Energy Optimal Control of Induction Motor Drives

Abrahamsen, Flemming

Publication date:
2000

Document Version
Publisher's PDF, also known as Version of record

Energy Optimal Control of Induction Motor Drives

by

Flemming Abrahamsen
Institute of Energy Technology, Aalborg University

February 2000

Institute of Energy Technology
Aalborg University
Pontoppidanstraede 101
DK-9220 Aalborg East

Printed in Denmark by Repro & Tryk A/S, Skive

ISBN 87-89179-26-9

2nd edition

Preface

This thesis is submitted to the Faculty of Engineering & Science at Aalborg University as part of the requirements for the degree of Ph.D. The research in energy optimal control of induction motors started for my part in August 1995. The first two years and three months with a research project financed by The Danish Energy Agency, entitled “Energy Optimal Control Strategies for Electro Motors - low-cost sensorless PWM-VSI based induction motor control”, journal no. 1253/95-0001. The project was followed by Design Engineer Erik Just Petersen from ABB Motors A/S, and by Manager of Control Engineering Paul Thøgersen from Danfoss Drives A/S. The results from this project, which focused on small drives, were in February 1998 published in a separate report. After that it was decided to extend the research with one year to investigate medium-size drives and permanent magnet motor drives. The last year was financed by the Danfoss Professor Program at Aalborg University and followed by Manager of Control Engineering Paul Thøgersen, Danfoss Drives A/S. The two research projects were supervised by Professor Frede Blåbjerg and Associate Professor John K. Pedersen, both from Institute of Energy Technology at Aalborg University.

The main purpose with a project like this it to promote technologies with a more efficient use of electrical energy. It is my hope that this thesis can be to help and inspiration for engineers who work with research and development of electrical drives, and to people who study efficient use of electrical energy in general.

Apart from this thesis and the report mentioned above, results from the project have been published in a number of papers and articles listed in the end of the thesis.

I would like to thank the Danfoss Professor Program for the financial support that enabled me to submit this thesis, and my supervisors Paul Thøgersen, Frede Blåbjerg and John K. Pedersen for help and good advises. I also want to thank Trine Lendrup Jacobsen for helping with the time-consuming efficiency measurements, and Paweł Grabowski for his assistance with programming the motor drive. I am thankful to Jens Birk, Danfoss Drives A/S, for his help during my stays at Danfoss Drives, and to Jukka Salonen, ABB Motors in Finland, for providing me with motor data.

February 2000, Flemming Abrahamsen

Summary

This thesis deals with energy optimal control of small and medium-size variable speed induction motor drives for especially Heating, Ventilation and Air-Condition (HVAC) applications. Optimized efficiency is achieved by adapting the magnetization level in the motor to the load, and the basic purpose is demonstrate how this can be done for low-cost PWM-VSI drives without bringing the robustness of the drive below an acceptable level.

Four drives are investigated with respect to energy optimal control: 2.2 kW standard and high-efficiency motor drives, 22 kW and 90 kW standard motor drives. The method has been to make extensive efficiency measurements within the specified operating area with optimized efficiency and with constant air-gap flux, and to establish reliable converter and motor loss models based on those measurements. The loss models have been used to analyze energy optimal control strategies by different steady-state calculations. Several control strategies were implemented and tested on a 2.2 kW scalar drive, both with respect to steady-state efficiency, convergence time in case of changing load, response to a large sudden load disturbance, and energy consumption in a realistic pump system. The dynamic performances were also evaluated in a vector controlled drive for CT applications. Based on these tests, the displacement power factor control and the direct air-gap flux control appeared to be best for small HVAC applications.

Energy optimal control of medium-size drives was analyzed separately to investigate the influence of converter losses. A new model-based control principle is proposed which can include converter losses, which does not depend on an analytical solution and which does only requires little computational power. A relation is established which can predict the efficiency improvement by energy optimal control for any standard induction motor drive between 2.2 kW and 90 kW.

A simple method to evaluate the robustness against load disturbances was developed and used to compare the robustness of different motor types and sizes. Calculation of the oscillatory behavior of a motor demonstrated that energy optimal control will sometimes improve and sometimes deteriorate the stability.

Comparison of small and medium-size induction motor drives with permanent magnet motor drives indicated why, and in which applications, PM motors are especially good. Calculations of economical aspects demonstrated the small difference in savings between the different motor types in a variable speed drive, compared with the constant speed drive.

Resumé

Denne Ph.D. rapport omhandler energioptimal styring af små og mellemstore asynkronmotordrev med variabel hastighed anvendt specielt i forbindelse med pumper, ventilatorer og kompressorer (HVAC). Virkningsgraden er optimeret ved at tilpasse magnetiseringsniveauet i motoren til lasten, og det grundlæggende formål er at vise, hvordan dette kan gøres i billige PWM-VSI drev, uden at stabiliteten forringes ud over det acceptable.

Fire motor drev er undersøgt med hensyn til energioptimal styring: 2.2 kW standard og højvirkningsgrad motor drev samt 22 kW og 90 kW standard motor drev. Den anvendte metode har været at udføre omfattende virkningsgradsmålinger indenfor hele det specificerede arbejdsområde, med optimal virkningsgrad og med konstant luftgabsflux, og at opstille pålidelige konverter og motor modeller baseret på disse målinger. Tabsmodellerne har været anvendt til at analysere energioptimale styrestrategier ved hjælp af forskellige stationære beregninger. Flere styrestrategier er blevet implementeret og afprøvet eksperimentelt på et skalært drev både med hensyn til stationær virkningsgrad, konvergenstid når lasten ændres, respons i tilfælde af en pludselig lastændring, og energiforbrug i et realistisk pumpesystem. De dynamiske egenskaber blev også afprøvet i et flux-vektororienteret drev. På baggrund af disse forsøg blev cos(φ)-styring og direkte flux-styring anset for at være de bedste styringsprincipper i små HVAC anvendelser.

Energioptimal styring af mellemstore drev blev analyseret separat med hensyn til indvirkningen af konvertertab. Et nyt modelbaseret styringsprincip, som kan medtage konvertertab, er foreslået. Det kræver ikke en analytisk løsning af optimeringproblemet og kræver kun meget lidt beregningskraft. Der er opstillet en sammenhæng, hvorved det er muligt at forudsige hvor meget virkningsgraden for et standard asynkronmotordrev mellem 2.2 kW og 90 kW kan forbedres ved at anvende energioptimal styring.

Der er etableret en simpel metode til at beregne hvor robust en motor er mod pludselige lastændringer, og den er anvendt på forskellige motortyper og motorstørrelser. Beregninger af resonanser i en motor har vist, at energioptimal styring i nogle tilfælde vil forbedre stabiliteten og i andre tilfælde forværre den. En sammenligning af små og mellemstore asynkronmotordrev med permanent magnet synkron motor drev har vist hvorfor, og i hvilke anvendelser, PM motorer er specielt gode. Økonomiske beregninger har vist, at i forhold til den store besparelse forbundet med indførelse af variabel hastighed, er der kun små forskelle i besparelserne mellem de forskellige motortyper i drev med variabel hastighed.

Chapter 1

Introduction

Many environmental experts see a connection between global changes in the climate and the emission of CO_2 in the atmosphere. During the last many years the global mean temperature has slowly increased and it has caused the political goal in many industrialized countries to reduce the emission of CO_2 in the future. The government in Denmark has in its plan “Energy21" committed itself to reduce the CO_2 emissions with 20 % by the year 2005 compared with the 1988 level. A UN panel of climate experts has estimated that to avoid serious changes in the climate, the CO_2 emissions should be halved from the year 1990 to 2030, and this might be the future goal for many industrialized countries. One of the ways to attain this goal is to reduce the electrical energy consumption, especially in a country as Denmark where most of the electrical energy is produced by coal fired power stations. These environmental considerations are the most important factors in Danish energy politics and the main reason to pursue reductions in energy consumption.

But there are other reason as well. The consumption of both thermal and electrical energy is growing, no matter the political intentions, so sooner and later very large investments in transmissions lines and power stations are required. If the growth in energy consumption can be reduced, then these investments can be postponed and a lot of money saved. For the end-user there is of course the simple incentive that he can save money if he can get the same work done with less energy by using more efficient energy conversion processes.

A large part of electrical energy is consumed by induction motors. They are used in various places including households, industry, commerce, public services, traction and agriculture. In fact, electrical motors consume around 56% of the total consumed electrical energy, and of this, induction motors account for 96% [1, p. 156]. This shows that around 53% of the total electrical energy is consumed by induction motors. The very extensive use of induction motors implies that if losses in induction motor drives can be reduced by just a few percent, it will have a major impact on the total electrical energy consumption.

The reasons for the wide use of this motor-type are well known: it is cheap, rugged, maintenance free, and has direct line start ability. Although the induction motor is inferior to for example permanent magnet synchronous motors and brush-less dc motors in terms of nominal efficiency, it is likely to remain the major electrical energy consumer for many years because of its many advantages and its wide use.

When the objective is to reduce the electrical energy consumed by induction motors, it is particularly interesting to deal with a segment of the consumer market called HVAC applications. HVAC, which stands for Heating, Ventilation and Air-Condition, is a group of applications that is often used in connection with induction motors. The devices employed in HVAC are typically ventilators, pumps, air-compressors and refrigerators. As will be shown later in this chapter, these devices consume a large part of the total energy consumed by induction motors. The reason why it is interesting to deal with these HVAC applications is that in many installations today, the application is driven by a constant speed induction motor, and the output of the process is being controlled by mechanical means, yielding a massive waste of energy. If, on the other hand, the HVAC application can be speed controlled, the loss of energy can be reduced dramatically.

Traditionally the induction motor has been operated directly from the grid, or possibly through a soft-starter, with almost constant shaft speed. But since the development of the power electronic converter in the early seventies, it is now also used in adjustable speed drives (ASD). This means that by inserting a converter between the motor in an existing installation, and the electrical grid, it is possible to obtain an adjustable speed motor drive and keeping all the advantages of the induction motor listed in the beginning of this section. In a HVAC application, by simply inserting a converter and leaving out the mechanical control (e.g. a valve), it is therefore possible to reduce the energy consumption remarkably. Since the HVAC applications account for a large proportion of electrical energy consumption variable speed control will contribute considerably to reduce energy consumption.

The newest progresses are improvements made to the motor drive itself. The motor efficiency is improved for so-called high-efficiency motors or premium-efficiency motors by improved construction and by use of more material in the motors. Furthermore the efficiency of the total drive is optimized by on-line energy optimal control.

This project will concentrate especially on the last issue, and seek to develop low cost control strategies for the converter and induction motor that minimize the energy losses in all load conditions. To do this in a rational manner the use of electrical motors in HVAC is analyzed further, so that the project can focus on the area with the highest potential for energy savings. In this introduction the control of HVAC applications is first discussed. Thereafter it is analyzed how much energy can be saved by speed control, in which applications and in what motor power range the highest savings can be obtained. This analysis leads to a more specific statement of the problem to be solved in this project.

1.1 Energy Efficient Control of HVAC Applications.

Typical tasks for HVAC installations are to control pressure, flow, temperature or liquid level, and which control method to choose is determined by several factors, including required control performance, installation cost and energy efficiency. A small comparison of control methods is given hereafter, see [2] for details.

- *On/off control.* Is used when only a fraction of full production is needed for long periods of time. The motor is turned on when the controlled parameter goes below a minimum limit, and the motor is turned off when the parameter exceeds a maximum limit. The number of starts and stops, which stress the installation mechanically, can be reduced by increasing a buffer size, for example a water tank for at water pump. If the plant is operating at rated load when the motor is turned on, the on/off control has a good energy efficiency, but otherwise the energy-efficiency will be degraded.
- *Stepwise control.* One large motor-drive-installation is divided into several smaller installations, each of them with on/off control. Each single motor is turned on or off depending on the production need. The advantage is that the motors and processes operate near rated load and with good energy-efficiency all the time. The disadvantages are increased installation costs and only stepwise control capability. It can, though, be combined with variable speed on one of the motors.
- *Mechanical process control.* It is used in applications where the process output parameter should be controlled continuously and the performance of on/off control and Stepwise control are not satisfactory. The induction motor is connected directly to the grid. The output parameter (e.g. pressure) is controlled mechanically, for example by a valve, a throttle-valve or a feedback shunt. The main drawback with this principle is that the mechanical control inevitably introduces high additional energy losses when full production is not needed. To express it in a popular way, it corresponds to running a car with full power and controlling the speed with the brake.
- *Variable speed control.* The motor is fed by a power-electronic converter which only consumes the amount of power that is required for the process. The process output is controlled only by varying the speed. Although the installation cost is high, variable speed may be chosen because of its control performance, possible energy saving or to reduce acoustic noise from for example fans.

From this small comparison between HVAC application control strategies, it can be concluded from an energy-economical point of view that the mechanical process control is not acceptable because of the high energy losses at reduced load. The choice between on/off control, stepwise control and variable speed control depends on the degree of loading and the required control performance. Plants where low production is needed for long periods of time

are in favor for the stepwise control and the variable speed control. On the other hand, when the production need is high and the performance of the on/off control is acceptable, the on/off control may be preferred because it is less expensive to install. A lot of energy can be saved in HVAC applications if good engineering is practiced during the design of the whole system, and in many cases on/off control or stepwise control will provide the best solution. There is no doubt, however, that in installations where good control performance is required, variable speed control makes up the only energy-effective alternative to mechanical control.

In general one should note that when designing the system it is important to consider the LCC (Life Cycle Costs). This includes all costs related to the given installation during its lifetime, including procurement, maintenance, repair, energy expense, environmental issues and disposal.

1.2 Energy Savings in HVAC Applications by Variable Speed Control.

The advantage of using variable speed control instead of mechanical control in HVAC applications is analyzed closer, taking a pump as an example. It will be concluded in which applications variable speed provides the highest potential energy saving.

1.2.1 Control of a Pump.

Four versions of a pump system are shown on Figure 1.1 - Figure 1.4. The first two are with constant speed and mechanical control, and the last two are with variable speed control. On Figure 1.1 and Figure 1.3 the pump is without head, and on Figure 1.2 and Figure 1.4 the pump is with head. The liquid flow is controlled so that in working point A the flow is 100% of rated flow, and in point B the flow is 50% of rated flow. The figures show the pressure-flow-curves of both the pump characteristic (PC) and of the tube-system, i.e. the system characteristic (SC). The operating point for the pump is defined by the intersection of the PC and the SC.

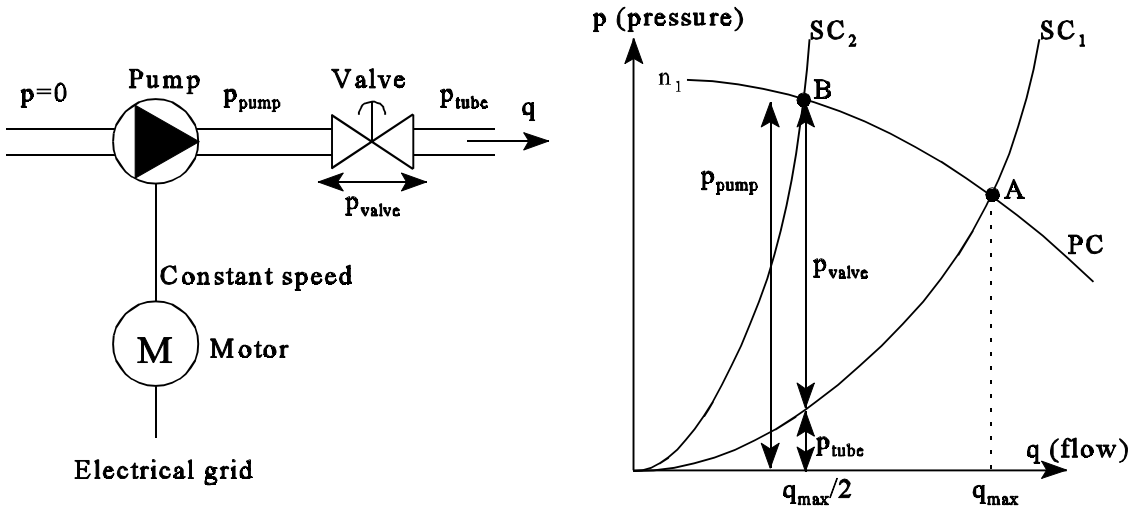

Figure 1.1: *Mechanical control of a pump without head. SC: system characteristic, PC: pump characteristic.*

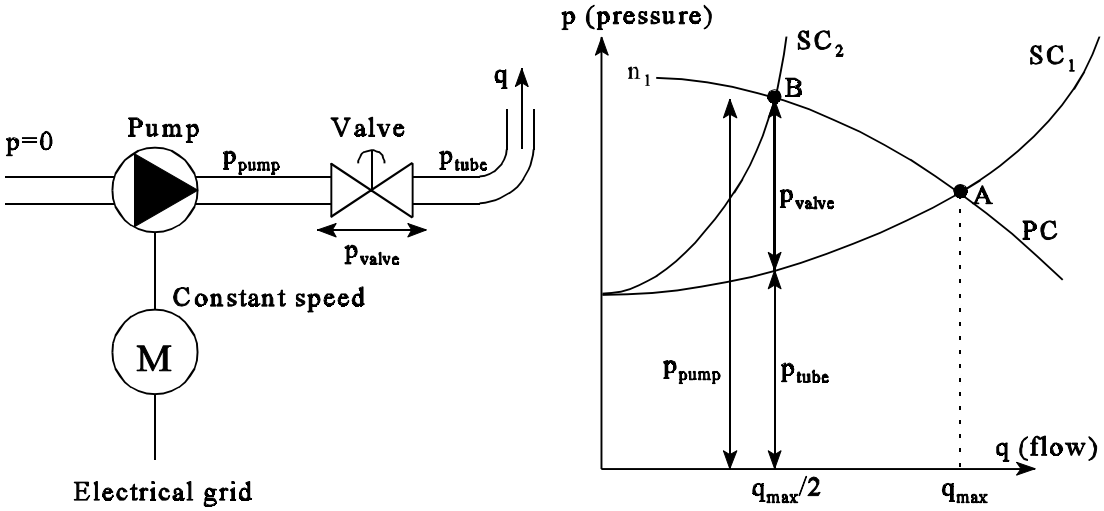

Figure 1.2: *Mechanical control of a pump with head. SC: system characteristic, PC: pump characteristic.*

It is seen from Figure 1.1 and Figure 1.2 that for the constant speed drive, the flow is reduced from A to B by using the valve to insert an extra resistance in the tube so that the system characteristic is changed from SC_1 to SC_2. In Figure 1.3 and Figure 1.4 the system characteristic is unchanged, but the change in speed changes the pump characteristic from PC_1 to PC_2, thereby changing the flow from A to B.

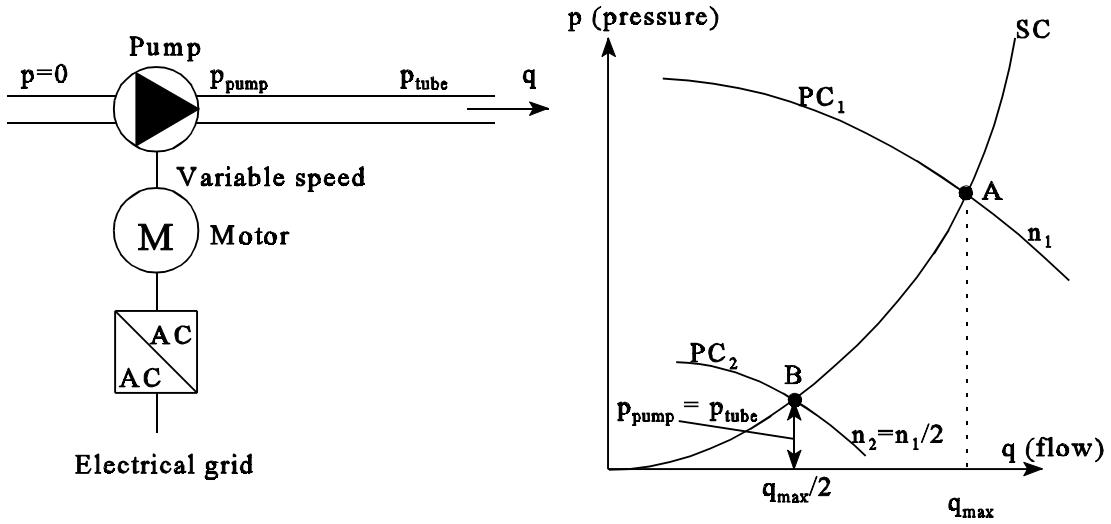

Figure 1.3: *Variable speed control of a pump without head. SC: system characteristic, PC: pump characteristic.*

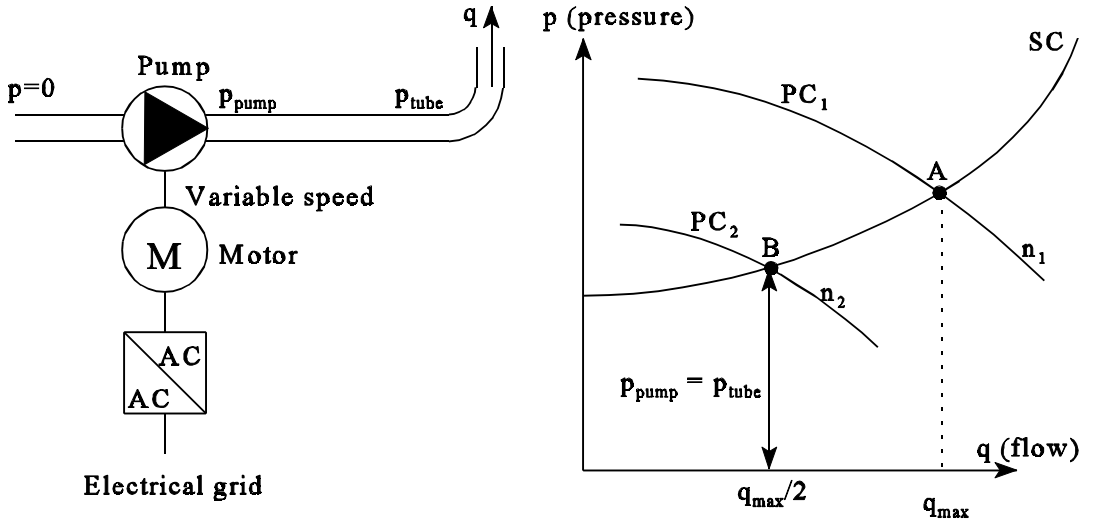

Figure 1.4: *Variable speed control of a pump with head. SC: system characteristic, PC: pump characteristic.*

Figure 1.5 shows that at full load (point A) the constant speed drive has the best efficiency because the power electronic converter in the variable speed drive causes additional losses in the motor and in the converter. At 50% flow (point B) the situation is opposite. At 50% flow without head there is a remarkable improvement with variable speed, compare bar-graph 1.1 with 1.3. Most of the loss in the constant speed drive is dissipated in the valve. In the case with head, compare bar 1.2 with 1.4, the difference is not that distinct. But still, the variable speed drive has the best efficiency.

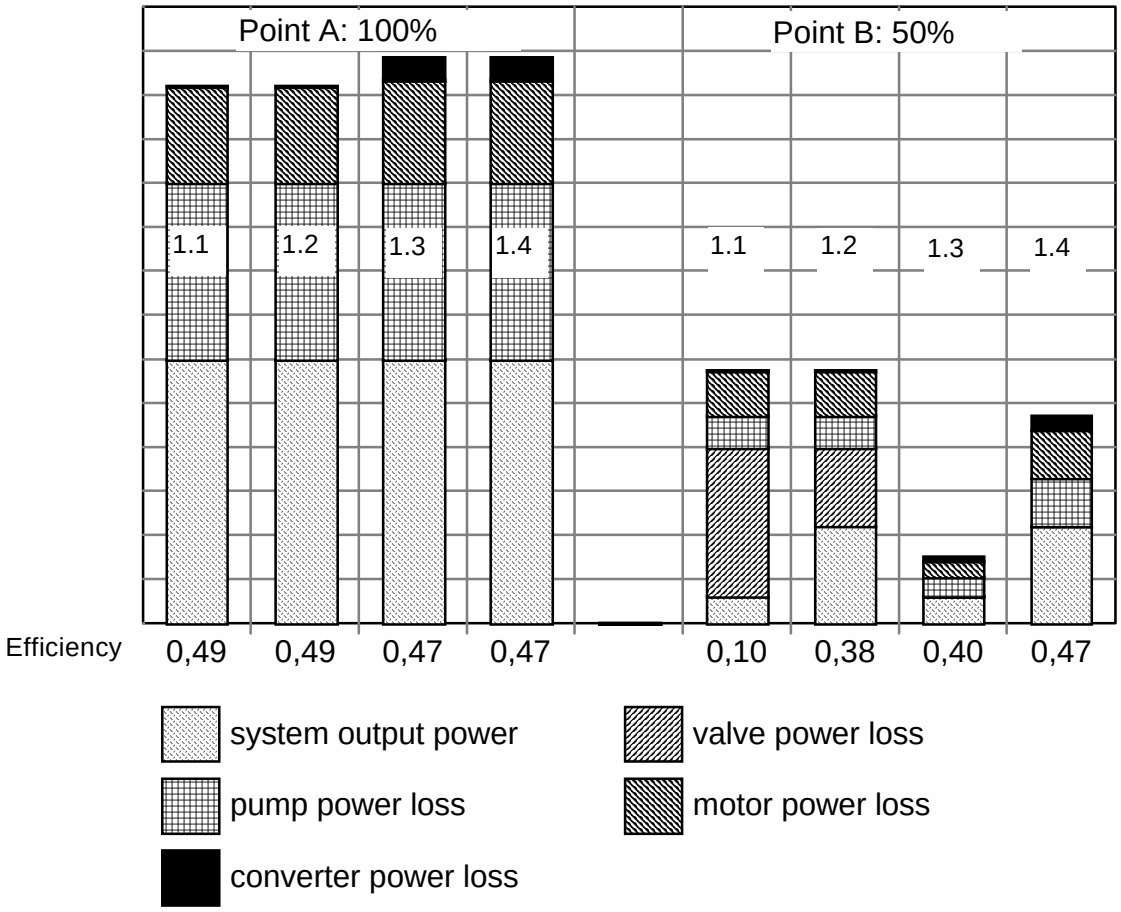

Figure 1.5: *Relative power distribution for the pump systems on Figure 1.1 - Figure 1.4. The efficiencies for the motor and pump are written below the bars-graphs.*

1.1: constant speed without head.
1.2: constant speed with head.
1.3: variable speed without head.
1.4: variable speed with head.

1.2.2 Applications with Potential for Energy Saving by Speed Control.

The previous analysis of a pump system made it clear that for a quadratic load type (in the ideal case the load torque increases with square of speed, in practice the increase is less than square), as a pump without head, variable speed control provides remarkable energy savings at part load compared to mechanical control. In the case with head, the savings are smaller. The results will now be extended to ventilators, air-compressors, and refrigerators. The conclusions are based on [2, pp. 28 ff] and [3, pp. 23-42].

Ventilation: The load is quadratic and is very well suited for speed control.

Pump: A pump without head is a quadratic load and very well suited for speed control, an example is a domestic heat water pump. A pump with head provides energy savings by speed control, but not as large, an example is a submersible pump.

Air compression: Speed control of an air-compressor corresponds somewhat to a pump with head and gives a good energy saving by speed control.

Refrigeration: Same as for air-compression.

The results are summarized in Table 1.1.

Table 1.1: Energy saving potential by speed control for four HVAC applications.

Process	Type	Torque, assuming ideal process	Energy saving by variable speed control
Ventilator	centrifugal	$\tau = K_1 q^2 = K_2 n^2$	very good
Pump	centrifugal without head	$\tau = K_1 q^2 = K_2 n^2$	very good
	centrifugal with head	$\tau = K_1 q^2 + K_2 = K_3 n^2 + K_2$	good
Air-compressor	screw, turbo, piston	Lightly increased with increased speed	good
Refrigerator	screw, turbo, piston	Lightly increased with increased speed	good

1.3 Statistics on the Use of Induction Motors.

In addition to the knowledge of which applications are especially well suited for variable speed control, it is valuable to know how extensive the use of these applications is, and in which motor power ranges they are primarily used. This knowledge shall be used to direct the research towards the area that have the highest potential for energy savings.

The knowledge is obtained by an analysis based on statistical material on the use of electro motors in Denmark [4]. The data is collected by energy-counselors in the period 1988-1992 in 1200 cases in the non-domestic sector. The 1200 cases comprise a total energy consumption of 900 GWh, equivalent to 750 MWh per case.

It can, of course, be discussed whether the data material is large enough to give a reliable result, but that is beyond the scope of this project. It just has to be kept in mind when analyzing the data that there is some uncertainty in the data. However, it is estimated that general conclusions can be drawn. Investigations on the use of induction motors have also been made in other countries, for example in the United States [1] and in Sweden [5], but they are not commented here.

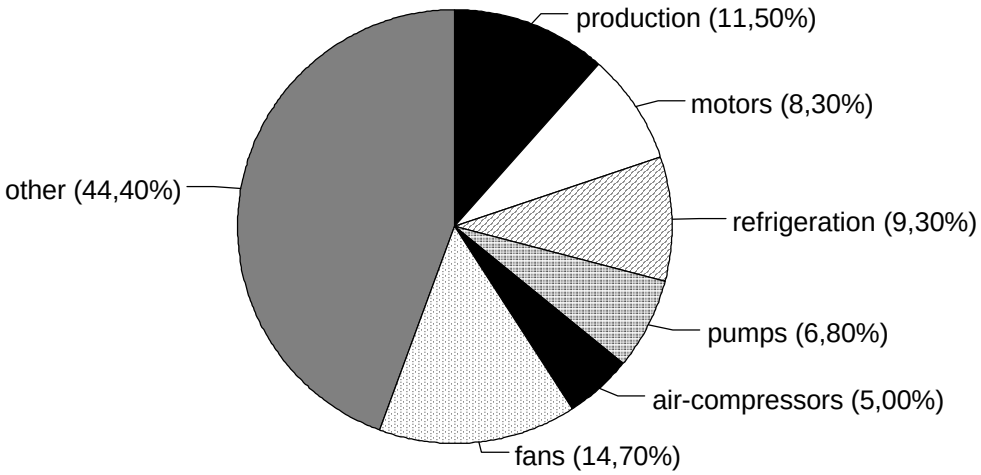

Figure 1.6: *Electrical energy consumption in Denmark in 1988-92 divided into applications [4, p. 11]. The domestic sector is not included.*

Figure 1.6 illustrates the electrical energy consumption divided into applications in the non-domestic Denmark. Knowing that electrical motors are used for both fans, air-compressors, pumps, refrigerators and production [4, p. 4], the pie-diagram shows that around 55.6% of the electrical energy is consumed by electrical motors, and that 35.8% of the total electrical energy consumption is used in HVAC applications, involving ventilators, air-compressors, pumps and refrigerators.

Not all electrical motors are induction motors. A small amount of the energy is consumed by other motors, including synchronous motors, dc-motors and stepper motors. Based on United States motor sales in 1989 it is estimated in [1, p. 156] that 96% of integral-horsepower drive power goes to induction motors. Although the number might be slightly different in Europe, it is certain that a very large amount of motor drive power goes to induction motors. It can be concluded that induction motors account for 53% ($0.556 \times 0.96 = 0.53$) of the total electrical energy consumption.

It is also investigated in which motor power range energy is consumed. In this analysis focus is put on the four HVAC applications: ventilators, pumps, air-compressors and refrigerators. It is interesting to look at the total energy losses per year on Figure 1.7. At low power ventilation and refrigeration are the most dominating applications, but in higher power ranges, the difference is smaller. It is interesting to see that as the consumption by ventilation goes down as the power range increases, the energy consumption of the other three application

reaches a maximum in the medium power range. The total energy loss per year, on Figure 1.8, which more or less decreases for all four applications for increasing power range, reflects the fact that the higher the power range, the higher is the energy efficiency. The total losses in the range above 53 kW are not important compared to the losses at low power. The power range is divided into small drives (<10 kW), medium-size drives (10-1000 kW), and large drives (>1000 kW).

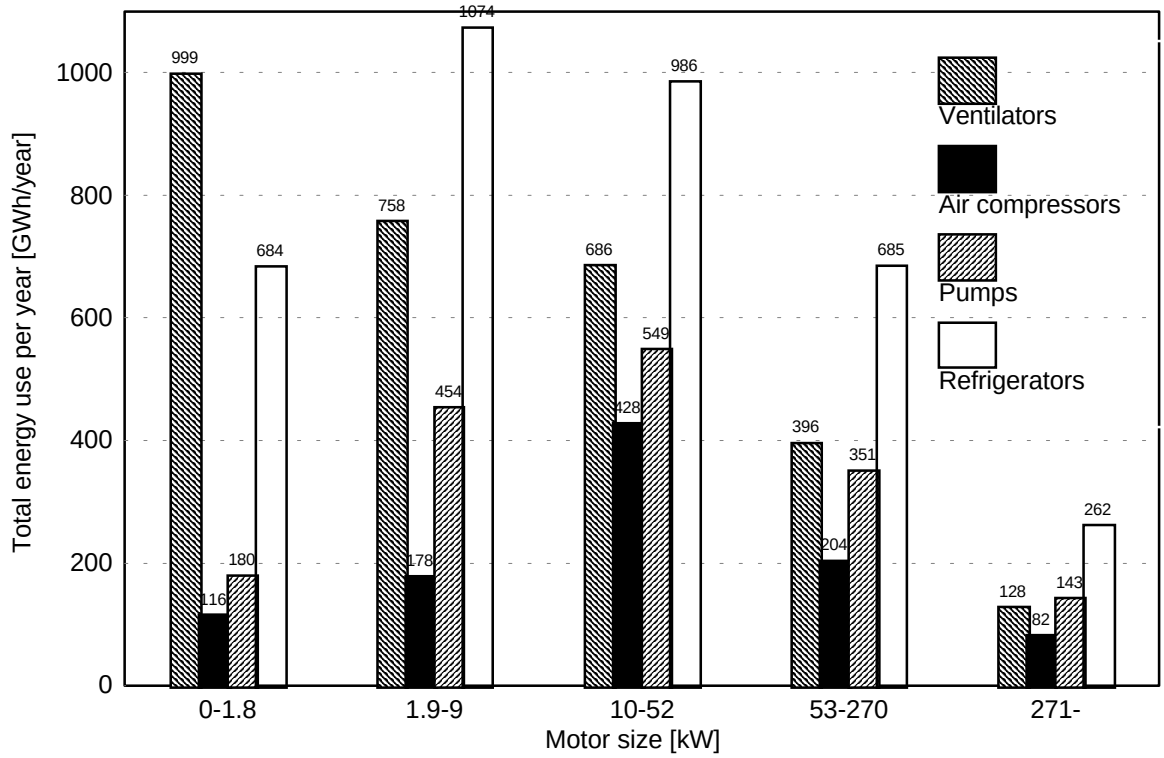

Figure 1.7: *Energy consumed by induction motors for ventilators, pumps, air-compressors and refrigerators in non-domestic Denmark in one year, divided into power classes [6, p. 22].*

The first conclusion that can be drawn with regard to the energy use in Denmark is that because the total losses in ranges above 53 kW are small, it is less interesting to try to reduce the motor losses in that power range. As most of the losses are located from 0-9 kW this is the most interesting power range to look at, but the medium power range can not be excluded either. Ventilation and refrigeration are the dominating applications, ventilation primarily at low power and refrigeration at medium power. Air-compressors and pumps are not important at low power, but gain increasing importance at medium power.

The energy use outside Denmark has not been investigated. A EU SAVE-project entitled "Penetration of Energy Efficient Motors and Drives" investigates the use of energy in HVAC applications in Europe, and the results will be published in year 2000. It is probable that the share of medium and large drives is more important in Europe in general than in Denmark alone.

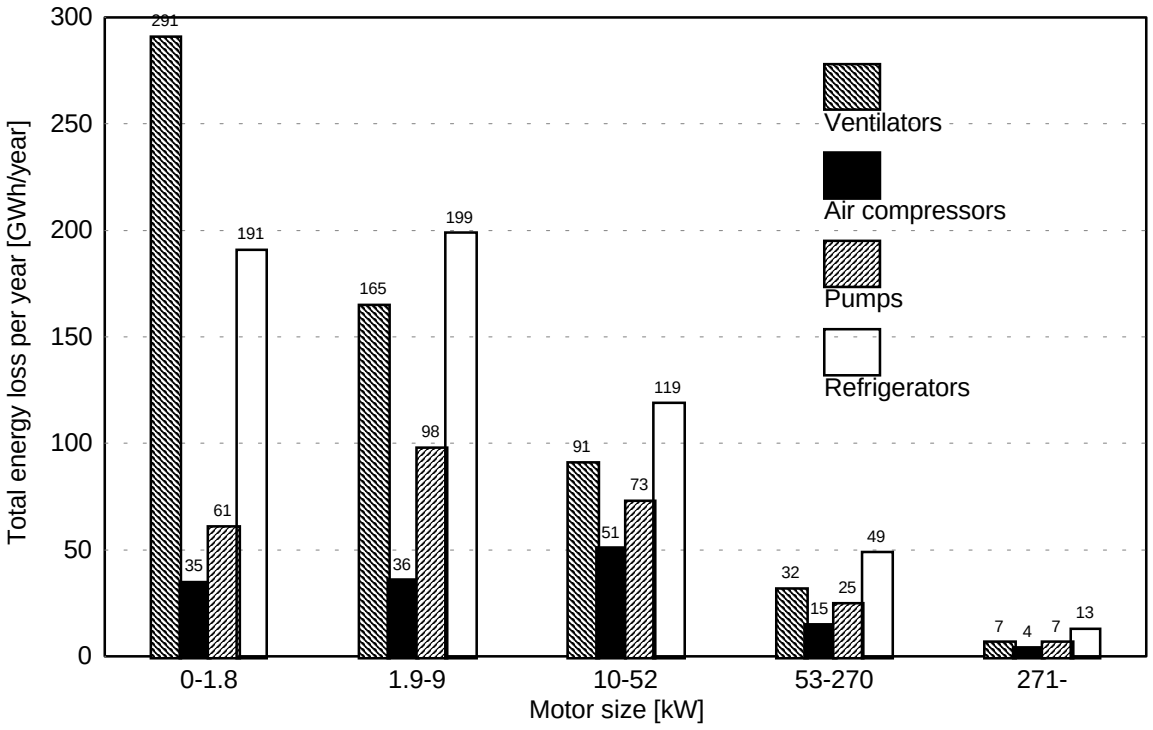

Figure 1.8: *Energy loss in induction motors for ventilators, pumps, air compressors and refrigerators in non-domestic Denmark in one year, divided into power classes [6, p. 24].*

1.4 Formulation of the Problem.

The initial analysis showed that the induction motor is a large consumer of electrical energy, and that a large part of the consumption goes to HVAC applications. As this is an area where variable speed control can offer several advantages, including good efficiency, it has been chosen to focus the work with energy optimal control on HVAC applications run by the standard PWM-VSI squirrel-cage induction motor drive on Figure 1.9.

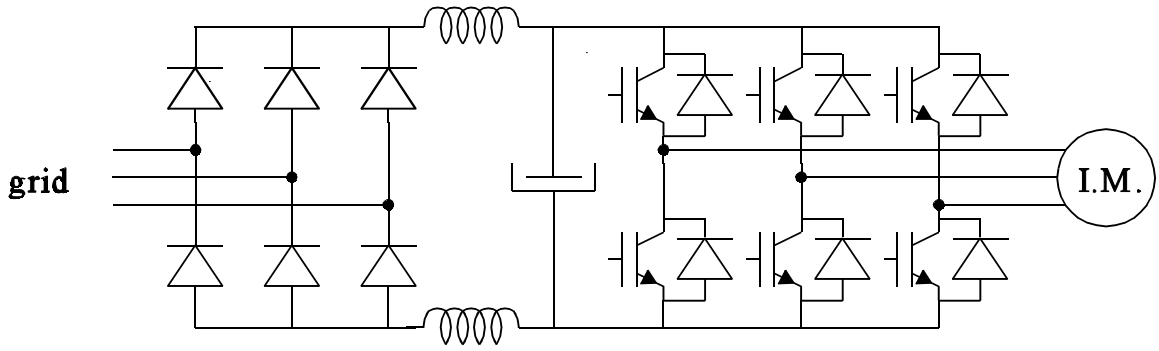

Figure 1.9: *PWM-VSI induction motor adjustable speed drive.*

The basic problem is to realize control of the induction motor drive which ensures that it always operates with optimal efficiency, keeping in mind that it must not reduce the reliability and other performance parameters of the drive below an acceptable level, and that the drive can be realized with low cost. This general goal brings about a number of more specific problems defined in the following, which are solved in this thesis.

1.4.1 Definition of the Problem.

The initial analysis showed that the main energy consumption and motor losses exist in connection with small drives (< 10 kW), so this thesis initially focuses on this size of drives. But the medium-size drives (10-1000 kW) are studied as well, paying special attention to the special characteristics of this class of drives compared with the small drives. As only HVAC applications are dealt with, the operating area is limited to 0 - 1 p.u. load torque and 0.2 - 1 p.u. speed, which is typical for such applications.

Small Drives.

For the energy optimal control of small drives it is chosen to study a 2.2 kW motor drive because it is typical for small drives, and because this drive size is easy to handle in the laboratory. The following issues have to be considered for small drives:

- What is the maximal increase in efficiency that can be obtained with energy optimal control compared with nominal air-gap flux control? This must be documented experimentally within the specified operating area.
- How important are the harmonic motor losses, and how do they depend on the control of the motor flux level? Should the harmonic losses be included in the energy optimal control algorithms? This also has to be documented by experiments.
- The above questions must be answered for both standard and high-efficiency induction motors, so that it can be clarified whether there are differences in the benefits of energy optimal control between the two motor types, and to see whether the type of motor influences how the energy optimal control algorithms should be designed.
- How can energy optimal control be realized, keeping in mind that the application is HVAC and the drive cost must be low? The last criterion restricts the solution to use a limited number of sensors, and a simple algorithm. The selection of proper control strategies should be founded on the extensive work which is already done within the field of energy optimal control, and possibly improvements should be suggested.
- The energy optimal control should be tested experimentally on a 2.2 kW test-bench within the whole operating area, both in steady-state and with regard to dynamic performance. Additionally the drive should be tested in a more realistic pump-system to see how much energy can typically be saved by energy optimal control. These tests must result in a proposal of which strategy is best suited for HVAC applications for small drives.

Medium-Size Drives.

The medium-size drives differ from the small drives by having a more important converter loss compared to the motor loss, and the following problems have to be solved with regard to energy optimal control of medium-size drives:

- Does the increased converter loss in medium-size drives influence much the point of optimal drive efficiency, compared with the small drives where the motor loss is dominating.
- Can energy optimal control algorithms for the small drives be used without problems in medium-size drives as well? Does the converter loss have to be included in the energy optimal control algorithm, and how can this possibly be done?
- The answers to the questions above must be based an experimental work, just as the performance of an energy optimal control strategy must be tested in terms of efficiency on a test-bench. 22 kW and 90 kW drives are selected for the experiments.

Energy Optimal Control in General.

The questions which must be answered to energy optimal control in general are the following:

- Possible stability problems could be a major disadvantage with energy optimal control. How serious is this problem, and how can it be overcome in drives for HVAC applications?
- Based on the work with the 2.2 kW, 22 kW and 90 kW drives, a relation should be established from which it can be estimated how much energy optimal control can improve the drive efficiency for any drive in the range of 2.2 - 90 kW compared with constant air-gap flux control.
- Is it important with regard to efficiency not to over-dimension an induction in a variable speed drive with energy optimal control?
- Finally it should be estimated how much energy can be saved with an induction motor drive in comparison with a permanent magnet motor drive in HVAC applications. The result must be presented in the form of energy saving, economical saving and pay-back time for the drives. The comparison should be made for a small and a medium-size drive.

1.4.2 Delimitation of the Project.

When the control algorithms are implemented for tests, they employ motor and converter parameters which are obtained by separate tests on the drive. For a possible industrial use it is assumed that these parameters are available, so methods of parameter estimation are not considered.

The control strategies are verified experimentally using a floating-point DSP to control the inverter. Such a DSP would be too expensive to use in most industrial drives, but it is very flexible and easy to use. The floating-point DSP could later be replaced with a fixed-point processor, but that is disregarded in this project.

Flux reduction has the advantage that is reduces the acoustic noise from both converter and motor, but acoustic noise is not considered in this thesis.

1.5 Structure of the Report.

The thesis is divided into three parts.

Part one includes this chapter and chapter 2, which reports on how losses can be reduced in motor drives, both in the construction phase and when the drive is operated.

Part two, which includes chapter 3 to chapter 6, provides a basic analysis and realization of energy optimal control applied to a 2.2 kW drive. Chapter 3 presents the motor and converter loss models which are used for analysis and experiments. A general steady-state analysis of energy optimal control is made in chapter 4, based on extensive experiments with 2.2 kW standard and high-efficiency motor drives. This analysis forms the basis for development of the control strategies which are selected and further analyzed in chapter 5. All control strategies are tested in chapter 6, both with respect to steady-state efficiency, dynamic performance and by energy consumption in a realistic circulating-water pump system.

Part three consists of three studies related to energy optimal control. The first in chapter 7 investigates energy optimal control in medium-size drive, supported by experiments with 22 kW and 90 kW motor drives. An analysis of stability is given in chapter 8, including robustness against load disturbances, and oscillations. Chapter 9 sets the energy optimally controlled induction motor drive in perspective by comparing it with a permanent magnet motor drive with respect to energy savings and economical issues.
Chapter 10 finally concludes on the whole thesis.

References.

[1] S. Nadel, M. Shepard, S. Greenberg, G. Katz, A. T. de Almeida, “Energy-Efficient Motor Systems”, 1992 by American Council for an Energy-Efficient Economy, 1001 Connecticut Avenue, N.W., Suite 801, Washington D.C. 20036, ISBN 0-918249-10-4.

[2] DEFU Teknisk rapport 322, “Energioptimering ved elmotordrift”, 1993. DEFU, Postbox 259, 2800 Lyngby, tel. +45 45 88 14 00. (Danish)

[3] T. Heilmann, “Pumper og regulering”, Heilmanns forlag, Højbjerggårdsvej 38, DK-2840 Holte. 1. udg., 1. oplag 1990. ISBN 87-983513-0-3. (Danish)

[4] DEFU Teknisk rapport 316 del 1, “Elprognose opdelt på slutanvendelser”, dec. 1992, DEFU, Postbox 259, 2800 Lyngby, tel. +45 45 88 14 00. (Danish)

[5] “Uppdrag 2000. Reducerede konsnader genom rät elmotorval”, Vattenfall 1991. (Swedish)

[6] DEFU Teknisk Rapport 352, “Elbesparelser gennem forbedret grundlag for projektering af elmotorer, 1995. DEFU, Postbox 259, 2800 Lyngby, tel. +45 45 88 14 00. (Danish)

Chapter 2

Induction Motor Drive Loss Minimization

This chapter describes various ways of optimizing the efficiency of an adjustable speed induction motor drive. The first part is devoted to give an overview of the losses in the drive and suggestion of how to improve efficiency by making changes in the construction of converter, motor and transmission. The losses generated in the distribution system are briefly discussed as well. The second part is a review of energy optimal control methods of induction motor drives. The main emphasis is put on variable speed drives, but control of fixed frequency converters, known as soft-starters, is briefly described as well.

2.1 Losses in an Adjustable Speed Induction Motor Drive.

Figure 2.1 shows how the power flows through an electrical motor drive from the power station to the process (ventilator, pump etc.). In every part of the chain there are losses associated with transportation of energy. The chain consists of:

Distribution system: Transmissions lines, distribution transformer and distribution line.

Converter: Power electronic unit which controls the motor stator voltage and stator frequency, typically a PWM-VSI with a three phase diode rectifier.

Motor: Three phase squirrel cage induction motor.

Transmission: Could be for example a direct shaft, a gear, a belt or a chain.

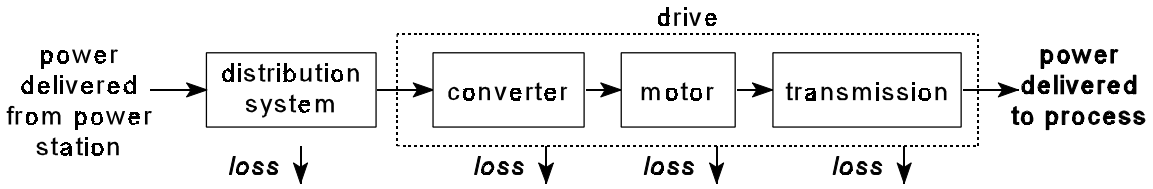

Figure 2.1: *Overview of power flow through an electrical motor drive.*

In this section the nature of losses in each of the four sections is briefly described, and it is explained, without going in details, how the losses can be reduced by optimization of the drive construction. A detailed description of motor and converter losses is given in chapter 3.

2.1.1 Frequency Converter.

The Pulse Width Modulated Voltage Source Inverter (PWM-VSI) topology with diode rectifier shown on Figure 2.2 is today used in standard drives up to several hundred kW. If the drive performs fast breaking or if it drives an active load, it can be necessary to dissipate power in a dc-link resistance or to use a thyristor rectifier in order to be able to regenerate power into the electrical grid, but neither of these cases are considered here.

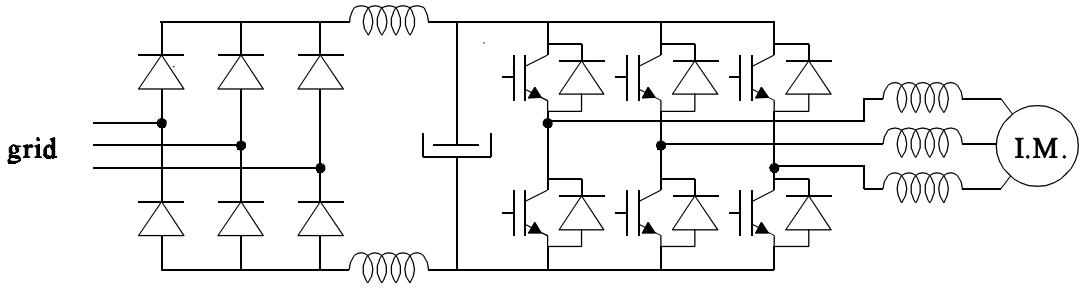

Figure 2.2: *Pulse Width Modulated Voltage Source Inverter (PWM-VSI) with diode rectifier commonly used in standard drives.*

The losses in the converter consist mainly of semiconductor switching loss and conduction loss, power supply for the control electronics, and choke conduction losses. The nominal efficiency is typically 0.96-0.98, depending on kVA rating and on whether forced or natural cooling is used.

The switching losses can be reduced by increasing the dv/dt of the switches, but on the other hand EMI regulation should be respected as well. It can also be a problem with a high dv/dt on the output, especially if the motor is fed through a long cable. In some converters the dv/dt on the motor terminals is limited with three output chokes. The choke copper losses can be reduced by increasing the wire size, but it increases the cost of the converter. The loss in the rectifier is not important.

The switching losses are also influenced by the inverter modulation strategy. It is possible to use a strategy where an inverter leg does not switch for 60 electrical degrees, and there are strategies with discontinuous modulating function where the switching losses are further reduced [1]. The choice of modulation strategy, however, depends on the requirements from the general motor control, and it is not commented further in this thesis.

2.1.2 Induction Motor.

Table 2.1 summarizes actions that can be taken to reduce losses in an induction motor given a constant core volume. It is seen that it is quite unproblematic to increase the amount of copper in the stator and to use thinner lamination steel with lower loss and with improved processing, although it is of course more expensive. The choice of steel, however, is also a compromise between low losses and good magnetic permeability. Steel with very low core

loss may have low permeability, whereby the saved core loss goes to stator copper losses because of increased magnetization current.

For a line start motor it is problematic to reduce the rotor resistance because of increased inrush current and decreased starting torque, but that is not a problem when the motor is fed with a converter. An improved, but unidirectional, fan for cooling the motor is only acceptable in some applications and probably not a good idea for a standard motor. Better bearings is a possibility. The actions to reduce stray load losses are not unproblematic, due to unacceptable adverse effects.

Table 2.1: Actions that can be taken to reduce induction motor losses [2].

Loss	Possible design changes	Positive effect on losses	Adverse effects
Stator copper loss	1. Increase amount of copper wire in slot.	1. Decrease stator resistance.	1. Increased cost & difficult to build.
	2. Increase stator slot size & amount of copper wire in slot.	2. Decrease stator resistance.	2. Increased cost & difficult to build.
	3. Decrease length of coil extensions.	3. Decrease stator resistance.	3. Possible increase of inrush current - difficult to build.
Core loss: hysteresis and eddy current	1. Change to lamination steel with lower loss.	1. Decrease hysteresis loss.	1. Increased cost & reduced availability of materials.
	2. Decrease lamination steel thickness.	2. Decrease eddy current loss.	2. Increased cost & availability of materials.
	3. Improve coreplating / annealing processes.	3. Decrease eddy current loss.	3. Increased cost and use of energy.
Rotor copper loss	1. Increase flux density in air-gap.	1. Decrease in slip & resulting rotor copper loss.	1. Increase in inrush current.
	2. Increase rotor bar size.	2. Decrease in rotor copper loss.	2. Maybe higher inrush current and decreased starting torque.
	3. Increase end-ring size.	3. Same as no. 2.	3. Same as no. 2.
	4. Increase rotor bar / end ring conductivity	4. Same as no. 2.	4. Same as no. 2.
Windage and friction loss	1. Optimize fan design.	1. Reduce operating temperatures.	1. Can cause increase in noise levels. May result in unidirectional fans.
	2. Optimize bearing selection.	2. Reduced friction loss.	2. May affect noise level or impose speed or bearing loading restriction.
Stray load loss	1. Insulate rotor bars.	1. Reduced bar to lamination currents.	1. Increased cost.
	2. Increased air-gap.	2. Reduce high frequency surface losses.	2. Reduced power factor.
	3. Eliminate rotor skew.	3. Reduction in rotor Cu loss.	3. May increase noise levels & affect speed-torque curves.
	4. Strand depth.	4. Reduced eddy currents.	4. Difficult to build, high cost.
	5. Transposed turns.	5. Reduced eddy currents.	5. Difficult to build, high cost.

If it is possible to increase the core volume, for example by increasing the stack length or the stator back iron, the permeance of the magnetic circuit can be increased. Then the number of stator windings can be reduced, giving room for thicker copper wires. The harmonic losses can be reduced by redesigning the rotor slot geometry, see for example [3].

2.1.3 Transmission.

Characteristics for different transmission types are listed in Table 2.2. It is clear from the table that there are quite large differences in efficiency between the transmission types. Especially the worm gear has very low efficiency, but there are also large differences between the different types of belts. There are mainly two types of belts: the synchronous belt with teeth, and the asynchronous belt such as the V-belt, cogged V-belt and flat belts. The V-belts are cheap and the maximal efficiency, which is not high for all types, is only reached if the belt is dimensioned, set up and maintained with care. The efficiency is also load dependent. If a V-belt has an efficiency of 98 % at nominal load it is reduced to around 92 % at 25 % load [4]. An advantage is that it can withstand chock loads as when a line start motor is started directly from the line. The flat and synchronous belts have higher efficiency but are more expensive. The synchronous belt does not withstand chock loads, but as these do not appear in speed controlled drives it is not a problem to use synchronous belts.

The best transmission solution is the direct shaft coupling, and variable speed makes it more often possible to select a direct shaft coupling than for a constant speed drive.

Table 2.2: Performances of motor drive transmissions [5, p. 86ff].

Type	Type	Losses	Efficiency	Advantage	Disadvantage
Shaft coupling	Shaft coupling	Low	99-100 %	High efficiency	Lower efficiency and wear on bearings when misaligned.
Gear	Helical (parallel) Bevel (right angle)	Friction between gears, in bearings and seals, windage, lubricant churning.	90-98 %	Remark: higher efficiency for higher rating and lower gear ratio.	
	Worm (right angle)		55-94 %, depends on gear ratio	High gear ratio.	Low efficiency
Belt	V-belt	flexing, slippage, windage	90-96 %	Withstands shock loads and motor jam, cheap	Efficiency < 90 % when not maintained
	Cogged V-belt	slippage, windage, flexing	1-3 % better than V-belt	less flexing loss. Takes shock loads and motor jam	20-30% more expensive than V-belt, needs maintenance
	Flat belt Poly-V belt	slippage, flexing	96-99 %	high efficiency, good for high speed.	Expensive
	Synchronous	windage, flexing	96-99 %	High efficiency, no slippage, no maintenance	Does not withstand shock loads and motor jam, expensive
Chain	Chain		up to 98 %	Withstands shock loads and high temperature	Needs maintenance

2.1.4 Grid Losses with an Adjustable Speed Drive.

For the line start motor the input current is nearly sinusoidal with a reactive component, and cos(φ) depends on the load. The three phase diode rectifier has a cos(φ) which is constantly near unity, but on the other hand the input current has an important harmonic content. The loss generated in the grid by the line start motor is:

$$P_{loss,grid} = 3R_{line}I_{line}^2 = 3R_{line}\left(\frac{P_{in}}{\sqrt{3}V_{line}\cos(\varphi)}\right)^2 = R_{line}\left(\frac{P_{in}}{V_{line}}\right)^2\frac{1}{\cos(\varphi)^2} \qquad (2.1)$$

where R_{line} : equivalent line series resistance.
I_{line} : RMS value of line current.
V_{line} : line voltage.
φ : phase lag angle.
P_{in} : motor input power.

The harmonic content is characterized by the Total Harmonic Distortion (THD), defined by:

$$THD = \frac{\sqrt{I^2 - I_1^2}}{I_1} \qquad (2.2)$$

where I : RMS value of rectifier input current.
I_1 : RMS value of fundamental rectifier input current.

If the grid voltage is sinusoidal, the harmonic current does not carry power and just generates losses in the grid. It can be shown that

$$I^2 = I_1^2(1 + THD^2) \qquad (2.3)$$

so that the loss generated in the grid by the diode rectifier is

$$P_{loss,grid} = 3R_{line}I_{line}^2 = 3R_{line}I_{line1}^2(1 + THD^2) = R_{line}\left(\frac{P_{in}}{V_{line}}\right)^2(1 + THD^2) \qquad (2.4)$$

The THD depends mainly on the size of the inductance in the dc-link filter and on the strength of the electrical grid. If the filter inductance is low, the THD becomes high. In commercial drives a THD on the input current of 40 % is common at nominal load. It is assumed here that the THD varies linearly with the motor output power from 2 at no-load to 0.4 at rated load. Figure 2.3 shows a comparison of the line RMS current for a 2.2 kW standard motor when it is connected directly to the grid and when it is fed through a frequency converter, and it demonstrates that the converter generates lowest loss in the grid. In [6] and [7] it is shown how the grid harmonics can be reduced by mixing single-phase and three-phase loads.

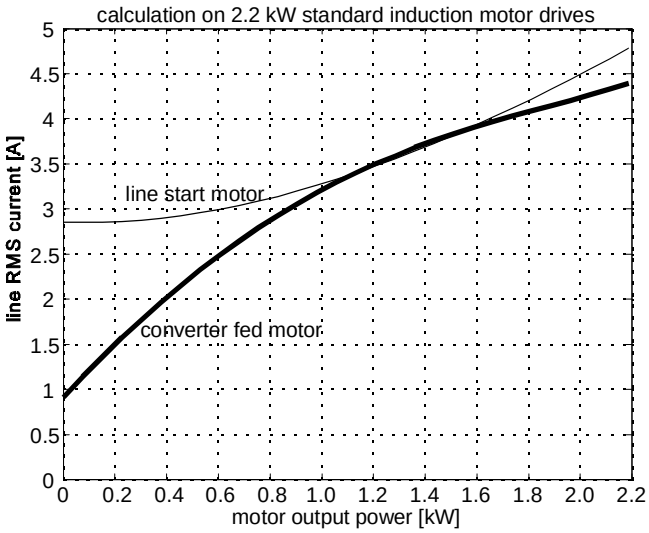

Figure 2.3: *Line RMS currents for a 2.2 kW induction motor when it is connected directly to the grid and when it is fed through a converter.*

2.2 Energy Optimization by Motor Flux Reduction.

Apart from improving the drive by changes in the construction, the losses can be reduced by energy optimal control, which is for a given speed and load torque to apply the set of stator voltage and frequency which minimize the drive losses [8, pp. 346-348]. The principle of energy optimal control is hereafter explained with main focus on motor losses.
The electro-magnetic torque of an induction motor is approximately

$$\tau_{em} = K \cdot I_m \cdot I_r \qquad (2.5)$$

where K : constant.
I_m : magnetizing current.
I_r : rotor current.

For a given load torque, the required electro-magnetic torque is therefore obtainable by an infinite number of combinations of magnetizing current and torque producing rotor current.

If I_m is large and I_r is small, then the core loss and the stator copper loss are large and the rotor copper loss is small. Contrarily if I_m gets smaller and I_r gets larger, then the core loss and the stator copper loss initially decrease and the rotor copper loss increases, but eventually the stator copper loss starts to increase also, so for a given load torque there is a ratio between the magnetizing current and the rotor current which generates a minimum of total losses. The motor is normally designed so that it operates with an optimum near rated load. But at low load there is an excess of magnetization, corresponding to a large I_m and a small I_r. The total loss can then be reduced by reducing I_m and increasing I_r.

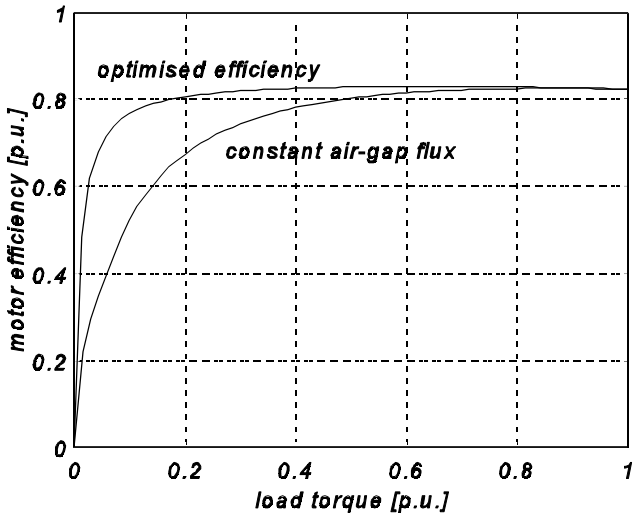

Figure 2.4: *Curves for motor efficiencies at rated speed for a 2.2 kW motor with constant air-gap flux and with optimized efficiency.*

The improvement in motor efficiency with minimized losses compared to conventional constant air-gap flux control is illustrated on Figure 2.4. It is seen that the difference between the energy optimized efficiency and the constant air-gap flux efficiency is largest in the low load region.

Energy optimal control is interesting for HVAC because it is highly probable that a motor in a HVAC installation will operate at reduced load for long periods of time. A HVAC application plant is normally dimensioned to handle an extreme load situation. For example a central heating warm-water circulating pump must be able to keep a house warm on the coldest day of the year. This means that for most of the year the motor and pump are only loaded with a fraction of rated power. Furthermore, the motor is normally larger than it needs to be in a given application, which is explained by the following two reasons [9, pp. 16f]:

- All motors from a motor manufacturer are not absolutely identical but lie inside the tolerances of a production line. Hence, the motor designer has to use a security factor for the rated power to insure that all motors fulfil the nameplate-data specifications.
- Because induction motors of the shelf are only available at certain power ratings, the engineer, having calculated the required rated motor power, has to choose the next motor size above the calculated value. Small standard induction motors, for example, are only available at 1.1, 1.5, 2.2, 3, 4, 5.5 and 7.5 kW.

Adding these factors, the result is that even when a plant is operating at full production, the induction motor is so large that the process (e.g. a pump) will never be able to subject the motor to full load. The conclusion is that there is a potential for energy savings in variable speed drives in HVAC applications by adapting the motor flux to the load.

The main disadvantage with energy optimal control is that flux reduction at low load makes the motor drive more sensible to load disturbances and degrades the dynamic performance.

If the losses in the drive were known exactly, it would be possible to calculate the energy optimal operating point and control the drive in accordance to that, but there are several reasons why this is not possible in real life:

- Even though the energy optimal operating point could be calculated exactly, it is probable that limitation in computation power in industrial drives would make this impossible.
- A number of losses are difficult to predict, including stray load losses, core losses in case of saturation changes and harmonic content, and copper losses because of temperature changes.
- All the measurable signals can not be acquired due to limited production cost of the drive. It means that certain quantities must be estimated, which naturally leads to an error. And some quantities, such as converter output voltage and dc-link current, are very difficult to measure precisely anyway.

2.3 Energy Optimal Control of VVFF Drive.

The use of a VVFF (Variable Voltage Fixed Frequency) converter (soft-starter) is in principle just a special case of the general problem of energy optimal control. As the name says, the stator voltage is variable and stator frequency is constant. But the harmonic content of the stator voltages differ so much from the PWM voltages that a total different performance is obtained because of the harmonic losses. That is the reason why the VVFF converter is treated separately in this review.

The first attempt to optimize the efficiency of an induction motor drive by converter control was indeed realized by use of a VVFF converter by Nola in 1977 [10]. It was discovered that by controlling the fire angle of a soft-starter converter, as seen on Figure 2.5 in a three-phase version, the fundamental stator voltage and thereby the efficiency can be controlled. The first control principle was to keep a constant fire angle of the thyristors. After that followed a number of articles and patents suggesting different control strategies for the same converter type [11]-[35].

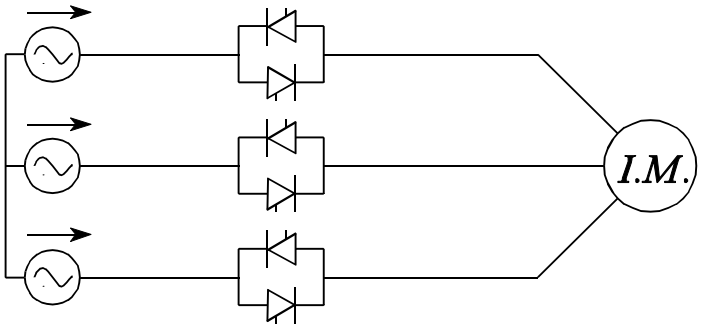

Figure 2.5: *Induction motor supplied by a VVFF converter (soft-starter).*

All control strategies are based on an attempt to select one variable, and to keep it constant or to minimize it. It could be a constant fire-angle, minimum or constant displacement power factor angle, minimum stator current or minimum input power. A comparison by Rowan and Lipo in 1983 [23] showed that minimum of power factor or minimum input power gives the best efficiency. The disadvantage with the VVFF converter is that the harmonic losses in the drive are so large, that the real improvement is questionable.

Rowan and Lipo [23] investigate the efficiency including harmonic losses of a VVFF controlled motor drive and compares it to a motor connected directly to the grid. At loads above 0.9 p.u. the VVFF converter is fully conducting so the thyristor conduction loss degrades the efficiency of the VVFF motor drive with 1.5 % compared to the uncontrolled motor. At loads below 0.45 p.u. the soft-starter-motor outperforms the uncontrolled motor. The conclusion is that for loads above 0.45 p.u. the efficiency improvement is negative, and therefore energy saving is only attainable in applications where the motor is operated with low load for significant periods of time.

As the power transistors developed, the soft-starter was left in favor of the PWM-VSI for energy optimization purposes, but the VVFF converter is still used as a soft-starter. The soft-starter is widely used in industry today and most of them also have an energy saving option. Modern soft starters have been tested recently by Blaabjerg et al. in 1995 [35], but the conclusion is that if the only purpose of the soft-starter is to save energy, there is no pay back on it. In addition, with energy optimization, stability problems can occur and harmonic grid current are increased making it possibly difficult to fulfil the new regulations IEC-1000. The conclusion is that the soft-starter is not a good solution to solve the energy efficiency optimization problem.

The main disadvantage is that the softstarter can not provide a large speed variation, whereby the primary source of energy savings in HVAC applications is lost. This converter topology will not be treated further in this thesis.

2.4 Energy Optimal Control of VVVF Drive.

The basic VVVF (Variable Voltage Variable Frequency) topology is shown on Figure 2.6. The output voltage is pulse-width-modulated. Today the pulse-amplitude-modulating inverter is only used in special applications such as high speed or low voltage, and it is not treated here.

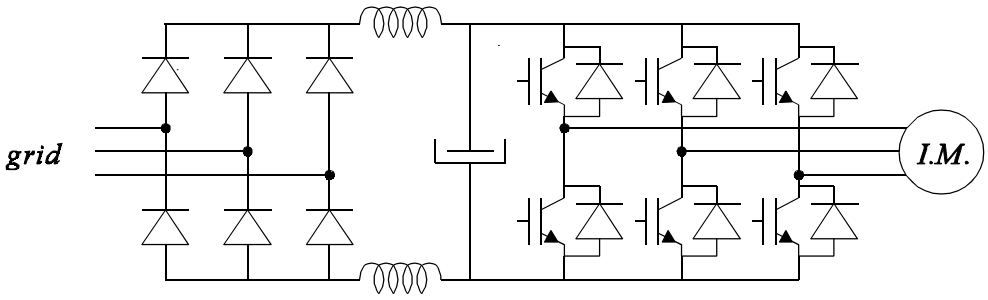

Figure 2.6: *A PWM-VSI with diode rectifier used in most ASDs today.*

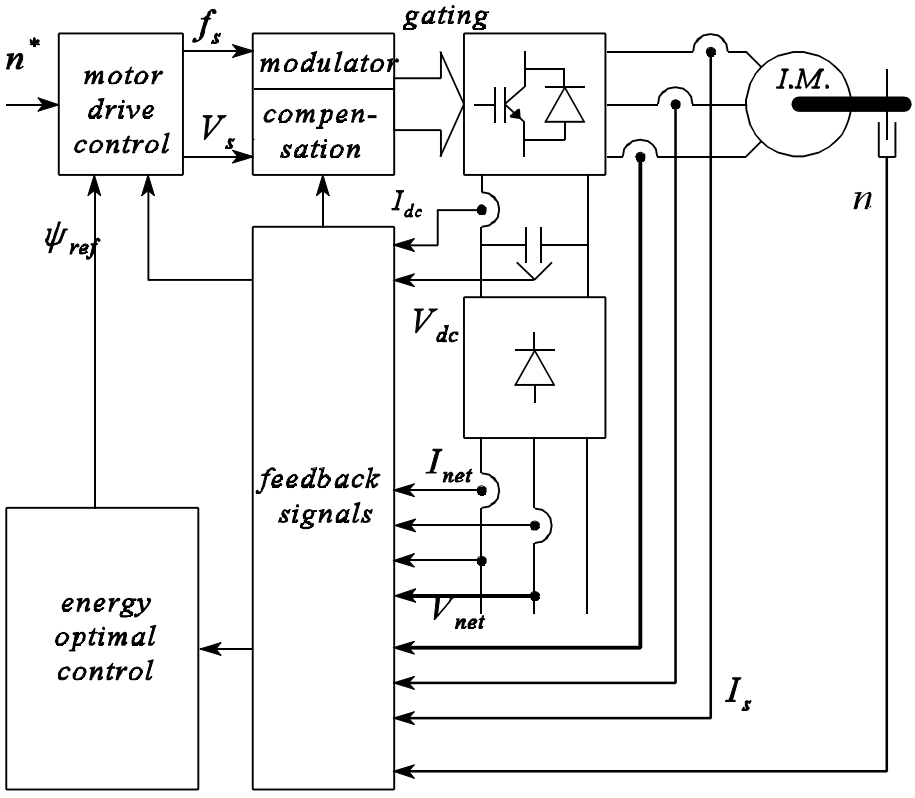

Figure 2.7: *Control diagram for efficiency optimization of a motor drive. Many possible feedback signals are indicated.*

Figure 2.7 shows a control diagram for an ASD with energy optimal control. Many measured feedback signal are indicated, but in most industrial drives only the dc-link voltage

and two or three phase currents are measured. In servo drives the speed may be measured as well. The diagram indicates that it is also possible to measure the dc-link current, and the currents and voltages at the input to the rectifier. The purpose of doing that would be to the measure in input power to the drive. This is, however, never done in industrial drives because of the extra cost. A solution for future drives could be to reconstruct the three stator currents from measurement of the dc-link current as suggested by Blåbjerg [102], which would also make it possible to measure the input power to the inverter without extra cost.

The energy optimal control methods are in the following divided into three categories: simple state control, model-based control and search control.

2.5 Simple State Control.

When an induction motor is operated with optimal efficiency it appears that some electrical parameters behave in a simple way. The most obvious parameters to control are cos(φ) and rotor slip frequency.

One simple control scheme, which does not include any of these two, was proposed, though, by Tomita in 1988 [45] and [46]. He suggests to control the motor in open-loop, and to determine the stator voltage as a function of stator current and stator frequency, see equation (2.6). This is basically a simple way of making the V/f-ratio load dependent by using the stator current as load torque indicator. The $K(f_s)$ compensates for the relatively larger voltage drop in the stator at low frequency.

$$\frac{V_s}{f_s} = K(f_s) \cdot I_s \qquad (2.6)$$

where $K(f_s)$: non-linear stator frequency dependent gain.

2.5.1 cos(φ) (Displacement Power Factor) Control.

The principle of cos(φ) control of inverter fed induction motors was described by Rosenberg et al. [36] in 1976, and it was mentioned in connection with energy optimal control for the first time in the patent by Earle [37] in 1981. Power factor control had previously been proposed by Nola [9] in 1977, but this was for a single phase motor fed by back-to-back mounted thyristors.

There is a large number of patents and papers on energy optimal cos(φ) control of induction motors: [37] - [39], [44], [47] - [55], and the claims are on ways to measure cos(φ) or to implement the control, see an example in Figure 2.8. There are also special proposals of how to generate the reference value.

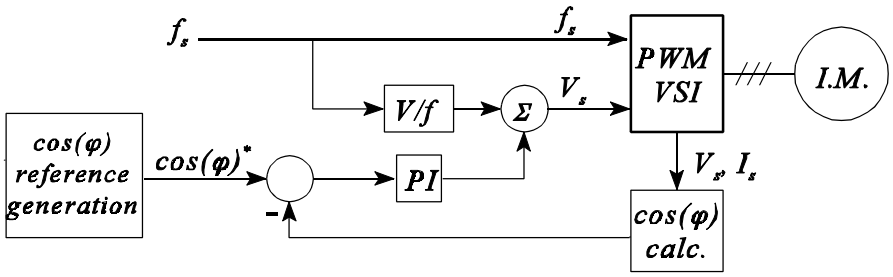

Figure 2.8: *An example of cos(φ) control in a scalar drive.*

The advantages of the cos(φ) control are that it is so simple and that it does not require speed information. One disadvantage is that the cos(φ) reference is only valid for one specific motor. For some motors it may be acceptable to keep a constant cos(φ) reference, and for other motors it may be an obligation to vary the reference as function of for example stator frequency or load, Andersen and Pedersen[55]. A careful analysis of this matter for different motor types and motor sizes has not been reported in literature.

2.5.2 Rotor Slip Frequency Control.

The first attempt to calculate energy optimal slip frequencies was done by Jian et al. [40] in 1983 for a constant frequency drive. They also discussed the influence of saturation on the reference values. Stanton et al. [57] suggested in 1983 to use a constant slip frequency reference in the low torque (low flux) region, assuming a linear magnetic circuit. It will be shown later in this report, however, that even when the magnetic circuit is linear, the influence of the presence of core losses deteriorates the performance of the constant slip frequency control. The same year Park et al. [41] proposed an implementation of slip frequency control in a current source inverter drive, see also the work by Kim et al. in 1984 [43]. In 1984 Park and Sul [42] proposed an energy optimal control strategy where the optimal rotor slip frequencies are put in a look-up table, see Figure 2.9. The values are based on off-line measurements on the motor drive, and for that given motor drive, the optimal slip frequency values were made dependent on the speed only.

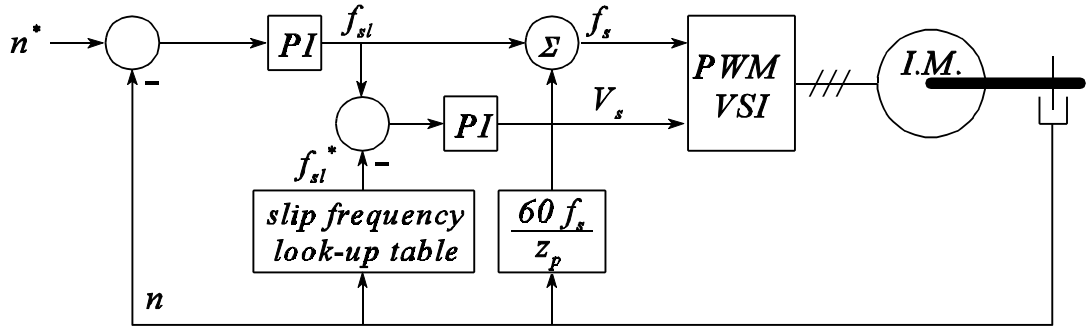

Figure 2.9: *An example of a rotor slip frequency control, with reference values in a look-up table [42].*

2.6 Model-Based Control.

Model-based control is a principle where the drive control contains equations which model the drive or the drive losses, and uses the equations to calculate the point of optimal efficiency. The motor parameters should be known beforehand. In a series production of drives with specific motors and converters designed to operate together it can be realized by off-line measurements. Otherwise automatic parameter estimation is required.

2.6.1 Scalar Drives.

Galler [56] proposed in 1980 to use the motor model to calculate an optimal stator frequency and to control the speed with the voltage. The calculated optimal stator frequency is based on the steady-state motor model disregarding core loss and assuming a linear magnetic circuit:

$$f_s = \frac{60n}{z_p} + \frac{1}{2\pi}\sqrt{\frac{R_s R_r^2}{R_s(L_m + L_r)^2 + R_r L_m^2}} \qquad (2.7)$$

where n : speed.
z_p : number of pole-pairs.
R_s : stator resistance.
R_r : rotor resistance.
L_m : magnetizing inductance.
L_s : stator inductance.
L_r : rotor inductance.

The method is also described by Kusko and Galler [58] 1983, and it is proposed to implement it as shown in Figure 2.10. The core losses can be included in the model, but then the optimal stator frequency must be computed numerically as

$$f_s = \frac{60 \cdot n}{z_p} + a \cdot n + b \qquad (2.8)$$

and the coefficients a and b will have to be calculated off-line. The last proposal is essentially just a look-up table similar to the scheme in Figure 2.9. The drawbacks of the equations (2.7) and (2.8) suggested by Kusko and Galler is that the model does not include saturation of the magnetic circuit, which makes it impossible to obtain good results.

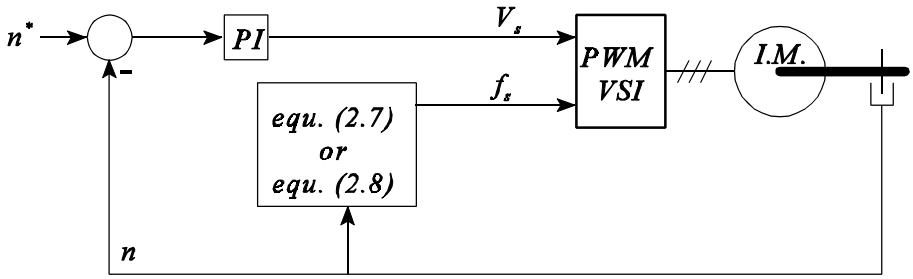

Figure 2.10: *Example of implementation of a model-based control in a scalar drive [58].*

Bose [59] claims in a patent the idea to optimize efficiency by use of a loss model. Stator current and air-gap flux are detected and used to calculate the model loss, including fundamental and harmonic copper losses, and core losses, taking also saturation into account. By measurement of stator voltages and currents, the input power and thereafter efficiency are calculated. The air-gap flux is varied in small steps until the optimal efficiency is found. The slip frequency is calculated from air-gap flux and torque. The proposed implementation will give a good result, but it is complex as it involves measurement of speed, air-gap flux, stator currents and stator voltages. The idea of searching for minimum loss by use of a loss model was also proposed by Kusko and Galler [58] in 1983.

Pedersen and Blaabjerg [63] proposed in 1992 for an electrical vehicle an expression where the efficiency optimal magnetizing current reference is determined as function of a torque reference and speed.

An idea was patented by Yamakawa [66] in 1994 for a motor controlled in open loop. The input power to the motor is measured, and the stator voltage is then calculated by

$$V_s = K \cdot \sqrt{P_{motor,in}} \cdot \sqrt[3]{f_s} \qquad (2.9)$$

In [72] Kioskeridis and Margaris, 1996, uses the steady state motor model to calculate the optimal air-gap flux as

$$\psi_{m,opt} = I_s G_s \sqrt{\frac{1 + \omega_m^2 T_s^2}{1 + \omega_m^2 T_{ps}^2}} \qquad (2.10)$$

where $\psi_{m,opt}$: efficiency optimal air-gap flux.
I_s : stator current.
G_s : motor specific constant which includes saturation.
ω_m : shaft angular velocity.
T_s : motor specific time constant.
T_{ps} : motor specific time constant.

The argument for the structure of equation (2.10) is as follows: the air-gap flux should increase with load, indicated by I_s. The denominator expresses that above a certain speed the flux should be reduced in order to limit the core losses, and the nominator expresses that at another speed the flux should increase in order to limit stray load losses due to armature reaction. The constants G_s, T_s and T_{ps} are determined by three experiments.

2.6.2 Field Oriented Vector Controlled Drives.

It is obvious to use model-based control in field-vector oriented drives because good speed information is available and some model parameters are already known. It should just be kept in mind that accurate models of core losses and of magnetic saturation are needed to obtain good loss minimization, and in most conventional field-vector controlled drives both core losses and saturation are disregarded.

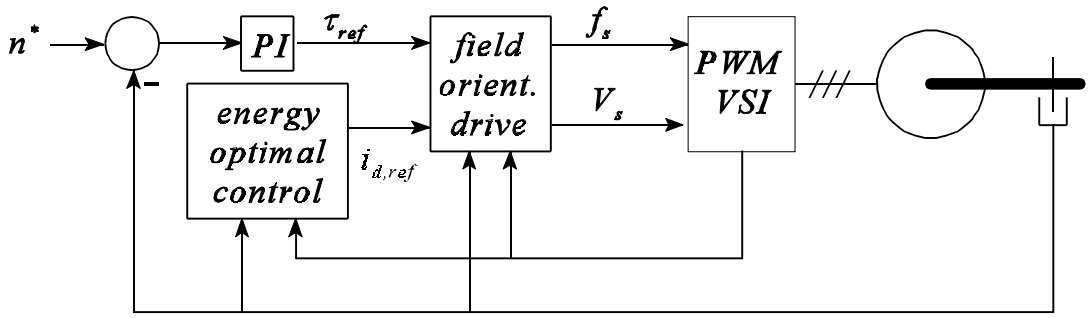

Figure 2.11: *An example of a motor model-based efficiency optimized control implemented in a field oriented reference frame.*

Most proposals are based on a loss function which is differentiated with respect to a flux related parameter to find minimum loss for a given load torque and a given speed. There are differences in how the result is presented. This is due to differences in representation of for example the core loss resistance and differences in implementation, but basically the idea is the same. In some cases the optimal rotor-flux reference is calculated directly as by Takahashi and Noguchi [60], Islam and Somuah [61], Mendes et al. [67], Baba et al. [73], Matsuse et al. [76] and Chang and Kim [77]. In other cases the optimal efficiency point is expressed as a ratio between field-current and torque-current, such as by Garcia et al. [65], Ashikaga et al. [69] and [74]. In [70], by Burtea and Ghita, an optimal slip frequency is calculated, and in [75], by Rasmussen and Thøgersen, the optimal efficiency point is found by equalizing the loss related to the torque producing current with the loss related with the field producing current by help of a PI-controller. As it will be shown in section 5.2, it compromises the result that saturation is not considered in any of the cases.

Mendes et al., [67] and [73], claim to minimize losses also in dynamic. This demands, however, that load torque and speed are known in advance. It is true in a limited number of

applications, for example in tool machines that work continuously in the same closed loop cycle. See also Lorenz and Yang [62].

Fetz et al. [64] made in 1993 a different approach to efficiency optimization of a rotor-flux oriented vector controlled drive. They used the maximum torque per ampere stator current as a criterion. This enables to calculate optimal field-current and torque-current references from a torque reference.

2.7 Search Control.

What here is called search control, has by other authors been called testing control, adaptive control or on-line optimization. It is the name for the control principle where a significant parameter is minimized or maximized by trial and error. The criterion could be maximum efficiency, minimum inverter input power, minimum dc-link power, minimum motor input power, minimum motor loss, minimum drive loss, minimum stator current or minimum dc-link current.

2.7.1 Traditional Search Control.

The principle was first mentioned in a patent by Geppert [78] in 1982 for an electrical vehicle drive. It was proposed to start the drive with a nominal V/Hz ratio, and when a constant torque demand is detected, to decrease the V/Hz ratio until a minimum of dc-link current is found.

For a general purpose drive, the idea was first mentioned by Kusko and Galler [58] in 1983. Kirschen et al. [79] were in 1985 the first to do simulations. Experimental results were reported in 1987 [80]. They implemented the search control in connection with a rotor-flux oriented vector control scheme, and minimized the drive input power, keeping the motor output constant by controlling the speed and assuming the load characteristic to be constant [103, p. 388], see Figure 2.12. A similar system was investigated by Chen and Yeh in 1991 [88].

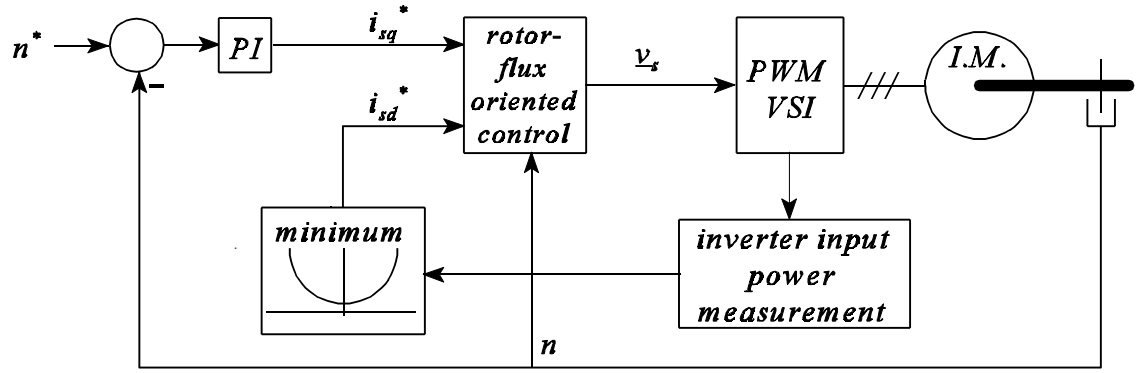

Figure 2.12: *Search control implemented with rotor-flux oriented motor control [80].*

The main advantage of the search control is that it does not depend on motor parameters as other control strategies do, and it finds the true optimal efficiency. On the other hand, the convergence time to reach the optimal efficiency is long (not less than 4 sec.), and there may be continuous disturbances in torque and speed, depending on how the algorithm is designed. The search algorithm may be difficult to tune in order to assure correct convergence under all circumstances. If a power is minimized, it needs extra and accurate sensors, unless the stator current are reconstructed from the dc-link current whereby the dc-link power can be acquired easily.

Kirschen et al. discuss in [79] and [80] the torque disturbance and damping of the drive. They find that near the point of optimal efficiency the disturbances for a given step in flux become larger and less damped, but that it can be compensated for by increasing the gain of the speed controller by simple gain scheduling.

A problem in rotor-flux oriented vector controlled drives, not only with search control but for all energy optimal control strategies, is the drive response when the flux is reduced and the drive meets a sudden large torque demand. When the flux is low, and the stator current is limited to the nominal current rating, the motor can not deliver full torque by just increasing the torque current. If no precautions are made to the drive, it will react by increasing the torque producing current until the current limit is met, but then the field current will not increase, so the drive will not be able to deliver the demanded torque. In [79] it is proposed to put an artificial limit on the torque current until the field has reached its nominal value, and thereafter to increase the torque current. This will only lead to a small decrease of the drive dynamics compared with the drive operating with continuous rated field.

Sul and Park [81] proposed in 1988 a type of search control for a motor driving a pump. It is assumed that the load characteristic is not changing. The load torque vs. speed characteristic is divided into several sections. During the start-up procedure, the motor drive runs through the load curve from zero to nominal speed, and in each section of the load curve it uses a search control algorithm to find energy optimal slip frequencies, and stores them in the memory. Under normal operation the drive is then slip frequency controlled, using the energy optimal slip frequencies as reference values. This results in a simple and fast drive control scheme under normal operation, but the slip frequency references of course have to be retuned if the load characteristic changes.

Moreira et al. [82] presented in 1989 and 1991 [85] search control for a scalar drive. The main invention was that instead of measuring the speed, it was estimated from the stator voltage third harmonic component. Additionally, for systems with essential fixed torque-speed characteristic, they proposed to disregard the speed measurement or estimation, and instead estimate torque and use that as an indication for the motor output power. In both cases they minimized the dc-link power. Parts of the control systems are patented in [86] and [87].

Kim [83] claimed in 1990 a patent on minimisation of the stator current by search control instead of minimisation of input power. But he demonstrates no actions to control the output power or speed, so it is not certain that the described drive will work in practice.

Kioskeridis and Margaris [94] documents in 1996 the advantage of minimizing the stator current instead of input power. The result is almost the same in terms of efficiency, the stator current has a more distinct minimum than the power, and it costs less sensors. Based on calculations they state that this is especially advantageous in larger drives, where the input power minimum is more difficult to detect.

Several authors have implemented search control with small variations in the application. Famouri and Cathey [84] minimized in 1991 inverter input power to a scalar drive by adjusting the rotor slip frequency. Blåbjerg and Pedersen [89] minimized in 1993 the dc-link power by adjusting the V/Hz ratio, see Figure 2.13.

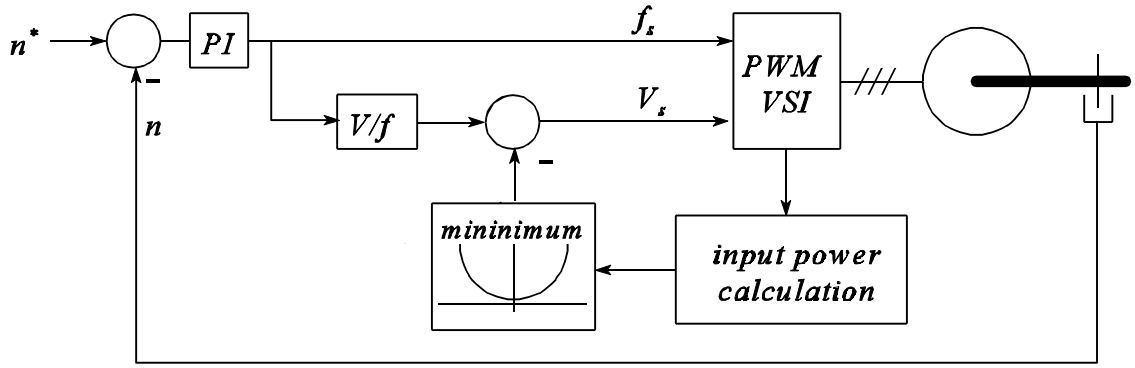

Figure 2.13: *An example of an search efficiency optimization implemented in a scalar drive.*

Cleland et al. [92] proposed in 1995 to implement search control in an open-loop controlled drive where the load characteristic is known. They claim to be able to adjust the speed without knowledge of motor parameters, by increasing the stator frequency each time the stator voltage is decreased. However, they have never proven this experimentally, and it is doubtful that it can work.

2.7.2 Fuzzy Logic and Neural Network Search Control.

The latest investigations in search control have been to use fuzzy logic in the optimization algorithm. Fuzzy control algorithms have an advantage over classical control methods when the system is not very well-known or when it is too complex to model. It therefore applies well for energy optimal search control, where the algorithm is applied without knowledge of the motor system model. In [97] it is stated that the main advantage of using fuzzy control instead of classical search control algorithms is that it makes the algorithm converge faster and that it can better accept inaccurate signals corrupted with noise. The credibility of the last statement is doubtful.

Fuzzy control was first introduced with energy optimal control by Sousa et al. [90] in 1993, and [93] in 1995, where they minimized the dc-link power of a rotor-flux oriented vector controlled drive, see Figure 2.14. They also introduced a q-axis feed-forward path to out-compensate the torque ripple when the field-current is stepped. In these two articles a convergence time of 4 sec. is reported. Fuzzy search control is also described by Cleland et al. [91] in 1995, by Wang and Liaw [96] in 1997, and by Bose [104, pp. 593-597].

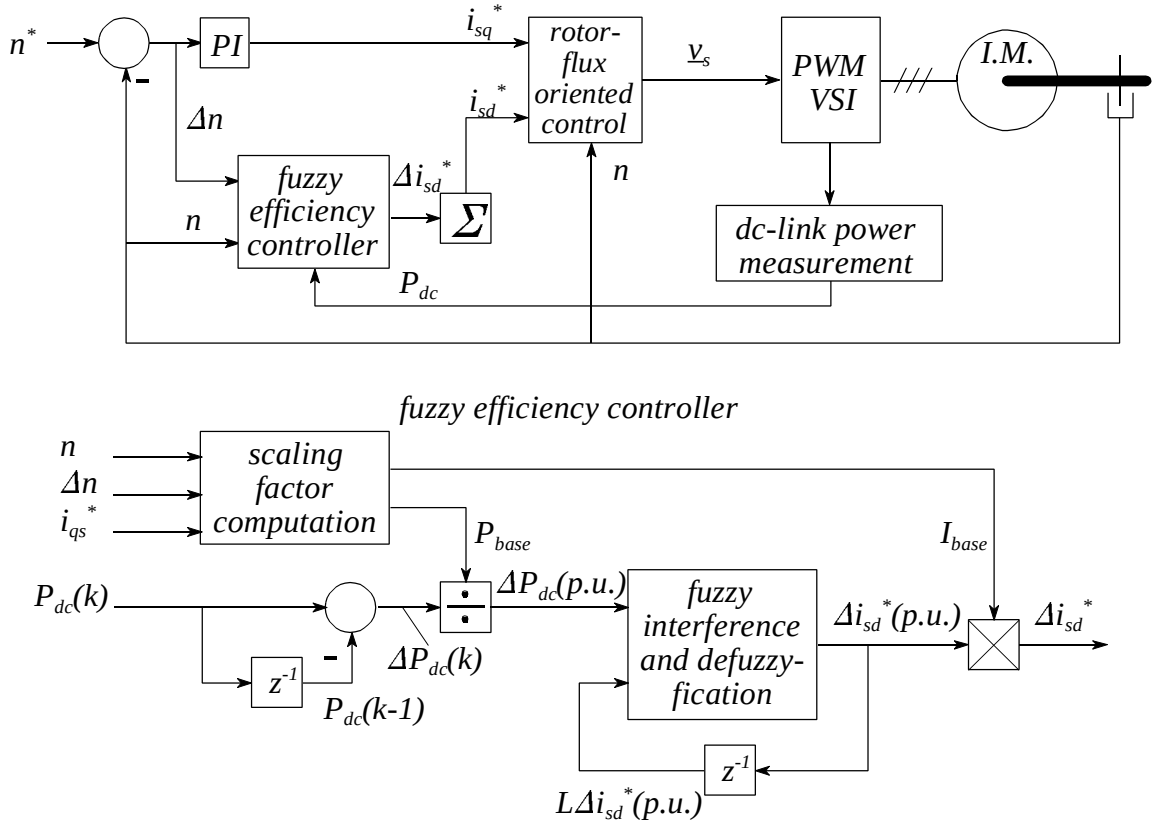

Figure 2.14: *Energy optimal fuzzy control implemented with field-oriented motor control [90].*

Bose et al. [97] introduced in 1997 fuzzy logic search control implemented in a sensorless stator-flux oriented vector control motor drive where they report a convergence time of 10 sec. It is also described by Bose and Patel [100] in 1997. It was the first time that search control was realized in a sensorless drive. They also proposed to reduce the flux following a ramp instead of a step, in order to reduce torque ripple. Furthermore they use the fuzzy logic control scheme to train a neural network that is used for the final implementation.

Also Choy et al. [95] in 1996 and Hasan et al. [101] in 1997 uses a neural network to perform the search control. In both cases they set up a model of the motor drive, and used a conventional search control algorithms to train the neural network in different operating points. Thereafter the search control is done by the neural network alone. This method seems

a bit awkward, because if they first have to set up a model to train the neural network, then they loose the advantage of the search control, which is that it should work without knowledge of the motor drive model. They could, of course, choose to train the neural network experimentally.

Moreno-Eguilaz et al., [98] and [99] both in 1997, carries out a comparison of different search control algorithms. Their conclusion is that fuzzy control offers the best and fastest convergence.

2.8 Summary.

On overview of the losses associated with an adjustable speed drive was initially presented, and it was shortly explained how the drive loss can be reduced by improving the construction and maintenance of converter, motor and transmission. The review of energy optimal control of electrical drives treated the variable voltage fixed frequency (VVFF) drive as well as the PWM-VSI based variable voltage variable frequency (VVVF) drive.

It is documented in literature that the VVFF drive is only able to save energy at very low loads, and that in general it is not well suited for energy optimization of integral horse-power electrical drives. And as is can not vary the speed very much, it is not interesting to use for HVAC applications. The control strategies for the VVVF drive are divided into the three categories listed in Table 2.3.

Table 2.3: Evaluation of induction motor drive energy optimal control methods.

Control Method	Simple State	Model Based	Search
Motor drive specific	yes	yes	no
Parameter sensible	yes	yes	no
Efficiency precision	medium	medium	high
Efficiency convergence	fast	fast	slow (4-10 sec.)
Complexity	simple	medium / complex	medium
Speed measured or identified	slip frequency: yes cos(φ): no	sometimes	yes (not if load torque is known)

The main disadvantage of the simple state control and the model based control is that they require knowledge of the motor parameters. But they are fast, and the simple state control can be very cheap to implement, especially the power factor control which does not require a speed sensor. The main disadvantage with the search control is that it requires a speed sensor and that the convergence time is long, but the advantage is that motor parameters are not required.

After 20-25 years of intensive research in the field of energy optimal control of induction motors, the general impression is that in some areas the research has reached a mature state, and in other areas development of new control strategies are still going on.

With respect to slip frequency control and displacement power factor control, the initial research and patents were concerned with how to implement the control in analog circuitry in a simple way. This is history, so the basic control is very simple to implement now. The only thing that can be discussed with respect to these methods is how to generate the references and possibly how to design the controller dynamics.

Research is still going on with search control, and it is especially important to develop ways of simplifying the design of the algorithm, and to develop algorithms with faster convergence time, for example by using fuzzy-logic control.

Model-based control is the field in which most research is going on. The proposed solutions differ a lot, depending on the drives they are designed for, and on how the losses are modeled. A general weakness with most solutions is that they do not include saturation, so there is still a need for simple methods which include saturation, and possibly also converter losses.

Looking more generally on the publications, it is characteristic that only a few of them compare different control strategies, and when it is done, it is only within one category of control strategies, for example a comparison of search control strategies. Generally the converter loss in not included in the controller design, which may come from the fact that most papers investigate drives of a few kW rated power. The importance of converter losses is barely untouched, as is also an investigation of how the converter losses can be included in the energy optimal control algorithms. Only one paper discusses a medium size drive, and the analysis is then done without experimental verification. A general analysis of stability with regard to energy optimal control has neither been seen in literature. So despite the many years of research in development of energy optimal control algorithms, and the mature state within some areas, there are still aspects of energy optimal control which are poorly covered, and which hopefully, among other things, will be clarified through the work documented in this thesis.

References.

[1] A. M. Trzynadlowski, R. L. Kirlin, S. Legowski, “Space Vector PWM Technique with Minimum Switching Losses and a Variable Pulse Rate”, Proceed. of IECON ‘93, 1993, pp. 689-694.

[2] A. H. Bonnett, “An Update on AC Induction Motor Efficiency”, IEEE Trans. Ind. App., Vol. 30, No. 5, Sep/Oct 1994, pp. 1362-1372.

[3] A. Arkkio, “Rotor-slot design for inverter-fed cage induction motors”, Proceed. of Speedam, Positano (Italy), May 1992, pp. 37-42.

[4] Mekaniske remtræk”, Projekt værktøjskassen, Projektsekretariatet, Lindelunden 65, 6705 Esbjerg Ø, tlf. 75 47 04 88.

[5] S. Nadel, M. Shepard, S. Greenberg, G. Katz, A. T. de Almeida, “Energy-Efficient Motor Systems”, 1992 by American Council for an Energy-Efficient Economy, 1001 Connecticut Avenue, N.W., Suite 801, Washington D.C. 20036, ISBN 0-918249-10-4.

[6] S. Hansen, P. Nielsen, F. Blaabjerg, “Harmonic Cancellation by Mixing Non-linear Single-phase and Three-phase Loads”, Proceed. of IAS '98, St. Louis, USA, October 1998, Vol. 2, pp. 1261-1268.

[7] P. Thøgersen, P. Nielsen, F. Abrahamsen, “Impacts on Energy Savings by Variable Speed Drives from Motor and Converter Technology”, Proceedings of PCIM '99, Nürnberg, Germany, June 1999.

[8] M. P. Kazmierkowski, H. Tunia, “Automatic Control of Converter-Fed Drives”, Elsevier, 1994, ISBN 0-444-98660-X.

[9] DEFU Teknisk Rapport 352, “Elbesparelser gennem forbedret grundlag for projektering af elmotorer, 1995. DEFU, Postbox 259, 2800 Lyngby, tlf. 45 88 14 00.

Variable Voltage Fixed Frequency (VVFF) Drive.

[10] F. J. Nola, “Power Factor Control System for AC Induction Motor”, U.S. Patent 4 052 648, Oct. 4, 1977.

[11] N. Mohan, “Improvement in Energy Efficiency of Induction Motors by Means of Voltage Control”, IEEE Trans. Power App. Syst., Vol. PAS-99, No. 4, July/Aug 1980, pp. 1466-1471.

[12] F. J. Nola, “Power Factor Control System for AC Induction Motors”, U.S. Patent 4 266 177, May 5, 1981.

[13] F. Nola, “Power Factor Controller - An Energy Saver”, Conf. Record IEEE IAS ‘80, pp. 194-198, 1980.

[14] M. Lee, “Power Factor Controller for Induc. Motor”, U.S. Pat. 4271386, Jun. 2, 1981.

[15] M. H. Lee, J. E. Keim, “Power Factor Controller for an Induction Motor using Transistor Switch Means with Variable Breakdown Voltage”, U.S. Patent 4 287 464, Sep. 1, 1981.

[16] E. C. Siemon, “Power Factor Control System for Inverter-driven A-C Induction Motor”, U.S. Patent 4 291 264, Sep. 22, 1981.

[17] R. W. Hedges, “Energy Economizer for Induction Motors”, U.S. Patent 4 297 628, Oct. 27, 1981.

[18] G. D. Opfer, “Power Dissipation Regulating Circuit for Induction Motor by Supply Voltage Control in function of Phase Angle”, U.S. Patent 4 298 834, Nov. 3, 1981.

[19] F. J. Bourbeau, “Load Responsive Control System for Constant Speed Induction Motor”, U.S. Patatent 4 355 274, Oct. 19, 1982.

[20] R. E. Davis, R. J. Becker, R. G. Foster, M. J. Westkamper, E. J. Timothy, R. H. Johnson, “Digital Induction Motor Control System”, U.S. Patent 4 361 792, Nov. 30, 1982.

[21] H. Sugimoto, “Power Control Circuit for Induction Motor”, U.S. Patent 4 379 258, Apr. 5, 1983.

[22] D. Green, S. Goldner, “Power Factor Controller”, U.S. Patent 4 388 578, Jun. 14, 1983.

[23] T. M. Rowan, T. H. Lipo, “A Quantitative Analysis of Induction Motor Performance Improvement by SCR Voltage Control”, IEEE Trans. Ind. App., Vol IA-19, No. 4, Jul/Aug 1983, pp. 545-553.

[24] R. W. Hedges, “Motor Protecting Improved Energy Economizer for Induction Motors”, U.S. Patent 4 414 499, Nov. 8, 1983.

[25] F. J. Nola, “Three Phase Power Factor Controller”, U.S. Patent 4 433 276, Feb. 21, 1984.

[26] F. J. Nola, “Motor Power Control Circuit for A.C. Induction Motors”, U.S. Patent 4 439 718, Mar. 27, 1984.

[27] R. J. Spann, “Power Factor Motor Controller”, U.S. Patent 4 454 462, Jun. 12, 1984.

[28] N. G. Muskovac, “Motor Slip Controller for AC Motors”, U.S. Patent 4 482 852, Nov. 13, 1984.

[29] F. J. Nola, “Solar Powered Actuator with Continously Variable Auxiliary Power Control”, U.S. Patent 4 489 243, Dec. 18, 1984.

[30] R. W. Hedges, “Energy Economizer Controlled-Current Start and Protection for Induction Motors”, U.S. Patent 4 636 702, Jan. 13, 1987.

[31] F. R. Rohatyn, “Energy Saving System for Larger Three Phase Induction Motors”, U.S. Patent 4 723 104, Feb. 2, 1988.

[32] P. J. Unsworth, “Controller for Induction Motors”, U.S. Patent 4 767 975, Aug. 30, 1988.

[33] P. J. Unsworth, “Apparatus and Method for Controlling Induction Motors”, U.S. Patent 4 800 326, Jan. 24, 1989.

[34] R. E. Davis, Jr. et al., “Induction Motor Control System”, U.S. Patent 4 950 970, Aug. 21, 1990.

[35] F. Blåbjerg, J. K. Pedersen, Søren Rise, H-H. Hansen, “A Comparative Study of Energy Saving Benefits in Softstarters for Three-phase Induction Motors”, Proceed. of IAS annual meeting, Vol. 1, 1995, pp. 367-374.

cos(φ) Control.

[36] S. A. Rosenberg, S. B. Dewan, G. R. Slemon, “Inverter Fed Induction Motor Drive Using Power Factor Control”, Journal of the 1976 annual meeting of the IEEE society, 1976.

[37] K. L. Earle, “Variable Speed Induction Motor Control System”, U.S. Patent, Feb. 3, 1981.

[38] K. Sakai, Y. Matsuda, M. Honbu, “Control System for Induction Motor using Inverter for AC Power Supply”, European Patent EP 0 053 916 A1, 16.06.82.

[39] W. P. Curtiss, G. P. Sharp, “Variable Speed Induction Motor Drive”, European Patent EP 0 065 245 A1, 24.11.82.

[40] T. W. Jian, N. L. Schmitz, D. W. Novotny, “Characteristic Induction Motor Slip Values for Variable Voltage Part Load Performance Optimization”, IEEE Trans. Pow. App. and Syst., Vol. PAS-102, No. 1, Jan 1983, pp.38-46.

[41] M. H. Park, S. K. Sul, D. Y. Yoon, T. W. Chun, “Optimal Efficiency Drive of Induction Motors with Current Source Inverter”, Proceed. 1983 International Power Electronics Conference IPEC, Tokyo, 1983, pp. 450-461.

[42] M. H. Park, S. K. Sul, “Microprocessor-Based Optimal-Efficiency Drive of an Induction Motor”, IEEE Trans. Ind. Elec., Vol. IE-31, No. 1, Feb 1984, pp. 69-73.

[43] H. G. Kim, S. K. Sul, M. H. Park, “Optimal Efficiency Drive of a Current Source Inverter Fed Induction Motor by Flux Control”, IEEE Trans. on Ind. Appl., Vol. IA-20, No. 6, Nov/Dec 1984, pp. 1453-1459.

[44] W. P. Curtiss, G. P. Sharp, “Self Generative PWM Voltage Source Inverter Induction Motor Drive”, U.S. Patent 4 469 997, Sep. 4, 1984.

[45] H. Tomita, “An Optimal Efficiency Control for Energy Saving of AC Motor by Thyristor Voltage Controller”, IEEE Proceed. of IECON’88, 1988, pp. 816-819.

[46] H. Tomita, S. Zheng, T. Haneyoshi, O. Miyashita, A. Maeda, T. Denki, “Optimal Efficiency Control for Energy Saving of Variable Speed AC Motor”, Proceed. of EPE’89, Achen 1989, pp. 819-822.

[47] T. Mukai, A. Yoshino, “Induction Motor Control System”, European Patent EP 0 330 477 A2, 30.08.89.

[48] T. Mukai, A. Yoshino, “Induction Motor Control System”, U.S. Patent 5 010 287, Apr. 23, 1991.

[49] T. Hatanaka, N. Kuwahara, “Energy-saving control apparatus and control method for induction motor”, European Patent EP 0 556 013 A1, 09.02.93.

[50] N. Kuwahara, T. Hatanaka, “Inudction Motor Control Apparatus”, U.S. Patent 5 204 606, Apr. 20, 1993.

[51] T. Hatanaka, N. Kuwahara, “Method and Apparatus for Controlling the Supply of Power to an Induction Motor to Maintain High Efficiency Under Varying Load

Condition", U.S. Patent 5 241 256, Aug. 31, 1993.

[52] Hatanaka et al., "Induction Motor Control Apparatus Providing High Efficiency with Rapid Response to Changes in Load Torque", U.S. Patent 5 442 271, Aug. 15, 1995.

[53] T. Hatanaka, "Supermizer - Energy Saving System for 3-phase AC Induction Motors", IEEE Proceed. of Power Electronics and Drive Systems PEDS 95, Vol. 1, Feb. 1995, pp. 110-116.

[54] T. Hatanaka, N. Kuwahara, "High-Efficiency Power Supply Control Apparatus for Variable-speed Induction Motor", U.S. Patent 5 500 581, Mar. 19, 1996.

[55] H. R. Andersen, J. K. Pedersen, "Low Cost Energy Optimized Control Strategy for a Variable Speed Three Phase Induction Motor", Record of PESC96, Vol. 1, 1996, pp. 920-924.

Model-Based Control.

[56] D. Galler, "Energy Efficient Control of AC Induction Motor Vehicles", Conf. Record of the IEEE Ind. Appl. Soc. Annual Meeting 1980, Sep. 1980, pp. 301-308.

[57] W. E. Stanton, D. B. Eisenhaure, R. D. Drescher, "Optimum Efficiency Control System", U.S: Patent 4 392 100, Jul. 5, 1983.

[58] A. Kusko, D. Galler, "Control Means for Minimization of Losses in AC and DC Motor Drives", IEEE Trans. Ind. App., Vol. IA-19, No. 4, Jul/Aug 1983, pp. 561-570.

[59] B. K. Bose, "Microprocessor-based Efficiency Optimization Control for an Induction Motor System", U.S. Patent 4 450 398, May. 22, 1984.

[60] I. Takahashi, T. Noguchi, "A New Quick Response and High Efficiency Control Strategy of an Induction Motor", IEEE IAS Annual Meeting 1985, pp. 496-502.

[61] S. M. Islam, C. B. Somuah, "An Efficient High Performance Voltage Decoupled Induction Motor Drive with Excitation Control", IEEE Trans. on Energy Conv., Vol. 4, No. 1, Mar 1989, pp. 09-117.

[62] R. D. Lorenz, S.-M. Yang, "Efficiency-Optimized Flux Trajectories for Closed-Cycle Operation of Field-Orientation Induction Machines Drives", IEEE Trans. Ind. Appl., Vol. 28, No. 3, May/Jun. 1992, pp. 574-580.

[63] J. K. Pedersen, F. Blåbjerg, “An Electrical Car Drive System Using an Energy-Optimized Control Strategy Based on an AC-machine and a Microcontroller”, Proceed. of the 11th International Electrical Vehicle Symposium, 1992, pp. 12.03.1-12.03.13.

[64] J. Fetz, K. Obayashi, “High Efficiency Induction Motor Drive with Good Dynamic Performance for Electric Vehicles”, Proceed. of PESC ‘93, 1993, pp. 921-927.

[65] G. O. Garcia, J.C. Mendes Luís, R. M. Stephan, E. H. Watanabe, “An Efficient Controller for an Adjustable Speed Induction Motor Drive”, IEEE Ind. Elec., Vol. 41, No. 5, Oct 1994, pp. 533-539.

[66] T. Yamakawa, “Device and Method for Controlling Motor”, European Patent 0 688 094 A1, 09.12.94.

[67] E. Mendes, A. Baba, A. Razek, “Losses Minimization of a Field Oriented Controlled Induction Machine”, Proceed. of IEE Electrical Machines and Drives Conf., Sep. 1995, pp. 310-314.

[68] P. Thøgersen, M. Tønnes, U. Jæger, S. E. Nielsen, “New High Performance Vector Controlled AC-Drive with Automatic Energy Optimizer”, Proceed. of EPE ‘95, Vol. 3, 1995, pp. 381-386.

[69] T. Ashikaga, M. Mori, K. Nagayama, T. Kobayashi, T. Kubo, “High Efficiency Induction Motor Control Method for Electric Vehicle”, Proceed. of IPEC-Yokohama ‘95, 1995, pp. 113-118.

[70] V. Burtea, C. Ghita, “Adaptive Control of Induction Motors with Optimal Efficiency”, Proceed. of Stockholm Power Tech Conf., 1995, pp. 7-12.

[71] N. Satou, “Control Device for Induction Motor”, U.S. Patent 5 426 357, Jun. 20, 1995.

[72] I. Kioskeridis, N. Margaris, “Loss Minimization Induction Motor Adjustable-Speed Drives”, IEEE Trans. Ind. Elec., Vol. 43, No. 1, Feb. 1996, pp. 226-231.

[73] A. Baba, E. Mendes, A. Razek, “Losses Minimisation of a Field-Oriented Controlled Induction Machine by Flux Optimisation Accounting for Magnetic Saturation”, 1997 IEEE International Electric Machines and Drives Conference Record, IEMDC’97, May 1997, pp. MD1 2.1-2.3.

[74] K. Jezernik, D. Drevensek, J. Korelic, “Robust VSS IM control for EVs”, Proceed. of PEDS’97, Vol. 2, 1997, pp. 804 -809.

[75] K. S. Rasmussen, P. Thøgersen, “Model Based Energy Optimizer for Vector Controlled Induction Motor Drives”, Proceed. of EPE’97, Trondheim, pp. 3.711-3.716.

[76] K. Matsuse, T. Yoshizumi, S. Katsuta, “High-Response Flux Control of Direct-Field-Oriented Induction Motor with High Efficiency Taking Core Loss into Account”, IAS annual Record, New Orleans, Oct. 1997, pp. 410-417.

[77] J. H. Chang, B. K. Kim, “Minimum-Time Minimum-Loss Speed Control of Induction Motors Under Field-Oriented Control”, IEEE Trans. Ind. Elec., Vol. 44, No. 6, Dec. 1997, pp. 809-815.

Search Control.

[78] S. Geppert, “PWM Inverter Control and the Application thereof within Electric Vehicles”, U.S. Patent 4 316 132, Feb. 16, 1982.

[79] D. S. Kirschen, D. W. Novotny, T. A. Lipo, “On-Line Efficiency Optimization of a Variable Frequency Induction Motor Drive,” IEEE Trans. Ind. App., Vol. IA-21, No. 4, May/Jun 1985, pp. 610-616.

[80] D. S. Kirschen, D. W. Novotny, T. A. Lipo, “Optimal Efficiency Control of an Induction Motor Drive”, IEEE Trans. Energy Conv., Vol. EC-2, No. 1, Mar 1987, pp. 70-76.

[81] S. K. Sul, M. H. Park, “A Novel Technique for Optimal Efficiency Control of a Current-Source Inverter-Fed Induction Motor”, IEEE Trans. Power Elec., Vol. 3, No. 2, April 1988, pp. 192-199.

[82] J.C. Moreira, V. Blasko, T. A. Lipo, “Low Cost Efficiency Maximizer for an Induction Motor Drive”, IEEE Proceed. of IAS ‘89, 1989, pp. 426-431.

[83] J.-S. Kim, “Circuit and Method for Power Efficiency Improvement of Induction Motors”, U.S. Patent 4 954 764, Sep. 4, 1990.

[84] P. Famouri, J. J. Cathey, “Loss Minimization of an Induction Motor Drive”, IEEE Trans. Ind. App., Vol. 27, No. 1, Jan/Feb 1991, pp. 32-37.

[85] J. C. Moreira, T. A. Lipo, V. , “Simple Efficiency Maximizer for an Adjustable Frequency Induction Motor Drive”, IEEE Trans. on Ind. App., Vol. 27, No. 5, Sep/Oct 1991, pp. 940-946.

[86] Wisconsin Alumni Research Foundation, T. A. Lipo, J. C. Moreira, “Air gap flux measurement using stator third harmonic Voltage and uses”, Patent No. 5 272 429, Dec. 21 1993.

[87] Wisconsin Alumni Research Foundation, R. D. Lorenz, K. T. Hung, T. A. Lipo, J. C. Moreira, “Motor torque control method and apparatus” Patent No. 5 334 923, Aug. 2 1994.

[88] S. Chen, S.-N. Yeh, “Efficiency Control of Field Oriented Operation Based on the Open-Loop VVVF Drivers”, IEEE Proceed. of IAS’91, 1991, pp. 58-64.

[89] F. Blåbjerg, J. K. Pedersen, “An Integrated High Power Factor Three -phase AC-DC-AC Converter for AC-machines Implemented in one Microcontroller”, Proceed. of PESC ‘93, 1993, pp. 285-292.

[90] G. C. D. Sousa, B. K. Bose, J. G. Cleland, “Fuzzy Logic Based On-line Efficiency Optimization Control of an Indirect Vector Controlled Induction Motor Drive”, Proceed. of IECON, Vol. 2, Nov. 1993, pp. 1168-1174.

[91] J. G. Cleland, V. E. McCormick, M. W. Turner, “A Fuzzy Logic-Based Energy Optimizer for AC Motors”, Proceed. of FUZZ-IEEE ‘95, Yokohama, March 1995, pp. 1777-1784.

[92] J. G. Cleland, V. E. McCormick, M. W. Turner, “Design of an Efficiency Optimization Controller for Inverter-fed AC Induction Motors”, Proceed. of Ind. App. Society, 1995, pp. 16-21.

[93] G. C. D. Sousa, B. K. Bose, J. G. Cleland, “Fuzzy Logic Based On-Line Efficiency Optimization Control of an Indirect Vector-Controlled Induction Motor Drive”, IEEE Trans. Ind. Elec., Vol. 42, No. 2, Apr 1995, pp. 192-198.

[94] I. Kioskeridis, N. Margaris, “Loss Minimization in Scalar-Controlled Induction Motor Drives with Search Controllers”, IEEE Trans. Power Elect., Vol. 11, No. 2, March 1996, pp. 213-220.

[95] I. Choy, S. H. Kwon, J. Y. Choi, J. W. Kim, K. B. Kim, "On-Line Efficiency Optimization Control of a Slip Angular Frequency Controlled Induction Motor Drive Using Neural Netword", Proceed. of IECON'96, pp. 1216-1221.

[96] J. B. Wang, C. M. Liaw, "Indirect Field-Oriented Induction Motor Drive with Fuzzy Detuning Correction and Efficiency Optimisation Controls", IEE Proc.-Electr. Power Appl., Vol. 144, No. 1, Jan. 1997, pp. 37-45.

[97] B. K. Bose, N. R. Patel, K. Rajashekara, "A Neuro-Fuzzy-Based On-Line Efficiency Optimization Control of a Stator Flux-Oriented Direct Vector-Controlled Induction Motor Drive", IEEE Trans. on Ind. Elec., Vol. 44, No. 2, Arp 1997, pp. 270-273.

[98] J. Moreno-Eguílaz, M. Cipolla, J. Peracaula, "Induction Motor Optimum Flux Search Algorithms with Transient State Loss Minimization using a Fuzzy Logic based Supervisor", Proceed. of PESC'97, pp. 1302-1308.

[99] J. Moreno-Eguílaz, M. Cipolla, J. Peracaula, "Induction Motor Drives Energy Optimization in Steady State and Transient States: A New Approach", Proceed. of EPE'97, Trondheim, 1997, pp. 3.705-3.710.

[100] B. K. Bose, N. R. Patel, "A Sensorless Stator Flux Oriented Vector Controlled Induction Motor Drive with Neuro-Fuzzy Based Performance Enhancement", IAS annual Record, New Orleans, Oct. 1997, pp. 393-400.

[101] K. M. Hasan, L. Zhang, B. Singh, "Neural Network Control of Motor Drives for Energy Efficiency and High Dynamic Performance", Proceed. Of IECON '97, New Orleans, Nov. 1997, pp. 488-492.

[102] F. Blaabjerg, J. K. Pedersen, U. Jaeger, P. Thoegersen, "Single Current Sensor Technique in the DC Link of Three-Phase PWM-VSI Inverters: A Review and a Novel Solution", IEEE Trans. Ind. Appl., Vol. 33, No. 5, Sep./Oct. 1997, pp. 1241-1253.

[103] D. W. Novotny, T. A. Lipo, "Vector Control and Dynamics of AC Drives", Oxford Science Publications, 1996, ISBN 0-19-856439-2.

[104] B. K. Bose, "Power Electronics and Variable Frequency Drives", IEEE Press, 1997, ISBN 0-7803-1084-5.

Chapter 3

Loss Models for Motor and Converter

In this chapter the individual loss components in the drive are described. The motor losses are separated into fundamental losses and harmonic losses, since the ways the two loss types are described are very different from each other. The importance of each of the two parts with respect to energy optimal control is evaluated. It is shown how the converter losses can be calculated for use in the analysis of energy optimal control. At last an approximated and simplified converter loss model is presented for use in real-time model-based energy optimal control calculations.

3.1 Fundamental Frequency Induction Motor Losses.

The losses which appear at fundamental frequency are stator and rotor copper losses, core losses (eddy current and hysteresis), stray load losses and mechanical losses (friction and windage). For a main connected motor the stray load losses are normally set to around 1 % of rated power at nominal load, but the number may vary at least between 0.5 % and 1.5 % depending on the motor. It is more uncertain how the stray load losses depend on load and flux level, and due to lack of generally accepted conventions of representing these losses, it is chosen to include them in the stator copper loss. The verification in Appendix B shows satisfactory results. The electrical losses are represented in the model shown on Figure 3.1 by the stator, rotor and core resistances.

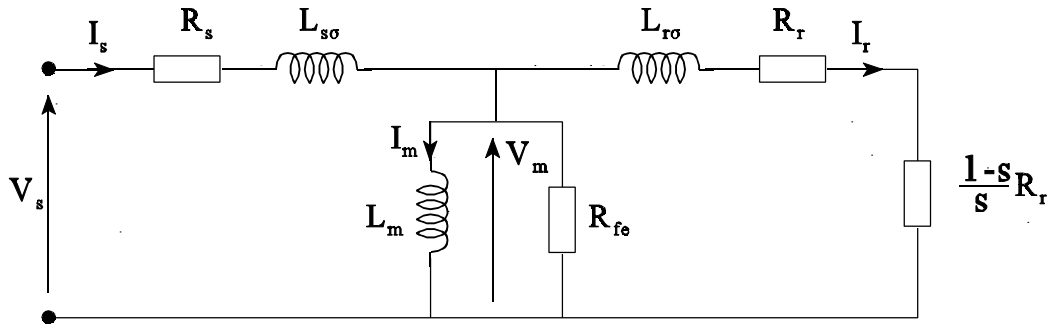

Figure 3.1: *A single phase stationary equivalent diagram for an induction motor.*

3.1.1 Stator Copper Loss.

The stator copper loss is calculated by:

$$P_{Cu,s} = 3 R_s I_s^2 \qquad (3.1)$$

where $P_{Cu,s}$: stator copper loss.
R_s : stator resistance.
I_s : stator current.

Skin effect is not taken into account in the stator. The resistance is compensated for the temperature drift of the winding by

$$R_s = R_{s0} \, (1 + \alpha_{Cu}(T - T_0)) \qquad (3.2)$$

where R_{s0} : stator resistance at temperature T_0.
α_{Cu} : temperature coefficient for copper.

3.1.2 Rotor Copper Loss.

The rotor copper loss is calculated by:

$$P_{Cu,r} = 3 R_r I_r^2 \qquad (3.3)$$

where $P_{Cu,r}$: rotor copper loss.
R_r : rotor resistance.
I_r : rotor current.

The resistance is compensated for the temperature drift of the winding by

$$R_r = R_{r0} \, (1 + \alpha_{Al}(T - T_0)) \qquad (3.4)$$

where R_{r0} : rotor resistance at temperature T_0.
α_{Al} : temperature coefficient for aluminum.

Aluminum is the most common rotor bar material in small motors, but copper may also be used. The rotor resistance is measured with a locked-rotor test at 10 Hz to account for the skin effect.

3.1.3 Core Losses.

The most common way of modeling the core losses in case of sinusoidal flux distribution is to use the following Steinmetz expressions of hysteresis and eddy current losses.

$$P_e = k_e \, \psi^2 \, f^2 \quad [W] \qquad (3.5)$$

$$P_h = k_h \, \psi^v \, f \quad [W] \qquad (3.6)$$

where P_h : hysteresis loss.
P_e : eddy current loss.
ν : coefficient that depends on the magnetic material.
k_h : hysteresis coefficient given by material and design of motor.
k_e : eddy current coefficient given by material and design of motor.
ψ : flux linkage.
f : fundamental frequency.

The total stator core loss is

$$P_{core,s} = k_{h,s}\ \psi_m^{\nu}\ f_s\ +\ k_{e,s}\ \psi_m^2\ f_s^2 \qquad (3.7)$$

where $P_{core,s}$: stator core loss.
ψ_m : air-gap flux.
f_s : stator frequency.

The total rotor core loss is calculated by using the stator core loss expression (3.7) but with slip frequency instead of stator frequency and by scaling with the ratio of the masses of rotor and stator core material.

$$P_{core,r} = \frac{m_r}{m_s}\left(k_{h,s}\ \psi_m^{\nu}\ s f_s\ +\ k_{e,s}\ \psi_m^2\ (s f_s)^2 \right) \qquad (3.8)$$

where $P_{core,r}$: rotor core loss.
s : slip
m_s : mass of the stator core
m_r : the mass of the rotor core.

The total fundamental core loss is

$$P_{core} = P_{core,s} + P_{core,r} = \left(1 + s\frac{m_r}{m_s} \right) k_{h,s}\ \psi_m^{\nu}\ f_s\ +\ \left(1 + s^2\frac{m_r}{m_s} \right) k_{e,s}\ \psi_m^2\ f_s^2 \qquad (3.9)$$

The equivalent per phase core loss resistance is

$$R_{fe} = \frac{3V_m^2}{P_{core}} = \frac{3(2\pi)^2 \psi_m^2\ f_s^2}{P_{core}(\psi_m, f_s, s)} \qquad (3.10)$$

where R_{fe} : parallel equivalent core loss resistance.

Equation (3.10) shows that the core loss resistance depends on air-gap flux, stator frequency and slip.

3.1.4 Mechanical Loss.

The friction and ventilation torques are given by

$$\tau_{fric} = \tau_{dry} + B\left(\frac{\pi}{30}\right) n \ , \quad \tau_{vent} = k_{vent}\left(\frac{\pi}{30}\right)^2 n^2 \qquad (3.11)$$

where τ_{fric} : friction torque.
τ_{dry} : dry friction torque.
B : viscous constant.
n : mechanical speed.
τ_{vent} : ventilator torque.
k_{vent} : ventilator constant.

The mechanical loss is

$$P_{mech} = \tau_{dry}\left(\frac{\pi}{30}\right) n + B\left(\frac{\pi}{30}\right)^2 n^2 + k_{vent}\left(\frac{\pi}{30}\right)^3 n^3 \qquad (3.12)$$

where P_{mech} : mechanical loss (friction + ventilation loss).

3.2 Harmonic Induction Motor Losses.

The aim of treating the harmonic motor losses here is not to give a profound and detailed description of them, that is a task far too complicated with this little space. It is here just interesting to know whether or not the harmonic losses should be taken into account in the energy optimal control algorithms.

First it is shown briefly how the individual harmonic loss components depend on harmonic frequency. This survey is based on the investigation of harmonic losses in [1]. Figure 3.2 illustrates the frequency dependence. The result is only qualitative, that is, it shows whether the individual losses increase or decrease with frequency. For a constant harmonic voltage, the harmonic current is only determined by the stray inductance, and the copper loss dependence of frequency is determined by how the stray inductance and the resistances depend on frequency. The figure shows that the copper losses almost only decrease for increasing frequency. The core loss decreases at low frequency, but the development at high frequencies is uncertain. The conclusion should be clear, however, that the total harmonic motor loss is decreasing for increasing harmonic frequency.

On the first axis of Figure 3.2 are indicated frequency numbers. These are only very approximate and they also depend on motor size, as for example skin effect starts at lower frequency in large motors than in small motors.

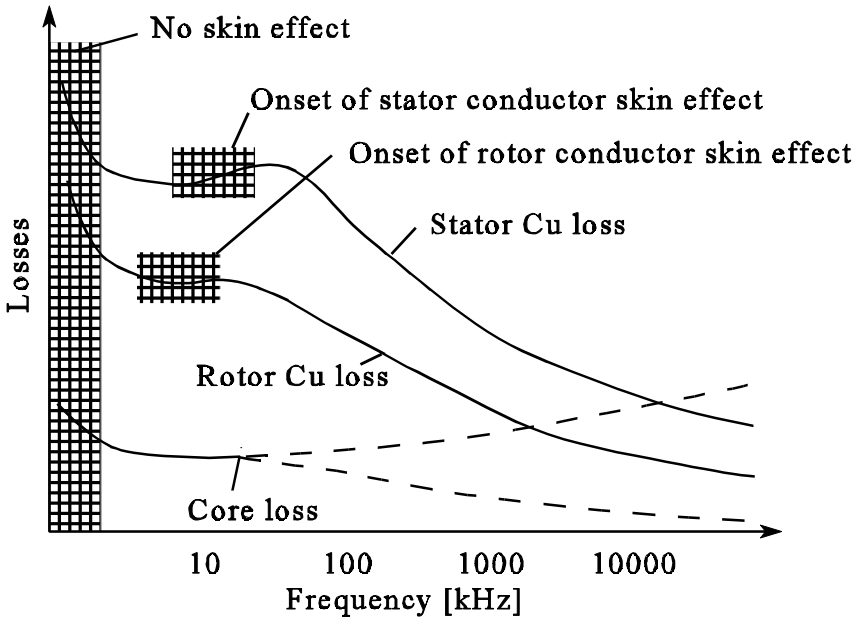

Figure 3.2: *Illustration of harmonic motor loss frequency dependence with constant harmonic stator voltage [2]. The first axis frequencies are very approximate and motor dependent. The high frequency core loss is not known exactly.*

A second stage would be to quantify the losses theoretically, but that is very difficult, and it seems like a lot research work still has to be done before the harmonic losses can be predicted theoretically with decent accuracy.

The harmonic losses are here determined by experiments on standard and high-efficiency 2.2 kW induction motors controlled by space-vector modulation with centered pulses. The total harmonic motor loss has been measured for different switching frequencies with a six-phase Norma Power Analyzer D6100 taken as the difference between the total motor input power and the fundamental motor input power. With this subtraction of two large numbers giving a small result, it is evident that the accuracy is limited. The measurements are shown on Figure 3.3 and Figure 3.4.

Figure 3.2 can not be compared directly with Figure 3.3, because Figure 3.2 shows losses for a single frequency and Figure 3.3 shows the loss for a whole spectrum of harmonic frequencies with different voltage amplitudes, but of course with the switching frequency as the dominating. The measurements show that the harmonic motor loss initially decreases and after 3-5 kHz switching frequency stays rather constant.

One conclusion which can be drawn from the experiment is that for a given motor drive there exist a switching frequency where the total harmonic loss of converter and motor has a minimum. For the tested 2.2 kW standard motor drive the minimum was found around 3-4 kHz, and this frequency should be chosen if energy efficiency was the only criterion. Similar measurements on a 2.2 kW high-efficiency motor, Figure 3.4, show the same frequency dependence, the losses are just smaller.

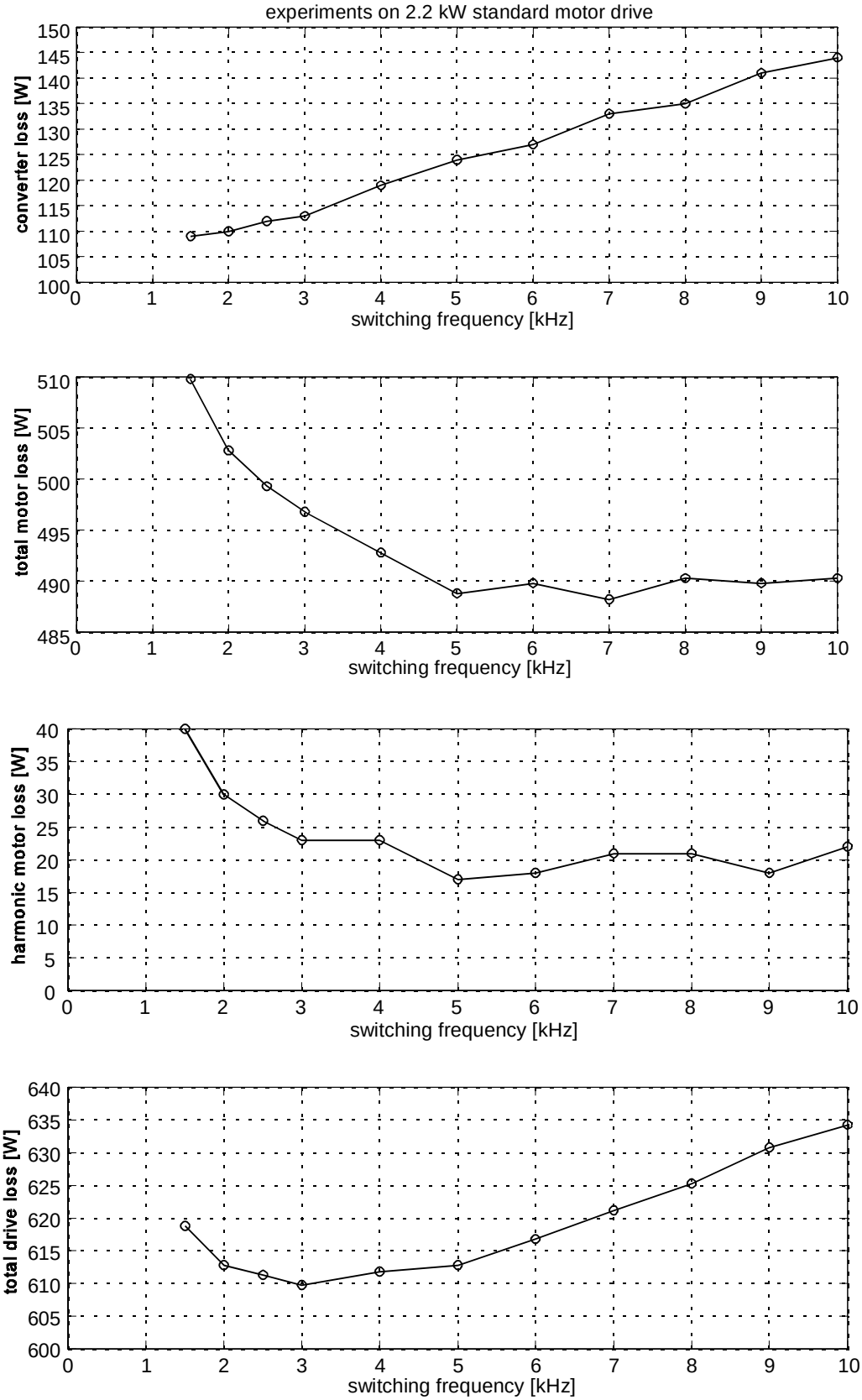

Figure 3.3: *Measured harmonic losses as function of switching frequency for a 2.2 kW standard induction motor drive.*

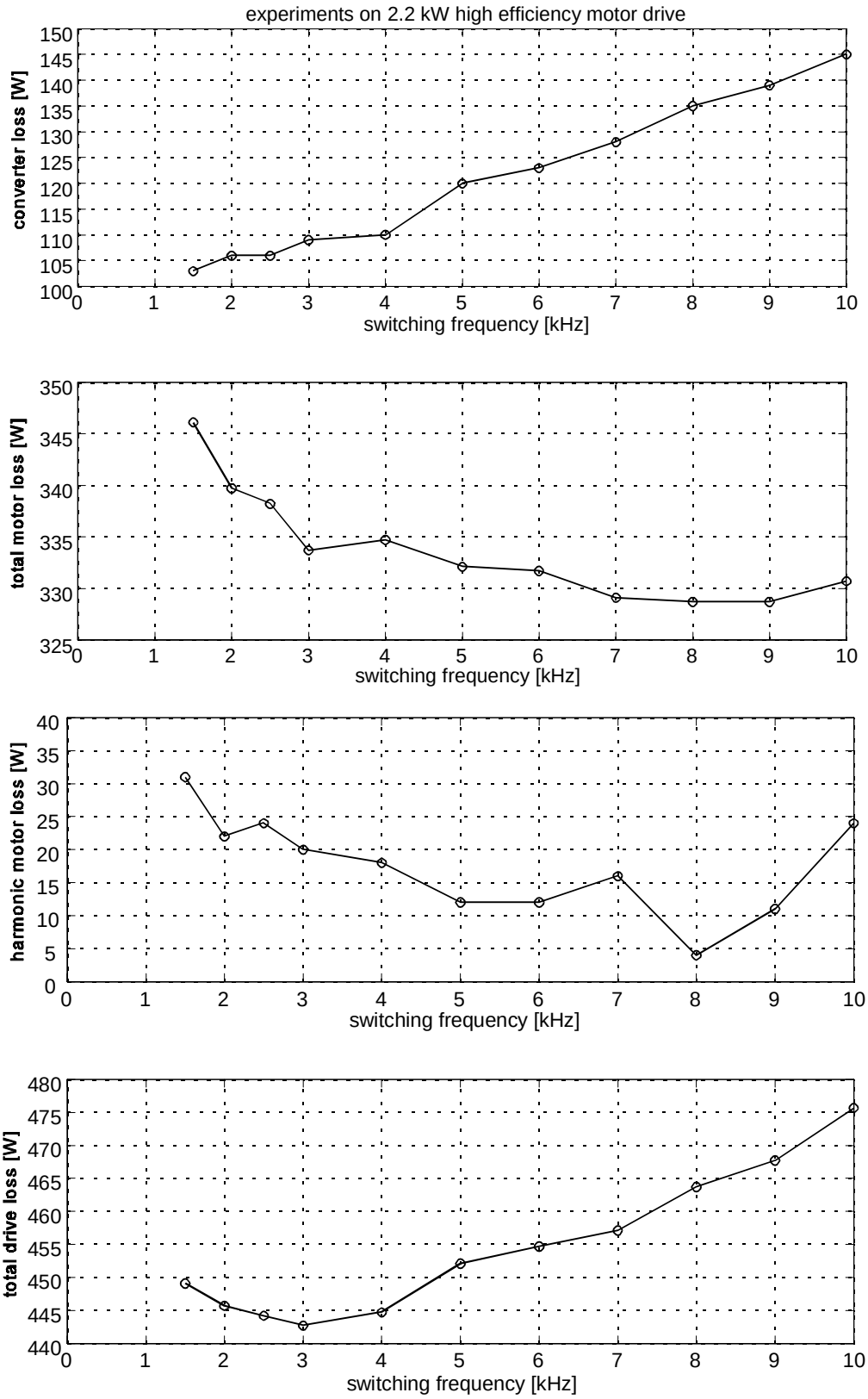

Figure 3.4: *Measured harmonic losses as function of switching frequency for a 2.2 kW high-efficiency induction motor drive.*

It is interesting to know whether the harmonic motor losses are influenced by the flux level in the motor in a way that they are obligatory to include in the energy optimal control algorithms. This question has been investigated experimentally by measurement of harmonic loss on a 2.2 kW standard induction motor. The measurement are those presented in chapter 4, namely when the motor is operating at different speeds and load torques, with constant air-gap flux and with optimized efficiency. The results on Figure 3.5 reflect the fact that it is very difficult to measure the losses precisely, which makes a conclusion unclear. It seems, however, that the losses are smaller with reduced flux than with constant air-gap flux. But the reduction is so small compared with the total loss, and so unpredictable, that it is chosen here not to include the harmonic motor losses in the energy optimal control algorithms.

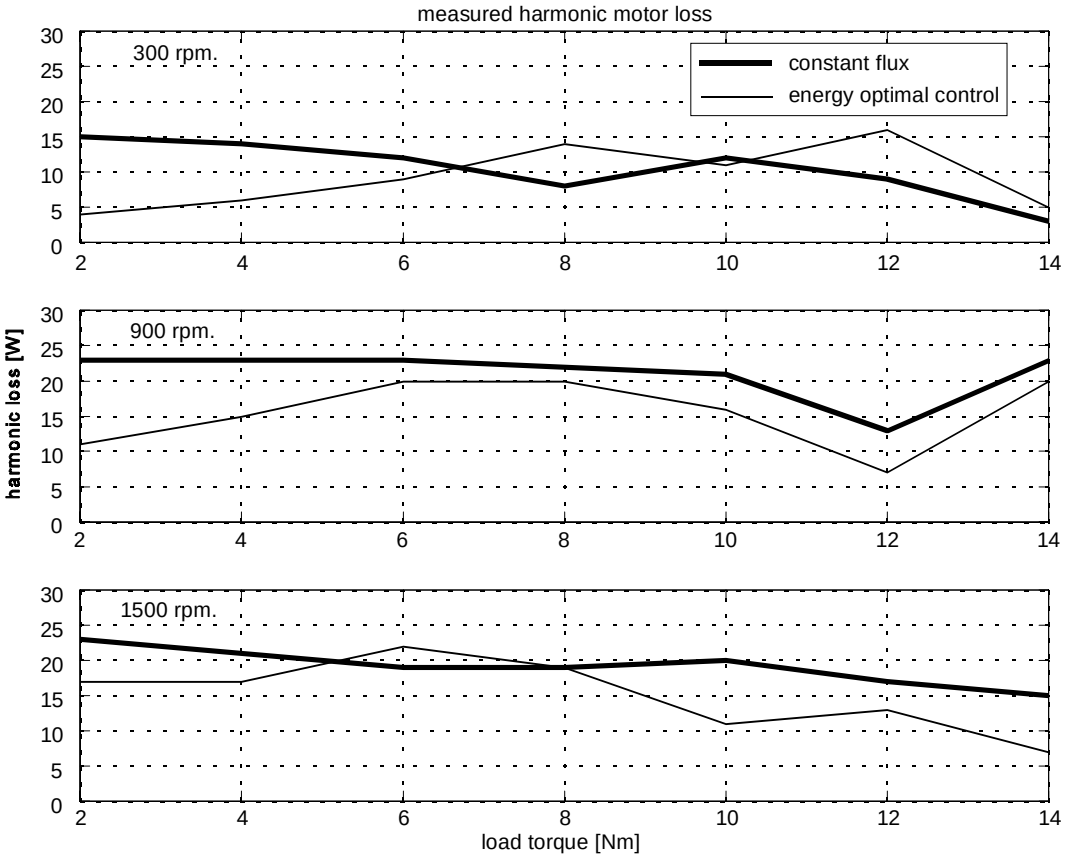

Figure 3.5: *Measured harmonic motor loss for a standard 2.2 kW induction motor operating with constant air-gap flux and with optimized efficiency.*

The conclusion with regard to harmonic drive losses is that they can be minimized by choosing the proper switching frequency and modulation strategy. These issues will not be further discussed in this thesis. A clear relation between harmonic motor loss and flux level has not been found, so the harmonic motor losses will not be included in the energy optimal control algorithms.

3.3 Converter Loss.

Two converter loss models are developed in this section. One which is used in the analysis of the motor drive in chapter 4, and one which is implemented in the drive to do real-time calculations of the converter loss. The second model is a simplified and approximate version of the first. The models apply to the converter topology on Figure 3.6, where the inverter is snubber-less.

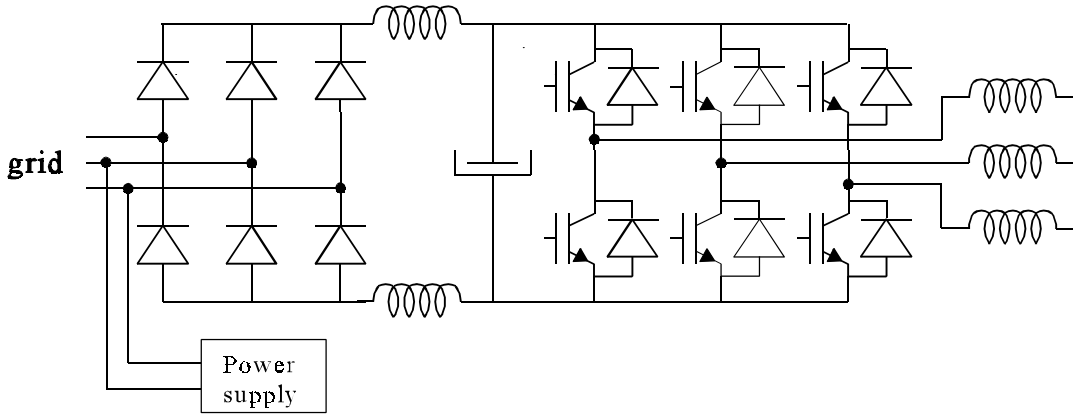

Figure 3.6: *Converter topology for which the loss models are developed.*

The following losses are considered:

- Rectifier conduction loss.
- Power supply.
- dc-link choke conduction loss.
- Conduction and switching losses in the inverter transistor and diodes.
- Output choke conduction loss.

The losses in the dc-link capacitor and in the iron-cores of the dc-link and output chokes are disregarded.

3.3.1 Rectifier Conduction Loss.

It is assumed that the rectifier diode voltage drop is constant. The loss of the three phase diode rectifier is calculated knowing that two diodes are conducting at a time:

$$P_{loss,rect} = 2 \cdot V_D \cdot I_{dc} = 2 \cdot V_D \frac{P_{rect,out}}{V_{dc}} \qquad (3.13)$$

where V_D : diode forward voltage.
$P_{rect,out}$: diode rectifier output power.
V_{dc} : dc-link voltage.

3.3.2 Electronics Power Supply.

The supply is modeled as a constant load. The load size is determined as the power input to the converter when the inverter is switching, but without a motor connected to the output terminals. The power consumption of the micro-controller, DSP and sensors is not included.

3.3.3 Choke Conduction Losses.

The conduction losses in the dc-link chokes are calculated as:

$$P_{loss,dc-choke} = R_{dc-choke}\left(\frac{P_{inv,in}}{v_{dc}}\right)^2 \qquad (3.14)$$

where $R_{dc\text{-}choke}$: total dc-resistance in the dc-link chokes.
$P_{inv,in}$: rectifier output power.
v_{dc} : dc-link voltage.

In equation (3.14) it is assumed that the output current of the rectifier is a pure dc current. Actually the current is a pulsating dc-current, so (3.14) is only approximate, but the small error is neglected. Also the core losses induced in the choke cores by the pulsations are ignored. In the real-time model the measured dc-link voltage is used. In the theoretical analysis a fixed dc-link voltage of 565 V is used. This is a simplification because the dc-link voltage varies with the load.

The conduction losses in each of the three output chokes are calculated as:

$$P_{loss,out-choke} = R_{out-choke}\, I_s^2 \qquad (3.15)$$

where $R_{out\text{-}choke}$: dc-resistance of output choke.
I_s : stator current.

Also here the core losses of the output chokes are ignored.

3.3.4 Inverter Loss.

Inverter Conduction Loss.

Figure 3.7 shows typical on-state voltages for diodes and transistors of an inverter. The diode respectively the transistor on-state voltages are modeled as:

$$v_{on,T} = v_{0,T} + r_{0,T}\cdot i_T^{B_{con,T}}, \qquad v_{on,D} = v_{0,D} + r_{0,D}\cdot i_D^{B_{con,D}} \qquad (3.16)$$

where $v_{0,T}$, $r_{0,T,}$ $B_{con,T}$: constants characterizing the transistor conduction loss.
$v_{0,D}$, $r_{0,D}$, $B_{con,D}$: constants characterizing the diode conduction loss.

$v_{on,T}$, $v_{on,D}$: transistor and diode on-state voltages.
i_T, i_D : transistor and diode forward currents.

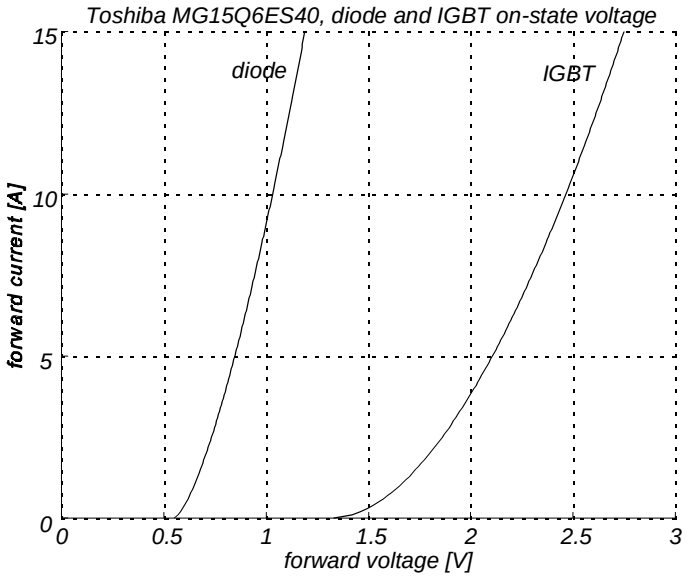

Figure 3.7: *On-state voltages for a 15 A IGBT-module used in a 4 kVA converter.*

The instantaneous diode and transistor power losses are then:

$$P_{on,T} = (v_{0,T} + r_{0,T} \cdot i_T^{B_{con,T}}) i_T \,, \qquad P_{on,D} = (v_{0,D} + r_{0,D} \cdot i_D^{B_{con,D}}) i_D \tag{3.17}$$

Inverter Switching Loss.

The losses relating to the switching between on and off states of the power components are difficult to calculate in a simple way, and in the data-sheets it is recommended not to use the provided turn-on and turn-off times to calculate switching loss, as the result will be very unreliable. It is therefore chosen here to measure the transistor turn-on loss, the transistors turn-off loss and the diode turn-off loss in a dedicated laboratory facility [3]. The current through the device and the voltage over it are measured, and by multiplication and integration, the energy dissipated in one switching is measured. This is done for different currents, and the result is shown in Figure 3.8 for a 15 A IGBT module.

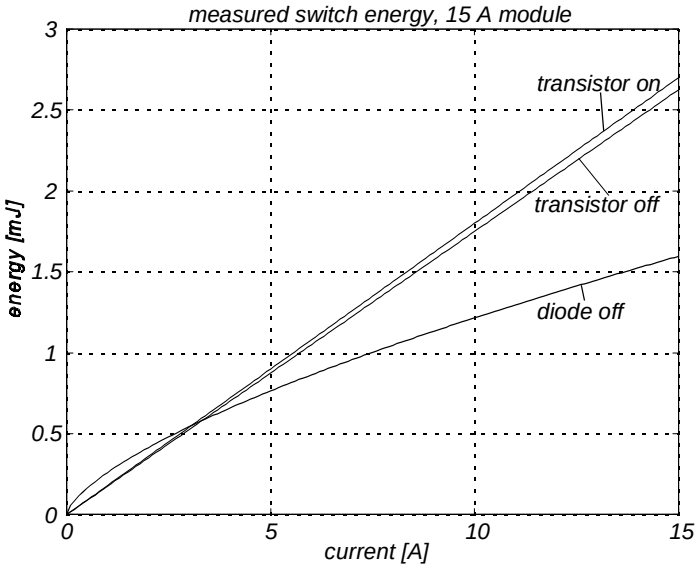

Figure 3.8: *Transistor turn-on, transistors turn-off and diode turn-off energy loss for a 15 A IGBT module used in a 4 kVA converter.*

The switch energy for each case is approximated by respectively

$$E_{sw,on,T} = A_{sw,on,T} \cdot i_T^{B_{sw,on,T}}$$

$$E_{sw,off,T} = A_{sw,off,T} \cdot i_T^{B_{sw,off,T}} \qquad (3.18)$$

$$E_{sw,D} = A_{sw,D} \cdot i_D^{B_{sw,D}}$$

where $E_{sw,on,T}$, $E_{sw,off,T}$: transistor turn-on and turn-off energy loss.
$E_{sw,D}$: diode turn-off energy loss.
$A_{sw,on,T}$, $B_{sw,on,T}$: constants characterizing the transistor loss at turn-on.
$A_{sw,off,T}$, $B_{sw,off,T}$: constants characterizing the transistor loss at turn-off.
$A_{sw,D}$, B_{swD} : constants characterizing the diode loss at turn-off.

The dissipated switching power loss in each device is:

$$P_{sw,on,T} = f_{sw} \cdot A_{sw,on,T} \cdot i_T^{B_{sw,on,T}}$$

$$P_{sw,off,T} = f_{sw} \cdot A_{sw,off,T} \cdot i_T^{B_{sw,off,T}} \qquad (3.19)$$

$$P_{sw,D} = f_{sw} \cdot A_{sw,D} \cdot i_D^{B_{sw,D}}$$

where $P_{sw,on,T}$: turn-on power loss in one transistor.
$P_{sw,off,T}$: turn-off power loss in one transistor.
$P_{sw,D}$: turn-off power loss in one diode.
f_{sw} : switching frequency.

Total Inverter Loss.

The way the total inverter loss is calculated is visualized on Figure 3.9, which shows two switching periods of the half fundamental period in which the mean power dissipation is calculated. This method was presented in [4].

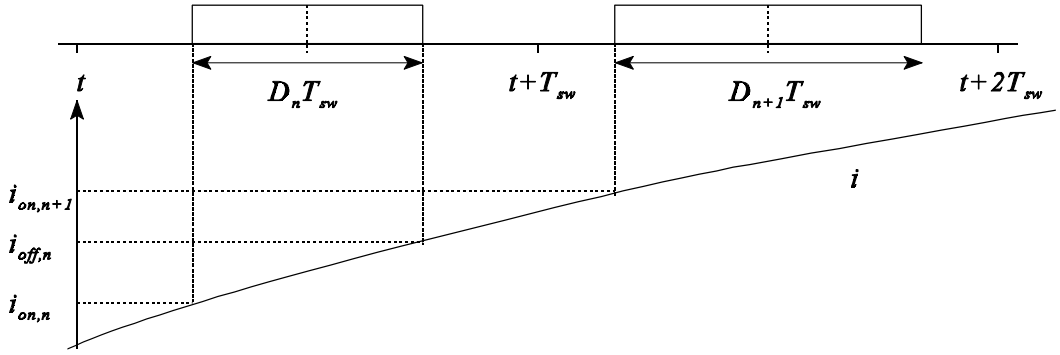

Figure 3.9: *Illustration of basis for inverter loss calculation showing the control signal for a branch and the phase current for two switching periods. The ripple of the phase-current is disregarded.*

The conduction energy loss from $t_{on,n}$ to $t_{on,n+1}$ is calculated as

$$E_{con,n} = 0.5\left((V_{0,T} + r_{0,t} i_{on,n}^{B_{con,T}})\, i_{on,n} \;+\; (V_{0,T} + r_{0,T} i_{off,n}^{B_{con,T}})\, i_{off,n}\right) D_n T_{sw} \;+$$
$$0.5\left((V_{0,D} + r_{0,d} i_{off,n}^{B_{con,D}})\, i_{off,n} \;+\; (V_{0,D} + r_{0,d} i_{on,n+1}^{B_{con,D}})\, i_{on,n+1}\right)\left((1 - D_n) + (1 - D_{n+1})\right) 0.5\, T_{sw} \qquad (3.20)$$

where $E_{con,n}$: conduction loss in one branch during a period of T_{sw}.
D_n : transistor dutycycle in switch period n.
D_{n+1} : transistor dutycycle in switch period n+1.

The switching energy loss in the same time interval is calculated as:

$$E_{sw,n} = A_{sw,on,T} \cdot i_{on,n}^{B_{sw,on,T}} + A_{sw,off,T} \cdot i_{off,n}^{B_{sw,off,T}} + A_{sw,D} \cdot i_{on,n}^{B_{sw,D}} \qquad (3.21)$$

where $E_{sw,n}$: Switching loss in one branch during a period of T_{sw}.

The inverter module loss can be calculated by:

$$P_{loss,inv} = 6 \cdot f_s \cdot \sum_{n=1}^{n=f_s/(2f_{sw})} \left(E_{con,n} + E_{sw,n}\right) \qquad (3.22)$$

where $P_{loss,inv}$: Total inverter power loss.
f_s : fundamental frequency.
f_{sw} : switching frequency.

3.4 Simplified Inverter Loss Expressions.

For an energy optimal control strategy where the inverter loss is an integral part of the algorithm, the method described above is too complex and time-consuming for real-time control calculations. Therefore a simplified method is used, providing almost the same precision, but requiring less calculations, see [5].

3.4.1 Simple Calculation of Conduction Loss.

Two main simplifications are made. First, the on-state voltages are modeled by linear first-order functions in (3.23) which are also depicted on Figure 3.10.

$$v_{con,D,lin} = v_{0,D,lin} + r_{0,D,lin} \cdot i_D \,, \qquad v_{con,T,lin} = v_{0,T,lin} + r_{0,T,lin} \cdot i_T \tag{3.23}$$

Secondly, in order to simplify the loss expressions it is necessary to use the duty-cycle pattern described by a fundamental with a third-harmonic injection, instead of the space vector modulation method which is used in experiments. The error is small because the switching functions are almost equal.

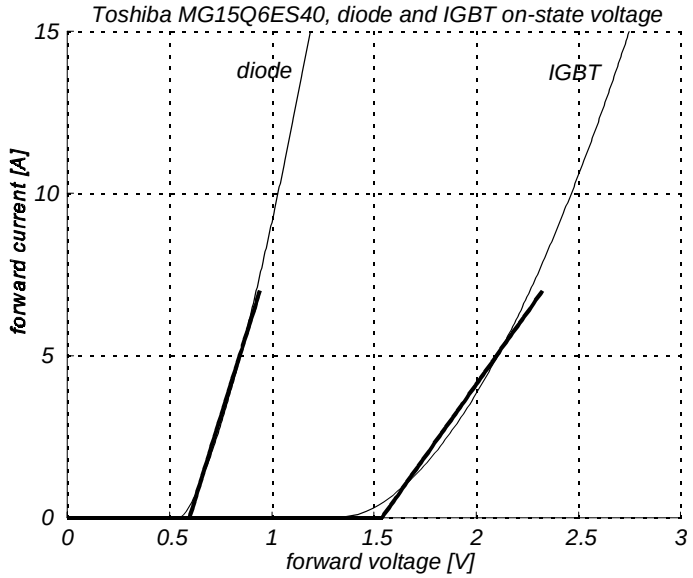

Figure 3.10: *Actual and linearized on-state voltages for a 15 A IGBT-module.*

For the conduction loss calculation it is assumed that the inverter switches infinitely fast, so the switches are either blocked or conduction.. At a given instant the stator current is given by:

$$i_s(t) = \sqrt{2} I_s \sin(\omega_s t) \tag{3.24}$$

where I_s : stator RMS current.

ω_s : stator angular velocity.

The duty cycle is expressed by the modulation function, which is leading the current by the phase shift angle, as:

$$D(t) = 0.5 + 0.5 \cdot m_i \left(\frac{2\sin(\omega_s t + \varphi)}{\sqrt{3}} + \frac{\sin(3(\omega_s t + \varphi))}{3\sqrt{3}} \right) \tag{3.25}$$

where m_i : modulation index, varying from 0 to 1.
φ : phase shift angle.

The transistor conduction energy loss for a period dt is then:

$$dE_{con,T} = i_s(t)\, v_{con,T,lin}(i_s(t))\, D(t)\, dt \tag{3.26}$$

where $v_{con,T,lin}$: linearized transistor on-state voltage.

The power loss is found by integrating the infinitesimal energy losses over a half fundamental period and dividing with the same time:

$$P_{con,T} = \frac{2}{T_s} \int_0^{T_s/2} i_s(t)\, v_{con,T,lin}(t)\, D(t)\, dt = \frac{1}{\pi} \int_0^{\pi} i_s(\theta)\, v_{con,T,lin}(\theta)\, D(\theta)\, d\theta \tag{3.27}$$

By inserting the above functions and performing the integration, the mean transistor conduction power loss is obtained:

$$\begin{aligned} P_{con,T} = {} & \frac{V_{0,T} I_s \sqrt{2}}{\pi} + \frac{I_s V_{0,T} m_i \cos(\varphi)}{\sqrt{6}} + \frac{R_{0,T} I_s^2}{2} \\ & + \frac{R_{0,T} I_s^2 m_i}{\sqrt{3}\cos(\varphi) 6\pi} - \frac{4 R_{0,T} I_s^2 m_i \cos(3\varphi)}{45\pi\sqrt{3}} \end{aligned} \tag{3.28}$$

Exactly the same procedure is followed for the diode conduction loss calculation. The only difference is that the diode dutycycle must be used:

$$D_D(t) = 0.5 - 0.5 \cdot m_i \left(\frac{2\sin(\omega_s t + \varphi)}{\sqrt{3}} + \frac{\sin(3(\omega_s t + \varphi))}{3\sqrt{3}} \right) \tag{3.29}$$

The mean diode conduction power loss is:

$$\begin{aligned} P_{con,D} = {} & \frac{V_{0,D} I_s \sqrt{2}}{\pi} - \frac{I_s V_{0,D} m_i \cos(\varphi)}{\sqrt{6}} + \frac{R_{0,D} I_s^2}{2} \\ & - \frac{R_{0,D} I_s^2 m_i}{\sqrt{3}\cos(\varphi) 6\pi} + \frac{4 R_{0,D} I_s^2 m_i \cos(3\varphi)}{45\pi\sqrt{3}} \end{aligned} \tag{3.30}$$

The mean conduction power loss for the whole inverter is:

$$P_{con,inv} = 3\left(P_{con,T} + P_{con,D}\right) \qquad (3.31)$$

3.4.2 Simplified Switching Loss Calculation.

A very simple formula for the total switching loss follows from the fact that it turns out to be nearly proportional to the switching frequency and proportional to the phase current. An example of the proportionalities is given on Figure 3.11, which shows the total switch energy as function of current.

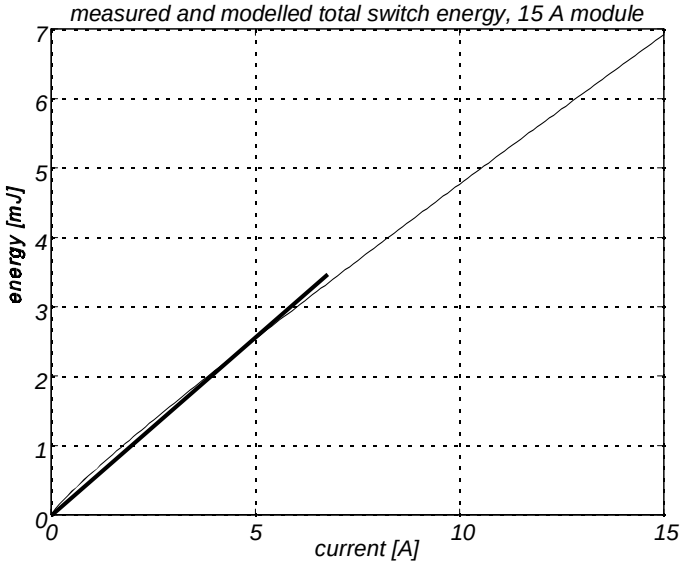

Figure 3.11: *Total switching loss as function of phase current for an inverter branch with 15 A modules. The thick line is the approximated switching loss within the normal operating area.*

The total switching loss is then approximately given by

$$P_{sw,lin} = K_{sw}\, I_s\, f_{sw} \qquad (3.32)$$

where K_{sw} : empirically determined constant.

3.4.3 Simple Calculation of Total Inverter Loss.

The total inverter loss can then be calculated by the simple analytical formulas (3.28), (3.30), (3.31) and (3.32), and it depends on the following parameters:

$$P_{loss,inv} = f(I_s,\ f_{sw}, \varphi, m_i) \qquad (3.33)$$

Hereby the inverter loss can be calculated easily and with a relatively good accuracy. The formulas will be used in chapter 7, where the inverter loss calculations are integrated in real-time in the model-based energy optimal control.

3.5 Summary.

The motor losses are separated into fundamental and harmonic losses. The fundamental losses are calculated with a conventional single phase model without separate representation of stray load losses. The harmonic losses were measured as function of the switching frequency for 2.2 kW standard motor and high-efficiency motor drives, and in both cases it was found that the drives loss reached a minimum around 3-4 kHz.

It was not possible to define a clear relation between measured harmonic motor losses and motor flux level. For that reason, and because these losses are not important, the harmonic motor losses will not be included in the energy optimal control algorithms.

The converter loss models are designed in two versions, one for theoretical analyses, and one simplified version for real-time converter loss calculations.

References.

[1] F. Abrahamsen “Energy Optimal Control Strategies for Electro Motors, low-cost and sensorless PWM-VSI based induction motor control”, Aalborg University, Denmark, ISBN 87-89179-23-4, 1998.

[2] D. W. Novotny, S. A. Nasar, B. Jeftenic, D. Maly, “Frequency Dependence of Time Harmonic Losses in Induction Machines”, Proceed. of ICEM90, 1990, pp. 233-238.

[3] S. Munk-Nielsen, F. Blaabjerg, J. K. Pedersen, “An Advanced Measurement System for Verification of Models and Data-sheets.”, 1994 PELS Workshop on Computers in Power Electron., 1994, pp. 234-239.

[4] F. Blaabjerg, U. Jaeger, S. Munk-Nielsen, J. K. Pedersen, “Power Losses in PWM-VSI Inverter Using NPT or PT IGBT Devices”, IEEE Trans. on Power Electronics, Vol. 10, No. 3, May 1995, pp. 225-232.

[5] J. W. Kolar, H. Ertl, F. C. Zach, “Calculation of the passive and active component stress of three-phase PWM converter systems with high pulse rate”, Proceed. of EPE’89, Aachen, Germany, Oct. 9-12, 1989, pp. 1303-1311.

Chapter 4

Experiments and Calculations on Drive with Optimal Efficiency

It is investigated in this chapter what the maximal obtainable efficiency of a motor drive is, and what characterizes the drive when it is efficiency optimized. The analysis is based on experiments on 2.2 kW standard and high-efficiency induction motor drives, on which efficiencies are measured with optimized efficiency and with constant air-gap flux. The measurements are used to validate the motor and converter loss models, and these are then used to analyze the drive by performing steady-state calculations. The drive is analyzed by steady-state calculations, both with optimized efficiency and with variations of flux around the points of optimal efficiency. From that analysis it is possible to chose several possible ways of implementing energy optimal control, and to evaluate how well they will perform.

4.1 Efficiency Measurements on 2.2 kW Standard Motor Drive.

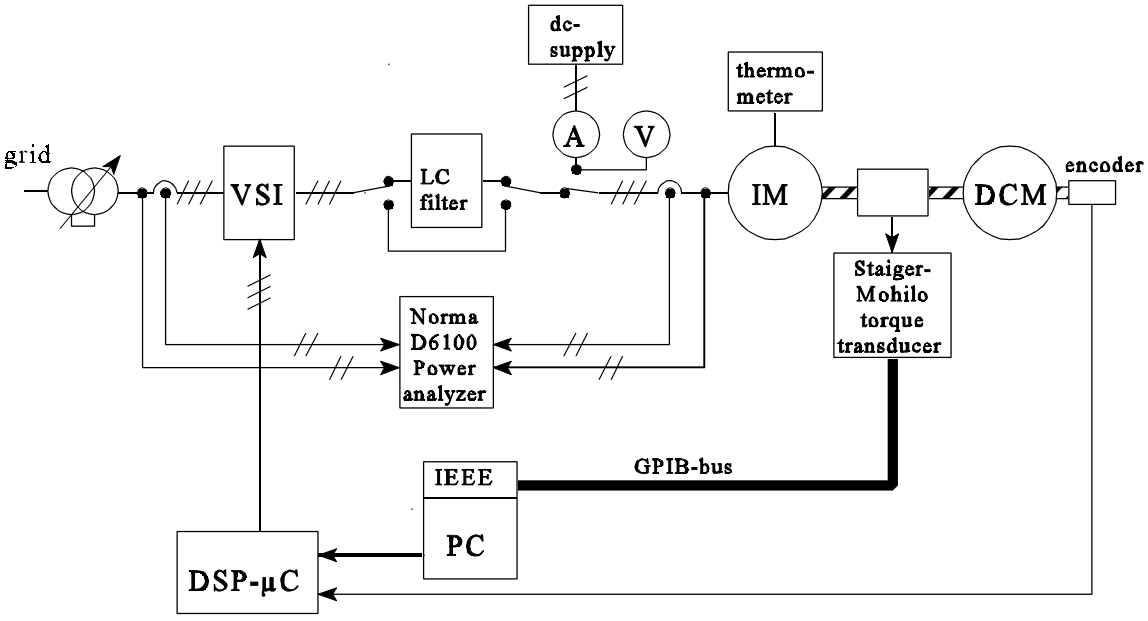

Figure 4.1: *Experimental setup for measurement of the induction motor drive efficiency.*

4.1.1 Execution of Experiment.

The experimental setup is shown on Figure 4.1. The motor and converter efficiencies are measured with a 12-channel Power Analyzer Norma 6100. The load is acquired by measurements of load torque and speed. For each efficiency measurement, the stator dc-resistance and the motor housing temperature are measured as well. Efficiency measurements are made both with PWM voltages imposed directly on the motor and with filtered stator voltages. When measurements in this way are made with both PWM and with sinusoidal voltages, it is possible to separate the harmonic motor loss arising from the PWM. All measurements are made inside the operating area: 0.2 - 1 p.u. speed and from 0.15 - 1 p.u. load torque.

When the motor is loaded, the thermal stability is reached within 2-3 hours. However, the measurement are for practical reasons performed with a time interval of 10-15 min. between two points. This allows the motor to accommodate its temperature to some degree. It is assumed that the error by doing so is not important.

The frequency converter is commanded by simple scalar control with compensation of the inverter non-linearities: dead-time, diode and transistor voltage drop, and dc-link ripple. During the measurements the speed is controlled in closed loop by adjusting the stator frequency. For the measurements with optimal efficiency, the stator voltage is adjusted until the drive input power read on the power analyzer has reached a minimum. For the constant air-gap flux control, the stator voltage is calculated in the following way:

$$V_s = abs(\psi_{m,nom}\ \omega_s + (R_s + j\,\omega_s L_{s\sigma}) I_s(\cos\varphi - j\sin\varphi)) \qquad (4.1)$$

where V_s : stator phase voltage.
$\psi_{m,nom}$: nominal air-gap flux.
ω_s : stator angular velocity.
R_s : stator resistance.
L_{so} : stator leakage inductance.
I_s : stator current.
φ : phase shift angle.

4.1.2 Results.

The results are presented graphically on the next pages. All measurement data are provided in [1, pp. 215ff].

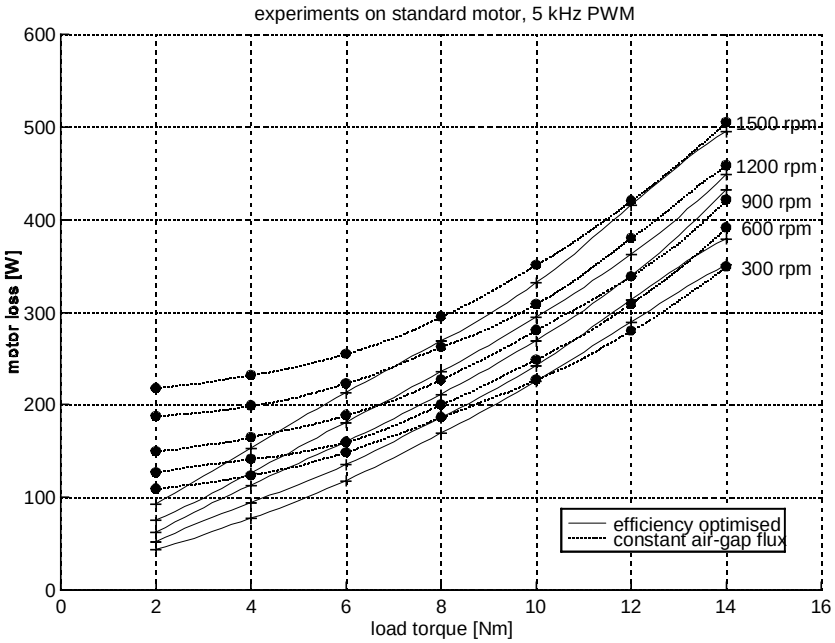

Figure 4.2: *Measured motor loss of a PWM inverter fed 4-pole 2.2 kW standard induction motor drive, and with both efficiency optimized and constant nominal air-gap flux control. Rotor speed is kept constant at 300, 600, 900, 1200 and 1500 rpm.*

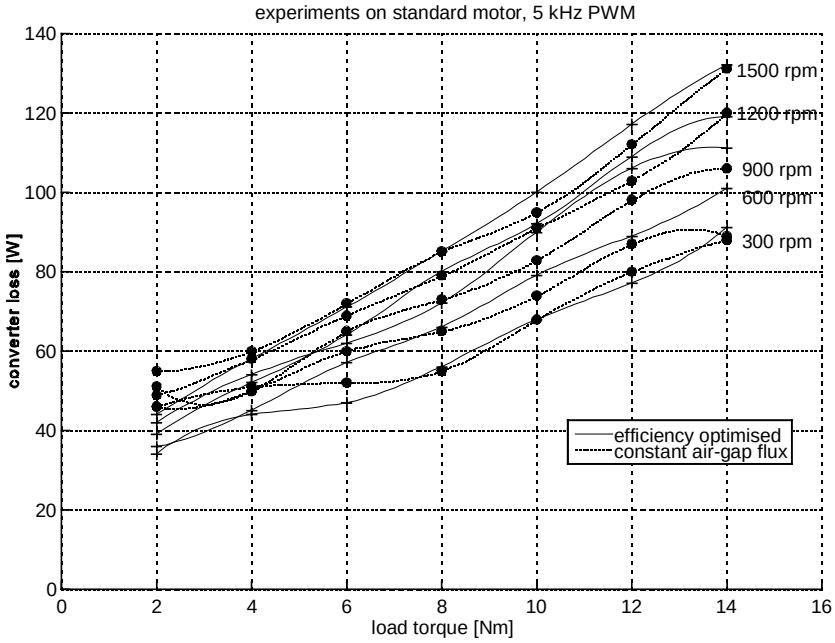

Figure 4.3: *Measured converter loss of a PWM inverter fed 4-pole 2.2 kW standard induction motor drive, and with both efficiency optimized and constant nominal air-gap flux control. Rotor speed is kept constant at 300, 600, 900, 1200 and 1500 rpm.*

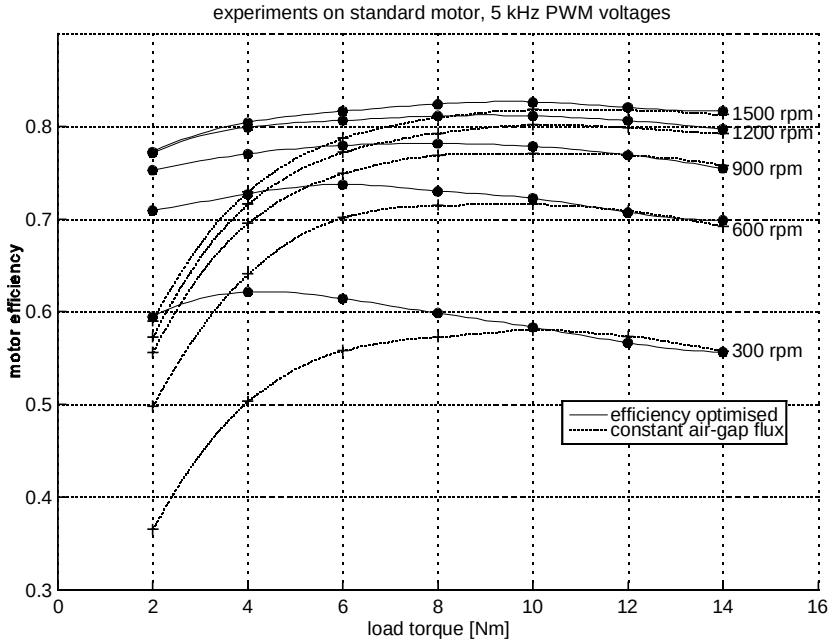

Figure 4.4: *Measured efficiencies of a 4-pole 2.2 kW standard induction motor supplied with PWM voltages and with both efficiency optimized and constant nominal air-gap flux control. Rotor speed is kept constant at 300, 600, 900, 1200 and 1500 rpm.*

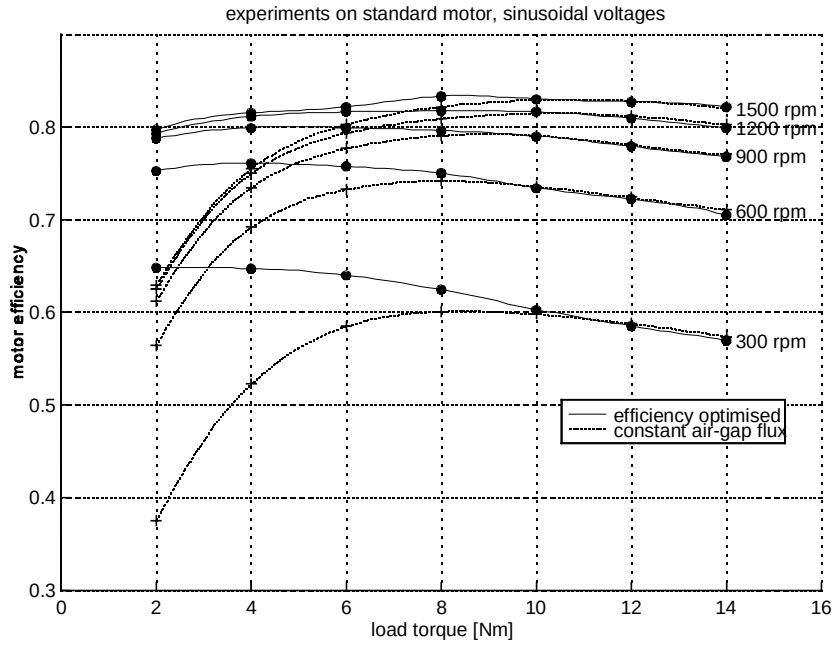

Figure 4.5: *Measured efficiencies of a 4-pole 2.2 kW standard induction motor supplied with sinusoidal voltages and with both efficiency optimized and constant nominal air-gap flux control. Rotor speed is kept constant at 300, 600, 900, 1200 and 1500 rpm.*

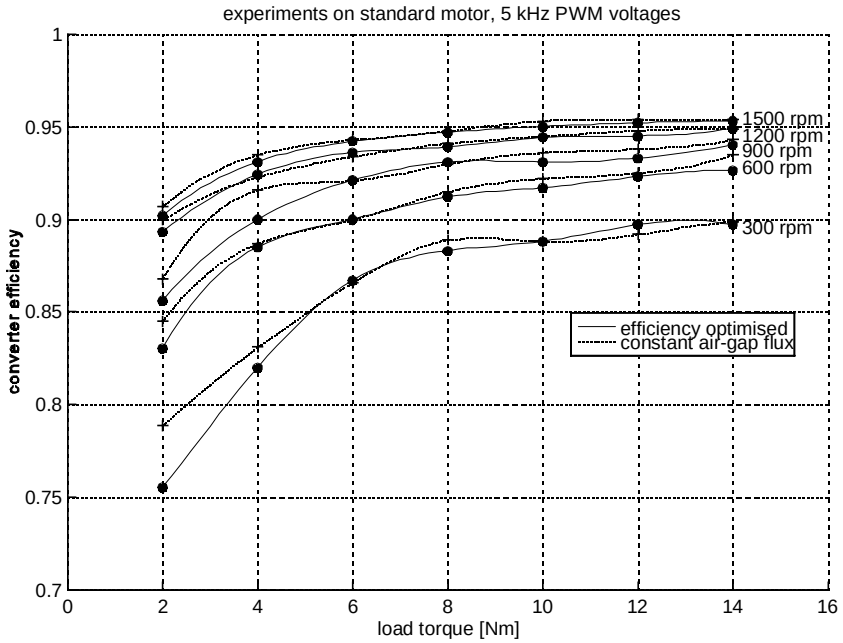

Figure 4.6: *Measured efficiencies of a converter supplying a 4-pole 2.2 kW standard induction motor with PWM voltages, and with both efficiency optimized and constant nominal air-gap flux control. Rotor speed is kept constant at 300, 600, 900, 1200 and 1500 rpm.*

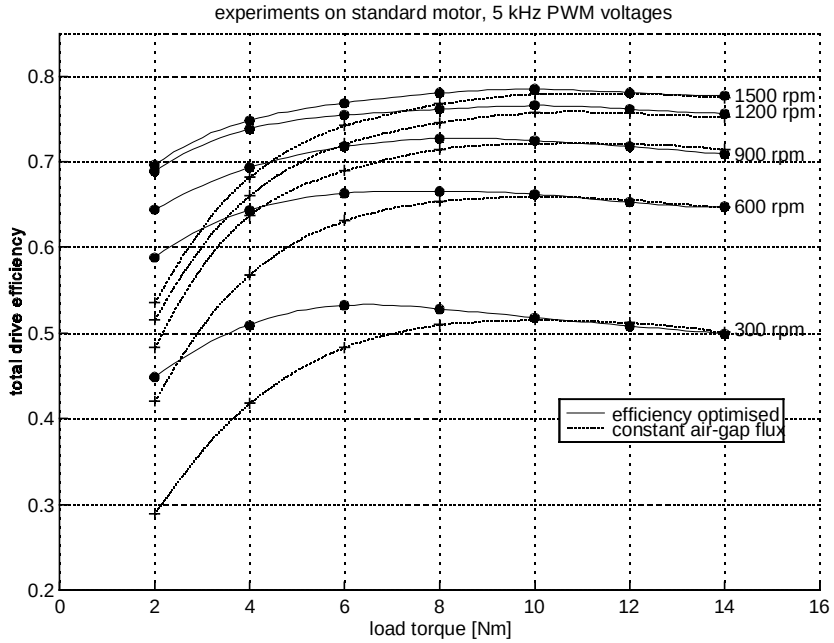

Figure 4.7: *Measured total drive efficiency of a PWM inverter fed 4-pole 2.2 kW standard induction motor, and with both efficiency optimized and constant nominal air-gap flux control. Rotor speed is kept constant at 300, 600, 900, 1200 and 1500 rpm.*

4.1.2 Discussion.

The reduction in motor loss with optimized efficiency is seen clearly from Figure 4.2, and it is present below around 10-12 Nm load torque (below around 0.6-0.7 p.u. load torque). By extrapolating the motor loss curves towards zero load torque it is seen that with optimized efficiency the motor losses go towards zero, and with constant flux the motor losses go towards final values. These are the no load losses consisting of core losses, and copper losses from the magnetizing current. At 300 rpm. the efficiency optimized motor loss is at high load higher than the constant flux motor loss, see Figure 4.2. This error can be caused by measurement inaccuracies or changed motor temperature.

For the converter losses on Figure 4.3 the improvements are only clear at loads below 4 Nm (0.3 p.u.). Extrapolation of the efficiency optimized curves towards zero load shows that the converter has a no-load loss around 30 W.

Although the stator current is almost constant for a given load torque irrespective of speed, the converter loss is higher at high speed. The reason is that at high speed the modulation index is high, so the transistors conduct for longer periods than the diodes. At low speed it is primarily the diodes that conduct, which leads to a lower loss.

The reduction seen on the motor losses are of course reflected into the motor efficiency curves on Figure 4.4 and Figure 4.5 also. The efficiency improvement at 0.25 p.u. load torque (3.5 Nm) is 8-10 % points at 1500 rpm. and 14 % points at 300 rpm. At first sight it may surprise that the optimized efficiency at low speed decreases as the load increases. The reason is that a high stator copper loss is generated at high load, where the core is saturated. It happens also at high speed, but to a lesser extent.

By comparing Figure 4.4 with Figure 4.5 it is seen that the motor efficiency is lowest with PWM voltages because of the harmonic motor loss with PWM voltages. The measured harmonic losses were discussed in chapter 3.2 and are not commented further here.

At this 2.2 kW motor power level the motor loss is approximately a factor three higher than the converter loss, see Figure 4.2 and Figure 4.3. So when the motor has a nominal efficiency of 0.82 (Figure 4.4), the converter has a nominal efficiency of 0.96 (Figure 4.6). The converter efficiency decreases with both load and speed, but not as much as for the motor.

The curves for the total drive efficiency (Figure 4.7), are the most interesting regarding efficiency optimization, because it is the input energy to the converter and not to the motor, which is paid for. An efficiency improvement is present up to 10 Nm (0.7 p.u.), and for 0.25 p.u. load (3.5 Nm) it is 8 % points at 1500 rpm. and 10 % points at 300 rpm. While the nominal efficiency for the motor alone is 0.82, the nominal system efficiency is reduced to 0.78.

4.2 Efficiency Measurements on 2.2 kW High-Efficiency Motor Drive.

The used high-efficiency motor is constructed with the same steel sheet geometry as the standard motor. The core losses are reduced by use of steel sheet which is both thinner and has lower specific losses. The stack-length is increased so the number of turns in the stator winding could be reduced and the cross section of the copper wire increased. The measurements are executed as for the standard motor drive in the previous section, and the results are shown on Figure 4.9 - Figure 4.14 in terms of losses and efficiency.

Figure 4.9 shows that the motor losses are reduced by energy optimal control below 9-14 Nm. The reduction of converter losses is small, Figure 4.10. The converter losses are slightly smaller with the high-efficiency motor than with the standard motor because the stator current is smaller for the high-efficiency motor.

The advantages of energy optimal control for the standard motor and for the high-efficiency motor are compared on Figure 4.8. The reduction of the drive loss is evaluated at 25% of nominal load torque (3.5 Nm) at the five different speeds. Although the illustration is distorted by the measurement inaccuracy, it is clear that the reduction is smaller for the high-efficiency motor than for the standard motor.

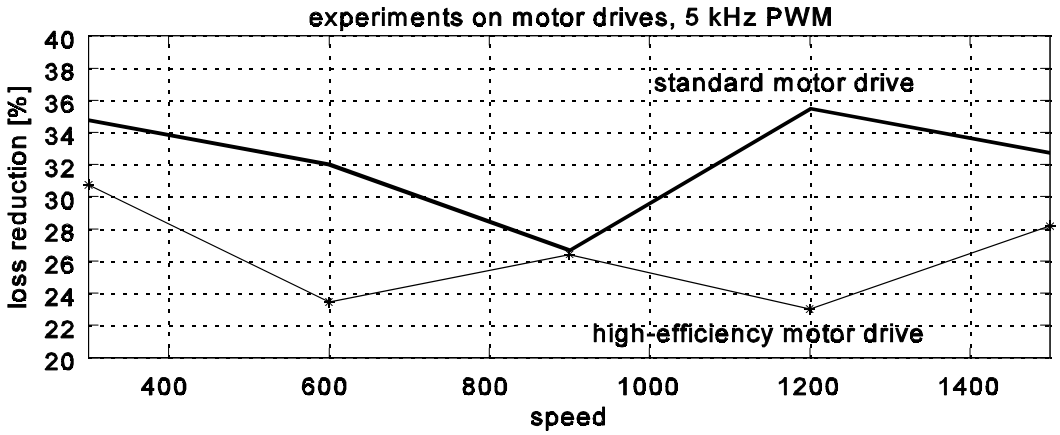

Figure 4.8: *Reduction of total drive loss at 25% load torque (3.5 Nm) for the standard motor and the high-efficiency motor.*

The high-efficiency motor efficiency, converter efficiency and drive efficiency are shown on Figure 4.11 - Figure 4.14.

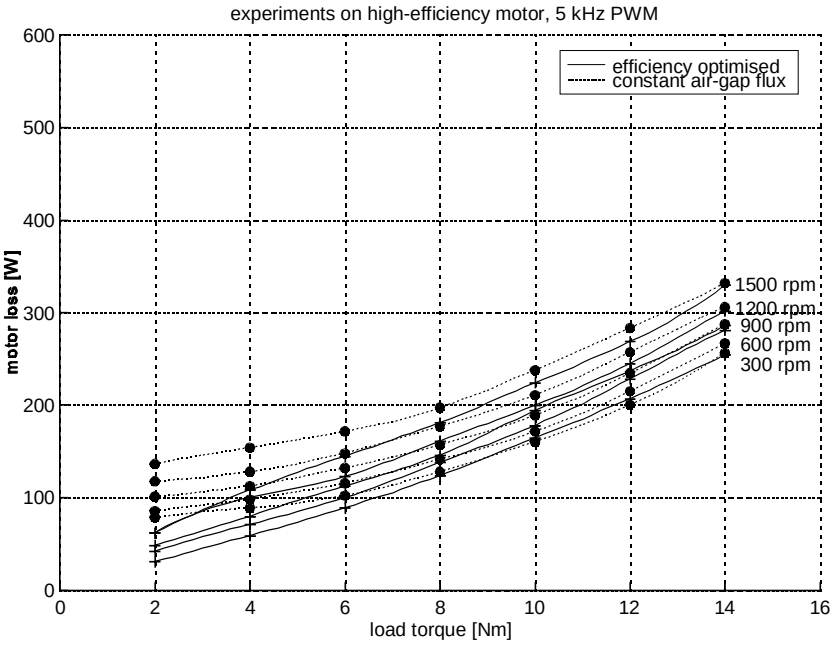

Figure 4.9: *Measured motor loss of a PWM inverter fed 4-pole 2.2 kW high-efficiency induction motor drive, and with both efficiency optimized and constant nominal air-gap flux control. Rotor speed is kept constant at 300, 600, 900, 1200 and 1500 rpm.*

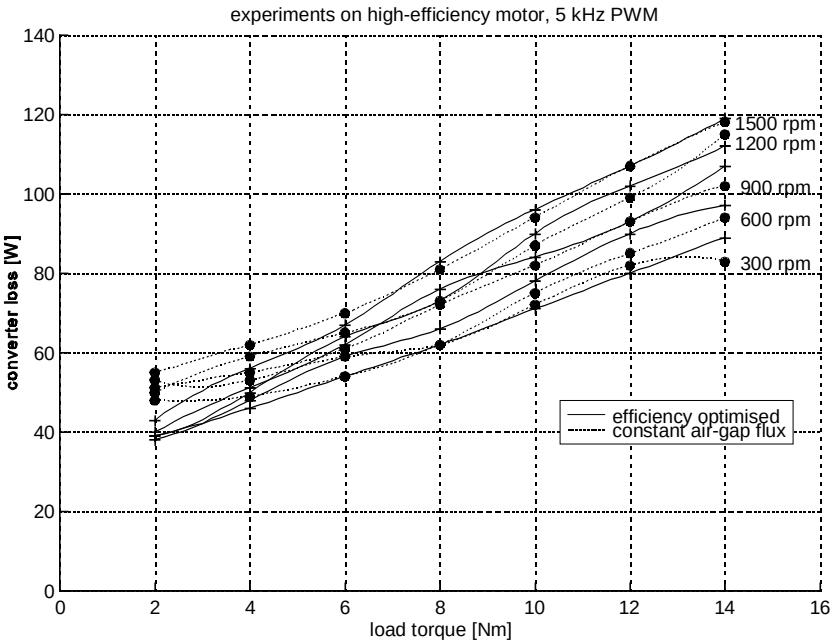

Figure 4.10: *Measured converter loss of a PWM inverter fed 4-pole 2.2 kW high-efficiency induction motor drive, and with both efficiency optimized and constant nominal air-gap flux control. Rotor speed is kept constant at 300, 600, 900, 1200 and 1500 rpm.*

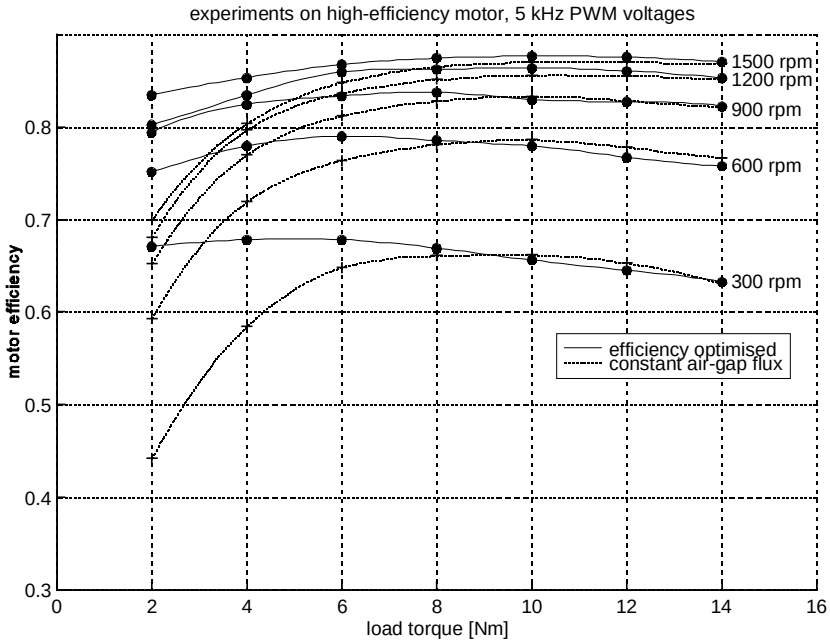

Figure 4.11: *Measured efficiency of a high-efficiency 4-pole 2.2 kW induction motor supplied with PWM voltages and with both efficiency optimized and constant nominal air-gap flux control. Rotor speed is kept constant at 300, 600, 900, 1200 and 1500 rpm.*

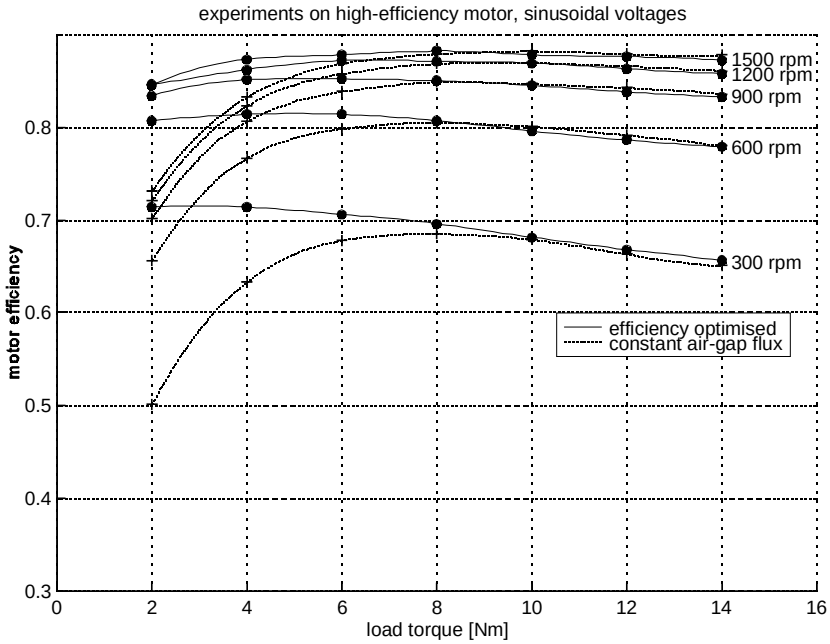

Figure 4.12: *Measured efficiencies of a high-efficiency 4-pole 2.2 kW induction motor supplied with sinusoidal voltages and with both efficiency optimized and constant nominal air-gap flux control. Rotor speed is kept constant at 300, 600, 900, 1200 and 1500 rpm.*

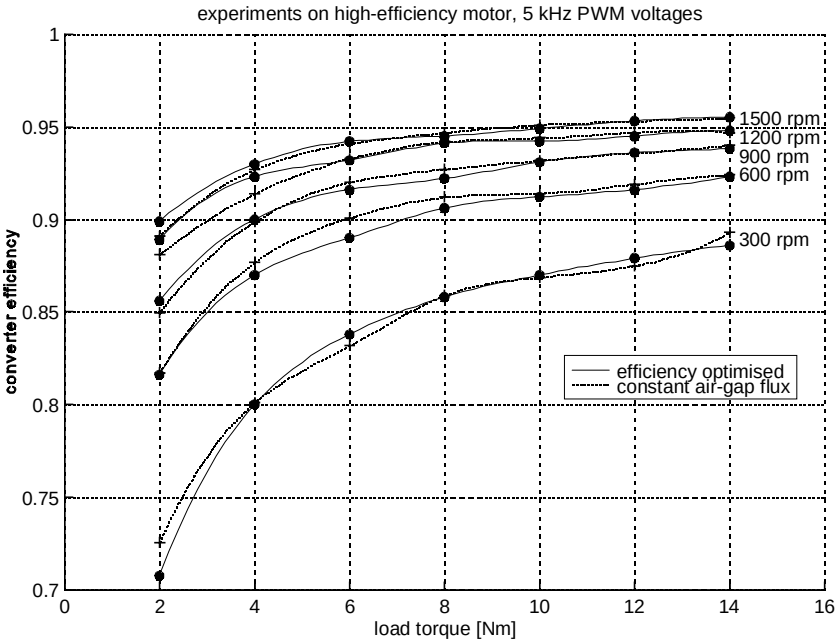

Figure 4.13: *Measured efficiency of a converter supplying a high-efficiency 4-pole 2.2 kW induction motor with PWM voltages, and with both efficiency optimized and constant nominal air-gap flux control. Rotor speed is kept constant at 300, 600, 900, 1200 and 1500 rpm.*

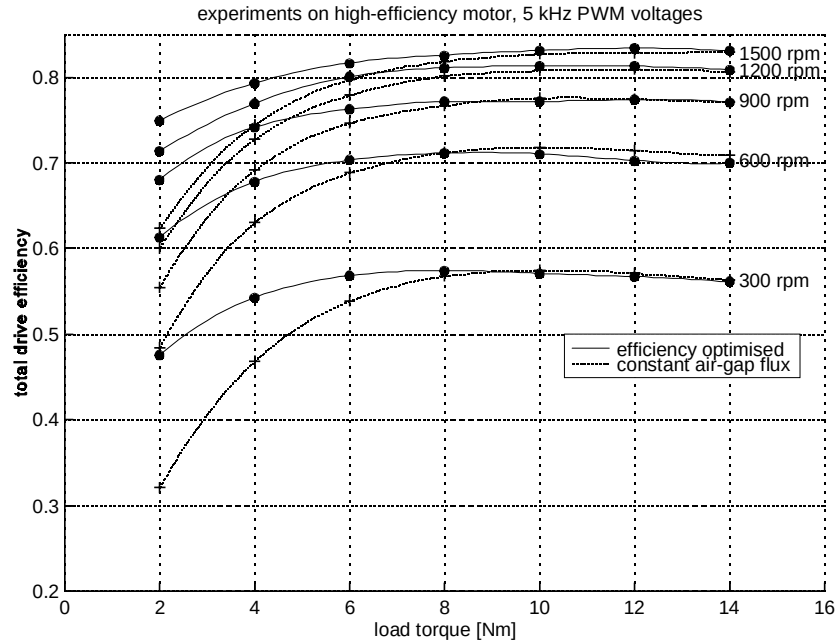

Figure 4.14: *Measured total drive efficiency of a PWM inverter fed high-efficiency 4-pole 2.2 kW induction motor, and with both efficiency optimized and constant nominal air-gap flux control. Rotor speed is kept constant at 300, 600, 900, 1200 and 1500 rpm.*

4.2 Calculation of Optimal Drive Efficiency.

The figures shown on the following pages present the result of two different analyses.

The first analysis which is referred to as optimized efficiency, for example Figure 4.15, is performed by calculations in a number of points given by a speed and load torque, and in each point the stator frequency and stator voltage are varied so as to minimize the drive input power. The calculations are done at five different speeds inside the nominal load range. The purpose of these calculations is to see the values of for example cos(φ), stator current and slip frequency, and whether these quantities can be used for an energy optimal control algorithm.

The second analysis is only done at 900 rpm., and four load points are selected for closer analysis: 2, 6, 10 and 14 Nm, see for example Figure 4.16. For each of the four load cases the air-gap flux is varied inside its nominal range. The points of optimal efficiency are denoted by a filled dot, and the corresponding operating points are also shown on the curves of the first analysis, compare for example the dots of Figure 4.15 and Figure 4.16. Because of limited space, calculations are only done at 900 rpm. here. In [1] they are made at 300 rpm. and 1500 rpm. as well, but they do not provide much extra information. The purpose of these calculations is to see, for example, how sensitive the efficiency is to changes in air-gap flux near optimal efficiency, and to get an idea of how an energy optimal control strategy will react to inaccurate and noisy feed-back signals.

4.2.1 Motor and Converter Models.

The models which are used to do calculations on the motor drive are those presented in chapter 3. The calculations are only done in steady-state, and as it is the energy efficiency of the drive which is of primary interest, it is sufficient to use the single phase motor equivalent circuit, but with accurate modeling of the losses in the motor and converter. The motor and converter losses are modeled as described in section 3.1 and section 3.3 respectively. It means that the harmonic losses are not included in the following analysis, but as it was stated in section 3.2, that is of no concern here because the harmonic losses have no influence of how the drive should be controlled.

The motor model parameters are measured by standard tests, see [1, pp. 83ff] for detailed information. The motor and converter loss models are validated by comparing them with the measurements with sinusoidal voltages in the previous section, and documentation for that is provided in appendix B. The only motor parameters which are adjusted to make the model fit the measurements are the ratio between the leakage inductances, and stator and rotor resistances which are made dependent on motor temperature. A linear dependence is established between motor temperature, and load torque and speed, based on measured values. So the motor is modeled in a relatively simple way but is has appeared to be sufficient for this purpose.

If a motor model on a more detailed level was to be used, for example the Magnetic Equivalent Circuit (MEC) model, the analysis would be much more complicated to carry out, and it is not even certain that the loss modeling would be much better than with the present simple model. For example, it is still a serious problem in MEC models to model the core losses accurately.

4.2.2 Result of Calculations.

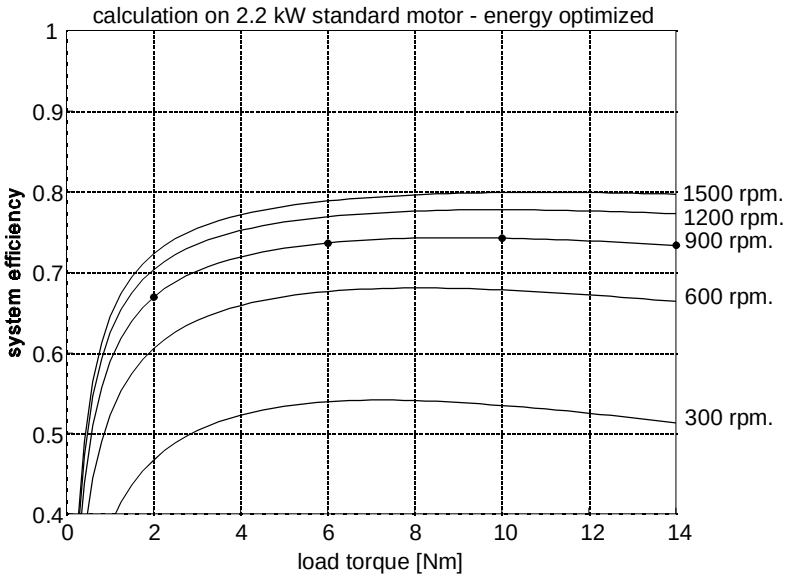

Figure 4.15: *Calculated system efficiency as function of load torque in case of optimal system efficiency. The dots denote operating points which are analyzed further in Figure 4.16.*

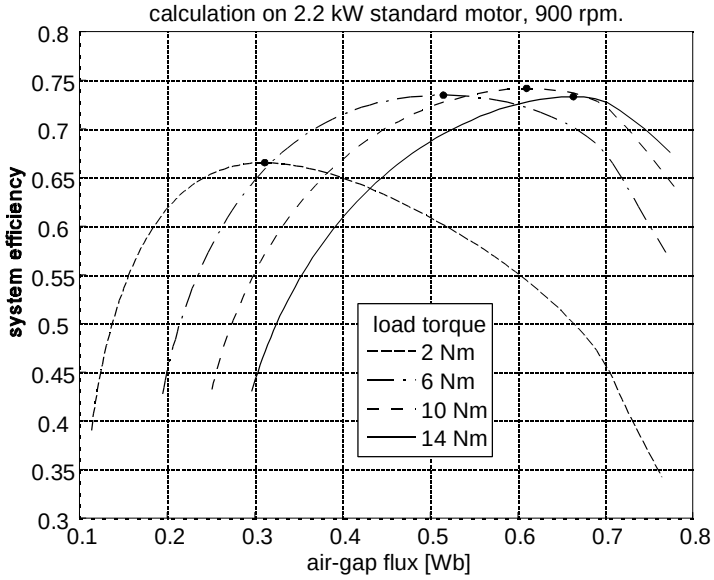

Figure 4.16: *Calculated system efficiency as function of air-gap flux, for the four operating points in Figure 4.15. The dots denote the points of optimal system efficiency.*

Figure 4.15 shows the maximal attainable system efficiency, and Figure 4.17 and Figure 18 the corresponding motor and converter efficiencies. For validation of the model with experiments, Figure 4.17 can be compared with Figure 4.5, and Figure 4.18 with Figure 4.6.

Figure 4.16 shows that at nominal load, the optimal efficiency is reached around the nominal air-gap flux of 0.658 Wb. The system efficiency curves are relatively flat on the top, indicating that it is not so important to hit exactly the air-gap flux of optimal efficiency. Figure 4.16 can be used to show that with a variation of +/- 0.02 Wb around the points of optimal efficiency, the maximal change in system efficiency appears at 14 Nm and is 0.13 % points.

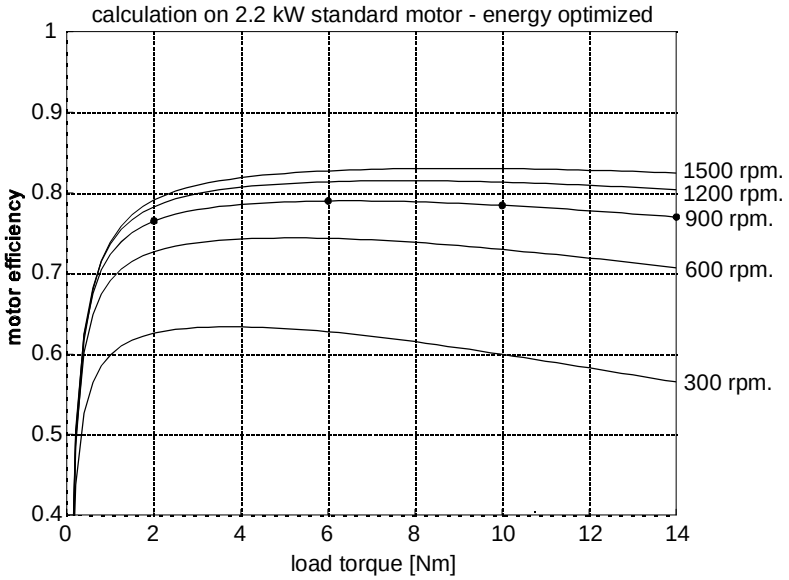

Figure 4.17: *Calculated motor efficiency as function of load torque in case of optimal system efficiency.*

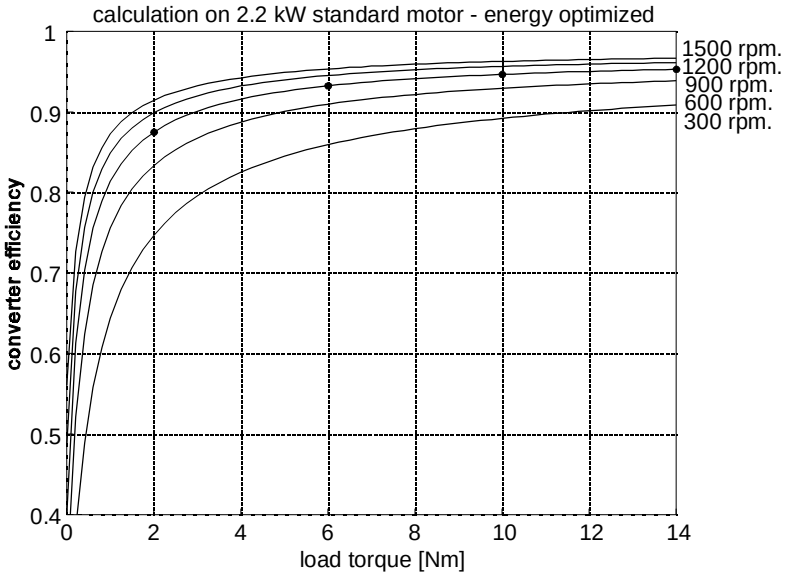

Figure 4.18: *Calculated converter efficiency in case of optimal system efficiency.*

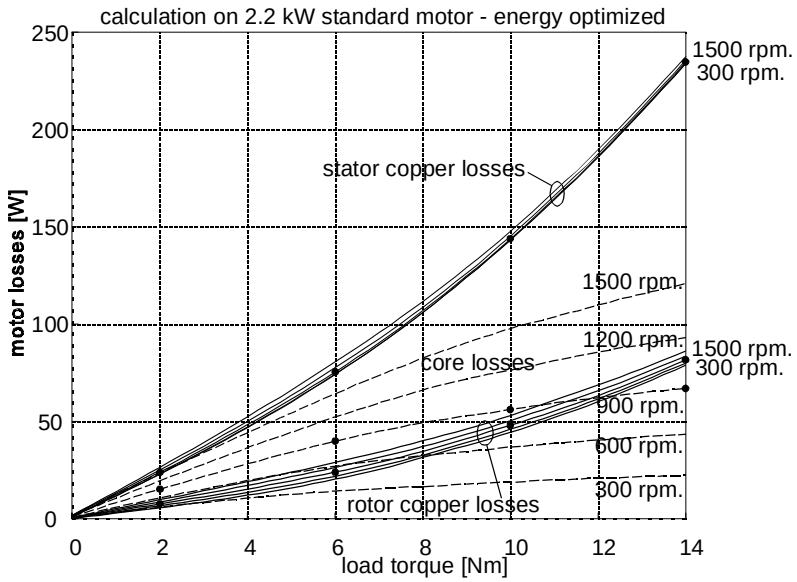

Figure 4.19: *Calculated motor loss as function of load torque in case of optimal system efficiency.*

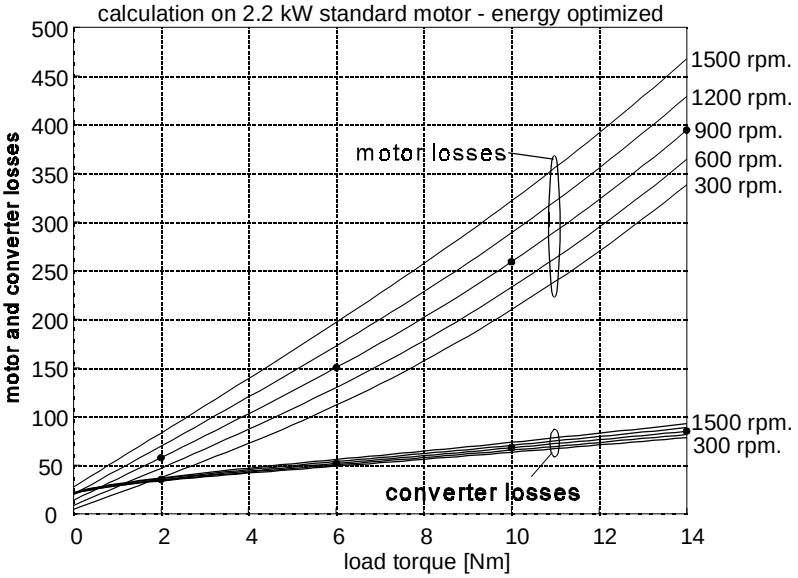

Figure 4.20: *Calculated converter loss as function of load torque in case of optimal system efficiency. The dots denote operating points which are analyzed further in Figure 4.21 and Figure 4.22.*

As shown on Figure 4.19 the copper losses are almost independent of speed, and at low speed the copper losses are by far dominating the motor loss. The motor loss is in general larger than the converter loss, see Figure 4.20, and especially at high load. It must be noticed, however, that in the low load area, where the energy optimal control is useful, the difference is not so large.

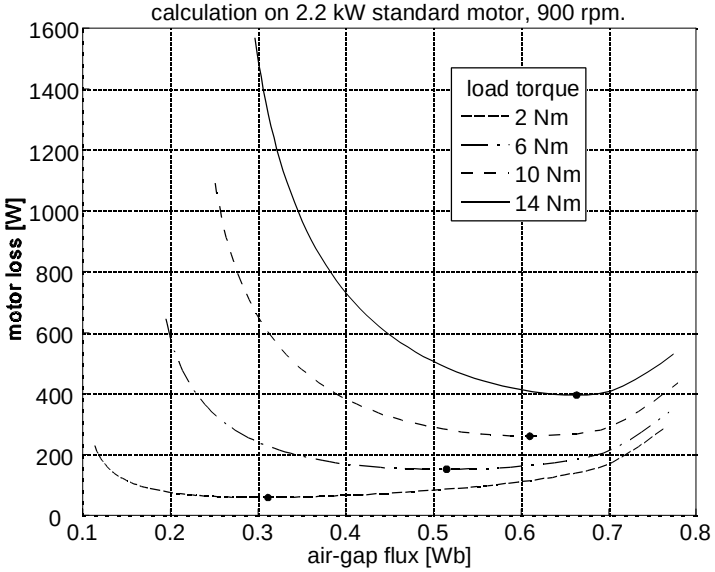

Figure 4.21: *Calculated motor loss as function of air-gap flux, for the four operating points in Figure 4.20. The dots denote the points of optimal system efficiency.*

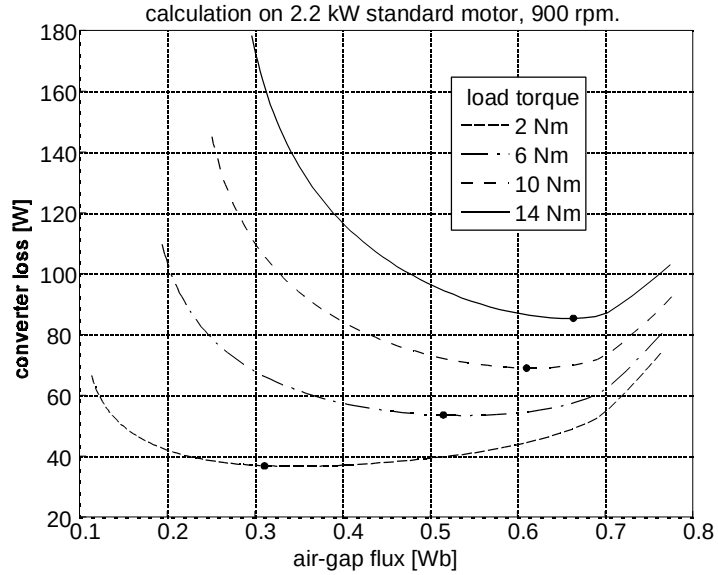

Figure 4.22: *Calculated converter loss as function of air-gap flux, for the four operating points in Figure 4.20. The dots denote the points of optimal system efficiency.*

The way the motor and converter losses depend on air-gap flux is almost identical, compare Figure 4.21 and Figure 4.22. The difference is the size of the loss. In both cases the loss minima are almost coincident with the system loss minima. This means that both minimum motor loss and minimum converter loss can possibly be used as indicator for optimal efficiency, and when one is used as indicator, the other can be disregarded.

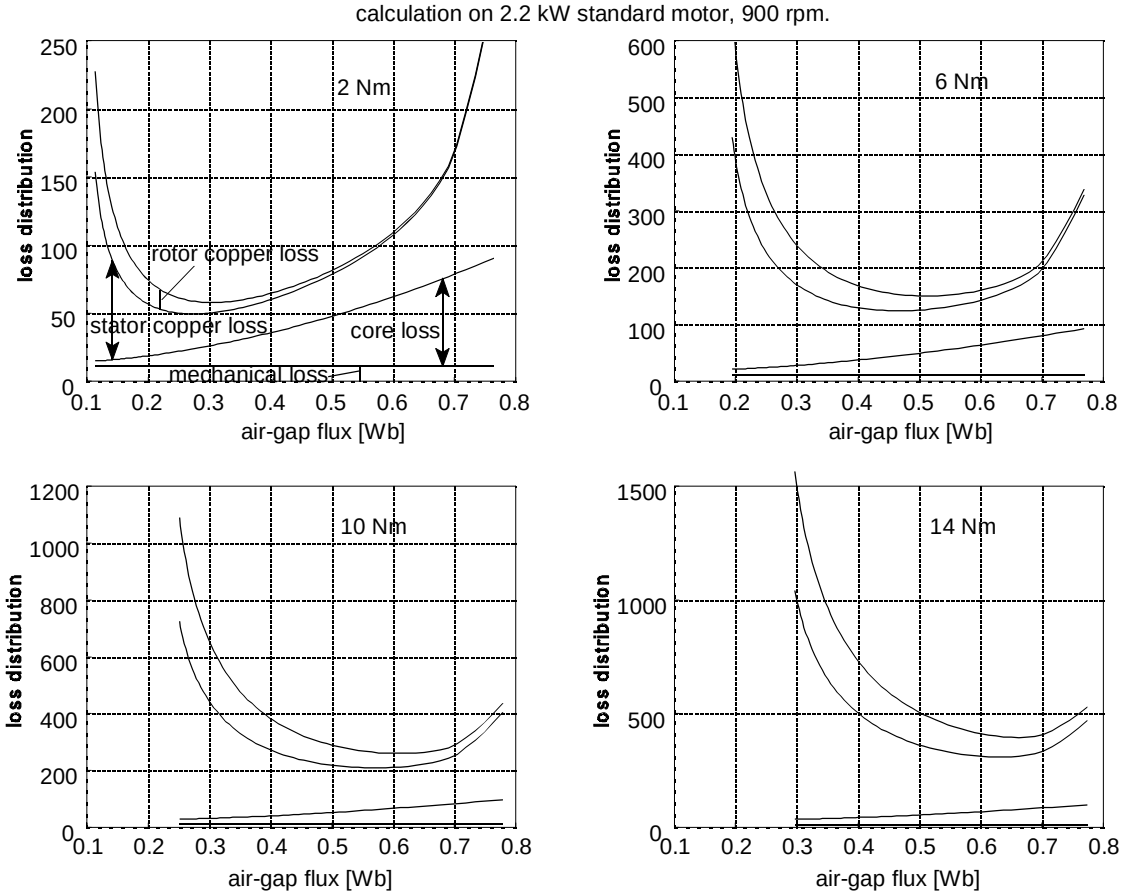

Figure 4.23: *Calculated distribution of motor losses as function of air-gap flux, for the four operating points in Figure 4.20.*

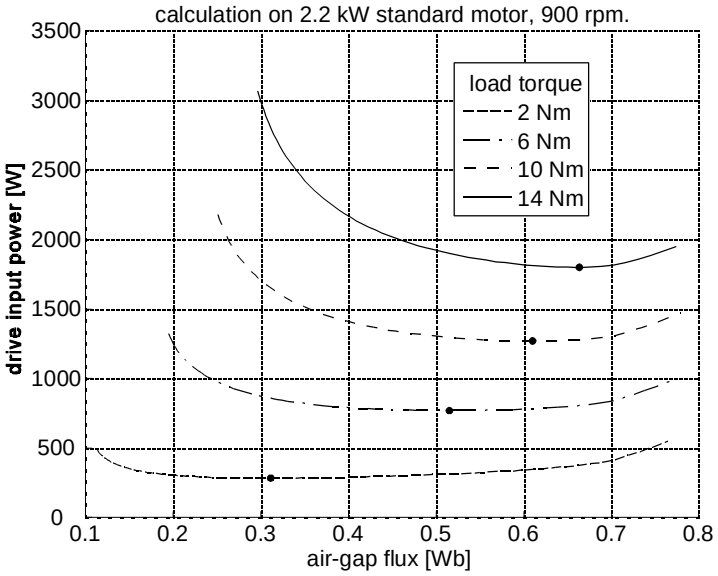

Figure 4.24: *Calculated input power as function of air-gap flux, in four operating points. The dots denote the points of optimal system efficiency.*

The distribution of motor losses are shown on Figure 4.23. From the 2 Nm load case it is seen that efficiency optimization by flux reduction is realized by reduction of core losses to 30 % and stator copper losses to 40 % of their nominal values (at 0.658 Wb). When looking on the losses, the minima are relatively well defined, but when it comes to the drive input power on Figure 4.24, the curves at low load are so flat that if the minimum must be detected precisely, by for example search control, a very precise power measurement is required, and it is obviously sensitive to noise on the measured signal.

The air-gap flux with optimal efficiency is shown on Figure 4.25. If speed and load torque (or stator current) are known, optimal efficiency is assured by setting an air-gap flux reference equal to the curves on the figure.

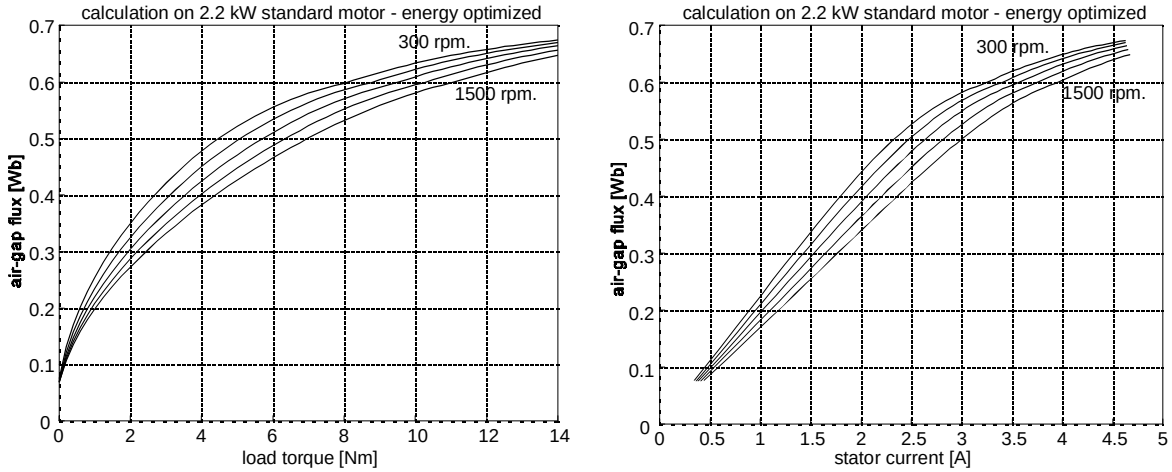

Figure 4.25: *Calculation on 2.2 kW standard motor with optimized drive efficiency. Left: air-gap flux as function of load torque for optimized efficiency, right: air-gap flux as function of stator current for optimized efficiency.*

The stator current with optimal efficiency is almost independent of speed, see Figure 4.26. One could be tempted to realize energy optimal control by setting a current reference which is a linear function of load. But there are two problems by doing that. First, just a small error in current would give a large deviation in flux and efficiency from the desired value, as can be observed from Figure 4.27. Next, if the control is implemented in a current controlled scalar drive, then the motor will pull out if the current reference for a given load is set below the curves shown on Figure 4.27. That can easily happen when the motor is operated near the point of optimal efficiency.

On the other hand, the current minima on Figure 4.27 are more well defined than the input power minima from Figure 4.24, and as the current minima are almost coincident with the point of optimal efficiency, it is better to use stator current than input power as search variable in search control.

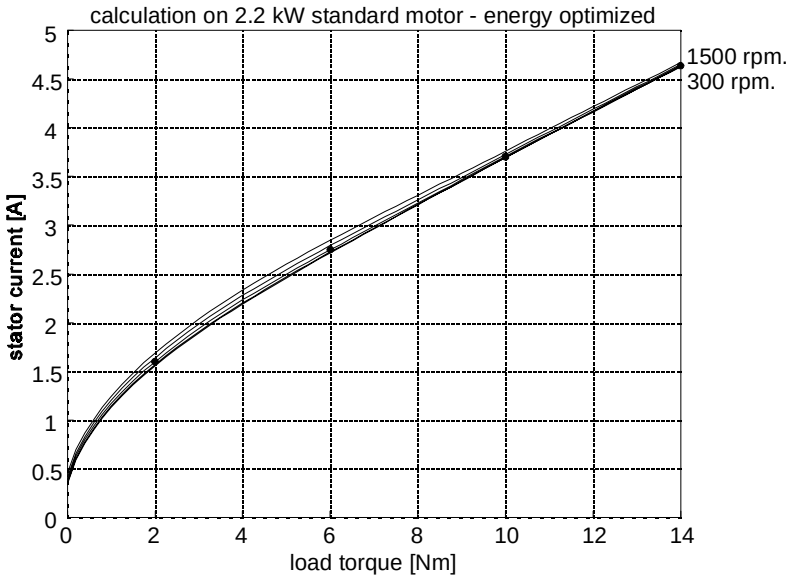

Figure 4.26: *Stator current as function of load torque in case of optimal system efficiency. The dots denote operating points which are analyzed further in Figure 4.27.*

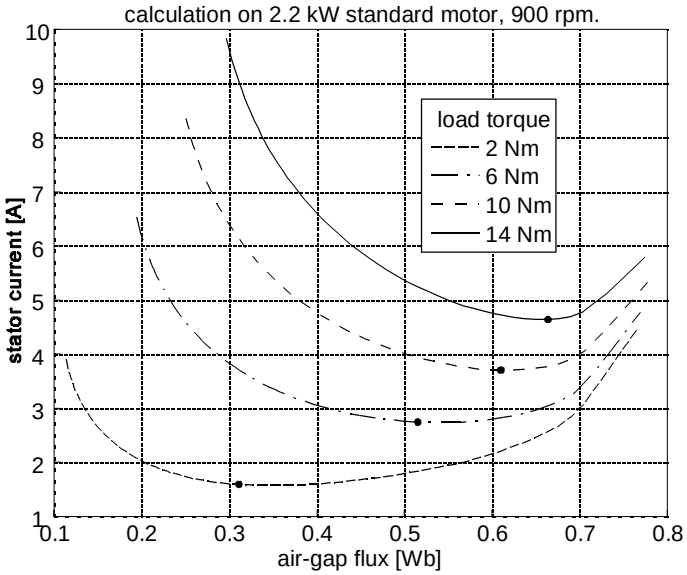

Figure 4.27: *Stator current as function of air-gap flux, for the four operating points in Figure 4.26. The dots denote the points of optimal system efficiency.*

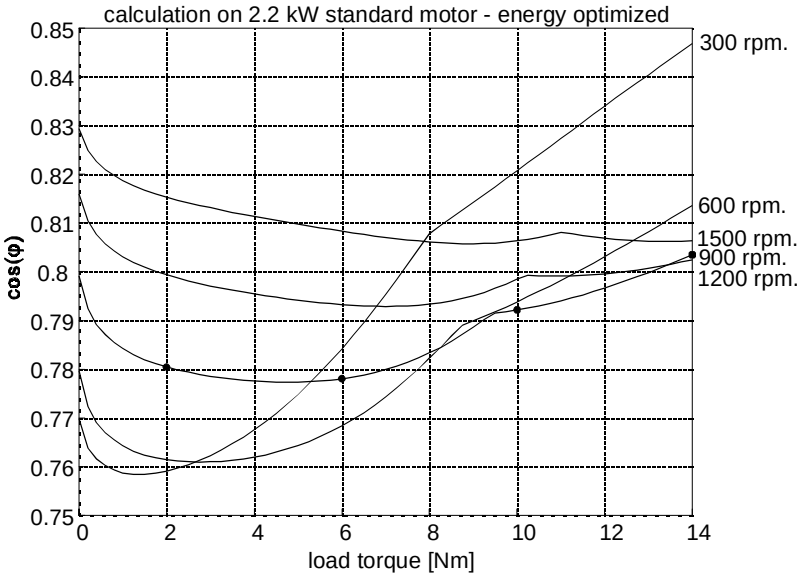

Figure 4.28: *Calculated cos(φ) as function of load torque in case of optimal system efficiency. The dots denote operating points which are analyzed further in Figure 4.29.*

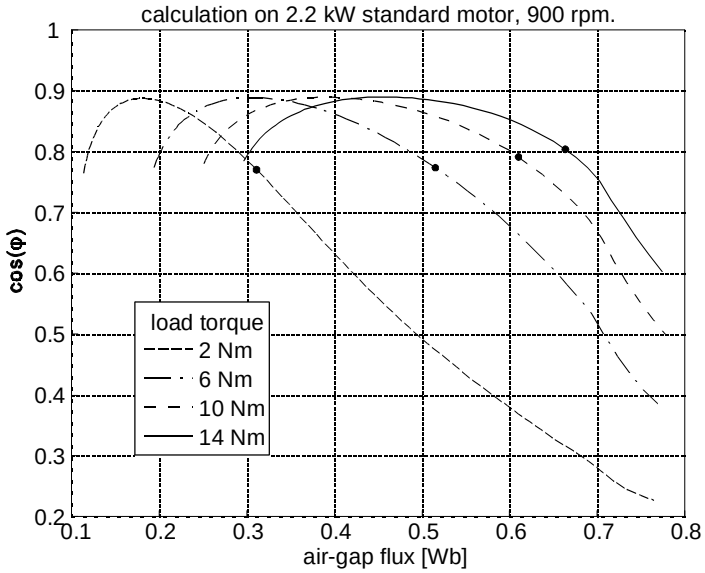

Figure 4.29: *Calculated cos(φ) as function of air-gap flux, for the four operating points in Figure 4.28. The dots denote the points of optimal system efficiency.*

The displacement power factor, cos(φ), is kept rather constant in case of optimized efficiency, Figure 4.28, although there are some deviations. But when these deviations are combined with Figure 4.29, it is obvious that the steepness of cos(φ) as function of air-gap flux means that the deviation in cos(φ) from a constant value has only little effect on the air-gap flux and efficiency. It is probably not worth trying to model the optimal cos(φ)-reference

as function of speed and load, partly because the improvement would be small and partly because it would complicate the control compared with constant displacement power factor control.

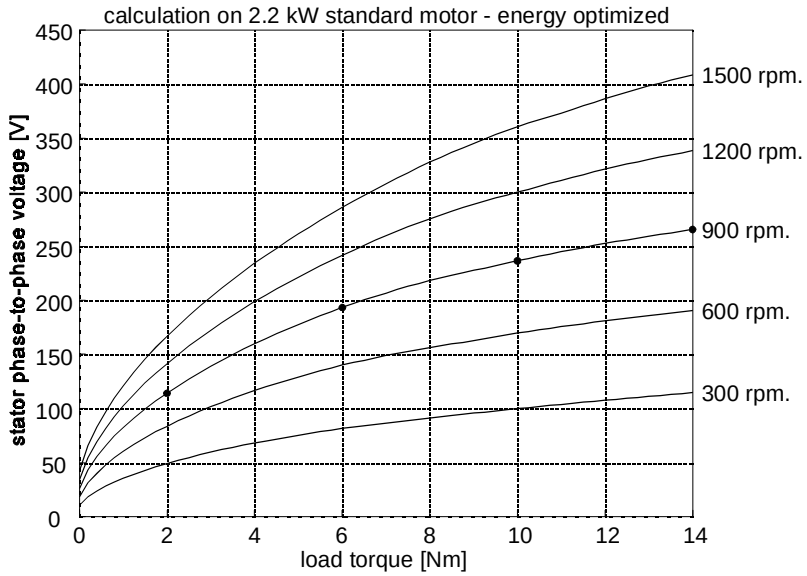

Figure 4.30: *Calculated stator voltage as function of load torque in case of optimal system efficiency. The dots denote operating points which are analyzed further in Figure 4.31.*

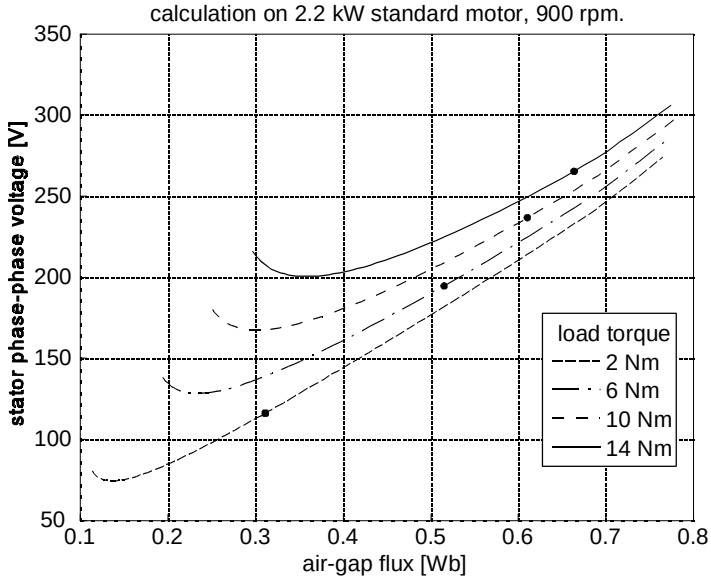

Figure 4.31: *Calculated stator voltage as function of air-gap flux, for the four operating points in Figure 4.30. The dots denote the points of optimal system efficiency.*

The curves on Figure 4.30 and Figure 4.31 show that flux reduction at low load, of course, is done by reduction the stator voltage. But it is not obvious to use the stator voltage as a direct parameter to control in energy optimal control.

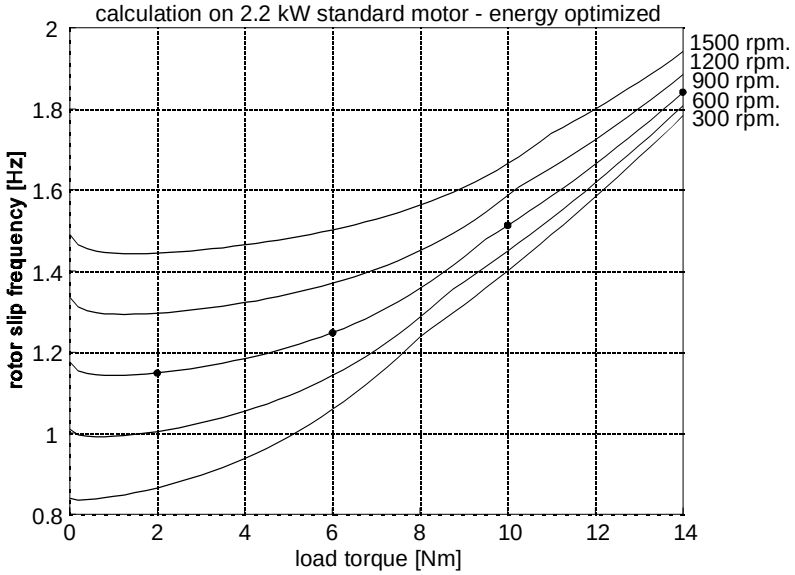

Figure 4.32: *Calculated slip frequency as function of load torque in case of optimal system efficiency. The dots denote operating points which are analyzed further in Figure 4.33.*

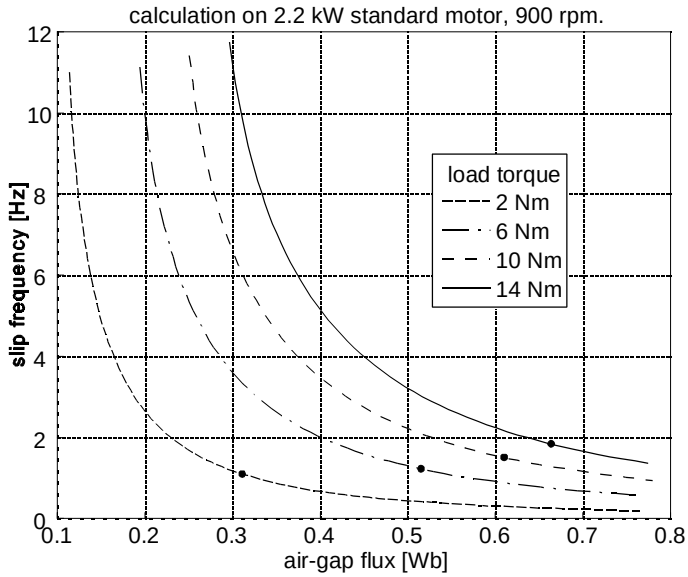

Figure 4.33: *Calculated slip frequency as function of air-gap flux, for the four operating points in Figure 4.32. The dots denote the points of optimal system efficiency.*

The value of slip frequency with optimal efficiency on Figure 4.32 varies with both speed and load, and when it is combined with Figure 4.33 it is seen that energy optimal control realized by setting a constant slip frequency reference does not yield a satisfactory performance in terms of efficiency. The reference value would have to be both speed and load dependent.

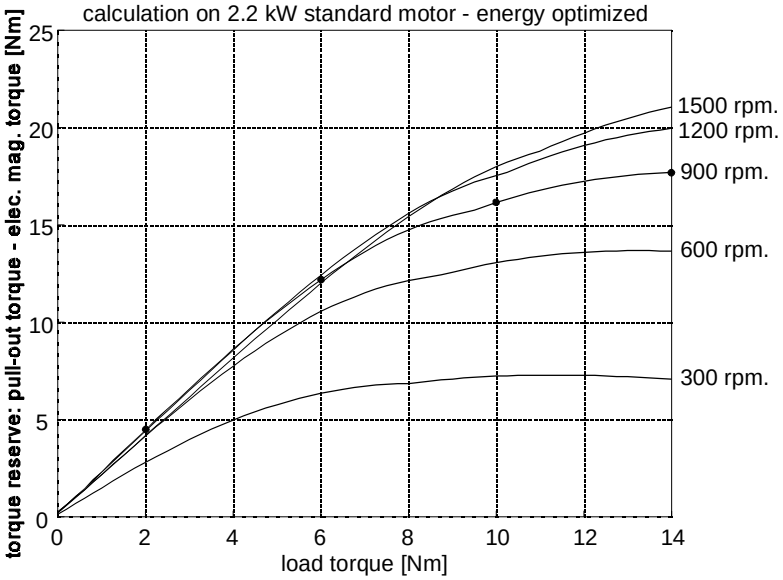

Figure 4.34: *Calculated torque reserve as function of load torque in case of optimal system efficiency. The dots denote operating points which are analyzed further in Figure 4.35.*

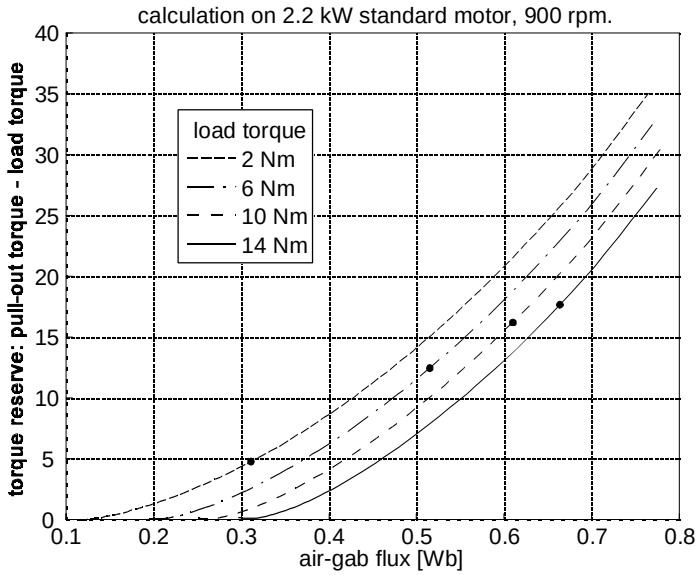

Figure 4.35: *Calculated torque reserve as function of air-gap flux, for the four operating points in Figure 4.34. The dots denote the points of optimal system efficiency.*

By the torque reserve on Figure 4.34 and Figure 4.35 is meant the difference between pull-out torque and developed electro-magnetic torque in a given operating point. When the torque reserve is zero the motor is on the edge of pulling out. When the flux is reduced, the torque reserve is diminished as well, making the drive more sensitive to load disturbances. The problem is most serious at low speed. For example at 300 rpm. and at 4 Nm load torque the reserve is 5 Nm, which means that the motor can not withstand nominal load if stator voltage

and stator frequency are kept unchanged. This emphasizes the need for load monitoring and fast reaction in case of sudden load disturbances.

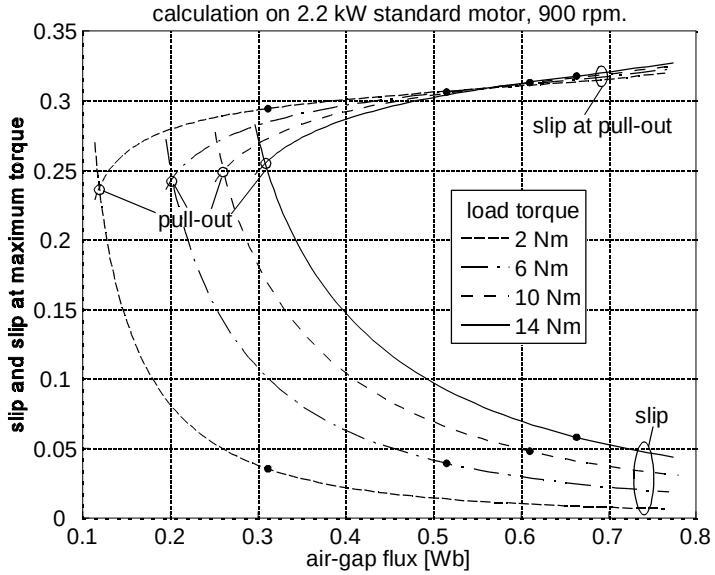

Figure 4.36: *Slip as function of load torque in case of optimal system efficiency. The dots denote the points of optimal system efficiency.*

Figure 4.36 illustrates, in a given load point, how far the motor is from pulling out, namely when the slip equals the slip at pull-out. It is seen that at optimal efficiency the motor does not come near that point, so if the load torque is remaining constant, the motor is not in danger of pulling out with optimized efficiency. Stability is investigated more closely in Chapter 8.

4.4 Summary.

It is quantified by measurement on 2.2 kW standard and high-efficiency motor drives how much energy optimal control can improve the system efficiency compared with constant air-gap flux control. For the standard motor drive the loss was reduced with 26-36 % at 0.25 p.u. load torque. This is mainly due to reduction of motor losses, and to a much lesser extent reduction of converter losses. For the high-efficiency motor drive the loss was correspondingly reduced with 23-31 %, so energy optimal control has a more positive effect on standard motors than on high-efficiency motors.

With steady-state converter and motor models verified by the experiments, calculations were done on the motor drive under optimized efficiency conditions. The following general observations were made for a 2.2 kW drive:

- As the efficiency vs. air-gap flux curves are quite flat near optimal efficiency, it is not important in energy optimal control to hit the commanded air-gap flux with high precision.
- When the system loss is minimized, both motor and converter losses are nearly minimized individually as well.
- With flux reduction at low load the motor becomes more sensitive to load disturbances, especially at low speed. The energy optimal controlled drive must have load monitoring and fast reaction on load disturbances in order to avoid instability.
- If the load remains constant, there is no risk that the energy optimally controlled motor should pull out.

The following observations were made with regard to development of energy optimal control strategies:

- It is easier to use stator current than input power as minimized variable for search control, and the results are almost identical in terms of efficiency.
- Displacement power factor control seems to be a good and simple energy optimal control method.
- Energy optimal control by setting a stator current reference value, for example being linearly dependent on load torque, may give problems, although simple at first sight.
- Energy optimal control by setting a constant slip frequency value does not seem promising in terms of efficiency. The reference value must be made a function of speed and load torque.
- If the drive losses are known throughly, a simple method is to set the air-gap flux directly, being a function of speed, and load torque or stator current.

These possibilities and other are analyzed further in the next chapter.

References.

[1] F. Abrahamsen “Energy Optimal Control Strategies for Electro Motors, low-cost and sensorless PWM-VSI based induction motor control”, Aalborg University, Denmark, ISBN 87-89179-23-4, 1998.

Chapter 5

Development of Energy Optimal Control Strategies

The review in chapter 2 listed a number of energy optimal control strategies, and the analysis in chapter 4 revealed both possibilities and problems regarding some of these. This chapter contains a deeper analysis and discussion of different possibilities for realizing energy optimal control.

As stated in chapter 1, the requirement is that energy optimal control is made for low-cost drives, which implies that a minimum of extra sensors should be used. Measurement of speed and load torque is definitely not possible, and measurement of input power is not wished either. But in for example pump applications the pump pressure may be fed back and used in closed loop pressure control. In such a case the measured pressure provides information of the load that enables to use the search control algorithms. Search control is therefore also investigated here.

One energy optimal control strategy can be implemented in varius ways, depending on how the motor is controlled. The possibilities include scalar voltage control, scalar current control and field-vector oriented current control. As the main application here is HVAC, where dynamic performance is not important, it is chosen to use a simple scalar voltage controlled drive, see Figure 5.1. The air-gap flux loop on the figure is not strictly necessary, but it eases the upper and lower limitation of the air-gap flux, on the other hand it slows down the response time for the stator voltage.

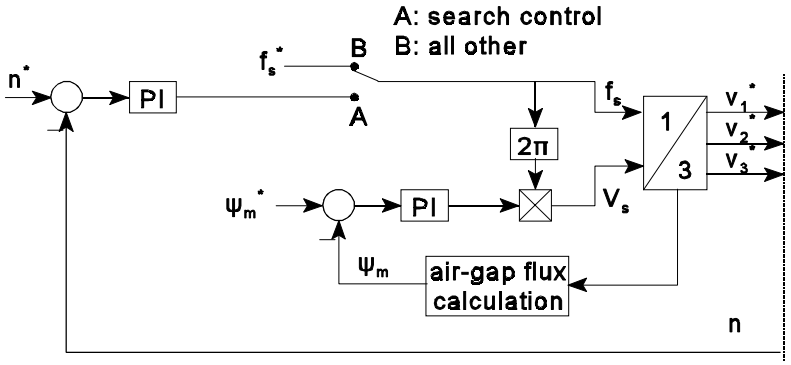

Figure 5.1: *Structure for the scalar drive control used to control the motor.*

The energy optimal strategies can be combined with either of the motor control principles, such as in chapter 6 where they are also implemented and tested in a rotor-flux oriented vector controlled drive. Only combination with a scalar current controlled drive may be problematic. The reason is that in the point of optimal efficiency the stator current is close to a minimum, and as the motor is current controlled, the current is commanded by a current reference set by the energy optimal control. If the reference in that case is set just slightly too low, the motor will not be able to produce the required torque and will pull out. A scalar current controlled drive is never used without a voltage or a speed feedback control loop [1, p. 68].

The following investigation is divided into three categories: simple state control, model-based control and search control.

5.1 Simple State Control.

Several methods of simple state control are already mentioned in chapter 2 and chapter 4:

- Slip frequency control.
- Direct control of air-gap flux as function speed, and of load torque or stator current.
- Displacement power factor control.

The problem with the slip frequency control is primarily that it is only simple in the absence of magnetic saturation and of core losses. Otherwise the slip frequency reference should be speed and load torque dependent, as shown in Figure 4.32.

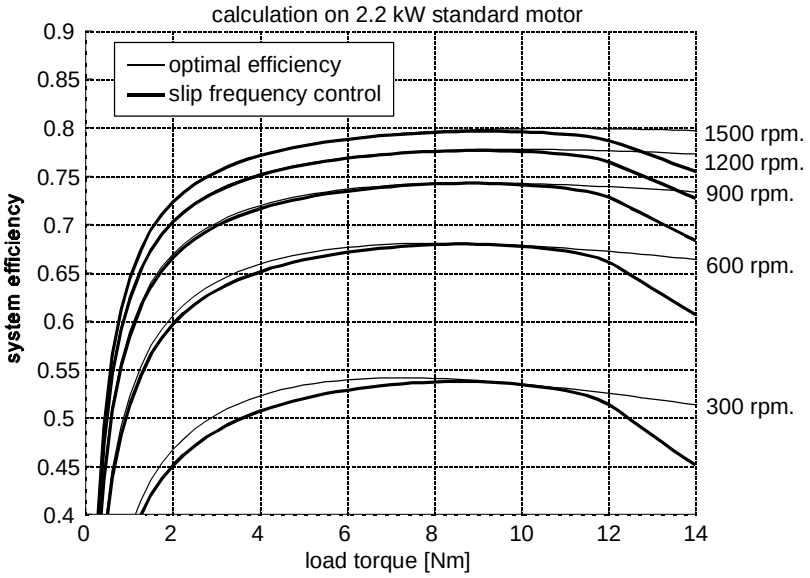

Figure 5.2: *Calculated system efficiency with slip frequency control (thick lines). The slip frequency reference is 1.4 Hz. The thin lines are the true optimized system efficiency.*

As an example of how poor a performance is obtained when a constant slip frequency is set as reference, the efficiency curves are shown on Figure 5.2 for a saturated motor. The slip frequency reference is set to 1.4 Hz, which is an approximate mean value of the curves on Figure 4.32. At high load, where the motor saturates, the efficiency is degraded to a degree which is not acceptable.

There are basically two categories of simple state control: those which require speed and load information, and those which do not. The slip frequency control clearly belongs to the last category, as the system efficiency could be improved by making the slip frequency reference a function of speed and load. The direct air-gap flux control also requires speed and load information for calculation of the air-gap flux reference. For both of these energy optimal control methods the speed and load do not have to be calculated very precisely, because the efficiency is not very sensitive to small variations in air-gap flux near optimal efficiency. In fact, a simple estimation of load and speed is sufficient for that purpose. But for the slip frequency controlled drive, a precise speed measurement is necessary to control the slip in closed loop, so this method is not advantageous and not investigated further here.

Displacement power factor control belongs to the category of simple state controls which is in the fortunate situation of not requiring neither speed nor load information. Analysis in chapter 4 showed that constant cos(φ) control will give a good efficiency performance, and is therefore also chosen for further investigation.

5.1.1 Direct Air-Gap Flux Control.

Air-gap flux references which yields optimal system efficiency are calculated off-line as function for speed and load torque, see Figure 4.25 and Figure 5.3 (thin lines). The control strategy where the air-gap flux is a function of stator current instead of load torque is not treated here, but it provides similar results. For on-line operation the approximate values, calculated by equation (5.1) and shown on Figure 5.3 with thick lines, are used as references.

$$\begin{aligned} \psi_{m,1500} &= -0.001835094 \cdot \tau_{est}^2 + 0.060535183 \cdot \tau_{est} + 0.159041338 \\ \psi_{m,opt} &= \psi_{m,1500} + 19.44 \cdot 10^{-6} \cdot (1500 - n_{est}) \cdot (4.5 - 0.35 \cdot |\tau_{est} - 4.5|) \end{aligned} \qquad (5.1)$$

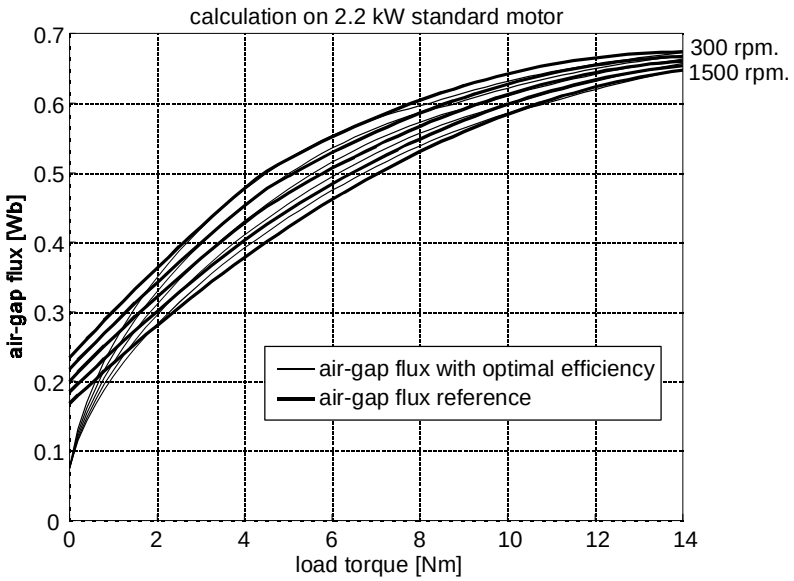

Figure 5.3: *Thin lines: air-gap flux values which optimizes system efficiency. Thick lines: approximated values calculated by equation (5.1). Speeds: 300, 600, 900, 1200, 1500 rpm.*

A schematic overview of the implementation is shown on Figure 5.4. The estimated torque and speed are calculated by use of the motor model. In order to ensure a smooth air-gap flux reference signal in case of transients, the calculated optimal air-gap flux needs to be filtered. The stator currents are filtered with a 5 Hz digital 1st order filter, and the air-gap flux reference is filtered with a 1 Hz 1st order digital filter.

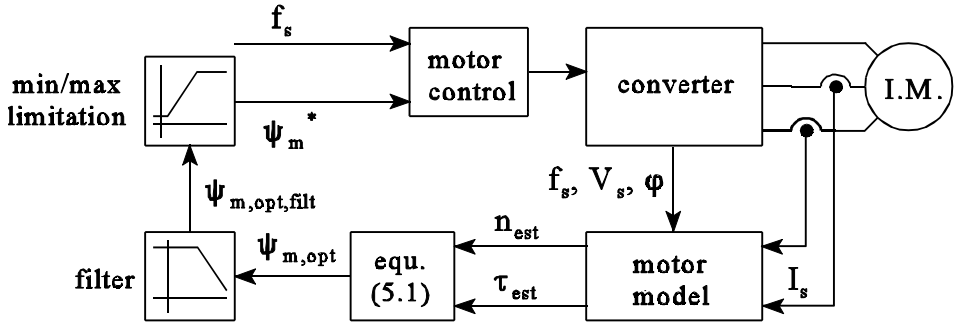

Figure 5.4: *Scheme for energy optimal direct air-gap flux control.*

The resulting system efficiency is shown on Figure 5.5, from which it is seen that there is almost no difference between the optimal efficiency and the efficiency obtained by energy optimal control.

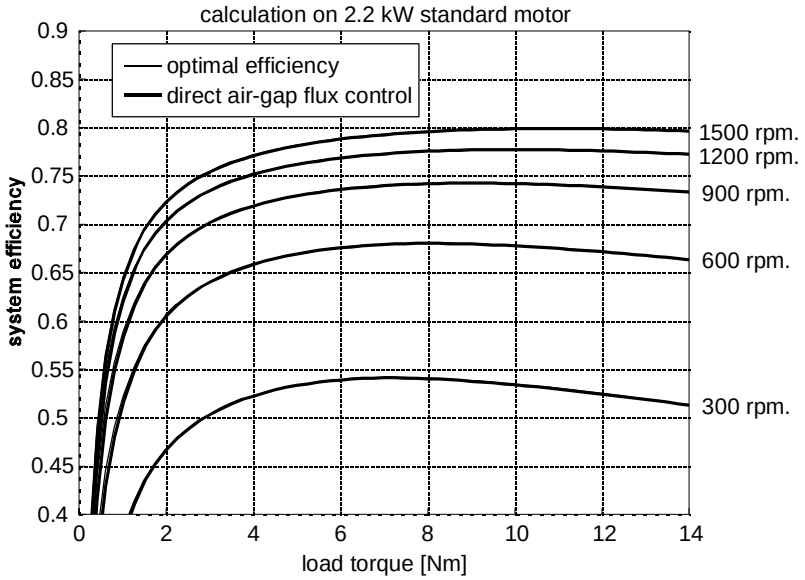

Figure 5.5: *Calculated system efficiency with direct air-gap flux control (thick lines). The thin lines are the true optimized system efficiencies.*

5.1.2 Displacement Power Factor Control.

The scheme for this very simple energy optimal control strategy is shown on Figure 5.1 for a scalar drive. The phase shift angle is calculated in each sampling period in the two-axis domain as the angle between the stator voltage reference and the measured stator currents. The error between the measured displacement power factor and the reference is eliminated with a PI controller.

It is not easy to set up a transfer function for the motor with air-gap flux as input and cos(φ) as output, so the cos(φ) controller is tuned in a simplified way. As the stator currents are filtered with a 5 Hz filter, the dynamics of the whole system is dominated by the slow filter. The cos(φ) controller is therefore dimensioned by ignoring the time constants in the motor and considering only the current filter. Afterwards the controller is fine-tuned by trial and error in order to optimize the dynamic performance. The calculated motor efficiencies with cos(φ) control are shown on Figure 5.7. The nominal cos(φ)=0.81 is set as reference in the whole operating area. It could be chosen to set the value a bit lower, for example to 0.78, which would assure a slightly higher flux at low load and less sensitivity to load disturbances, without changing the efficiency much. The air-gap flux should then be limited to the nominal value in order to avoid a stator current higher than the nominal value at nominal load.

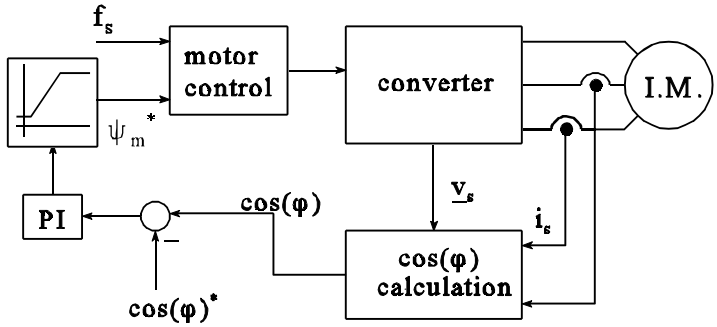

Figure 5.6: *Scheme for energy optimal cos(φ) control in a scalar drive.*

A load disturbance is detected by observing the measured air-gap flux and its reference value. If the air-gap flux is more than 0.02 Wb below its reference value, it is interpreted as a large load disturbance, and then the air-gap flux is reset to its nominal value.

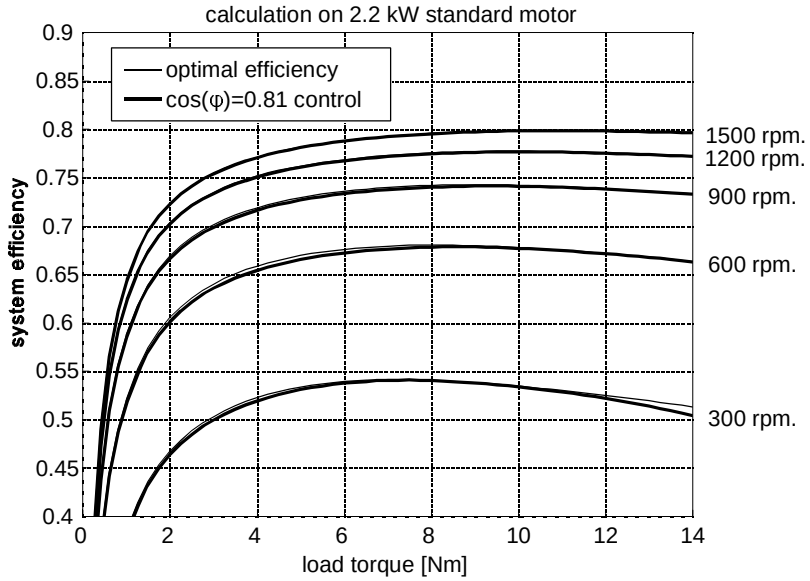

Figure 5.7: *Calculation of system efficiency with cos(φ)=0.81 control (thick lines), compared with the optimized system efficiency (thin lines).*

5.2 Model-Based Control.

It is assumed that motor and converter model constants are known beforehand, including saturation of the magnetizing inductance, and the flux and frequency dependence of the core loss resistance. It was shown in chapter 4 that converter losses are not important in small drives compared with motor losses. Therefore motor losses are only considered here. In chapter 7 where medium-size drives are treated, the converter losses are included in the model-based energy optimal control.

Many of the model-based control strategies quoted in the state-of-the-art were not found useful for the application in this work. Those which were, are based on the rotor-flux oriented motor model, and the one which it is chosen to test here, has the advantage that it includes core losses, that is applies to both scalar drives and rotor-flux oriented drives, and that solution to the optimization problem is done by a PI-controller which may reduce calculations a bit. The method was presented in [2].

5.2.1 Derivation of the Optimal Solution.

The motor model which is used is shown on Figure 5.8. The model is the steady-state case of the transient rotor-flux oriented motor model, so the model includes all three phases of the motor. Core losses are represented in the model with a resistance in parallel with the rotor inductance. Except for a scaling factor, this model is equivalent to the single phase steady-state inverse-gamma motor model.

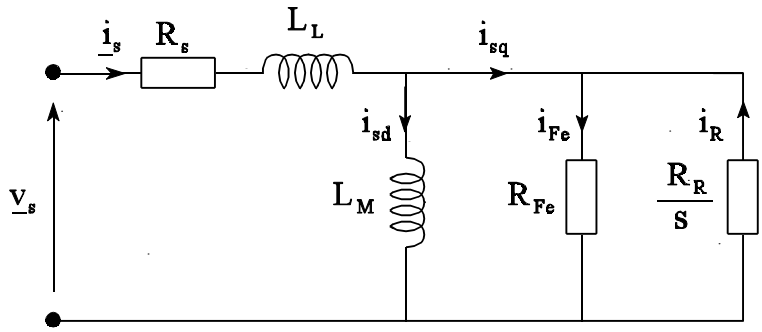

Figure 5.8: *Steady-state rotor-flux oriented model of the induction motor including core losses.*

Examining the rotor-flux oriented motor model on Figure 5.8 and using the power-invariant 3-to-2 axis transformation, it can be shown that the motor loss in steady state is equal to the sum of the following three components:

$$P_{loss,d} = \left(\frac{(\omega_s L_M)^2}{R_{Fe}} + R_s + (\omega_s L_M)^2 \frac{R_s}{R_{Fe}^2} \right) i_{sd}^2 \qquad (5.2)$$

$$P_{loss,q} = (R_R + R_s)\, i_{sq}^2 \qquad (5.3)$$

$$P_{loss,dq} = -2\,\omega_s L_M \frac{R_s}{R_{Fe}} i_{sd} i_{sq} \qquad (5.4)$$

where ω_s : stator angular velocity.
L_M : rotor-flux magnetizing inductance (equal to rotor inductance).

R_{Fe} : core loss resistance in parallel to rotor inductance.
R_s : stator resistance.
R_R : rotor resistance in the rotor-flux oriented model.
i_{sd} : d-axis stator current (field-producing in steady-state).
i_{sq} : q-axis stator current (torque-producing in steady-state).

The developed electro-magnetic torque is:

$$\tau_{em} = z_p L_M \; i_{sd} \; i_{sq} \tag{5.5}$$

where z_p : pole-pair number.

With the definition of A as

$$A = \frac{i_{sq}}{i_{sd}} \tag{5.6}$$

and combination with equation (5.5), the following is obtained:

$$i_{sq}^2 = A \; \frac{\tau_{em}}{z_p L_M} \quad , \quad i_{sd}^2 = \frac{1}{A} \; \frac{\tau_{em}}{z_p L_M} \quad , \quad i_{sd} i_{sq} = \frac{\tau_{em}}{z_p L_M} \tag{5.7}$$

Using equations (5.2)-(5.4) and (5.7) the total motor loss becomes

$$\begin{aligned} P_{loss} &= P_{loss,d} + P_{loss,q} + P_{loss,dq} \\ &= \frac{\tau_{em}}{z_p L_M} \left[\left[\frac{(\omega_s L_M)^2}{R_{Fe}} + R_s + (\omega_s L_M)^2 \frac{R_s}{R_{Fe}^2} \right] \frac{1}{A} + (R_s + R_R) A - 2 \omega_s L_M \frac{R_s}{R_{Fe}} \right] \end{aligned} \tag{5.8}$$

For a constant torque, the loss minimum is found by differentiating the loss expression with respect to A, and assuming that the model parameters are independent of A. This is not entirely true, because the magnetizing inductance and the core loss resistance depend on the flux level, which is contained in A. However, it is assumed initially that these errors can be ignored.

$$\begin{aligned} &\frac{\partial P}{\partial A} = 0 \\ &\Updownarrow \\ &-\left[(\omega_s L_M)^2 \frac{1}{R_{Fe}} + R_s + (\omega_s L_M)^2 \frac{R_R}{R_{Fe}^2} \right] \frac{1}{A^2} + (R_R + R_s) = 0 \\ &\Updownarrow \\ &P_{loss,d} = P_{loss,q} \end{aligned} \tag{5.9}$$

The motor losses thus reach a minimum when the motor loss depending on the current direct with the rotor flux is equal to the loss depending on the current in quadrature to the rotor flux. In [2] it is proposed to solve this equation with a PI-controller, as shown in Figure 5.9.

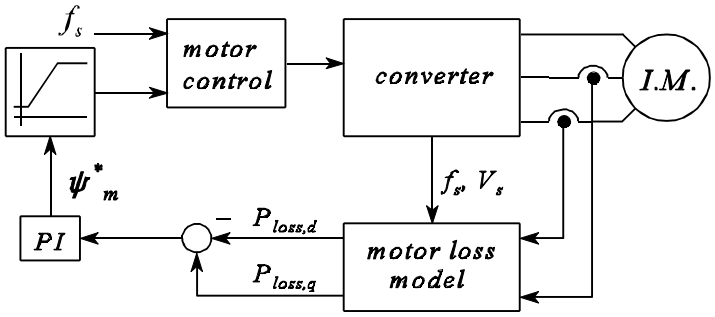

Figure 5.9: *Scheme for energy optimal model-based control.*

In a scalar drive there is not direct access to the rotor-flux oriented magnetizing and torque producing currents. The two loss components are then found by doing calculations on the single phase inverse-gamma motor model, see Figure 5.10.

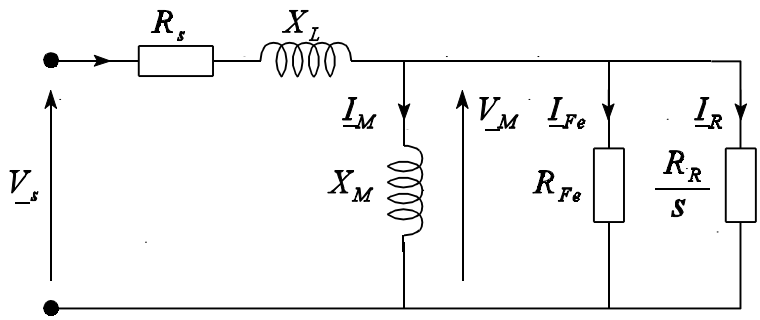

Figure 5.10: *Steady-state inverse-gamma single phase model of an induction motor.*

The relations between the inverse-gamma model parameters and the T-model parameters are:

$$\begin{aligned} R_R &= R_r(X_m/X_r)^2 \\ X_L &= X_s - X_m^2/X_r \\ X_M &= X_m^2/X_r \end{aligned} \qquad (5.10)$$

where X_m : magnetizing reactance of the T-model.
X_s : stator reactance of the T-model.
X_r : rotor reactance of the T-model.
X_M : magnetizing reactance of the inverse-gamma model.
X_S : stator reactance of the inverse-gamma model.
X_R : rotor reactance of the inverse-gamma model.
R_r : rotor resistance of the T-model.
R_R : rotor resistance of the inverse-gamma model.

The magnetizing voltage is

$$\underline{V}_M = \underline{V}_s - (R_s + jX_L)\underline{I}_s \tag{5.11}$$

The core loss resistance is

$$R_{Fe} = \frac{3V_M^2}{P_{core}} \tag{5.12}$$

where P_{core} : core loss.

The field producing current and the torque producing current are:

$$\underline{I}_M = \frac{\underline{V}_M}{jX_M} \tag{5.13}$$

$$\underline{I}_R = \underline{I}_s - \underline{I}_M - \frac{\underline{V}_M}{R_{Fe}} \tag{5.14}$$

The three loss components are then

$$P_{loss,d} = 3\left(R_R\left(\frac{X_M}{R_{Fe}}\right)^2 + R_s + \frac{X_M^2}{R_{Fe}}\right)I_M^2 \tag{5.15}$$

$$P_{loss,q} = 3(R_s + R_R)I_R^2 \tag{5.16}$$

$$P_{loss,dq} = 3z_p R_R \frac{X_M}{R_{Fe}} I_M I_R \tag{5.17}$$

The calculated motor efficiencies with the model-based control are shown on Figure 5.11. It is seen clearly that the result in not very good at high load and especially at low speed. Figure 5.12 shows that the calculated air-gap flux values are too high at high load. The reason is that at high load with saturation the differentiation in equations (5.9) does not hold because L_M and R_{Fe} do depend on A. It has not been possible to solve the differentiation analytically including saturation and core losses. In chapter 7 it is shown how the problem can be solved numerically.

One could argument, however, that the model-based control is acceptable for HVAC applications. The squares on the curves of Figure 5.11 indicate the operating points with a quadratic load, for example a ventilator. It is seen that in the region where it operates, the efficiency is near the optimal efficiency.

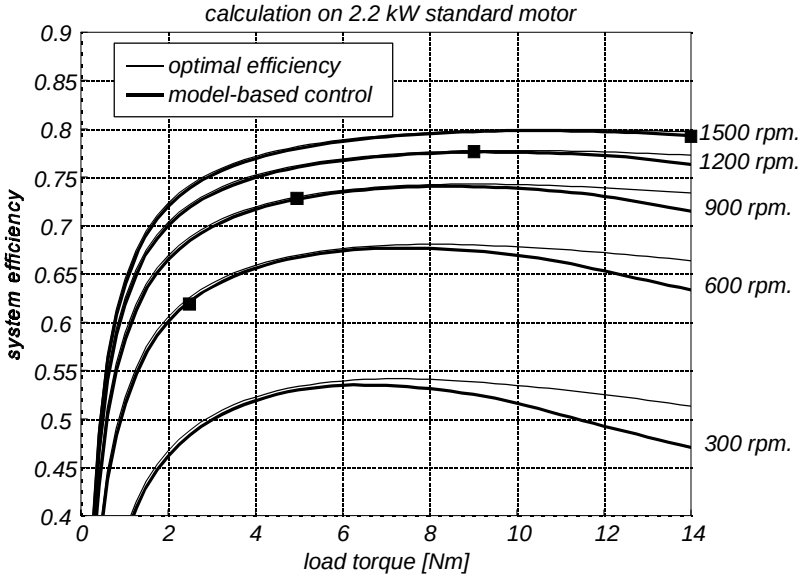

Figure 5.11: *Calculation of air-gap flux with model-based control without limit the air-gap flux. This is compared with the optimal motor efficiency air-gap flux. The squares denote load points of a HVAC application with a square load torque profile.*

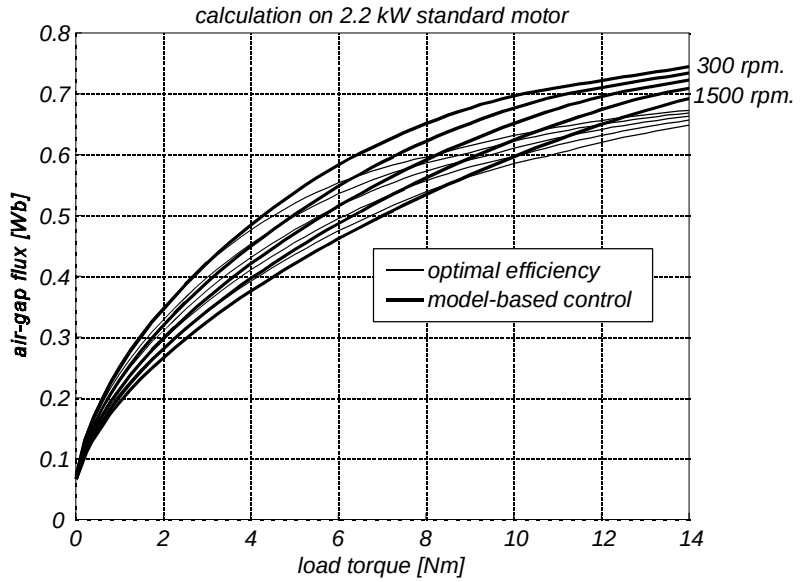

Figure 5.12: *Calculation of motor efficiency with model-based control without limit the air-gap flux. This is compared with the optimal motor efficiency.*

An easy way to compensate for the unacceptable error at high load could be to limit the air-gap flux to its nominal value. When doing that the results on Figure 5.13 and Figure 5.14 are obtained. The result is still not optimal, but clearly better than before.

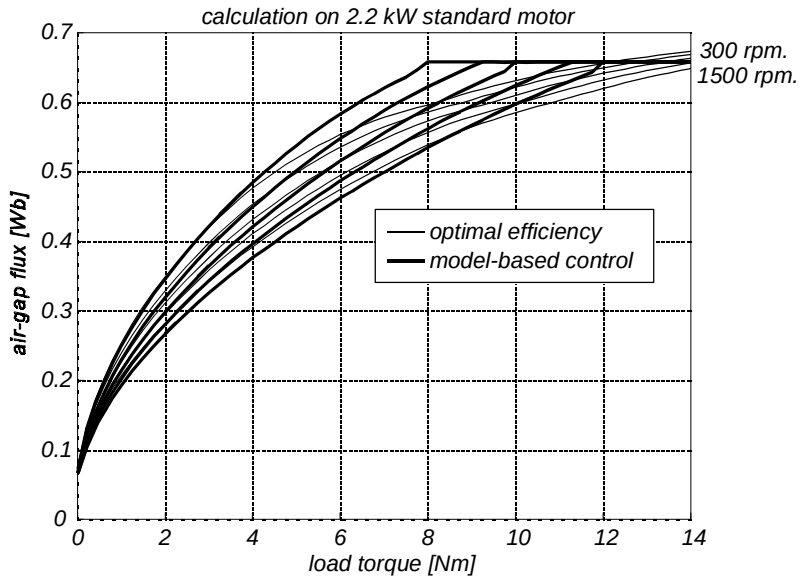

Figure 5.13: *Calculation of motor efficiency with model-based control, where the air-gap flux is limited to its nominal value. This is compared with the optimal motor efficiency.*

It is not straightforward to design the controller which equalizes the two loss components for a certain response-time. The reason is that as the loss changes heavily with load, the effective transfer function from air-gap flux to ($P_{loss,d}$-$P_{loss,q}$) changes likewise. A fast response-time is not a primary concern for energy optimal control, so therefore the controller is just tuned by trial and error and with a primitive gain-scheduling. The integration time of the PI-controller is constant while the gain of the PI-controller is made a linear function of stator frequency so the gain is high when the stator frequency is low.

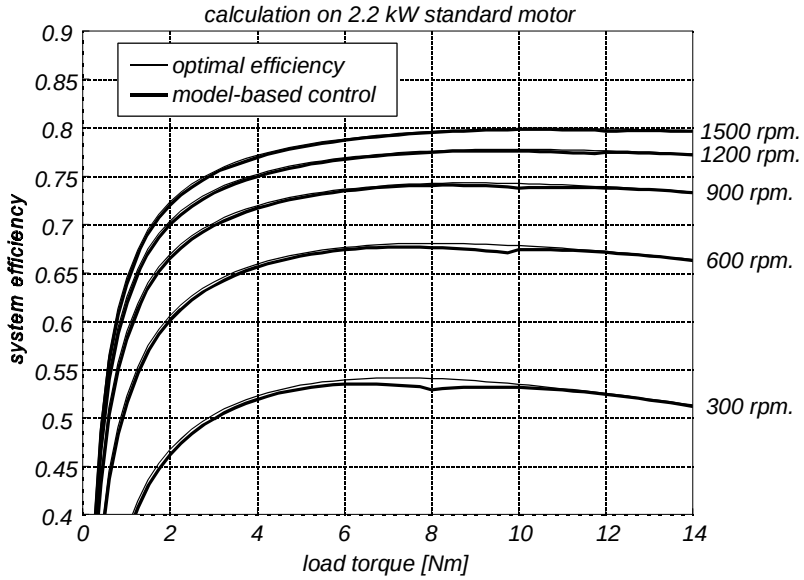

Figure 5.14: *Calculation of air-gap flux with model-based control, where the air-gap flux is limited to its nominal value. This is compared with the optimal motor efficiency air-gap flux.*

5.3 Search Control.

The search method only applies to systems with precise load information, in most cases obtained with a speed feed-back by assuming a constant load torque. This is of course not useful in most HVAC-applications where speed is not measured. But in some special application there is load information also in HVAC. In chapter 6 is an example with a pump-system, where the differential pressure over the pump is used a feed-back whereby search control is implemented without speed-feedback. Therefore search control is investigated here.

The principle of the search control is to keep the output power of the motor constant and to find the operating point where the input power has a minimum. This minimum is found by measuring the input power, and iteratively changing the flux level in small steps until the input power minimum is detected. The output power is normally kept constant by keeping the speed constant and assuming a constant load torque, see Figure 5.15.

Two search control schemes were reported in literature, as mentioned in Chapter 2: minimization on input power and minimization of stator current. The analysis in chapter 4 made it clear that current minimization is easier and costs less sensors, yet giving almost the same result as input power minimization.

The calculations in this chapter show the steady-state efficiency performances. The dynamic experimental performances are shown in chapter 6. The fuzzy-logic approaches which have been reported recently are not considered here.

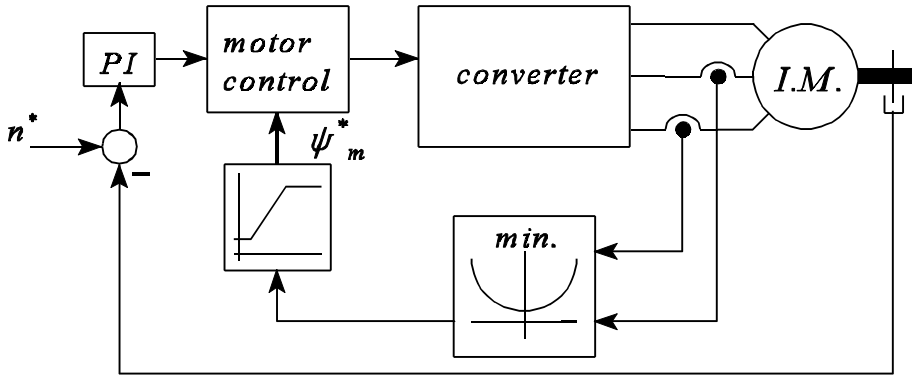

Figure 5.15: *Scheme for energy optimal search control with stator current minimization.*

The main advantage of the search method is that the point of optimal efficiency is found without knowledge of motor or converter parameters. The major disadvantage is that the speed should be measured. Typically the convergence time to find the point with minimal losses is not less than 4 s, so the method is unusable if the load is changing more often than that. A problem is that the input power as a function of air-gap flux is very flat near the point of optimal efficiency, so the power measurement must be very precise and noiseless.

In this project it is chosen to implement the search control in the following way. The air-gap flux is initially stepped with a fixed step. Once a minimum is detected and the air-gap flux is increased again, the air-gap flux step size is reduced with 25%, and every time the direction of the step is changes, the step size is reduced. The minimum step size is 25% of the initial step size. The parameters which have to be tuned by trial and error are:

- initial step size.
- time period between each step.
- Tolerances in speed for detection of load disturbances.
- Bandwidth and order of filters for input power and stator current.

Figure 5.16 and Figure 5.17 show the calculated system efficiencies for minimized stator current and minimized inverter input power, respectively. In the first case there is a difference between the optimized and obtained efficiency a low load and high speed. In the rest of the area, and also in the second case, the steady-state performance is very good.

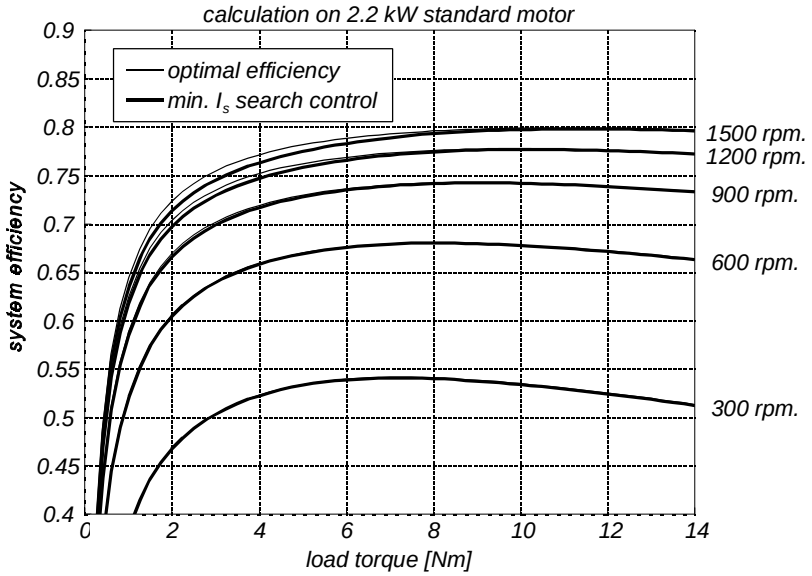

Figure 5.16: *Calculation of system efficiency with minimum stator current search control, compared with the optimized system efficiency.*

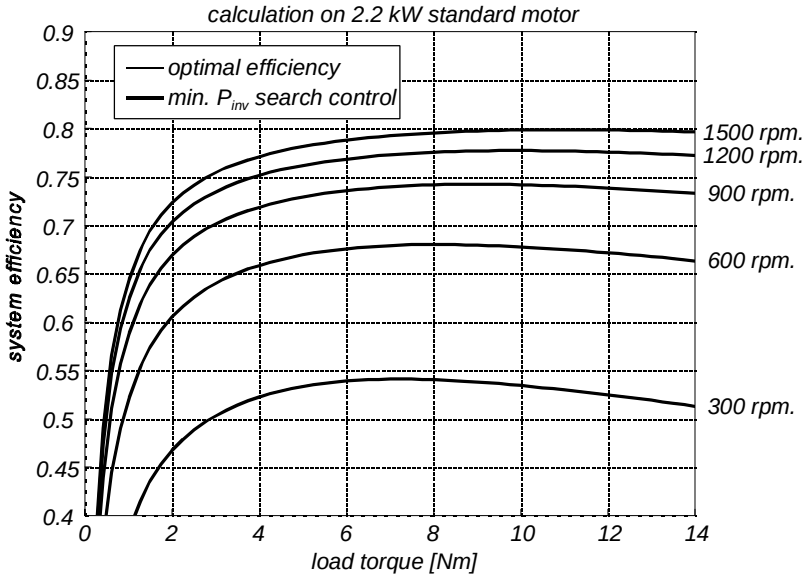

Figure 5.17: *Calculation of system efficiency with minimum inverter input power search control, compared with the optimized system efficiency.*

5.4 Summary.

As this thesis focuses on drives for HVAC applications, it is chosen to implement the energy optimal control in a scalar drive without speed measurement. When search control is considered anyway it is because there are special applications where the required speed measurement can be replaced by for example an existing pressure measurement for a pump applications, see section 6.3.

With regard to simple state control it was found that constant slip frequency control, contrary to what has been reported in many papers, does not give a satisfactory result. In fact, constant slip frequency does only guarantee minimized losses when neither magnetic saturation nor core losses exist, and neither is true for commercial motors. The method of setting the air-gap flux directly, being a function of speed, and torque or stator current, is simple and provides good result. But, of course, it requires good knowledge of the motor parameters. The displacement power factor control was analyzed by setting the reference value to the nominal value, and calculations showed good results.

A model-based control method in which the losses associated with the torque producing current are equalized with the losses associated with the field producing current was analyzed. The derivation of the analytical solution to the optimization problem was solved by disregarding the magnetic saturation, like it has been reported in literature. This, however, appeared to give a solution which is not satisfactory, as it produces an air-gap flux at high load which is well above the optimal air-gap flux value. The problem is here solved simply by

limiting the air-gap flux to its nominal value, and the result is, if not satisfactory, then acceptable.

Both input power minimizing and stator current minimizing search control show good results with regard to steady-state efficiency.

It is chosen to implement and test the direct air-gap flux control, displacement power factor control, model-based control with limitation of air-gap flux, stator current and input power minimizing search control. Especially it is important to test the dynamical performances which were not investigated in this chapter.

Reference.

[1] M. P. Kazmierkowski, H. Tunia, "Automatic Control of Converter-Fed Drives", Elsevier, 1994, ISBN 0-444-98660-X.

[2] K. S. Rasmussen, P. Thøgersen, "Model Based Energy Optimizer for Vector Controlled Induction Motor Drives", Proceed. of EPE'97, Trondheim, pp. 3.711-3.716.

Chapter 6

Test of Energy Optimal Control Strategies

The energy optimal control strategies which were treated in the previous chapter are now tested experimentally. The control strategies are:

- Direct air-gap flux control.
- Displacement power factor control, $\cos(\varphi)=0.81$.
- Model-based control with limitation of the air-gap flux to the nominal value.
- Stator current minimizing search control.
- Inverter input power minimizing search control.

The first test is steady-state measurement of efficiencies in the whole operating area. Next the dynamic performances are tested, both when implemented in a scalar drive and when implemented in a rotor-flux oriented vector controlled drive. At last the energy optimal control strategies are tested in a realistic pump system.

6.1 Steady-State Test of Energy Optimal Control.

6.1.1 Experimental Setup.

The tests are made with the setup on Figure 6.1. The motor drive is tested at three speeds: 300, 900, 1500 rpm., and at seven different load torques: 2, 4, 6, 8, 10, 12, 14 Nm. The speed is during the tests controlled by the induction motor drive. The speed is measured, and with a closed speed loop, the speed is controlled by adjusting the stator frequency. The induction motor is loaded with a permanent-magnet synchronous machine, and the load torque is controlled in closed loop by the computer PC2 on Figure 6.1.

PC2 is connected to the Norma Power Analyzer and acquires all measured values: speed, torque, stator voltage, stator current, power factor, and power at the input and at the output of the converter. The input to the converter is measured with a 2-watt-meter method, and the output of the converter is measured with a 3-wattmeter method, using the motor neutral as the fourth wire.

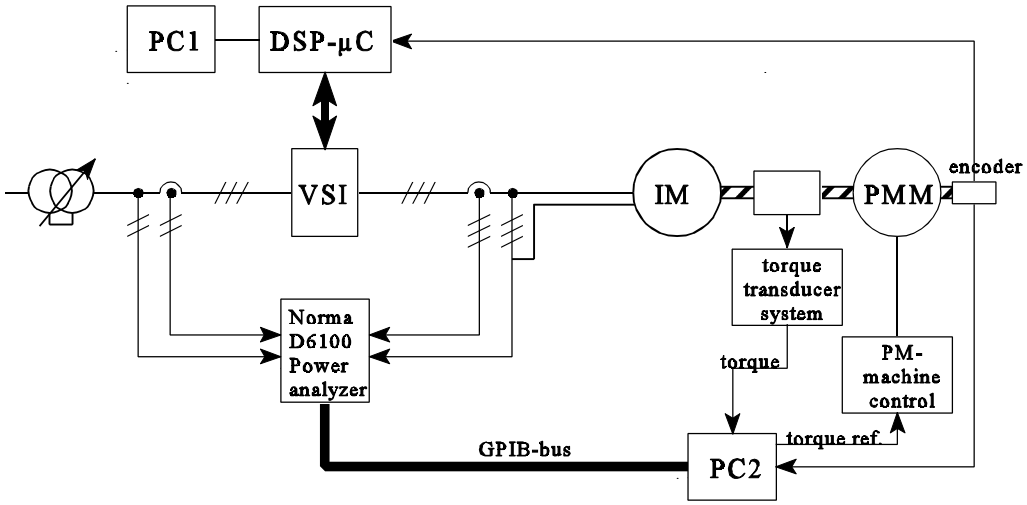

Figure 6.1: *Experimental setup for measurement of the motor drive efficiency.*

The measurement procedure is the following: the motor runs for an hour at 300 rpm. and 14 Nm until it is warm. The first measurements are made at 14 Nm, and with first 300 rpm., then 900 rpm. and at last 1500 rpm. Then the load is reduced to 12 Nm, the measurements are made at the same three speeds. The procedure is followed down to 2 Nm. Making the measurements in this way, the first measurement is made where the motor is warmest and the last one is made when it is coldest. As the measurement in each operating points lasts around 10 min., it is reasonable to make all the measurements continuously without waiting for the temperature to stabilize.

The induction motor is controlled with scalar control according to the schemes shown previously in chapter 5, and the switching frequency is 5 kHz. The measurements can not be compared directly with the measurements in chapter 4. One reason is that the motor is not the same, although it is the same motor type. But as there may be a small difference from motor to motor due to tolerances in manufacturing, the measurements are not exactly comparable. Another reason is that the measurements in chapter 4 were made with an inverter with filter chokes at the output, and the measurements in this chapter are made with the filter chokes taken out of the inverter. This means that filter choke losses in the inverter are eliminated and that the output voltages contain a higher content of harmonics which will generate additional losses in the motor. It is, however, probable that the additional motor losses are so small that they are not measurable.

6.1.2 Measured Motor and Converter Losses.

The measured motor losses are shown on Figure 6.2 for all six control strategies. The motor loss highly depends on both speed and load torque. There are only small differences between the losses for the five energy optimal control strategies, whereas the difference for the constant flux control is clear at low load.

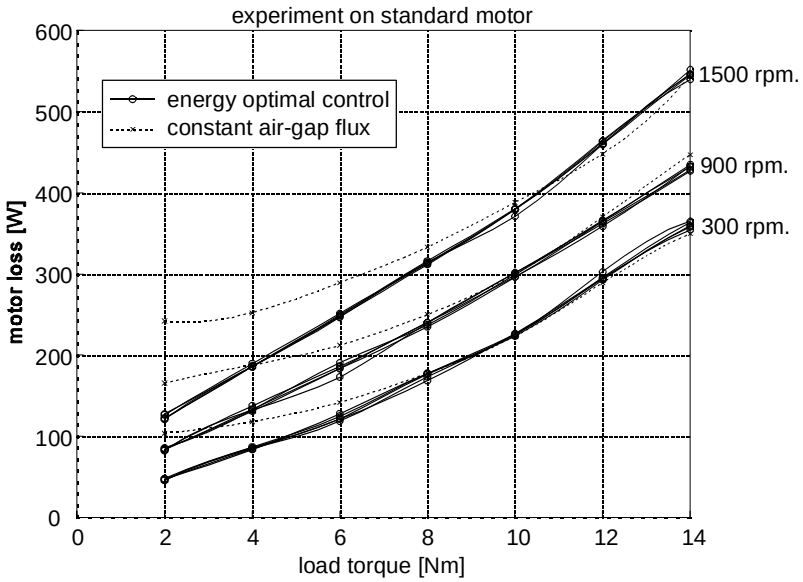

Figure 6.2: *Experiments on standard motor at 300, 900 and 1500 rpm. Measured motor loss with all the five energy optimal control strategies and with constant air-gap flux control.*

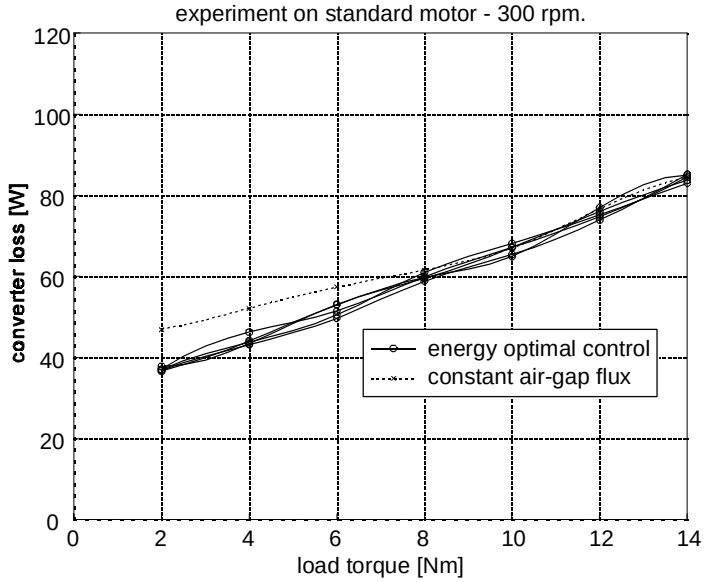

Figure 6.3: *Experiments on standard motor at 300 rpm. Measured converter loss with all the five energy optimal control strategies and with constant air-gap flux control.*

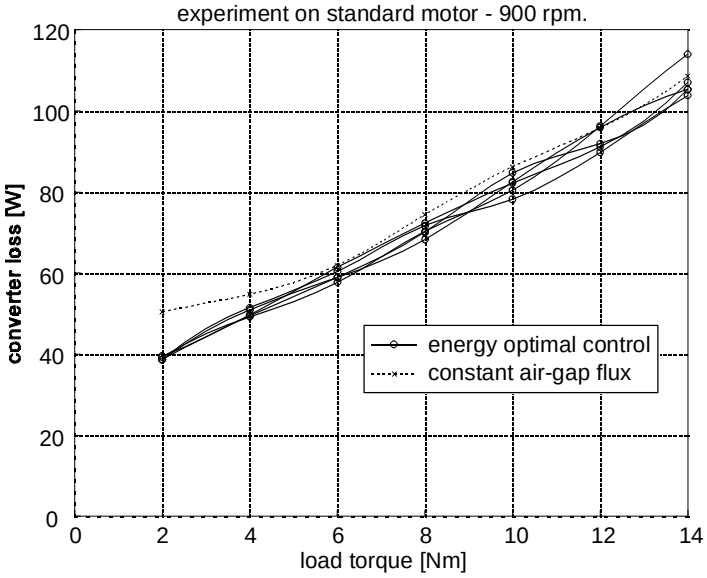

Figure 6.4: *Experiments on standard motor at 900 rpm. Measured converter loss with all the five energy optimal control strategies and with constant air-gap flux control.*

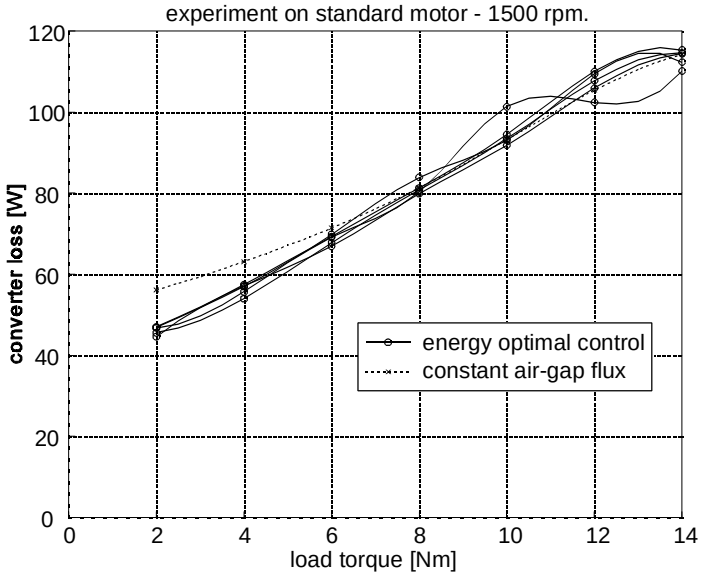

Figure 6.5: *Experiments on standard motor at 1500 rpm. Measured converter loss with all the five energy optimal control strategies and with constant air-gap flux control.*

The converter losses are shown on Figure 6.3 - Figure 6.5 for all six control strategies. The converter loss mostly depends on load torque and to a smaller degree on the speed. Comparing these figures with Figure 6.2 it is seen that the converter loss is 3-5 times smaller than the motor loss. The converter losses are slightly reduced at light load with energy optimal control. There is no remarkable difference between the losses for the five energy optimal control strategies.

6.1.3 Measured Motor Drive Efficiency.

The measurements for alle control strategies are shown in terms of system efficiency on Figure 6.6. The efficiency curves for the individual control strategies are shown on Figure 6.7 - Figure 6.11.

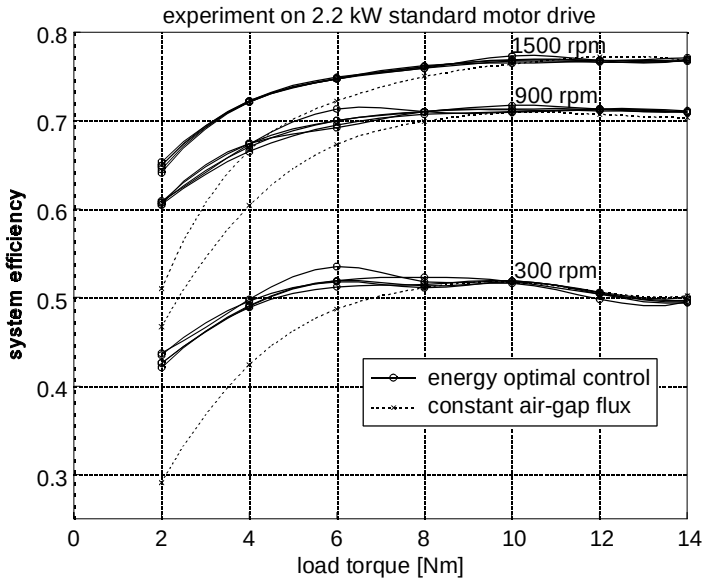

Figure 6.6: *Experiments on standard motor at 300, 900 and 1500 rpm. Measured drive efficiencies with all the five energy optimal control strategies and with constant air-gap flux control.*

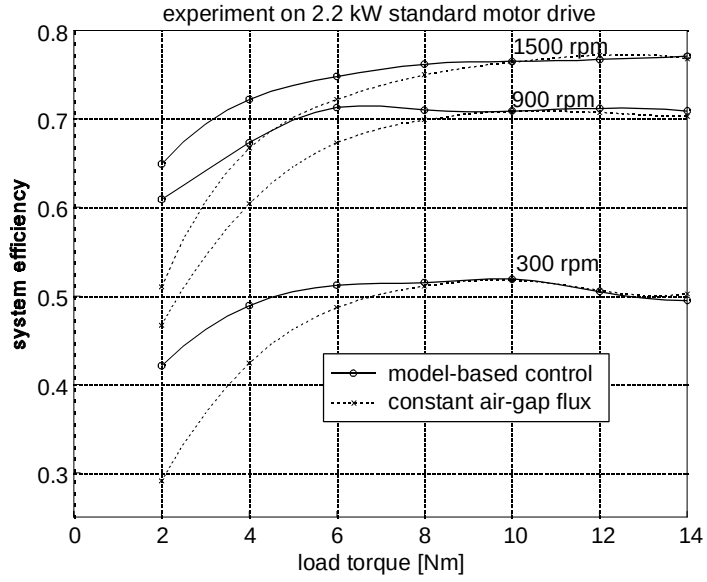

Figure 6.7: *Experiments on standard motor at 300, 900 and 1500 rpm. Measured drive efficiencies with model-based control and with constant air-gap flux control.*

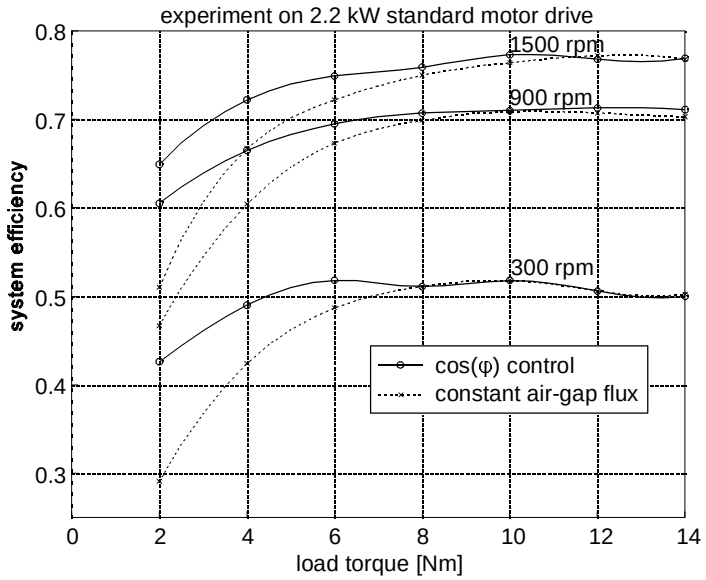

Figure 6.8: *Experiments on standard motor at 300, 900 and 1500 rpm. Measured drive efficiencies with cos(φ) control and with constant air-gap flux control.*

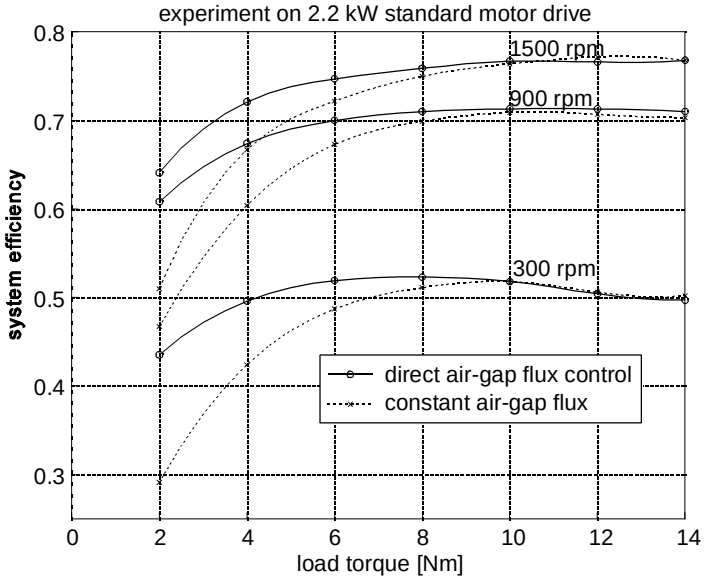

Figure 6.9: *Experiments on standard motor at 300, 900 and 1500 rpm. Measured drive efficiencies with direct air-gap flux control and with constant air-gap flux control.*

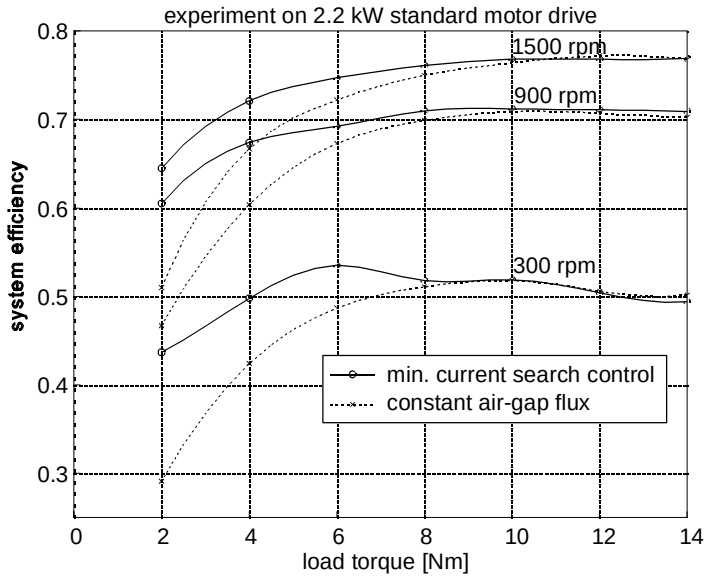

Figure 6.10: *Experiments on standard motor at 300, 900 and 1500 rpm. Measured drive efficiencies with stator current minimizing search control and with constant air-gap flux control.*

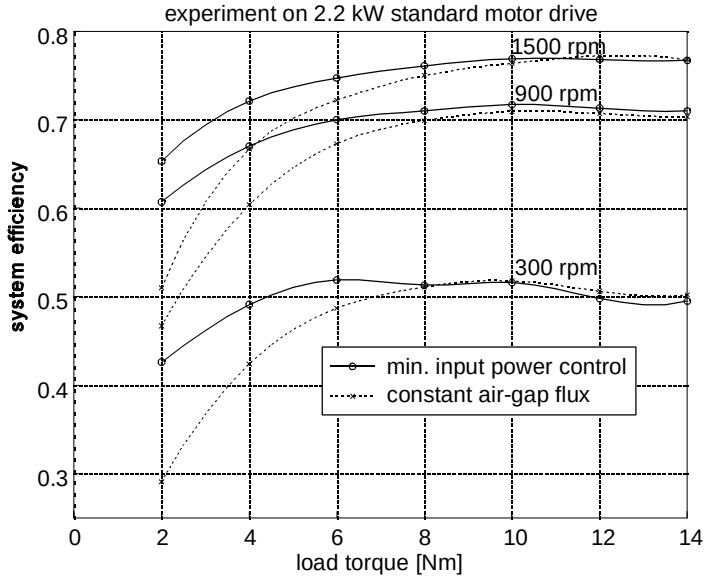

Figure 6.11: *Experiments on standard motor at 300, 900 and 1500 rpm. Measured drive efficiencies with input power minimizing search control and with constant air-gap flux control.*

Unfortunately, the measured efficiencies can not be compared with the efficiencies calculated previously in this chapter, because the calculated efficiencies do not include harmonic motor losses. It is, however, interesting to see whether the tendencies of the calculated efficiencies can be identified on the measurements. For example, Figure 5.16 showed that the motor efficiency for the stator current minimizing search control is degraded at high speed and low load. The same should be seen on the measurements compared to the other energy optimal control strategies. After investigating this, the conclusion is, however, that these minor differences between the energy optimal control strategies are not noticeable on the measurements. The differences may either not be present, or they are to some degree hidden in measurement inaccuracies.

The experimental results confirm that an efficiency improvement is obtainable below 8 Nm (approximately 0.6 p.u. load torque) by energy optimal control. The nominal efficiency is reduced to 0.78, from the 0.82 of the nominally loaded motor which is connected directly to the electrical grid.

6.2 Dynamic Test of Energy Optimal Control.

In this section the dynamic properties of the different energy optimal control strategies are investigated experimentally. Although the scalar drive has most importance in this thesis because it focuses on HVAC applications, the experiments are also made with an indirect rotor-flux oriented current controlled drive in order to give a reference for comparison.

6.2.1 Experimental Execution.

The experiments on the induction motor drive are made with a dc-generator as a load. The dc-generator has a constant field excitation and a variable resistance connected to the armature.

What is important for a drive in an industrial installation is how fast the energy optimal control can adapt to the point of optimal efficiency in case of changes in load or changes in speed. With the available laboratory setup it is not possible to vary the load quickly from, for example, 14 Nm to 2 Nm. It is therefore chosen to test the dynamic performance by initially running the drive with nominal magnetization, then turning the energy optimal control on, and see how fast it converges. The energy optimal controllers are tuned as described in chapter 5 for the scalar control.

6.2.2 Experimental Results with Turn-On of Energy Optimal Control.

The results of the tests are shown on Figure 6.12 - Figure 6.14. Each figure shows the transient at turn-on of the energy optimal control with both the scalar drive and with the vector drive. The tests are made 300, 900 and 1500 rpm., and with 2 Nm load torque in the point of optimal efficiency.

A summary of the response times is listed in Table 6.1.

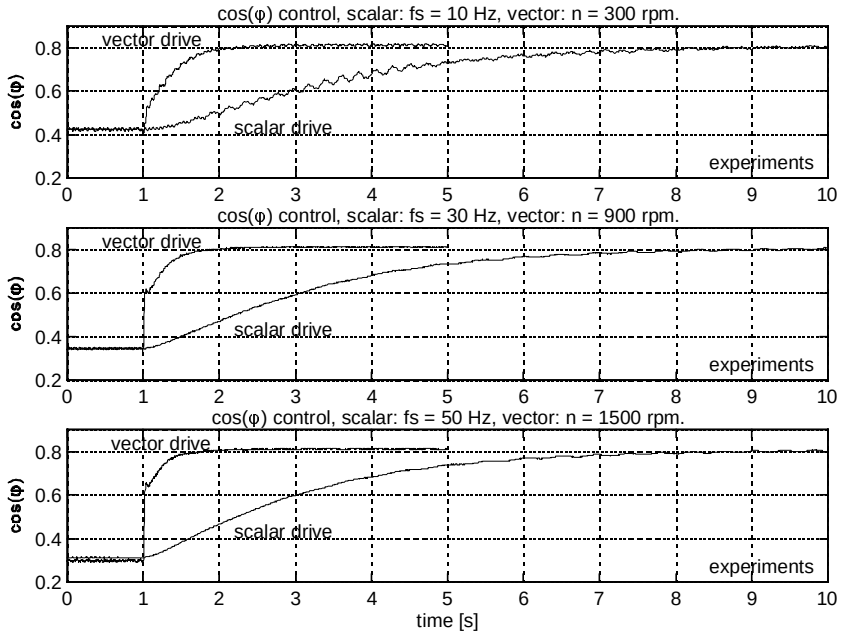

Figure 6.12: *Experiments with turn-on of the cos(φ) control, for both the scalar drive and the vector drive. $\cos(\varphi)^*=0.81$. The load torque is 2 Nm. cos(φ) is filtered with following filters; scalar drive: 5 Hz filter, vector drive: 10 Hz filter.*

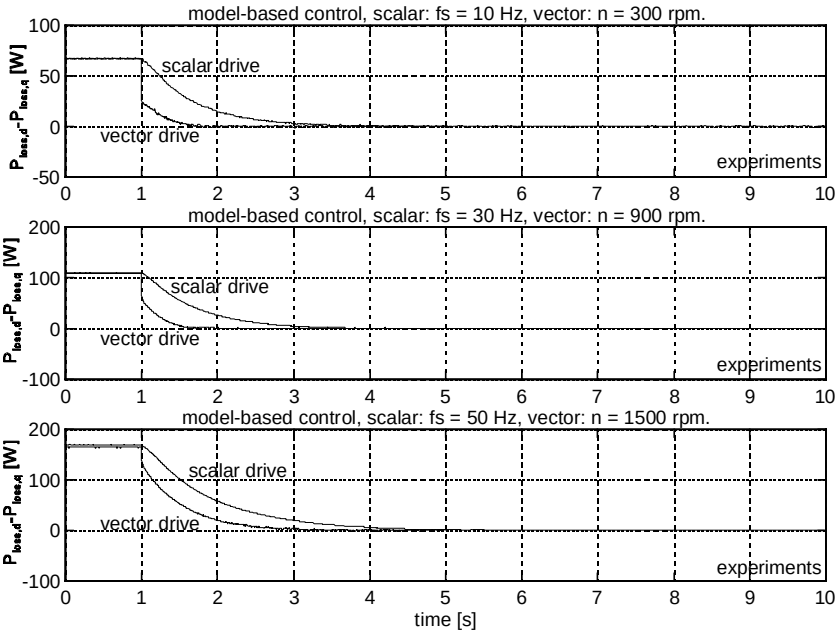

Figure 6.13: *Experiments with turn-on of the model-based control, for both the scalar drive and the vector drive. The load torque is 2 Nm. The powers are filtered with following filters; scalar drive: 5 Hz filter, vector drive: 10 Hz filter.*

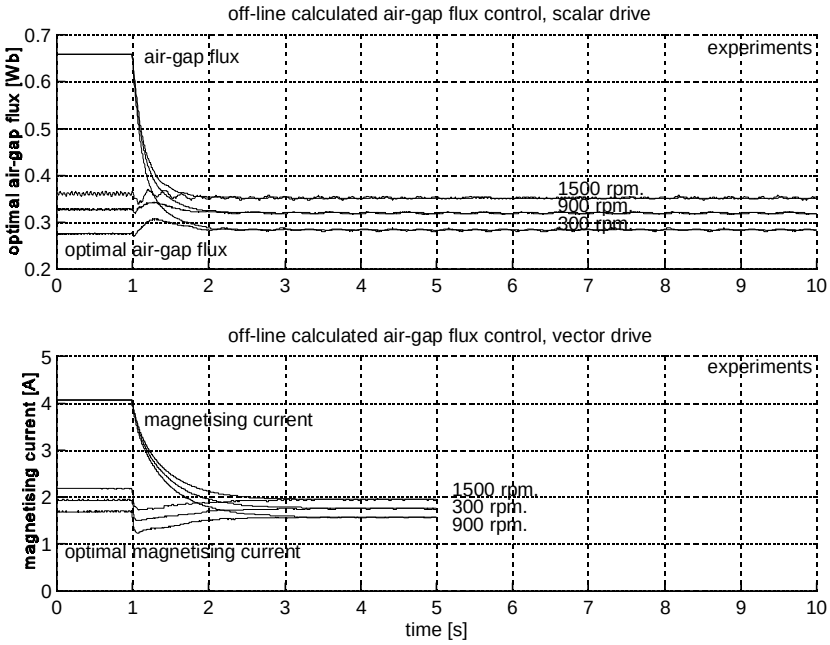

Figure 6.14: *Experiments with turn-on of the off-line calculated air-gap flux control, for both the scalar drive and the vector drive. The load torque is 2 Nm. The air-gap flux is filtered with a 5 Hz filter.*

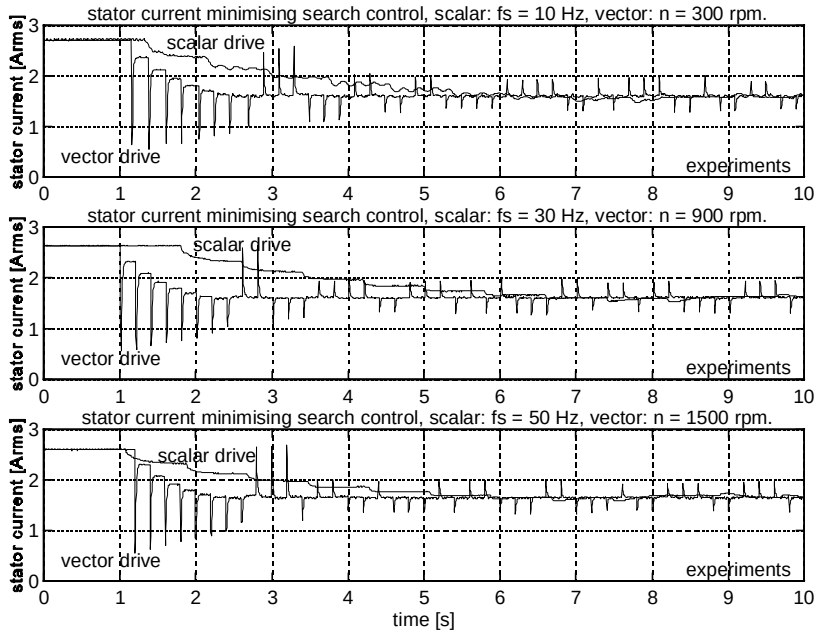

Figure 6.15: *Experiments with turn-on of the stator current minimizing search control, for both the scalar drive and the vector drive. The load torque is 2 Nm. The stator current is filtered with following filters; scalar drive: 5 Hz filter, vector drive: 10 Hz filter.*

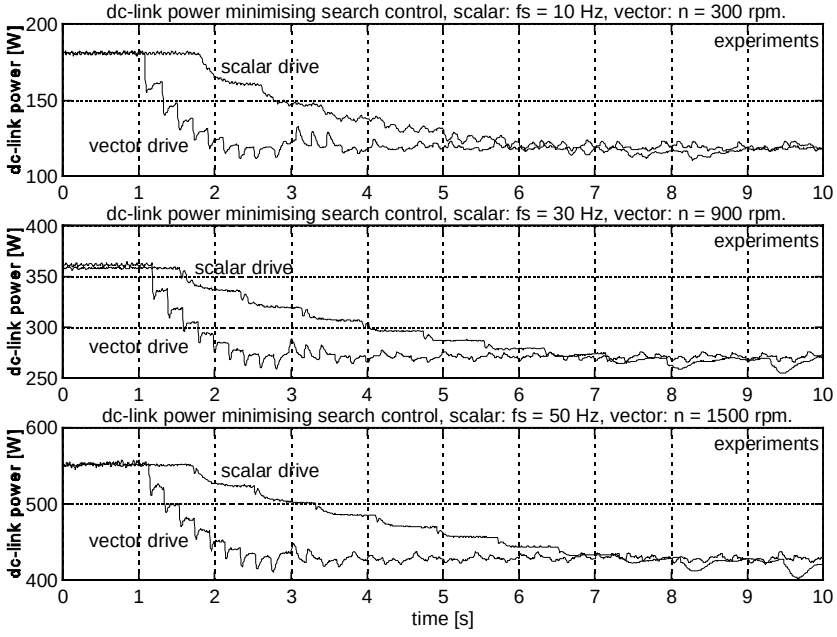

Figure 6.16: *Experiments with turn-on of the dc-link power minimizing search control, for both the scalar drive and the vector drive. The load torque is 2 Nm. The dc-link power is filtered with a 3 Hz filter.*

Table 6.1: Response times by turn-on of energy optimal control.

Energy optimal control strategy.	Scalar Drive	Vector Drive
cos(φ)	7 s	1 s
Model-based	2-3 s	0.5-2 s
Off-line calculated air-gap flux	1 s	2 s
Stator current minimizing search control	7-8 s	3 s
dc-link power minimizing search control	9 s	4 s

The summary in Table 6.1 makes it clear that the model-based control and the off-line calculated air-gap flux control are fastest. The scalar drive cos(φ) control response time is very slow. The reason is that the air-gap flux control loop has a slow response time of 1 s. For the vector drive, however, the response of the cos(φ) control is fast. The slow scalar drive air-gap flux control does not seem to have any major retarding effect on the model-based control. The response time for the scalar drive off-line calc. control is equal to the response time of the air-gap flux control loop. For both the scalar drive and the vector drive, the search control algorithms have the largest response times.

For the first three energy optimal control strategies, the controlled parameters are smooth in both transient and steady-state. For the search control strategies, on the other hand, the stator current and dc-link power are distorted in both transient and steady-state. Therefore it must be concluded that although the search control strategies find the points of optimal efficiency, the dynamic quality of these strategies are poorer than the dynamic quality of the three first strategies.

Until now there has not been made any distinction between the terms energy optimization and efficiency optimization, but the dynamical tests indicate that there is a difference. While all control strategies provide almost the same optimized efficiency in steady-state, the tests in the next section will show that the search control, due to its poor dynamical properties, does not provide a good energy optimization in a realistic test.

6.3 Energy Measurement in a Pump System.

As a final examination of the developed energy optimal control strategies for small motors, the strategies are applied in an ASD for a water pump system. The purpose is to do experiments in the laboratory which are as close to a real life application as possible. The strategies are compared by measuring the motor energy consumption when running through a predefined test-cycle with a duration of 6 min.

6.3.1 Description of the Pump-System.

A schematic diagram of the pump system, together with the ASD, is shown on Figure 6.17. The PC, the control unit, the AD-converter and the VSI are the same as used with the load system previously in this thesis. An impression of the physical dimensions of the system is gained from the picture on Figure 6.18.

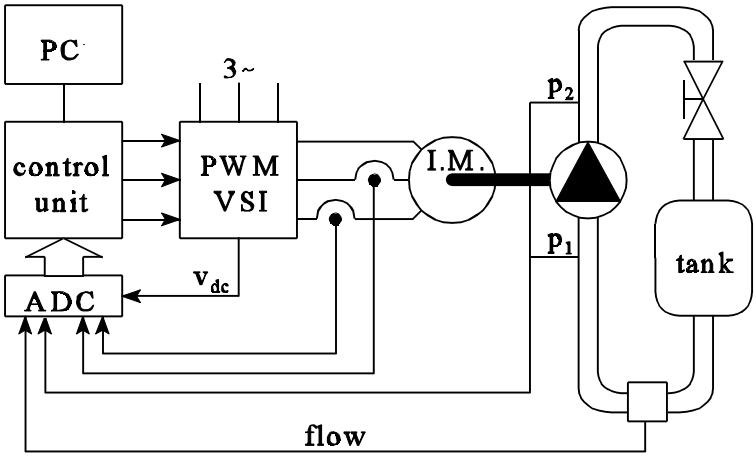

Figure 6.17: *Pump-system to test HVAC applications.*

The pump is of the type:	Grundfos, LM 65-200/202	
	rated speed:	1400-1420 rpm.
	max. lifting height:	14 m = 1.37 bar.
	max flow rate:	46 m^3/h = 12.8 l/s.
	internal tube diameter:	65 mm.

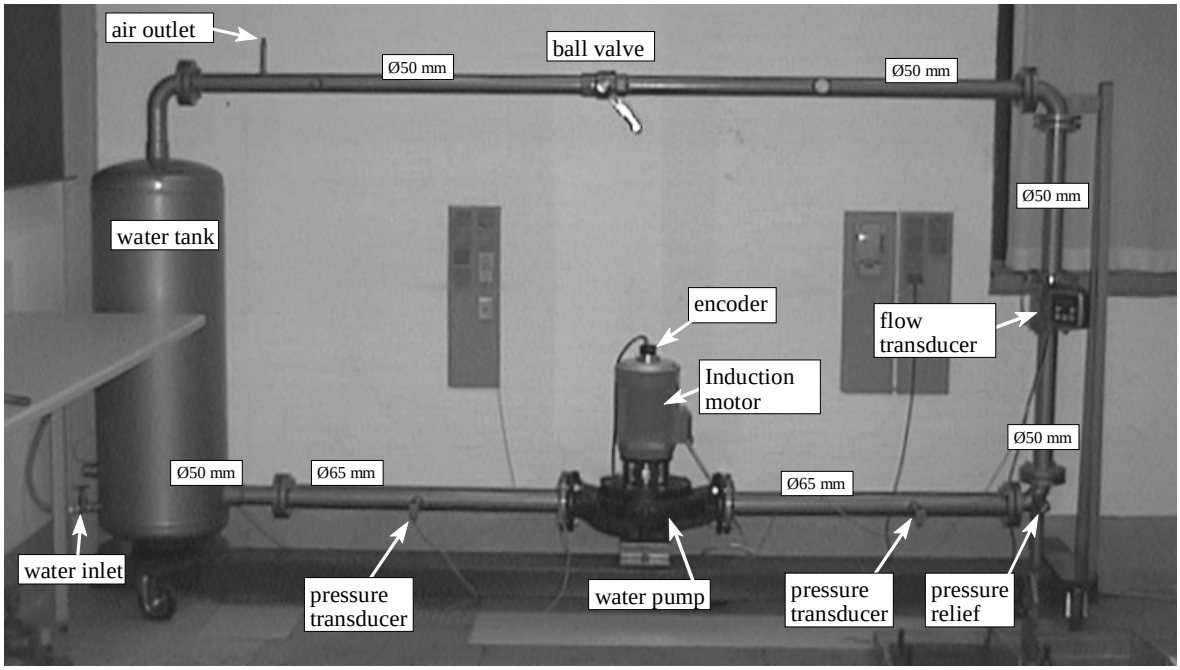

Figure 6.18: *Picture of the pump-system.*

6.3.2 Pump System Control

Because a pump system is a low-dynamic system, it is irrelevant to use vector control of the motor. The scalar control which is seen on Figure 6.19 is therefore used. The water pressure is measured before and after the pump, and the difference between them is the input to the control loop. The pressure is controlled by adjusting the stator frequency, and thereby the speed. The air-gap flux reference is set by the energy optimal control.

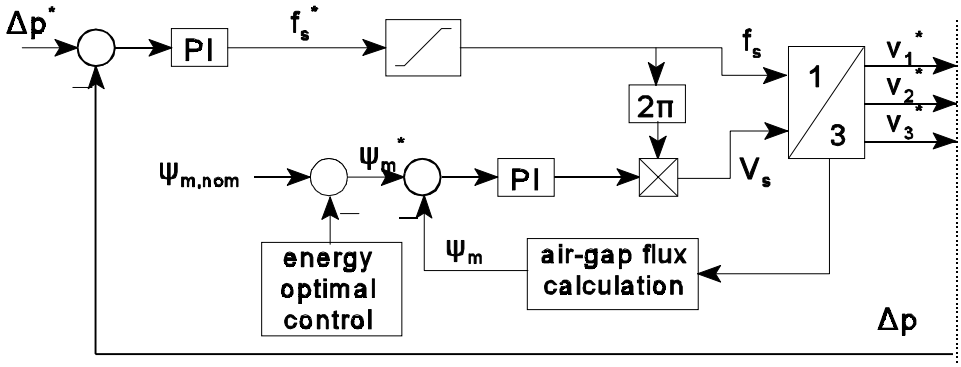

Figure 6.19: *Diagram showing the control of the pump system. The difference (Δp) between the pressure after the pump and the pressure before the pump is controlled in closed loop.*

The load cycle which is used for testing the energy consumption with different energy optimal control strategies is shown on Figure 6.20. Initially the pressure reference is 0.2 bar and the valve is half-closed. After 40 s the pressure slowly increases up to 1.2 bar and then down to 0.2 bar. At 140 s the pressure reference suddenly increases to 1.2 bar and at 170 s it

suddenly goes down to 0.2 bar again. After 200 s the valve is suddenly opened, half-closed again at 230 s and then opened at 260 s. At 290 s the pressure reference is set to 0.85 bar, which corresponds to full load of the pump. At 320 s the pressure reference is set back to 0.2 bar. The resulting flow is shown on the lowest graph on Figure 6.20.

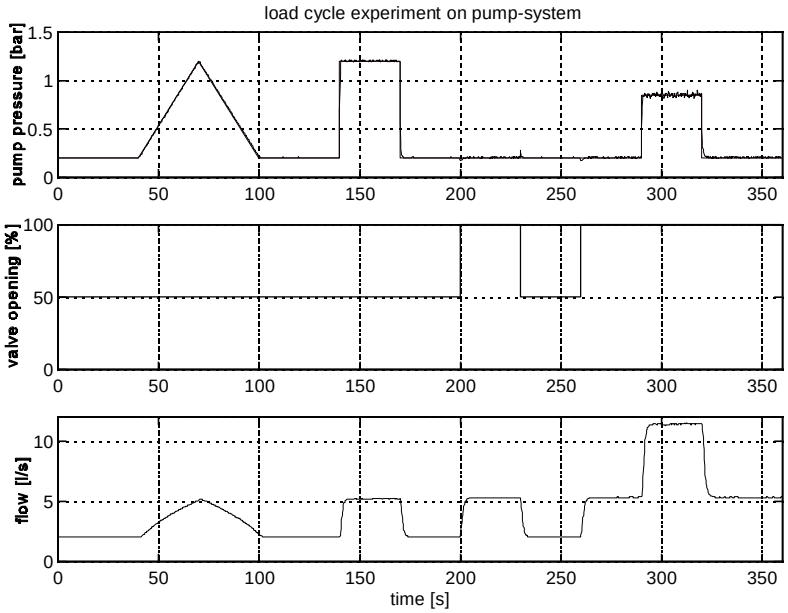

Figure 6.20: *Load cycle for test of energy optimal control strategies with a pump-system. The figure shows the differential pressure over the pump, the valve opening and the water flow.*

Six motor control strategies are tested with the mentioned load cycle:

- Nominal magnetization.
- cos(φ) control. cos(φ) = 0.81.
- Model-based control.
- Direct air-gap flux control.
- Stator current minimizing search control.
- dc-link power minimizing search control.

The control strategies are identical to those described in chapter 5.

Before the test, the system has run for several hours so that it is thermally stable. Each of the control strategies are first tested once, one after the other, and then they are similarly all tested a second time. For every test, air-gap flux reference, pump pressure, flow and calculated motor input power are recorded with a sampling time of 0.2 s, which corresponds to 1800 points in 360 s. The energy consumption is measured with a power analyzer (Voltech 3000 A), which is inserted between the VSI and the motor.

6.3.3 Measured Energy Savings for a Prespecified Test-Cycle

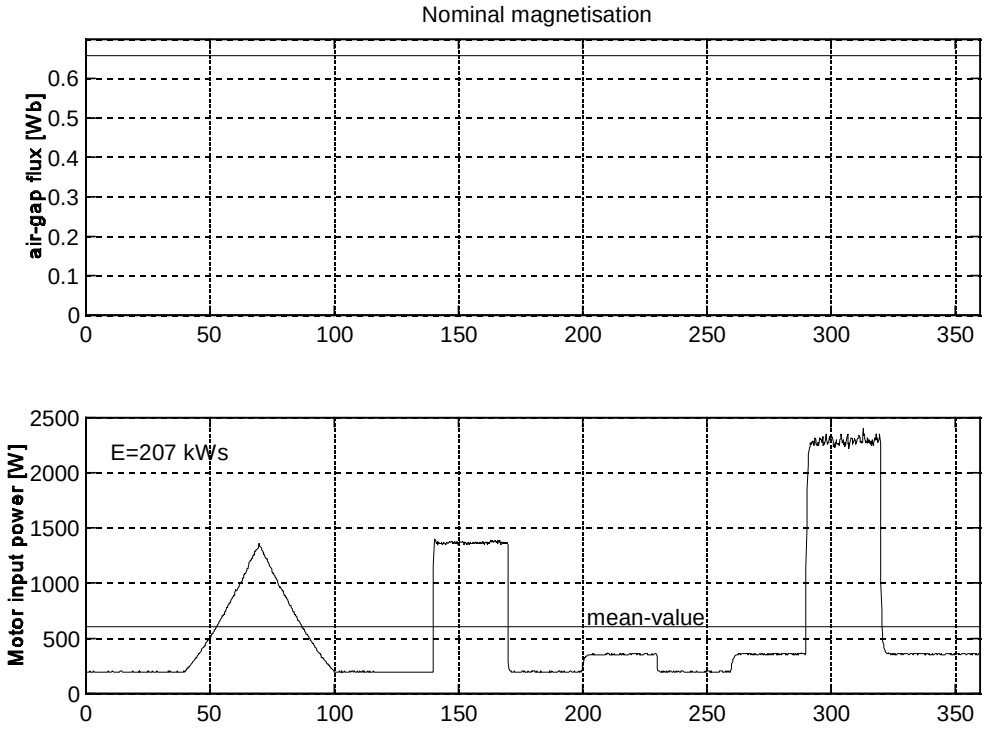

Figure 6.21: *Air-gap flux and motor input power for the load cycle with nominal magnetization for test 2.*

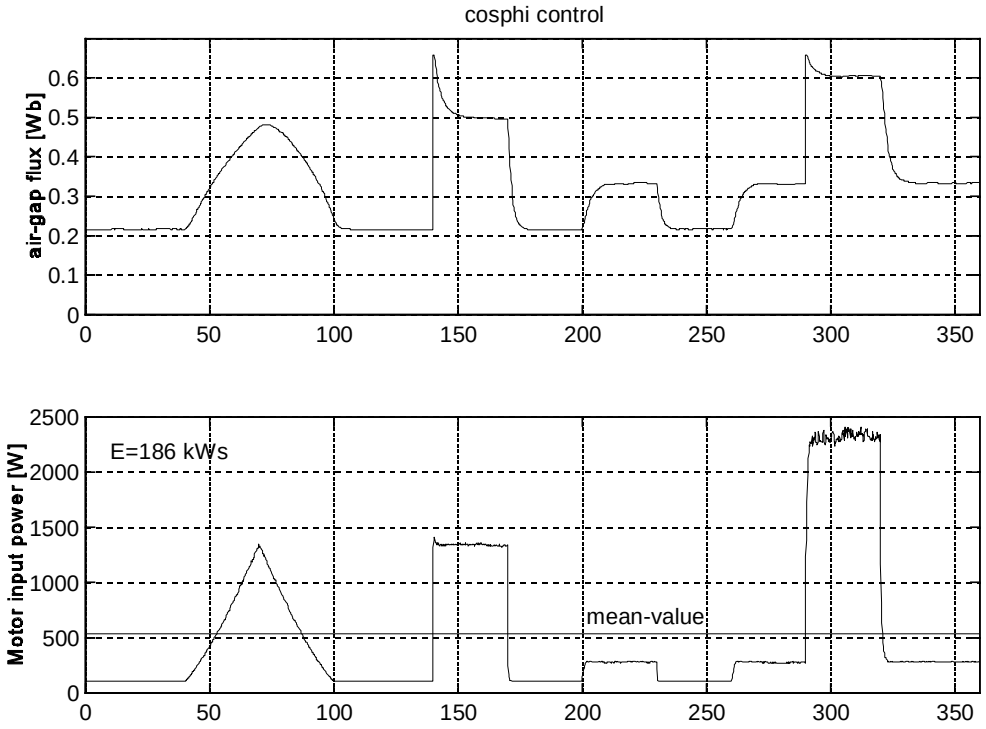

Figure 6.22: *Air-gap flux and motor input power for the load cycle with cos(φ) control for test 2. cos(φ)=0.81.*

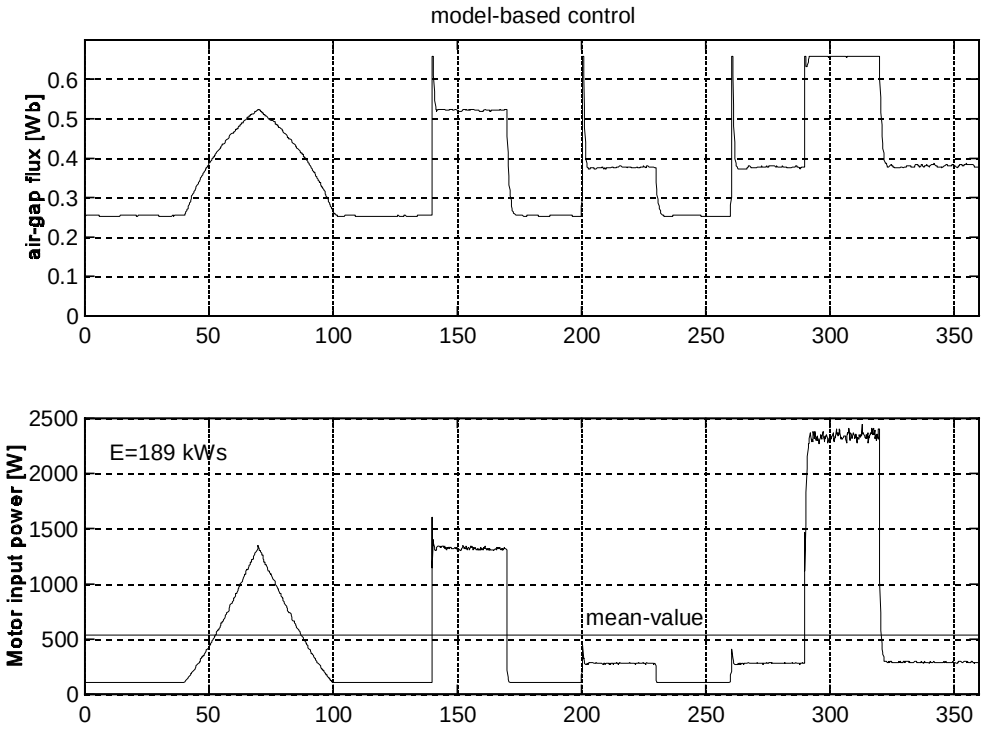

Figure 6.23: *Air-gap flux and motor input power for the load cycle with model-based control for test 2.*

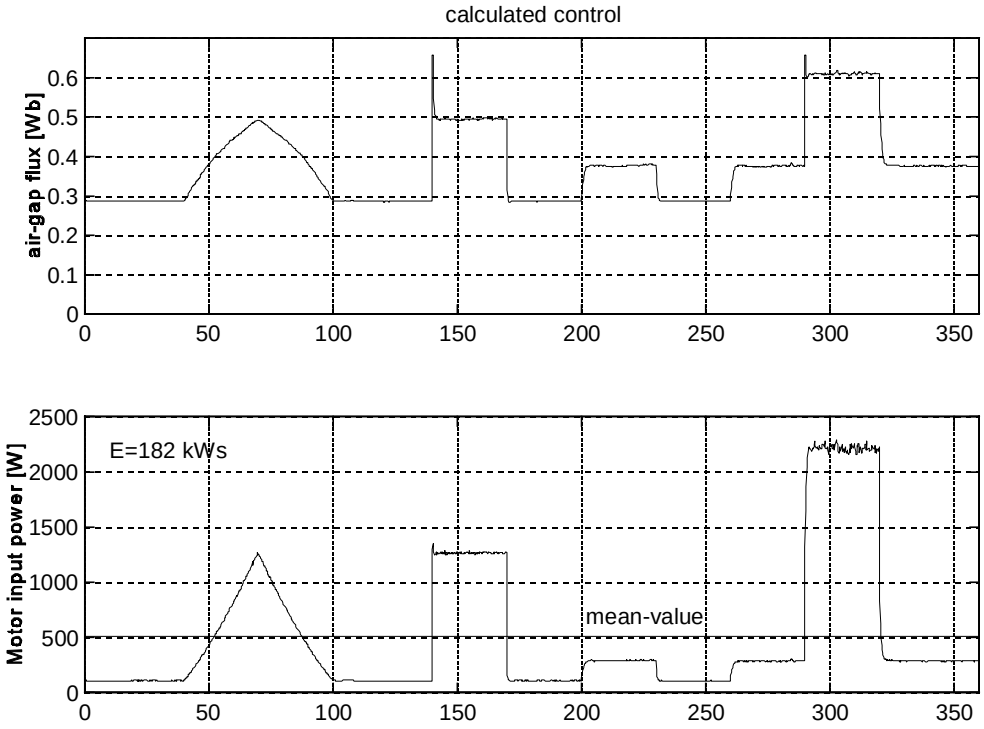

Figure 6.24: *Air-gap flux and motor input power for the load cycle with off-line calculated air-gap flux control for test 2.*

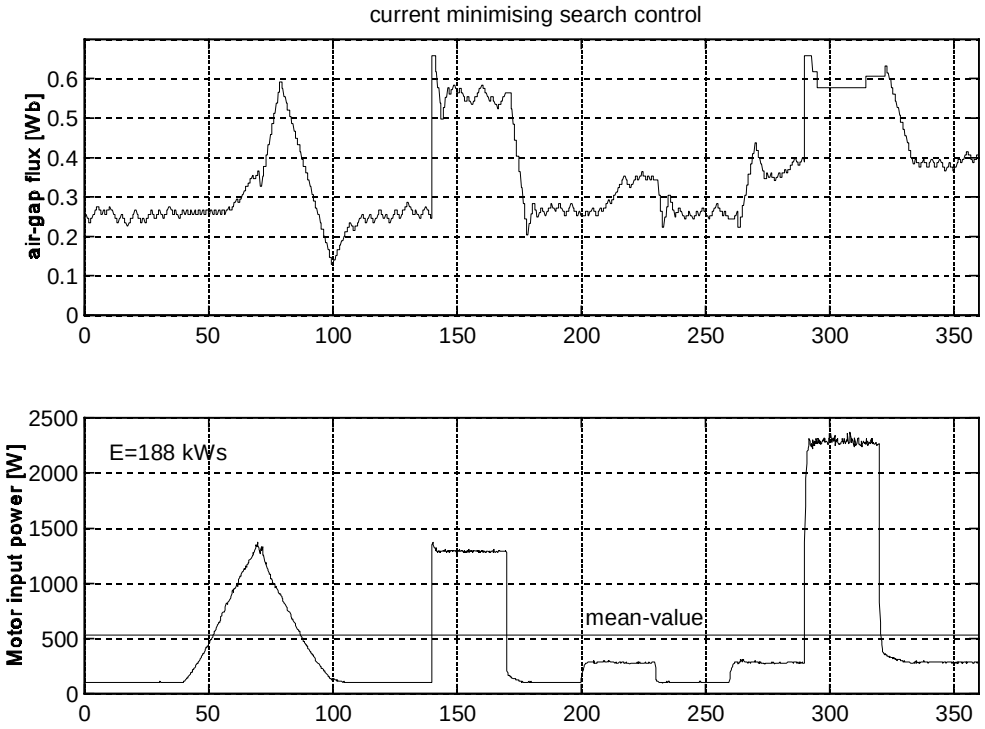

Figure 6.25: *Air-gap flux and motor input power for the load cycle with stator current minimizing search control for test 2.*

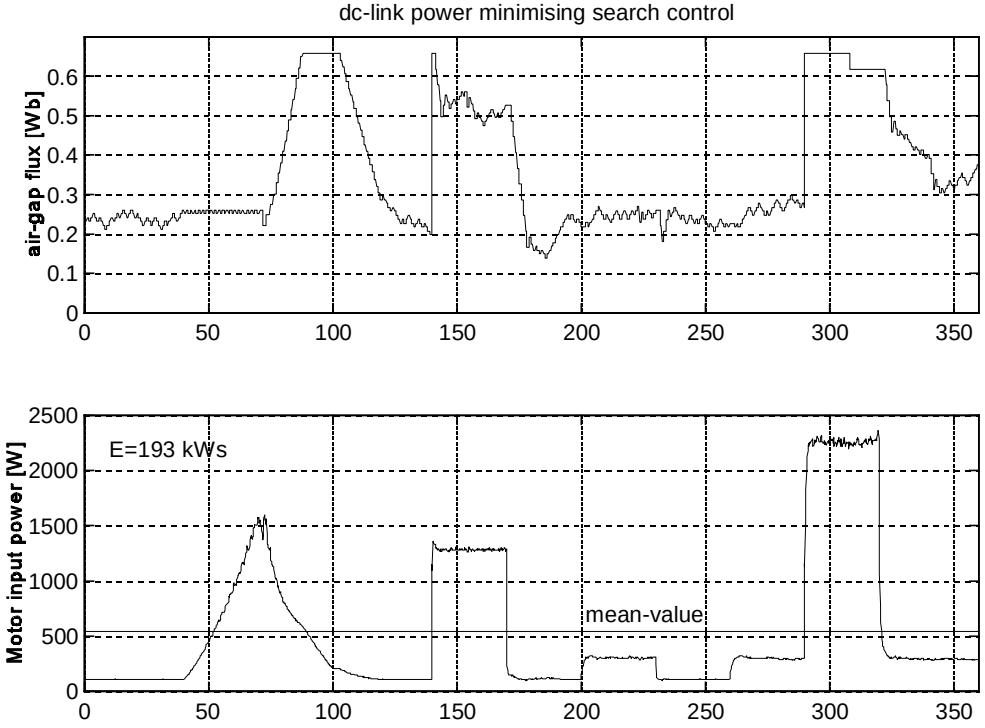

Figure 6.26: *Air-gap flux and motor input power for the load cycle with dc-link power minimizing search control for test 2.*

The measured energy consumption is listed in Table 6.2. The right column shows the energy consumption as a ratio of the energy consumption with rated air-gap flux. The averaged values are used to calculate these percentages. There are observed some differences between test 1 and test 2, which indicate that there is some inaccuracy related to the measurements. Differences in motor and water temperature for the two tests may be one explanation. For the search control, the reason may be that even if the same test is made two times, one right after the other, the control does not behave in exactly the same way in the two tests.

Table 6.2: Measured energy consumption for the two runs of the test-cycle. The result is calculated from the averaged values of the two tests.

	Energy consumption test 1 [kWs]	Energy consumption test 2 [kWs]	Energy consumption average [kWs]	% of case with nominal air-gap flux
Nominal air-gap flux	209.1	207	208.1	100%
cos(φ) control	186.5	185.9	186.2	89.5%
model-based control	185.8	189.4	187.6	90.1%
off-line calc. air-gap flux control	181.6	182.1	181.9	87.4%
stator current min. search control	183	188	185.5	89.1%
dc-link power min. search control	188.7	193	190.8	91.7%

The control method based on off-line calculations has the lowest energy consumption, whereas cos(φ) control, model-based control and stator current minimizing control are quite equal. The dc-link power minimizing control has the highest energy consumption of the energy optimal control strategies.

Figure 6.21 - Figure 6.24 show that the first four control strategies have nice and quiet courses. This is, however, not true for the two last search control algorithms, see Figure 6.25 and Figure 6.26. They have both a problem to find the correct magnetization when the pressure reference is varying slowly (between 40 s and 100 s). Also when the valve is changed (between 200 s and 260 s) the search algorithms are very slow because the steps in the air-gap flux are very small. So although the power minimizing search control theoretically should be the best method in steady-state, these tests illustrate the difficulties for the search control under non-ideal conditions.

It can be concluded that the cos(φ) control, the model-based control and the off-line calculated air-gap flux control all give good energy savings and show good behavior, no matter which disturbances occur. The search control algorithms give relatively good energy savings, but the dynamic properties are not satisfactory.

6.4 Summary.

Steady-state measurements confirmed what was already found from calculations, namely that by energy optimal control of a 2.2 kW standard motor drive it is possible to improve the efficiency below 8 Nm (approximately 0.6 p.u. load torque). It is from measurements not possible to distinguish clearly between the efficiencies of the individual control strategies as is was the case for the calculations. It is most probable that the differences are smaller than or equal to the measurement inaccuracies. This confirms the already indicated statement that it is not important to hit exactly the optimal magnetization level.

On the other hand there are large differences in the dynamic responses. Tests of how fast the energy optimal control can adapt the flux level when the energy optimal control is enabled showed fast and smooth transition of the direct air-gap flux control and the model-based control. The response of the displacement power factor control is slowed by the slow air-gap flux loop. Likewise the search control is slow and has a very distorted response. Tests with a rotor flux oriented vector controlled drive showed that the transition time for search control can be brought down below 4 seconds, and for the other control strategies below 2 seconds.

The problem with search control is illustrated very well when applied in a pump system. Although the energy saving with search control is only a little smaller than for the other control strategies, the courses of the air-gap flux shows that errors occur when the load and references change slowly. It may in some cases be seen as a problem that the search control is not deterministic, understood in the way that for a given load and speed it is not possible to say at what flux level the motor operates.

It should be emphasized that the transient behavior measured here can not be generalized, as it depends on the type of drive control, how the measured signals are filtered and on how the controllers are tuned. In this case the controllers are coarsely tuned from simple consideration and then fine-tuned by trial and error using simple gain scheduling to optimize the dynamics. The problem with the scalar drive is that the transfer function of the controlled system is very complex, and further work needs to be done for the controllers to be tuned in a systematic way. However, once the controllers are tuned, they are independent of the application. The main problem with the search control is that several constants have to be tuned by trial and error in every new application. It is obvious that work has to be done that can automate this process, before one can start to discuss using search control industrially.

Measurements of energy consumption for a six-minute test-cycle in the pump-system showed a reduction of the energy consumption with up to 12.6 % with energy optimal control compared with constant air-gap flux control. The average load of the motor was approximately 20 % of rated power.

A final conclusion is that search control is not a good solution for energy optimal control in HVAC applications. The three other strategies all perform well, and which one to choose may depend on the existing drive control and on processor performance available.

Chapter 7

Energy Optimal Control of Medium-Size Motor Drive

The induction motor drives which have been investigated so far can be categorized as small drives. Medium-size drives then refers to drives in the range of 10-1000 kW. For the 2.2 kW drives the converter losses were disregarded in the energy optimal control algorithms. For larger drives the converter losses are more important, and it is the purpose here to analyze how this influences the energy optimal control algorithms.

Only one paper has been found which analyzes the difference between small and medium-size motor drives with regard to energy optimal control [1], and it concentrates on search control. They do calculations on 1 kW and 75 kW motors with search control and find that because of the relatively small drive loss in medium-size drives it is easier to minimize the stator current than to minimize the input power. But although this takes away the need for sensors to measure the input power, the method is still not good in industrial HVAC drives for the same reasons as for the small drives: continuos disturbances, difficulties to tune algorithm parameters, and need for precise output power indication, for example by a speed sensor. Search control is not investigated in this chapter as it is not considered relevant in HVAC and especially not in medium-size and large drives.

It order to make an analysis of energy optimal control it is essential to have reliable and experimentally verified motor and converter models, otherwise one can easily reach false conclusions. The analysis is here done on a 90 kW drive, and for that purpose the loss models from Chapter 3 have been verified against extensive loss measurements. Next, the influence of the converter loss in energy optimal control is calculated, and a proposed energy optimal control algorithm is tested on a 22 kW drive. At last, aspects of over-sized motors are described and relations between drive size and efficiency improvement by energy optimal control are established. The unique contributions of this chapter are a general analysis of energy optimal control in medium-size drives based on experiments, a proposal for a new way of implementing model-based control, and a means to determine the benefits of energy optimal control at different drive sizes.

7.1 Motor and Converter Loss Ratio.

The ratio between motor and converter loss depends on the size of the drive and on how it is operated. The ratio is first illustrated from Figure 7.1 which shows nominal motor and converter efficiencies for drives between 2.2 kW and 250 kW. While the motor efficiencies increase rapidly with size, especially at low power, the converter efficiency only increases slowly. The ratio between the motor loss and converter loss approaches, but does not reach unity, and the ratio is lowest for the high-efficiency motors.

In the following the motor/converter loss ratio is calculated with loss models of the four investigated drives: 2.2 kW standard and high-efficiency motor drives, 22 kW and 90 kW motor drives. The structure of the loss models for the 22 kW and the 90 kW drives are the same as for the small drives, see chapter 3 for details. The loss models are verified in the whole operating area, see Appendix B. It should be noted that the 2.2 kW motor models do not include harmonic losses. The 22 kW and 90 kW motor models do include harmonic losses because there were no output filters available for the experiments with these two drives. The harmonic losses of the 2.2 kW motors range between 10-30 W, see also section 3.2.

The measured losses for the 22 kW and 90 kW drives at 900 rpm. are shown on Figure 7.3 together with the measured losses for the small drives on Figure 7.2. The measurements are only shown here for 900 rpm. while the corresponding measurements for 300, 1400 and 1500 rpm. are shown in Appendix B. It is seen that the converter losses are relatively larger for the larger drives.

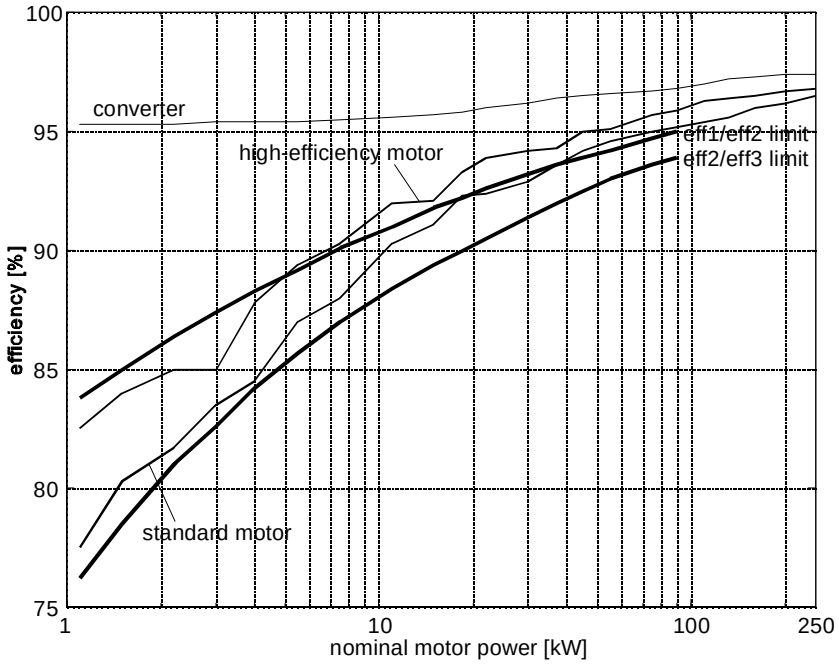

Figure 7.1: *Nominal efficiencies for 400 V converters and motors. The converters are with diode rectifier and PWM inverter. The motors are catalogue data for AAB 4-pole, 50 Hz motors. The thick lines indicate the limits between the European Commission motor classes.*

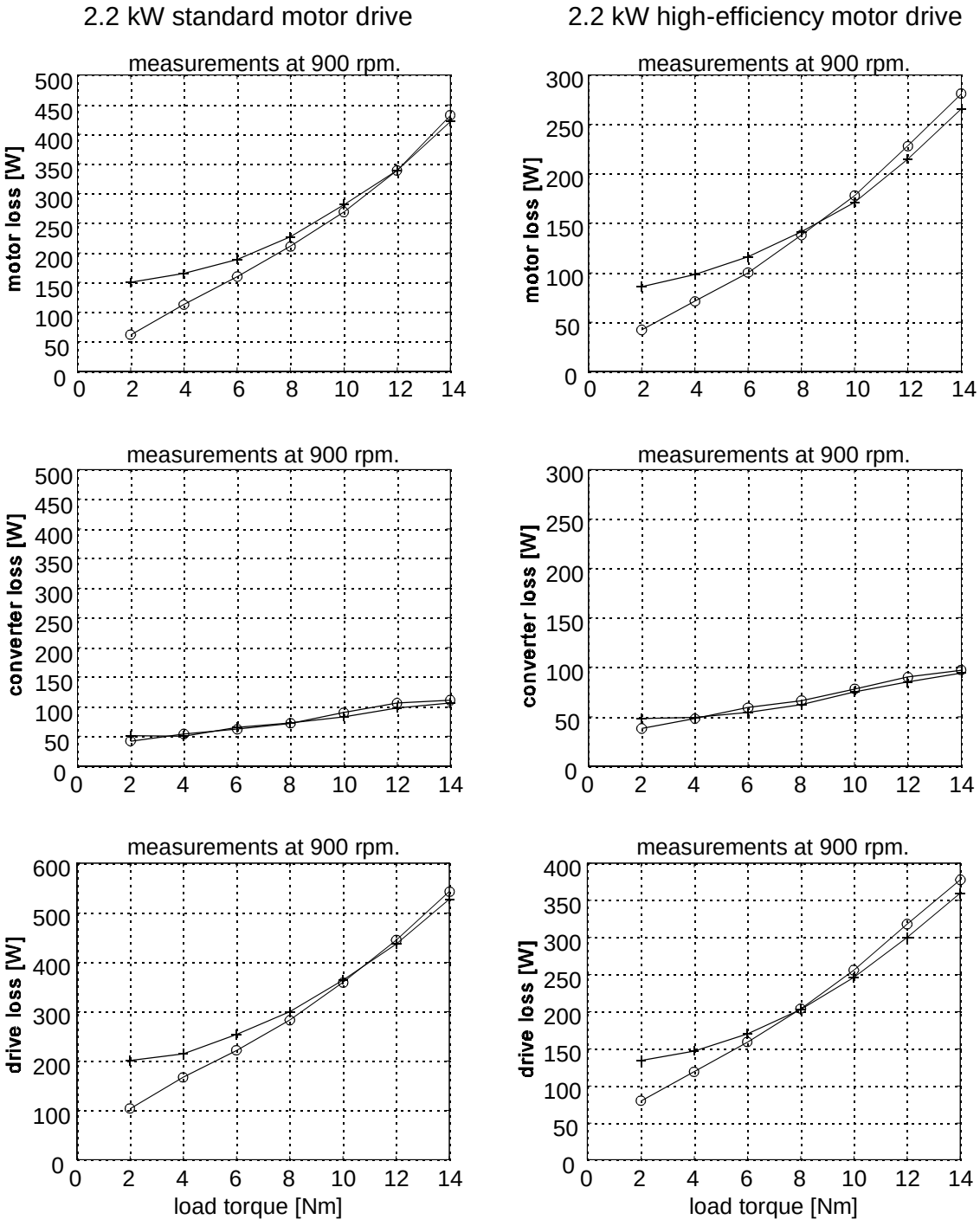

Figure 7.2: *Measured losses in 2.2 kW standard motor and high-efficiency motor drives. Crosses: constant nominal air-gap flux. Circles: energy optimal control.*

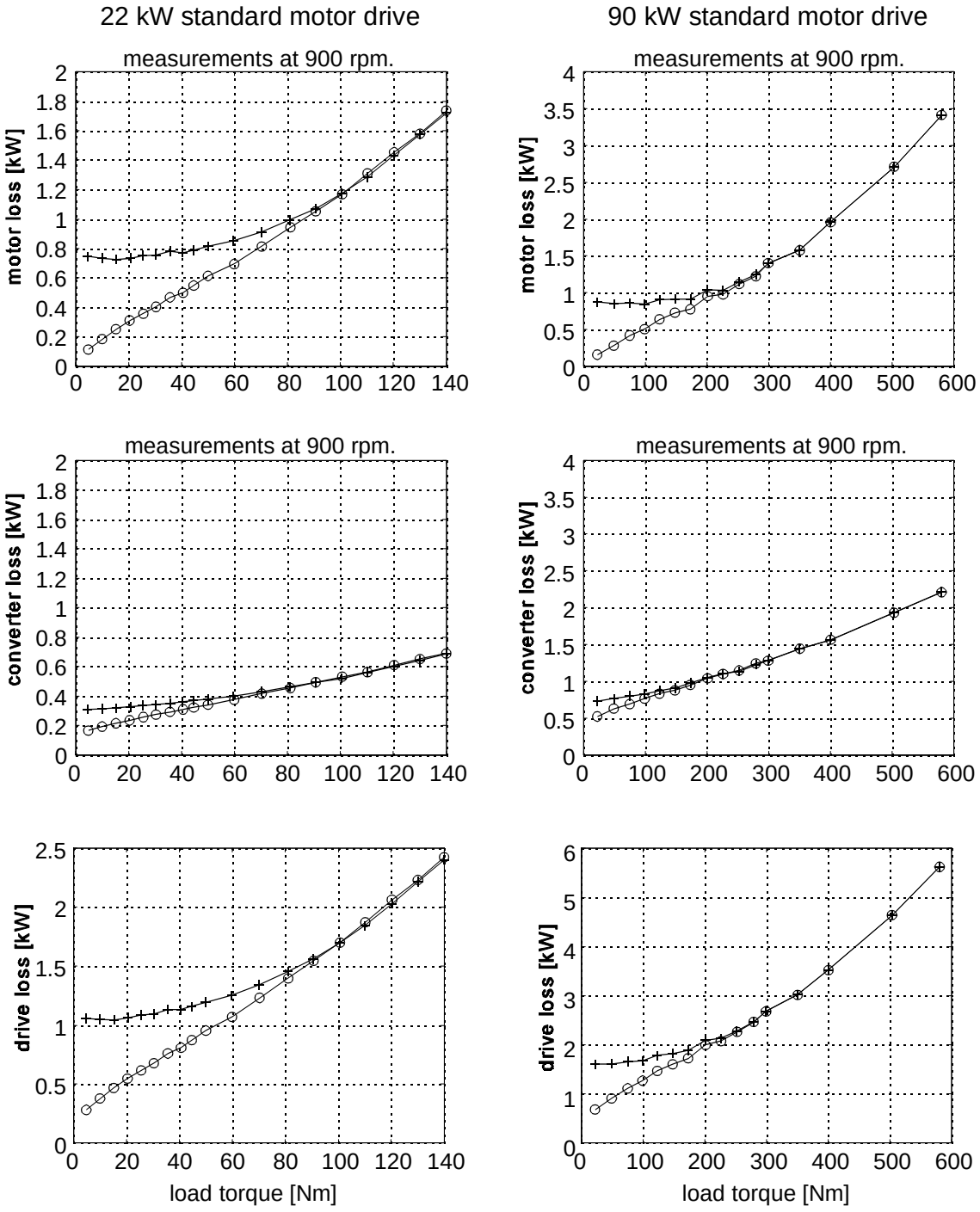

Figure 7.3: *Measured losses in 22 kW and 90 kW motor drives. Crosses: constant nominal air-gap flux. Circles: energy optimal control.*

The per-unit motor constants and loss components of the four investigated drives are compared in Table 7.1. It is characteristic that the largest motor has better efficiency because the stator and rotor resistances are smaller, and the magnetizing reactance and the core loss resistance are larger. While the nominal converter loss is almost the same for all motors, the nominal motor losses (copper and core losses) are reduced for the large motors, so that the ratio between the motor loss and the converter loss goes from 3.9 in the standard 2.2 kW motor drive to 1.8 for the 90 kW motor drive.

Table 7.1: Nominal Induction Motor Drive Constants and Losses in Per-Unit.

	2.2 kW standard	2.2 kW high-eff.	22 kW standard	90 kW standard
stator resistance	0.061	0.048	0.019	0.014
rotor resistance	0.040	0.037	0.021	0.010
stator leakage reactance	0.083	0.074	0.072	0.077
rotor leakage reactance	0.11	0.10	0.11	0.16
magnetizing reactance	1.82	1.80	1.66	2.98
core loss resistance	22.9	44.0	35.6	110.8
copper losses	0.10	0.070	0.033	0.022
core losses	0.035	0.019	0.025	0.0081
converter losses	0.028	0.028	0.035	0.030
Pmotor/Pconverter	3.9	2.7	2.6	1.8

7.2 Influence of Converter Loss on the Loss Minimization.

The importance of including the converter loss in the energy optimal control is investigated by performing calculations on the motor and converter loss models. These are only done on the 90 kW drive, which is the case with the highest relative converter loss of the investigated drives. Calculations of the drive loss (motor and converter loss) are done at 300, 900 and 1500 rpm. with varying air-gap flux, and from low to nominal load torque.

7.2.1 Calculations with a Fixed Switching Frequency.

The calculations are first made with 4 kHz switching frequency, see Figure 7.4 - Figure 7.6, which corresponds to the experiments made on the 90 kW drive. The circles denote the points of minimum drive loss and the stars denote the points of minimum motor loss. Figure 7.4 shows that at 300 rpm. there is almost no difference between these two criteria. The differences increase at higher speed, see Figure 7.5 and Figure 7.6. In terms of drive loss, however, the flat bottom shape curves lead to that even a noticeable difference in air-gap flux has almost no effect on the drive loss. So from the point of view of drive loss minimization the minimum motor loss criterion is just as good as the minimum drive loss criterion.

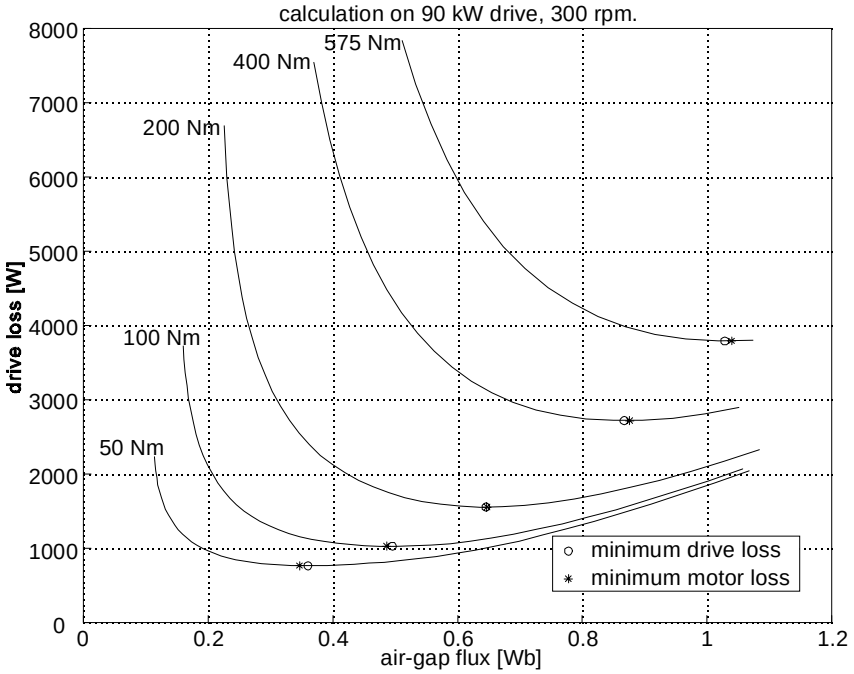

Figure 7.4: *Calculation of the loss for a 90 kW induction motor drive at 300 rpm. The circles denote minimized drive loss and the stars denote minimized motor loss.*

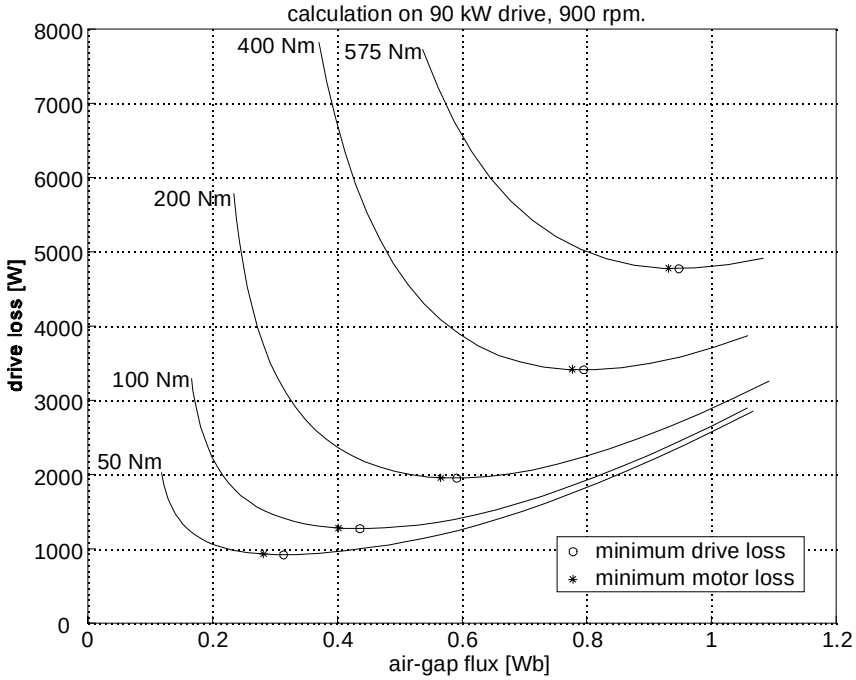

Figure 7.5: *Calculation of the loss for a 90 kW induction motor drive at 900 rpm. The circles denote minimized drive loss and the stars denote minimized motor loss.*

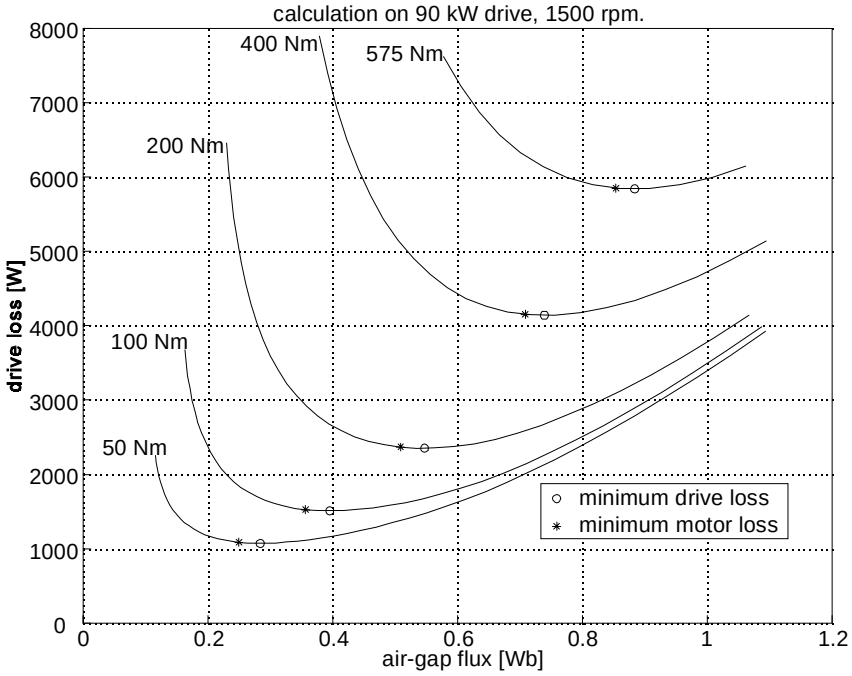

Figure 7.6: *Calculation of the loss for a 90 kW induction motor drive at 1500 rpm. The circles denote minimized drive loss and the stars denote minimized motor loss.*

7.2.2 Influence of Increased Switching Frequency.

The drive is now analyzed for increased switching frequency: 5 kHz, 10 kHz and 15 kHz, see Figure 7.7 - Figure 7.9.

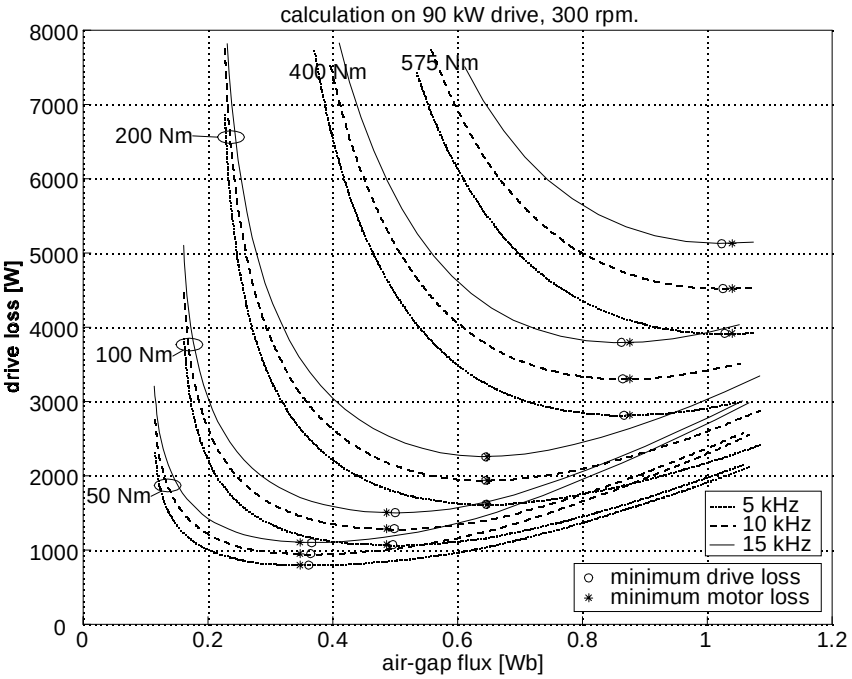

Figure 7.7: *Calculation of the loss for a 90 kW induction motor drive at 300 rpm. The circles denote minimized drive loss and the stars denote minimized motor loss.*

The result is the same as before, with the only change that the differences between the two loss minimization criteria become more important the higher the switching frequency is.

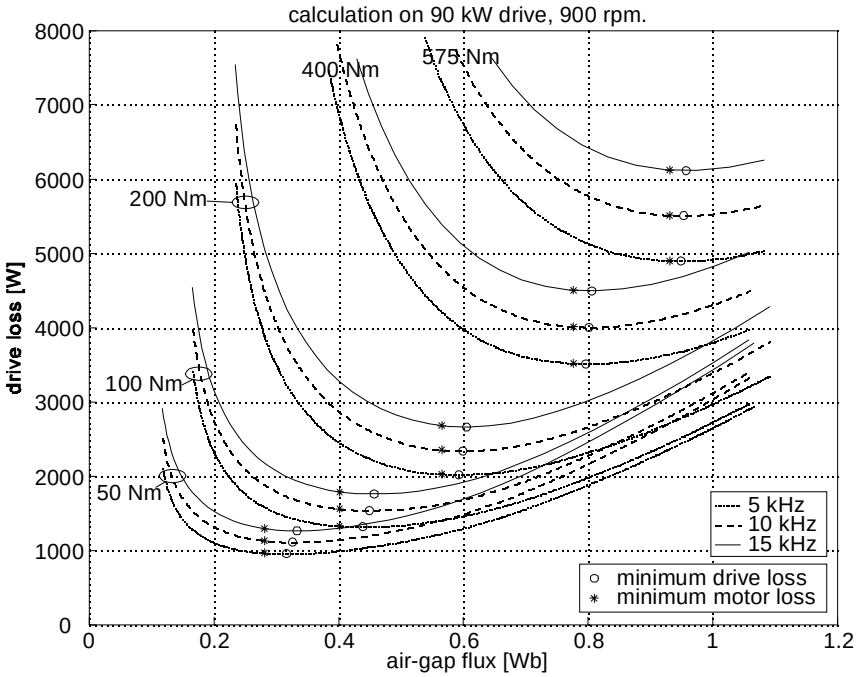

Figure 7.8: *Calculation of the loss for a 90 kW induction motor drive at 900 rpm. The circles denote minimized drive loss and the stars denote minimized motor loss.*

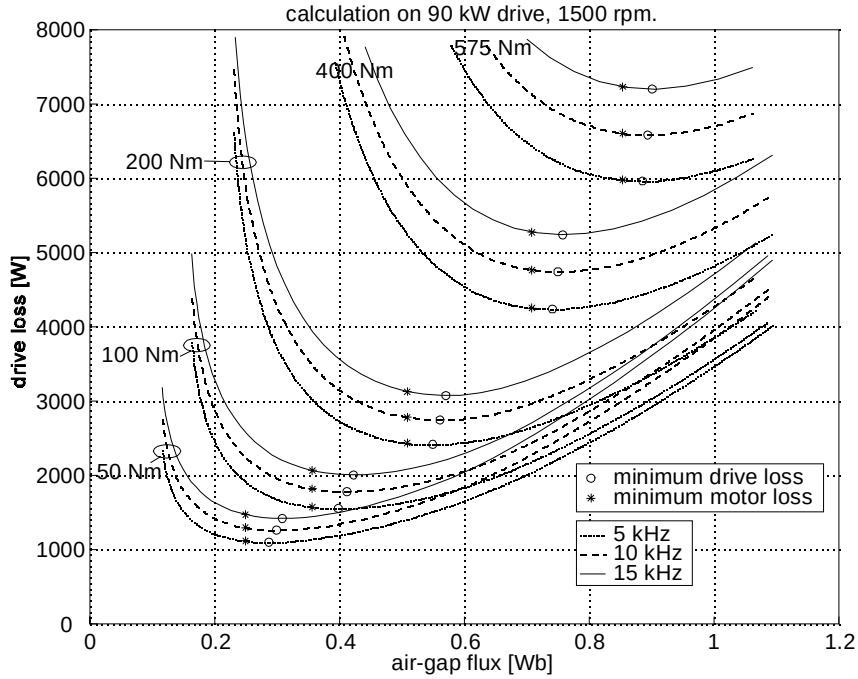

Figure 7.9: *Calculation of the loss for a 90 kW induction motor drive at 1500 rpm. The circles denote minimized drive loss and the stars denote minimized motor loss.*

7.3 Evaluation of Energy Optimal Control Strategies.

Two energy optimizing control strategies are evaluated by doing calculations with the 90 kW drive model: displacement power factor control (cos(φ) control) and model-based control.

7.3.1 Cos(φ) Control.

The cos(φ) control was described in section 5.1. Figure 7.10 shows calculation of cos(φ) as function of air-gap flux at several speeds and load torques. The points of optimal drive efficiency, which are indicated on the figure vary between 0.70 and 0.82. It is chosen here to use a constant cos(φ) reference value, and it is determined as the average of the indicated optimal points. In this case the reference value is 0.76.

The calculated drive loss with cos(φ) control is shown on Figure 7.11 at 300, 900 and 1500 rpm. The figure shows that the drive loss with cos(φ) control is very close to the minimized loss.

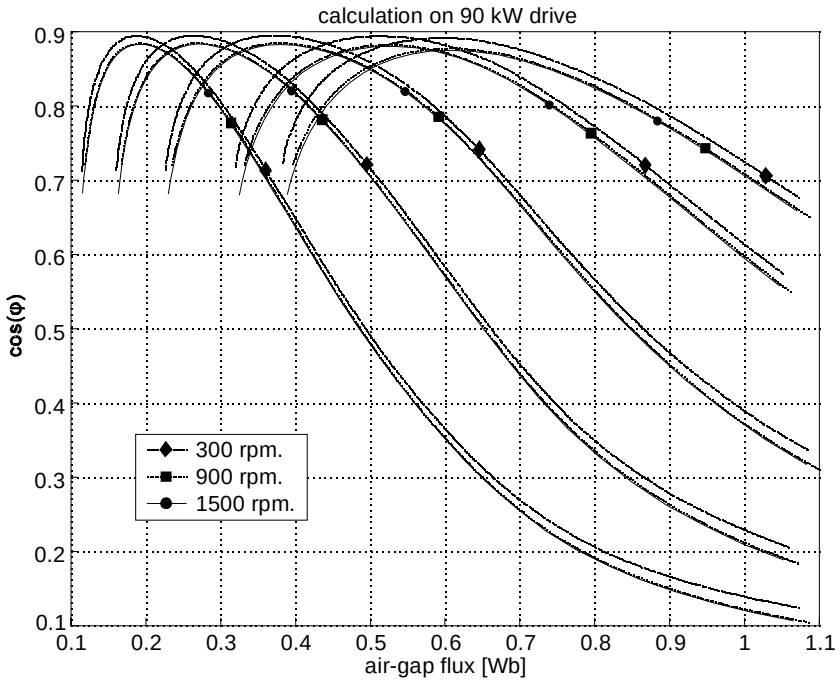

Figure 7.10: *Calculated cos(φ) for 90 kW drive at 300, 900, 1500 rpm. The points of optimal drive efficiency are denoted by individual markers. Switching frequency: 4 kHz.*

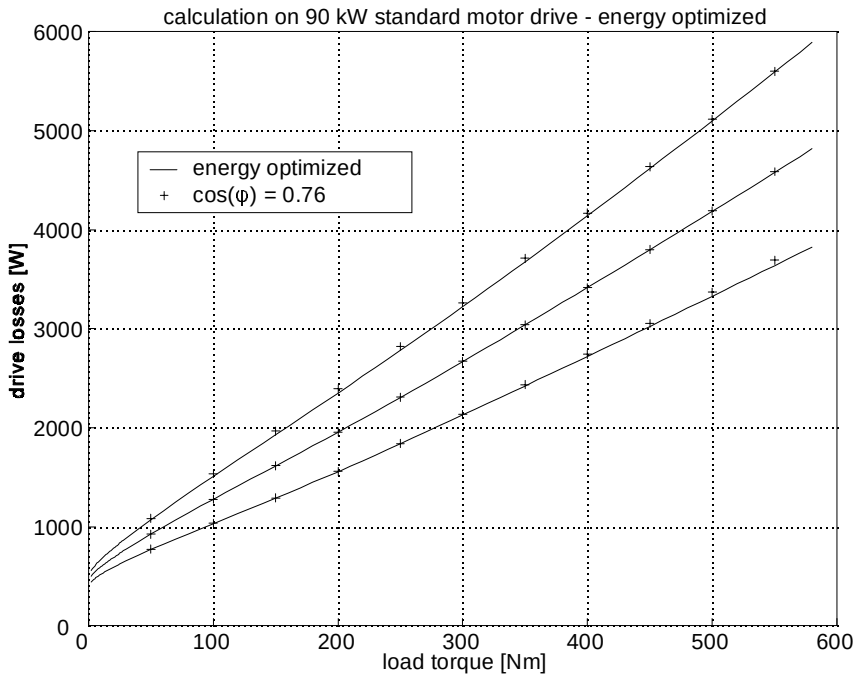

Figure 7.11: *Calculated drive loss (motor and converter) for 90 kW drive. Lines: optimized efficiency. Crosses: cos(φ) control, cos(φ)* = 0.76.*

7.3.2 Model-Based Control.

Assuming that the motor and converter models are known, it is possible to find the point of optimal efficiency in every operating point defined by a load torque and speed. The major problem is to determine an estimate of the load torque. There are several possibilities, ranging from advanced dynamic estimation techniques to simple techniques such as measuring the air-gap power and dividing with the stator angular velocity. It is done here by simply using the relation between stator current and load torque with optimized efficiency, see Figure 7.12. The relation is almost independent of the speed, and it is approximated here with a piece-wise linear function which is shown with a thick line on Figure 7.12. The calculated drive loss which is obtained with model-based control and the simple load torque estimation is shown on Figure 7.13. It gives the same good result as with the cos(φ) control. In practice the result will, of course, be worse than that because of inaccuracies in the loss model, and because the real motor constants vary with time and only settles with temperature after several hours. The temperature variations can be taken into account with a time-domain thermal model of the motor and converter.

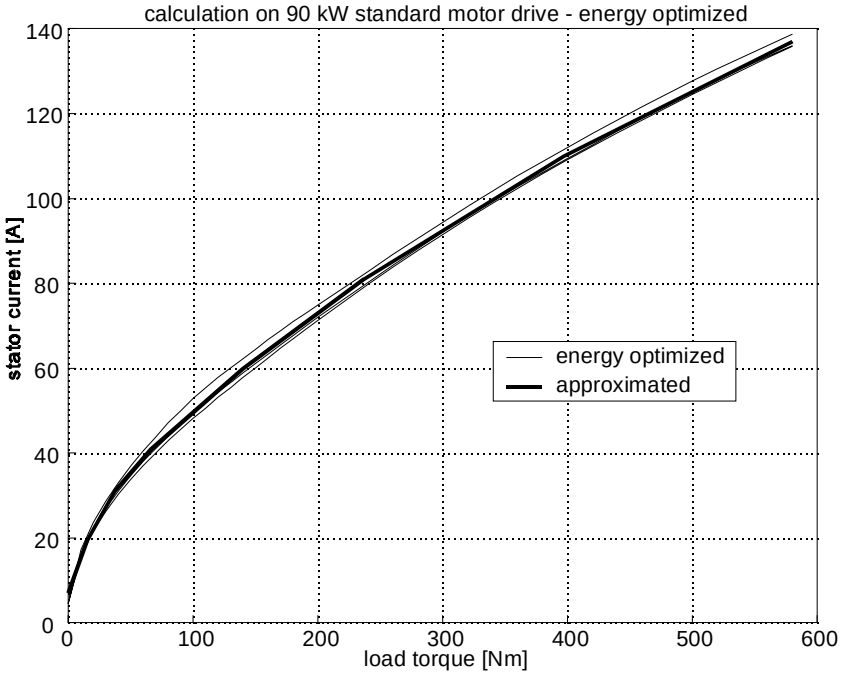

Figure 7.12: *Calculation on 90 kW standard motor drive. Thin lines: stator current with optimized drive efficiency. Thick line: stator current used to estimate load torque.*

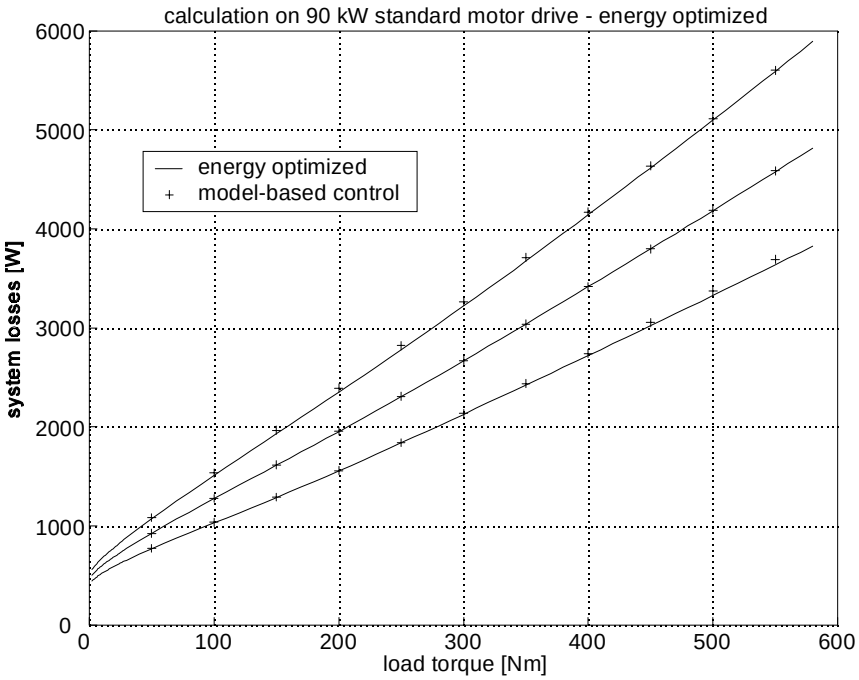

Figure 7.13: *Calculated system loss (motor and converter) for 90 kW drive. Lines: optimized efficiency. Crosses: Model-based control with estimated load torque.*

7.4 Experiments with Model-Based Control.

One energy optimal control strategy is tested experimentally. The model-based control is chosen for that purpose, while the cos(φ) controller could have been tested without problems also. The tests should have been made on the 90 kW drive, but because it was no available the tests had to be carried out on the 22 kW drive.

As it is very difficult to find an analytical solution to the minimum drive loss problem, it is proposed to solve the minimization-problem numerically. The concept was proposed in [2] for a dc-motor drive. Given an operating point defined by an estimated load torque and speed, loss calculations are performed, including both motor and converter losses, and by a numerical minimization algorithm the stator voltage and stator frequency are found which minimize the total drive loss, and they are set as references.

7.4.1 Experiments on a 22 kW Drive.

The model-based control principle was implemented and tested, see Figure 7.14 - Figure 7.16. Two curves are shown on each graph, with energy optimization and with model-based energy optimal control. The model-based control is done as described above. The measurements with energy optimization are in practice done with calculations on loss models also, but with measured speed and load torque as input to the models.

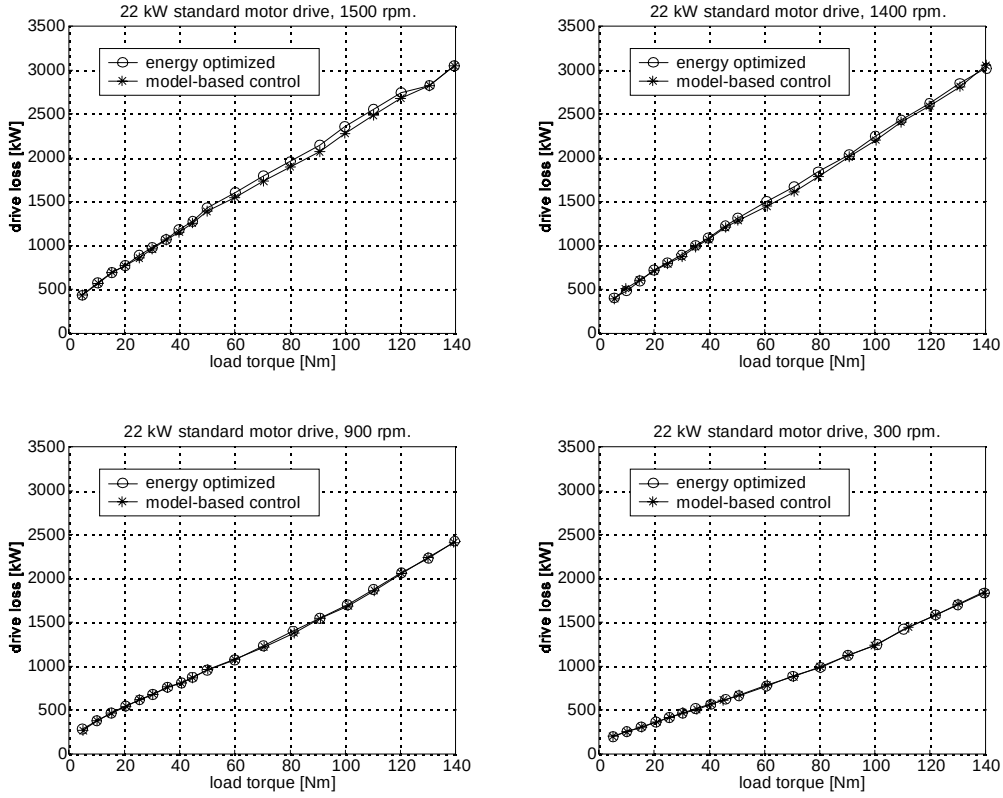

Figure 7.14: *Measured drive loss for 22 kW drive. Circle: energy optimal control, stars: model-based control with estimated load torque.*

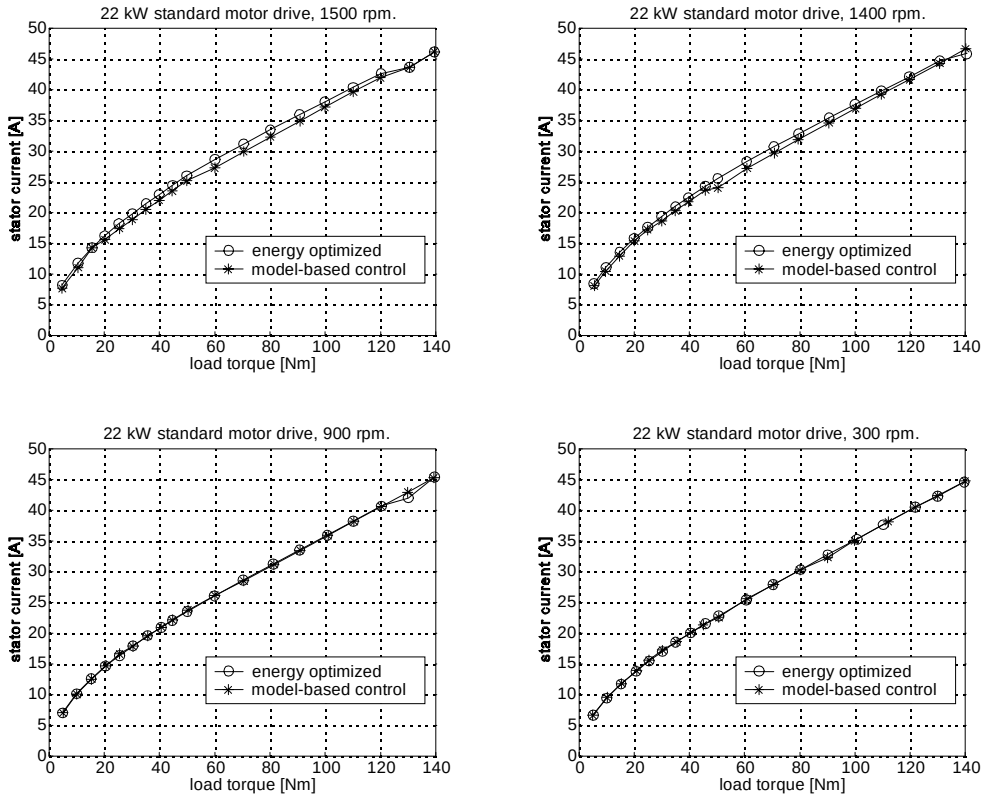

Figure 7.15: *Measured stator current for 22 kW drive. Circle: energy optimized, stars: model-based control with estimated load torque.*

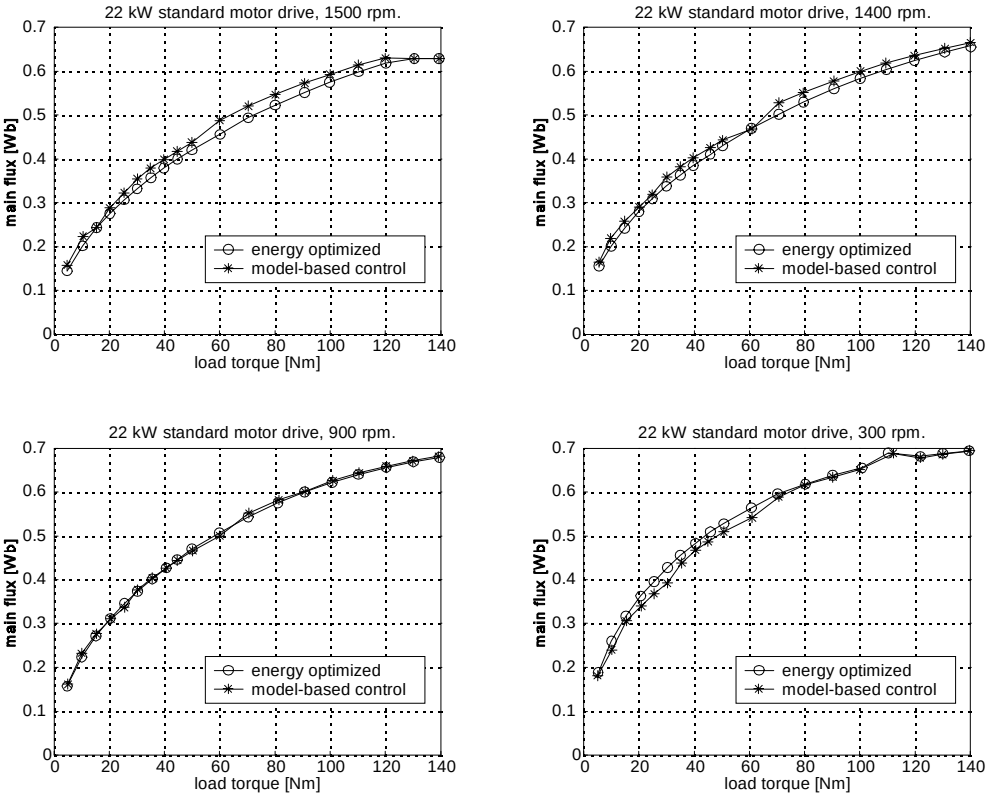

Figure 7.16: *Measurement on 22 kW drive, air-gap flux calculated from measured stator voltage and current. Circle: energy optimized, stars: model-based control.*

Figure 7.14 shows that the model-based control provides good loss minimization. The only major differences between the curves occur at 1400 and 1500 rpm. at high load, where the drive loss with model-based control is actually lower than the loss which was supposed to be the minimized drive loss. The error occurs because at high speed and high load the inverter modulation index is forced into saturation by the low dc-link voltage, and the phenomenon is not included in the converter loss model. From Figure 7.15 and Figure 7.16 it is seen that the model-based control achieved the lower loss compared with the energy optimized case by commanding a higher air-gap flux and which gave a lower stator current.

7.4.2 Practical Implementation of Model-Based Control.

In the beginning of this section it was briefly described how the model-based energy optimal control can be solved numerically. The different ways of practical implementation are discussed here.

For the experiments here, it was chosen to run the energy optimal control algorithms as a background process in the DSP. This means that the basic drive control and PWM calculations are put in an interrupt routine which is launched once every sampling period, see Appendix A.3. In the time between two interrupt routines the DSP then has time to perform the energy optimization algorithm. This means that the air-gap flux reference is not updated every sampling period, but on the other hand it is not necessary with a very powerful processor, and the loss models are not limited in complexity to the same degree as if all the loss model calculations should be carried out every sampling period. Of course, the processor must have a certain amount of overhead time, so the reference value updating does not become too slow. What this means in practice depends on the dynamics of the outer process which is operated by the drive. One rule of thumb could be that the reference updating should be at least ten times faster than the dynamics of the process. When this principle is used, where the loss model calculations are carried out continuously, it is also possible to let the model parameters vary with for example temperature.

Another way of implementation could be to do all the loss model calculations once and for all at commissioning or at start-up. The calculations would then determine the energy optimized relation between air-gap flux, speed and stator current, or between stator voltage, stator frequency and stator current. The relation could be stored in a two-dimensional table, and during operation the drive would simply have to be controlled according to this table. This is a solution with very little demands to the processor performance.

7.5 Over-sized Motors.

Induction motors in HVAC applications are frequently severely over-sized, and it was explained in section 2.2 why it is so. The result of over-sizing is that the motors most of the

time operate with very low load. For mains connected motors low load is equivalent to poor efficiency, so it is important to select a main-connected motor carefully. Indeed, campaigns have been made in Danmark, encouraging engineers not to over-dimension induction motors. In this section it is investigated whether proper motor dimensioning has the same importance in energy optimized variable speed drives.

The question is examined by comparing the 2.2 kW standard motor with a 3 kW standard motor with the same shaft height. The only differences between the motors are that the 3 kW motor has a longer stack, windings with less turns, and thicker stator wire. The comparison is based on calculations, and the model of the 3 kW motor is established by making few modifications to the 2.2 kW motor model. It is shown in Appendix B how the modifications are done. The 2.2 kW motor has a nominal efficiency of 0.820 and a maximal efficiency of 0.823. The 3 kW motor has a nominal efficiency of 0.833 and a maximal efficiency of 0.837.

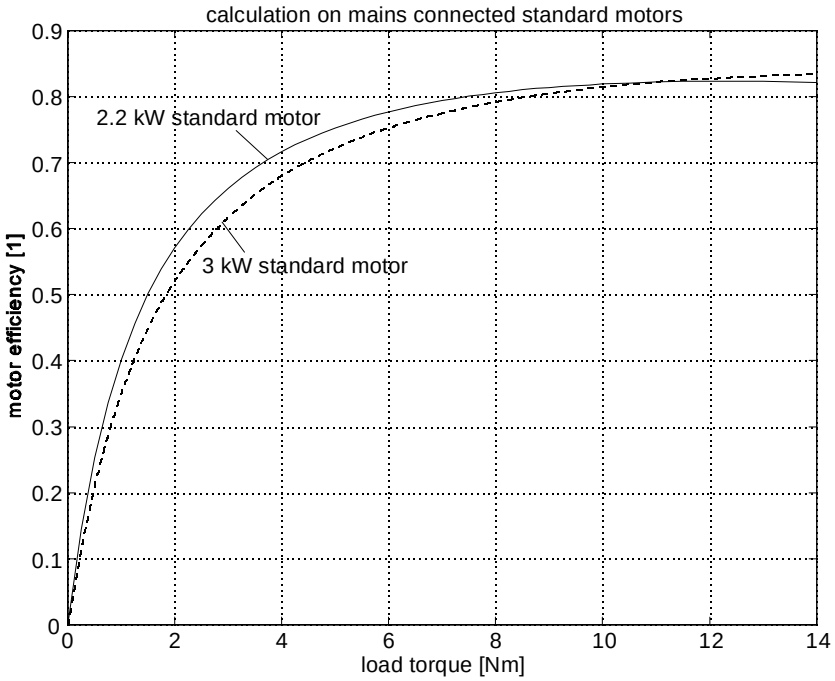

Figure 7.17: *Calculated efficiency of 2.2 kW and 3 kW standard induction motors connected directly to the mains (400 V, 50 Hz). 14 Nm is nominal load for the 2.2 kW motor.*

An illustration of the above mentioned problem is shown on Figure 7.17, where the efficiencies of a 2.2 kW motor and a 3 kW are depicted when they are connected to the mains and are loaded from zero to nominal load for the 2.2 kW motor. The problem of using the 3 kW motor appears below 10 Nm where its efficiency is up to 4.9 % point lower than the 2.2 kW motor efficiency. The reason why it is better to use the 2.2 kW motor is that the core losses are larger in the 3 kW motor, and at low load also the stator copper loss is larger than in the 2.2 kW motor.

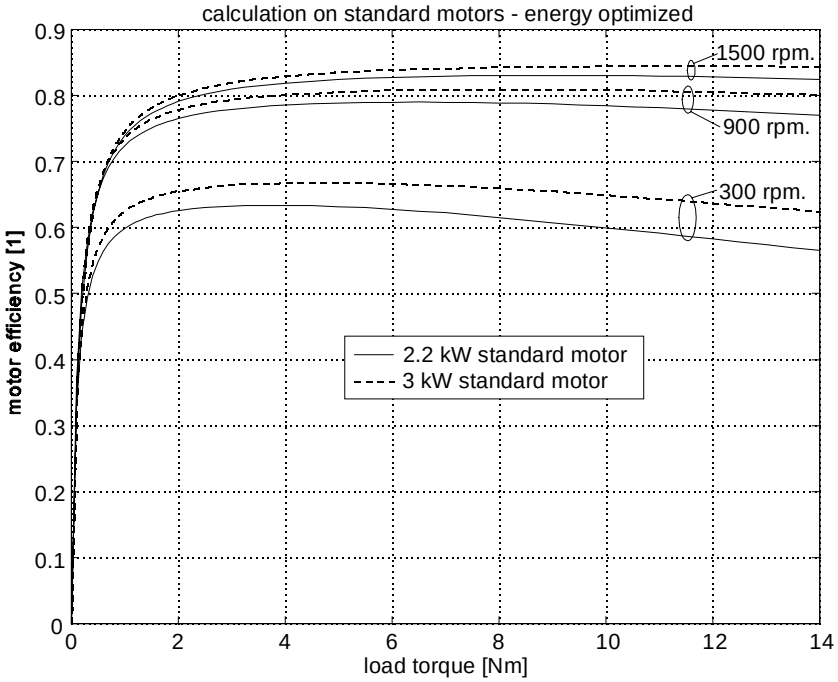

Figure 7.18: *Calculated efficiency of 2.2 kW and 3 kW standard induction motors fed by a converter and with optimized motor efficiency. 14 Nm is nominal load for the 2.2 kW motor.*

The motor efficiencies are now calculated when the motors are fed by converters and with minimized motor loss. Harmonic losses are not taken into account. The results are shown on Figure 7.18 at 300, 900 and 1500 rpm.

The result is that when it is possible to adapt the flux level to the load torque, it is not a disadvantage to use a motor which is too large for the load, indeed the opposite is true. In the whole operating area the 3 kW motor has higher efficiency than the 2.2 kW motor, and especially at low speed. The reason why it is better to use the 3 kW motor in the variable speed drive is that the core losses are almost equal in the two motors, but the stator copper losses are much smaller in the 3 kW motor because of the lower winding resistance.

In the case investigated here, the maximal stator current of the 3 kW motor is 10 % higher than of the 2.2 kW motor, so it would probably be possible to use the same converter with both motors.

The immediate conclusion would be that in variable speed drives it is good to use a motor which is larger than necessary. It should be kept in mind, however, that if the building sizes are not equal as it was the case here, the mechanical losses may be more important in the larger motor. So the result of Figure 7.18 may not be true in a general sense, but anyway it is clear that the problem with over-sized motors does not exist in variable speed drives with energy optimization.

7.6 Energy Optimal Control - Drive Size and Efficiency Improvement.

As three standard induction motor drives (2.2 kW, 22 kW, 90 kW) have been investigated in relation to energy optimal control, both experimentally and with derived loss models, it is possible to set up approximated relations between motor drive size and how much the drive efficiency can be improved by energy optimal control compared with constant air-gap flux control, both as function of speed and as function of load torque.

The relations are illustrated on Figure 7.19 - Figure 7.21 at 300, 900 and 1500 rpm. respectively. These figures show the difference in drive efficiency with and without energy optimal control (drive efficiency improvement in % point). The points between the three motor drives are connected with spline interpolations.

The general tendency is, as expected, that the improvement get smaller the larger the motor drive is, and the higher the load torque is. But the figures also show that in some cases the improvement for the 22 kW is higher than for the 2.2 kW drive. It is believed that this occurs because the 22 kW motor is relatively poor in respect to energy efficiency. Table 7.1 shows, for example, that the per-unit magnetizing inductance of the 22 kW motor is lower than for the 2.2 kW motor. Equally, the core losses and the converter losses for the 22 kW drive are relatively high. This is seen as the reason why the 22 kW motor drive takes so good advantage of the energy optimal control. Despite this fact, the curves may be useful for a general investigation of energy efficiency of induction motor drives.

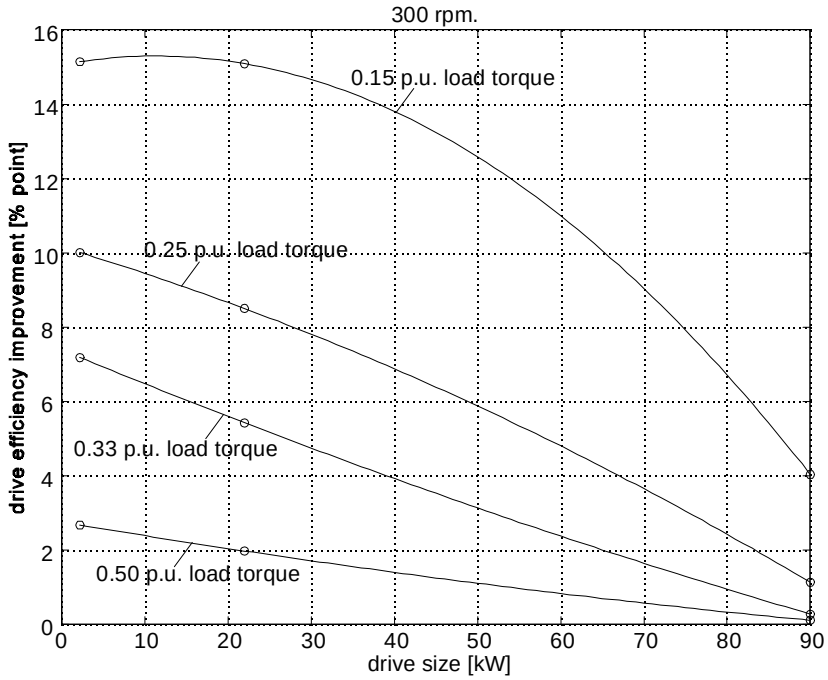

Figure 7.19: *Difference between drive efficiency with constant air-gap flux and drive efficiency with optimized drive efficiency. Standard induction motors at 300 rpm.*

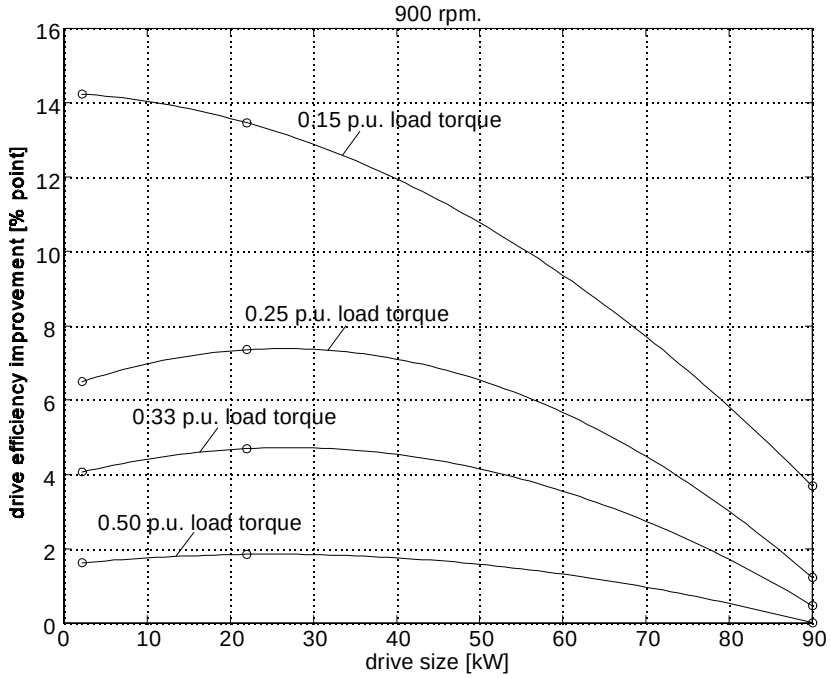

Figure 7.20: *Difference between drive efficiency with constant air-gap flux and drive efficiency with optimized drive efficiency. Standard induction motors at 900 rpm.*

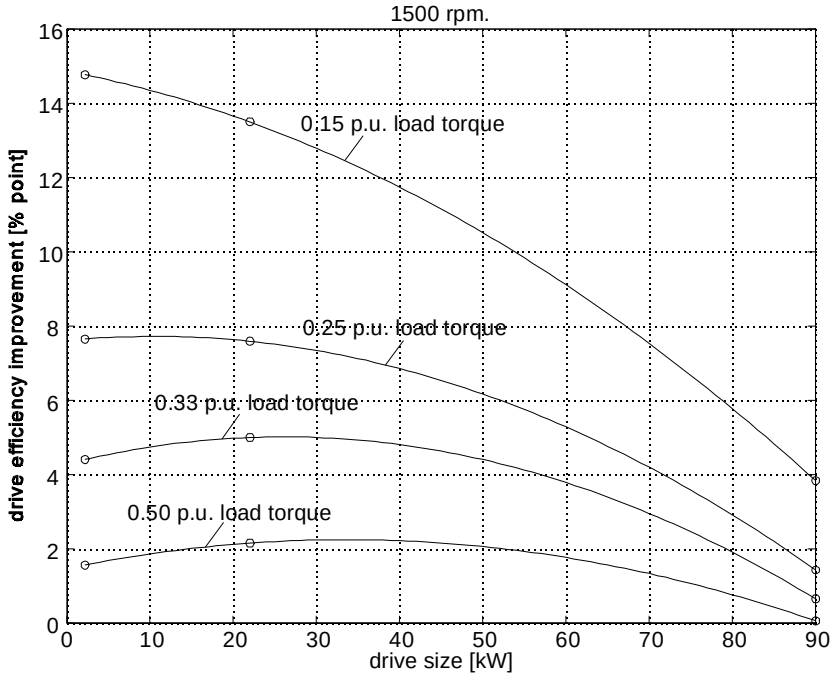

Figure 7.21: *Difference between drive efficiency with constant air-gap flux and drive efficiency with optimized drive efficiency. Standard induction motors at 1500 rpm.*

7.7 Summary.

Motor and converter loss models have been established and verified against extensive measurements in 22 kW and 90 kW standard induction motor drives. Further analysis with these models have shown that it has only very little influence on the drive loss which minimization criterion is used: minimum motor loss or minimum drive loss. So with respect to efficiency, the converter losses do not need to be taken into account in the control algorithm. The only reason to include the converter losses is that it guarantees a higher robustness against load disturbances.

Calculations were done with cos(φ) control and model-based control, both giving very good results. The conclusion is that in medium-size drives it is most important to use an efficiency optimizing control strategy which is simple and provides good quality operation. This is the case with the two investigated strategies, but is for example not the case with search control.

A model-based control with simple load torque estimation was tested on a 22 kW drive with a very satisfactory result, where the losses are significantly reduced at low load for all speeds.

A new energy optimal control strategy is proposed which is based on model-based control, but which converts the control principle into simple state control, according to the terms used in this thesis. The method can be used in drives where motor and possibly converter loss models are known. Instead of doing on-line calculations on the loss-models, all the time-consuming model calculations are done off-line or as a back-ground process, and the drive is controlled according to a simple relation between for example stator voltage, stator frequency and stator current.

Relations have been set up between drive power rating and drive efficiency improvement by energy optimal control in the power range 2.2 - 90 kW. So for a given motor drive in this power range it is possible to estimate the advantage of energy optimal control compared with constant air-gap flux control. One should just keep in mind that the relation is approximate, as the improvement depends on how well the motor drive construction is optimized.

Finally it is proven that the problem of degraded efficiency for over-sized mains-connected motors does not exist in variable speed drives with energy optimal control.

References.

[1] I. Kioskeridis, N. Margaris, “Loss Minimization in Scalar-Controlled Induction Motor Drives with Search Controllers”, IEEE Trans. Power Elec., Vol. 11, No. 2, March 1996, pp. 213-220.

[2] A. Kusko, D. Galler, “Control Means for Minimization of Losses in AC and DC Motor Drives”, IEEE Trans. Ind. App., Vol. IA-19, No. 4, Jul/Aug 1983, pp. 561-570.

Chapter 8

Motor Drive Stability

As stability could be a critical issue when the motor flux is reduced at low load, it is important to analyze this problem. There are two different aspects included in motor stability. The first is related to the risk of stalling the motor in case of a load disturbance, and it is analyzed by simulation and experimentation. The second has to do with oscillation, and it is analyzed by analytical calculation of resonance frequencies and damping.

8.1 Stability in Case of a Load Disturbance.

The problem with stability towards stalling is illustrated by Figure 8.1, where the motor is operating with the load torque and the speed in point OP. Point A is the pull-out torque with nominal air-gap flux. Point B is the pull-out torque with energy optimal control where the air-gap flux is reduced and the stator frequency is increased.

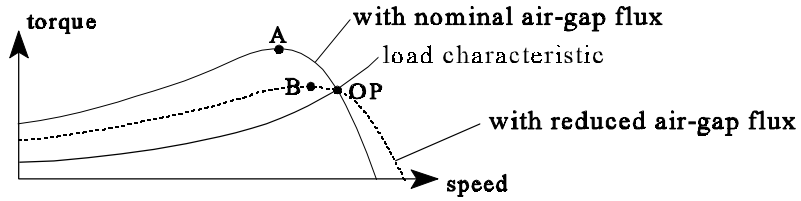

Figure 8.1: *Torque-speed curves with the motor operating in OP. A is the pull-out torque with nominal flux and B is the pull-out torque with reduced flux.*

It is observed that as a result of energy optimal control, the pull-out torque of the motor is reduced. In case of a load disturbance, the motor therefore has an increased risk of pulling out if the stator frequency and the stator voltage are kept unchanged. In a drive with speed feedback the problem is not serious because the speed controller will make sure to increase the produced torque. In fact, a field-oriented vector controlled drive can not pull out, but will just loose speed. The critical case is the open loop controlled drive.

The load disturbance problem is analyzed in two ways. The first is to simulate a sudden load step on a motor with constant voltage and frequency supply using a transient motor

model. The second is do experiments with a sudden load step and compare the responses for different control strategies.

8.1.1 Simulations of a Load Step.

The purpose of simulating a motor exposed to a load step while it is supplied with a constant stator voltage and frequency, is to analyze whether the risk for the motor to pull out depends on how the load step is applied. The two cases which are compared here are a suddenly applied load step and a load which is constant. In case of the constant load, the motor pulls out when the load exceeds the pull-out torque of the motor, which is calculated with the stationary motor model. Figure 8.2 shows the static torque-speed curves is case of nominal stator voltage and in cases where the motor is on the limit of pulling out. Simulations are then made of the motor with the same voltage supplies, but when the load is applied as a step from zero load. These simulations are also shown on Figure 8.2. It can be observed that if the motor can withstand a load applied as a static load, it can withstand the same load even if it is applied as a sudden load step. This is also true even if the speed momentarily goes below the speed of static pull-out. This indicates that the limit of pull-out does not have any relation to how the load is applied, and the problem can be analyzed from purely stationary considerations, for example as it was done on Figure 4.34.

Figure 8.3 and Figure 8.4 show calculated torque reserve for 2.2 kW motors with energy optimization. Torque reserve is here defined as pull-out torque minus developed torque. It is seen, for example, from Figure 8.3 that at 900 rpm. and 30 % of rated torque, the torque reserve is 70 % of rated torque. This means that at this load the motor can remain stable if the load is increased to rated load and the stator voltage and frequency remain unchanged. For the high-efficiency motor at the same load, Figure 8.4, the torque reserve is 90 % of rated load, so the high-efficiency motor is more robust against load disturbances.

The same calculations for the 22 kW motor and 90 kW motor are shown on Figure 8.5 and Figure 8.6. These show that the 22 kW motor is more robust at low speed, but at high speed it is not much better than the high-efficiency motor. The 90 kW motor has generally the best robustness.

The pull-out torque is calculated from equation (8.1) by disregarding core losses. The equation shows that it is especially a high magnetizing inductance which gives a high pull-out torque, as it is also learned from the previous comparisons of different motors.

$$\begin{aligned} \frac{R_r}{s_{pull-out}} &= \left(\frac{(X_r X_s - X_m^2)^2 + (R_s X_r)^2}{R_s^2 + X_s^2} \right)^{\frac{1}{2}} \\ \tau_{pull-out} &= \frac{6}{\omega_s} X_m^2 V_s^2 \frac{R_r}{s_{pull-out}} \left((R_s \frac{R_r}{s_{pull-out}} - (X_r X_s - X_m^2))^2 + (R_s X_r + X_s \frac{R_r}{s_{pull-out}})^2 \right)^{-1} \end{aligned} \qquad (8.1)$$

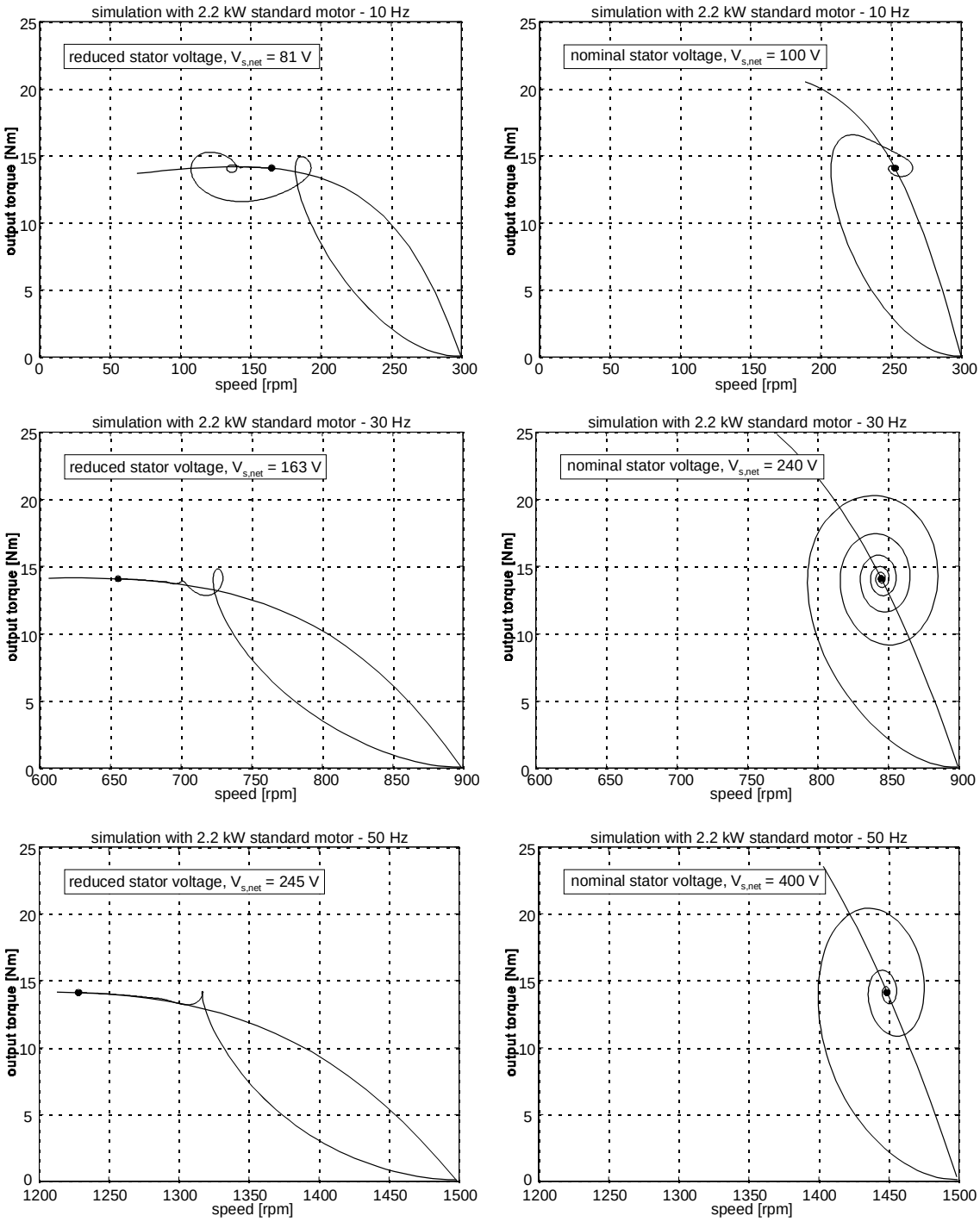

Figure 8.2: *Simulation of 2.2 kW standard motor with reduced stator voltage (left column) and nominal stator voltage (right column). Shown are the static torque-speed characteristic, and the torque-speed trajectory when the load is stepped from 0 to 14 Nm. Stator frequency: 10 Hz (above), 30 Hz (middle) and 50 Hz (below). Inertia: $J = 2\ J_{motor}$.*

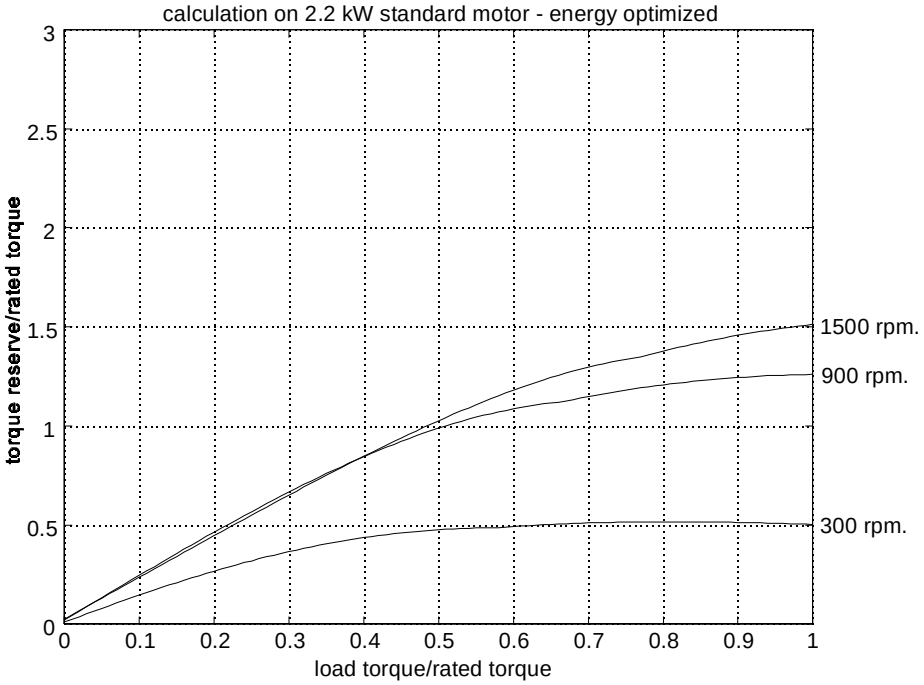

Figure 8.3: *Calculation on 2.2 kW standard motor of torque reserve (pull-out torque minus developed torque) with energy optimization.*

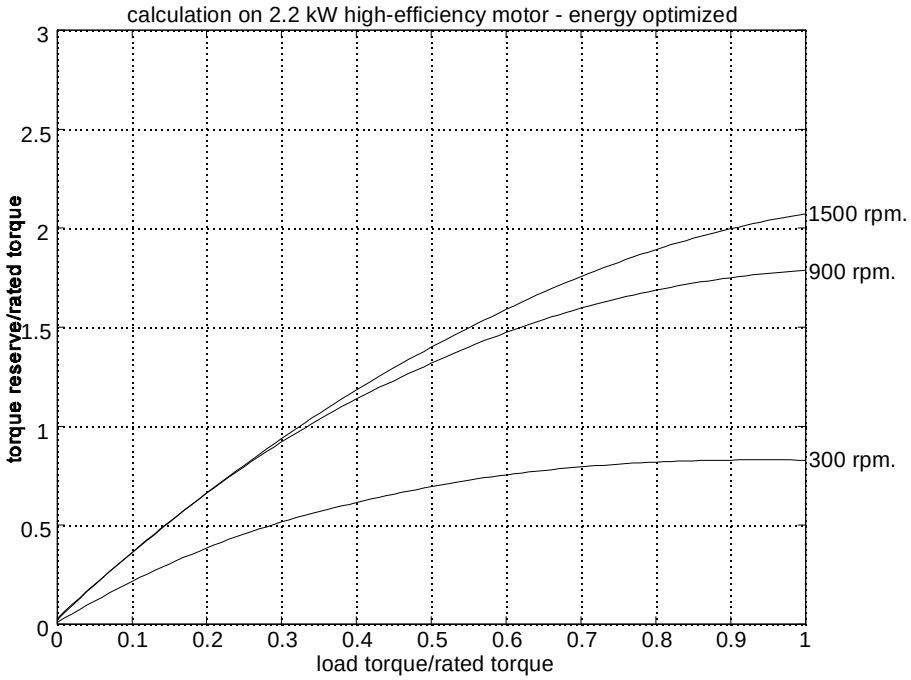

Figure 8.4: *Calculation on 2.2 kW high-efficiency motor of torque reserve (pull-out torque minus developed torque) with energy optimization.*

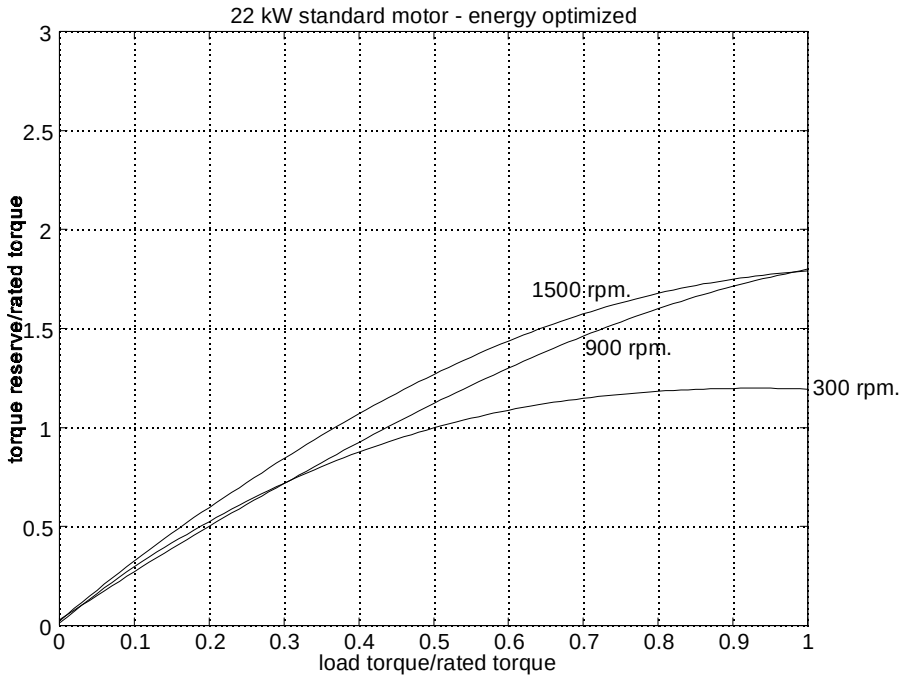

Figure 8.5: *Calculation on 22 kW standard motor of torque reserve (pull-out torque minus developed torque) with energy optimization.*

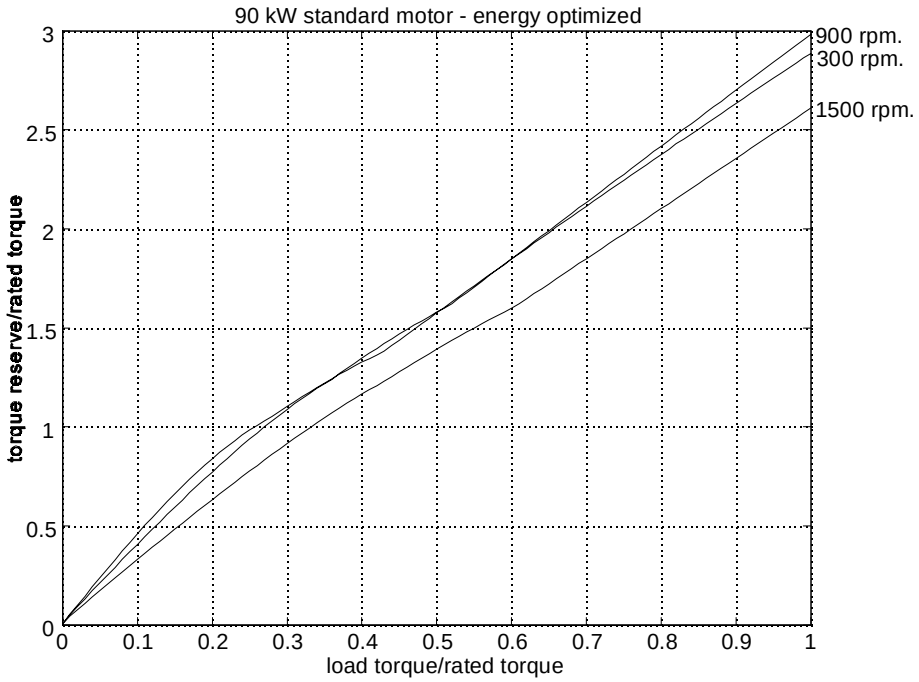

Figure 8.6: *Calculation on 90 kW standard motor of torque reserve (pull-out torque minus developed torque) with energy optimization.*

8.1.2 Experiments with Load Step.

The experiments with a load step are slightly different from the simulations. The simulations were carried out with fixed stator frequency and fixed stator voltage. The experiments are made with a control strategy that forces the air-gap flux to the nominal value if a large load disturbance is detected. By doing that, pull-out is avoided even with a large load step.

During the experiments the motor drive is initially run with energy optimal control at no-load and then the load is suddenly increased to 14 Nm. The induction motor is loaded with a separately magnetized dc-generator, and the load change is realized by switching in an armature load resistance. By realization of the load step in this way it is not certain exactly how the torque is stepped from low to full load, only that it is done rapidly compared with the dynamics of the energy optimal control. Two experiments are shown on Figure 8.7 for the scalar controlled drive operating at 30 Hz stator frequency, and on Figure 8.8 for a rotor-flux oriented vector controlled drive operating at 900 rpm. As mentioned, the air-gap flux is forced to its nominal value when a large load disturbance is detected, and the detection is done by observing the air-gap flux. If the air-gap flux decreases below 98% of the reference air-gap flux, the air-gap flux is forced to its nominal value. In the scalar controlled drive this is done by turning to simple V/f control and applying a voltage which is 10 % above rated voltage for the given stator frequency. In the vector controlled drive the flux is reset to its nominal value by setting the magnetizing current reference to its nominal value. For both drives the energy optimal control is turned on again after 0.5 seconds.

The speed reduction with the scalar drive on Figure 8.7 shows clearly that the nominally excited motor is much more stiff than when the flux is reduced. The difference is smaller for the vector drive, Figure 8.8. The experiments show that it is possible to prevent an energy optimally controlled motor drive from pulling out in case of a load disturbance from low to nominal load. Apart from that, it is difficult to make a general conclusion because the responses depend to a great extent on the way the energy optimal control is programmed to react on load disturbances, and on the dynamic performance of the drive.

The way the motor responds to a load disturbance depends both on the speed and on the flux level. This was seen clearly from the simulations on Figure 8.2, as the responses in some cases are very undamped and in other cases well damped. This leads to the next stability issue, which is an analysis of the resonance frequencies and damping of the motor.

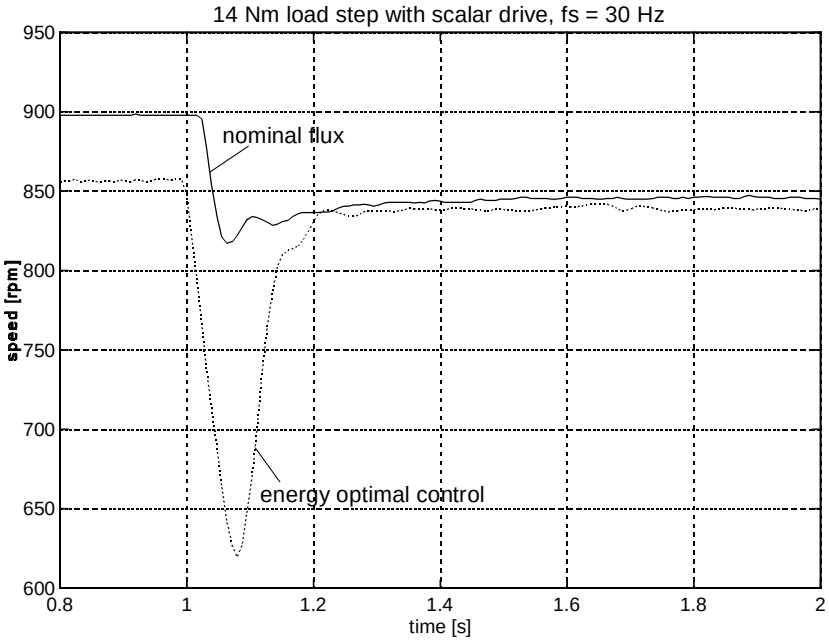

Figure 8.7: *Experiments with sudden step from no-load to full 14 Nm (full load) with the scalar drive. The stator frequency is 30 Hz.*

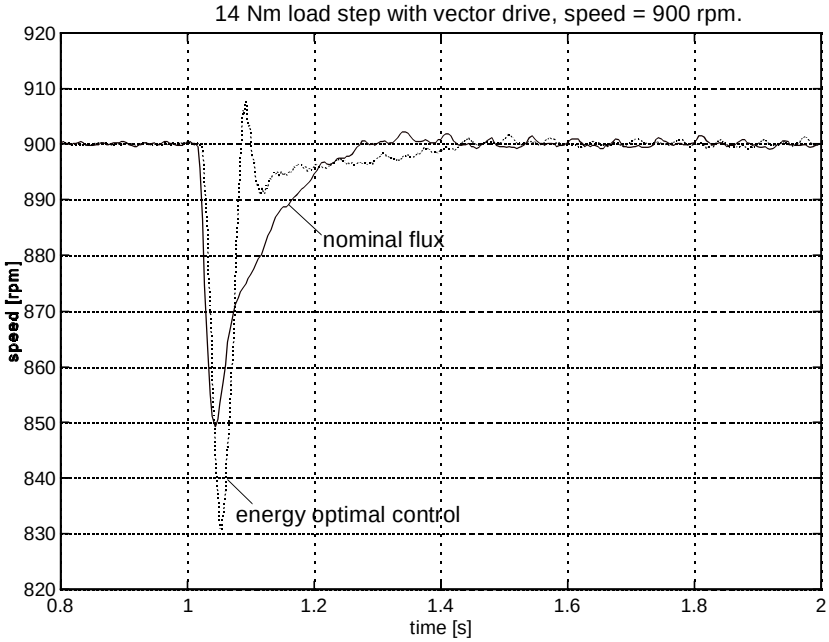

Figure 8.8: *Experiments with sudden step from no-load to full 14 Nm (full load) with the vector controlled drive. The speed reference is 900 rpm.*

8.2 Oscillations.

In an inverter driven motor, oscillations can be excited by three sources:

Load disturbances: When the load itself can not provide sufficient mechanical damping, as for fan blowers, or when the load torque contains a periodic component, as for a piston compressor.

Motor Construction: Eccentricity.
Asymmetry of windings.
Slotting.

Inverter non-linearities: dc-link ripple.
Dead-time.
Switching time and component voltage drop.

8.2.1 Methods of Analysis.

There are two different approaches to the analysis of motor oscillations. One method, suggested in [1], is to use a linearized motor model. The motor is described as a fifth order system, with five poles and five zeros. The damping of the motor is expressed by the damping of the dominating poles. Evaluating the dominating poles in the whole operating area, the worst case is found in the point where the damping is smallest. One difficulty is that in certain areas it is not well defined which poles are the dominating ones, and then it is difficult the define the motor damping factor. Another inconvenience is that the damping factor comes out as a numerical value so there is no information of how it related to the motor parameters.

Another method, which is less time consuming and more informative, is suggested in [2] and [3]. It utilizes the fact that there are two modes of resonance in the motor: parallel resonance and series resonance. The nature of the two modes is illustrated on Figure 8.9. In the series resonance mode the angle between the stator flux and the rotor flux oscillates, the amplitudes being constant and the leakage inductance acting as a spring. In the parallel resonance mode the angle is constant and the flux amplitudes oscillate.

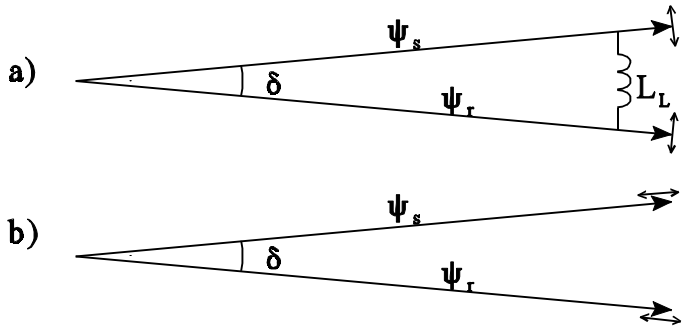

Figure 8.9: *Illustration of a) series resonance and b) parallel resonance in an induction motor.*

The calculation of the resonance frequencies is based on the Γ-model of the motor, see Figure 8.10.

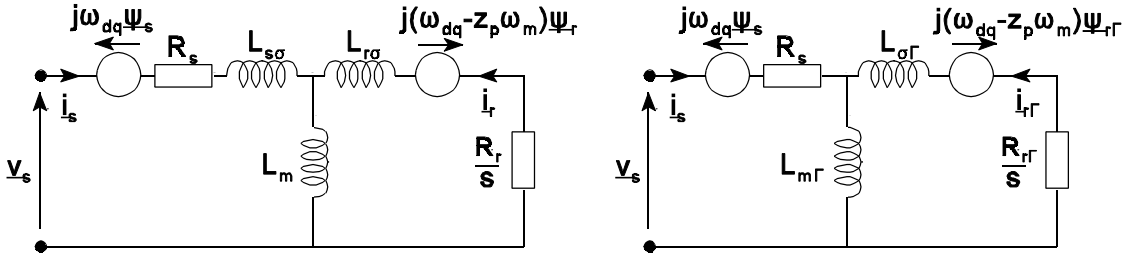

Figure 8.10: *Transient T-model and Γ-model of an induction motor.*

There are the following relations between the T-model and the Γ-model parameters:

$$
\begin{aligned}
R_{r\Gamma} &= \left(\frac{L_m + L_{s\sigma}}{L_m} \right)^2 R_r \\
L_{m\Gamma} &= L_m + L_{s\sigma} \qquad (8.2) \\
L_{\sigma\Gamma} &= (L_m + L_{s\sigma}) \left(\frac{(L_m + L_{s\sigma})(L_m + L_{r\sigma})}{L_m^2} - 1 \right)
\end{aligned}
$$

Four simple equations, which are derived in [2], express the resonance frequency and the corresponding damping for each of the two resonance modes, using the Γ-model parameters in per-unit, see equation (8.3).

The series resonance frequency and damping are calculated under the assumption that the magnetizing inductance is infinite, so the stator current equals the rotor current with opposite sign, but this approximation does not distort the result very much.

The parallel resonance is calculated under several assumptions, for example that the leakage inductance is zero and the flux amplitudes are constant. Therefore the calculated parallel resonance values are not as exact as for the series resonance. However, they still describe how the different motor parameters influence the resonance properties.

$$\omega_{ser,p.u.} = \frac{\psi_{s,p.u.}}{\sqrt{J_{p.u.} L_{\sigma\Gamma,p.u.}}} \quad , \quad \zeta_{ser} = \frac{R_{s,p.u.} + R_{r\Gamma,p.u.}}{2\psi_{s,p.u.}} \sqrt{\frac{J_{p.u.}}{L_{\sigma\Gamma,p.u.}}}$$

$$\omega_{par,p.u.} = \frac{\psi_{s,p.u.}}{\sqrt{J_{p.u.} L_{m\Gamma,p.u.}}} \quad , \quad \zeta_{par} = \frac{\psi_{s,p.u.}}{2R_{s,p.u.}} \sqrt{\frac{L_{m\Gamma,p.u.}}{J_{p.u.}}} \qquad (8.3)$$

where ω_{ser}, ω_{par} : series and parallel resonance angular velocity.
ζ_{ser}, ζ_{par} : series and parallel resonance damping factor.
ψ_s : stator flux.
J : moment of inertia.
$R_{r\Gamma}$: rotor resistance of the Γ-model.
$L_{\sigma\Gamma}$: leakage inductance of the Γ-model.
$L_{m\Gamma}$: magnetizing inductance of the Γ-model.

From the analytical expressions in equation (8.3) it is seen that the damping of the series resonance is increased with increasing stator resistance while it is opposite for the parallel resonance. This indicates that parallel resonance is a problem in small machines and series resonance is a problem in large machines. Flux reduction decreases the parallel resonance damping and increases the series resonance damping. A small leakage inductance and a large magnetizing inductance always increase the damping.

Expressed in absolute values, equation (8.3) becomes:

$$f_{s,ser} = \frac{1}{2\pi}\sqrt{\frac{3}{2}}\frac{\psi_s z_p}{\sqrt{J L_{\sigma\Gamma}}} \quad , \quad \zeta_{ser} = \frac{R_{s\Gamma} + R_{r\Gamma}}{2\psi_s z_p}\sqrt{\frac{2}{3}\frac{J}{L_{\sigma\Gamma}}}$$

$$f_{s,par} = \frac{1}{2\pi}\sqrt{\frac{3}{2}}\frac{\psi_s z_p}{\sqrt{J L_{m\Gamma}}} \quad , \quad \zeta_{par} = \frac{\psi_s z_p}{2R_{s\Gamma}}\sqrt{\frac{3}{2}\frac{L_{m\Gamma}}{J}} \qquad (8.4)$$

These equations are now used to calculate the resonance frequencies and damping of different induction motors.

8.2.2 Calculation of Oscillations.

The resonance frequency and damping are evaluated with constant air-gap flux and with optimized efficiency, both for the 2.2 kW motors, the 22 kW motor and the 90 kW motor, see Figure 8.11 - Figure 8.14.

The influence of energy optimization can be seen from for example Figure 8.11. As the flux is reduced at low load, both the series and the parallel resonance frequencies decrease. But while the flux reduction increases the series resonance damping, the parallel resonance becomes more undamped.

The series resonance of the high-efficiency motor can be expected to be less damped as its resistances are smaller, and this is also seen by comparing the series damping of the two 2.2 kW motors, Figure 8.11 and Figure 8.12, but in both cases the damping factor is above one. The series resonance is more likely to cause problems for the larger motors, as the damping factor then goes below one. At low load the problem can be reduced by flux reduction, so in that case the parallel resonance is not likely to cause any problems. But the parallel resonance can cause problems in situations when it is not possible to reduce the flux, like during start-up. The 90 kW motor, for example, has a resonance frequency around 5 Hz where the damping factor is only 0.6.

Another risk is if the motor is loaded with a large inertia with little damping, e.g. a fan, because the parallel resonance damping is then brought down by the inertia-factor, see equation (8.4). This is especially dangerous during start-up because the poor damping is then combined with a long starting time.

One approach to reduce the oscillations is to eliminate the exciting sources, that is changing to a less perturbating load, improving the motor design, and linearizing the inverter by compensating for its non-linearities.

Another approach is to increase the damping by control means, which is proposed in [3]. If the stator flux is controlled, it corresponds to having a zero stator resistance, whereby the parallel resonance is infinitely damped, but the series resonance becomes less damped. By correcting the voltage in the q-axis of the stator flux oriented drive, the stator resistance can be virtually increased and the series resonance be more damped.

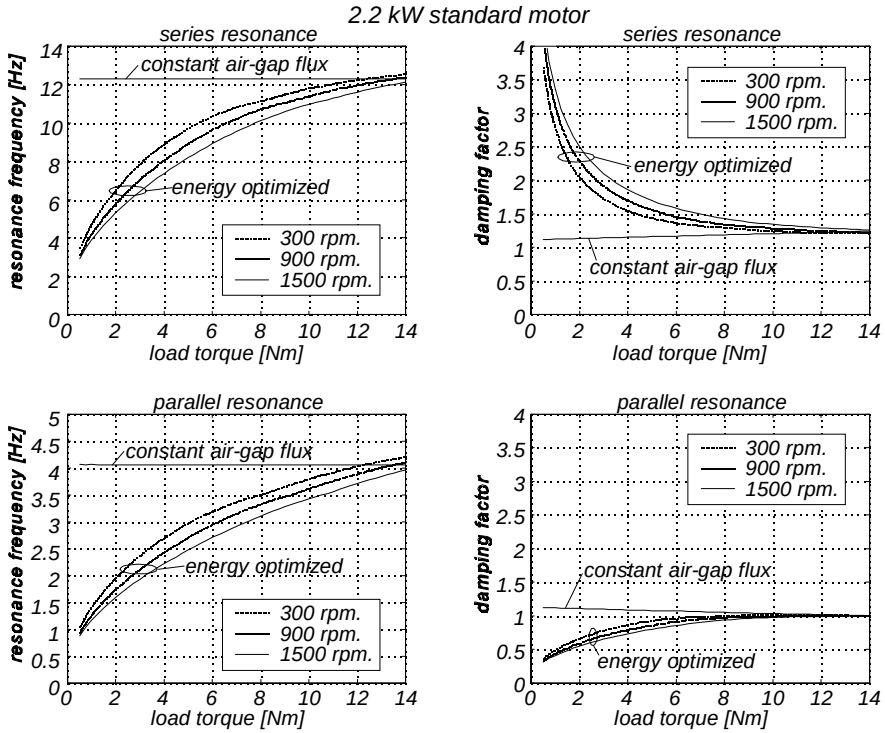

Figure 8.11: *Calculation of resonance stator frequency and damping of the 2.2 kW standard motor with constant air-gap flux and with optimal efficiency. Speeds: 300, 900, 1500 rpm.*

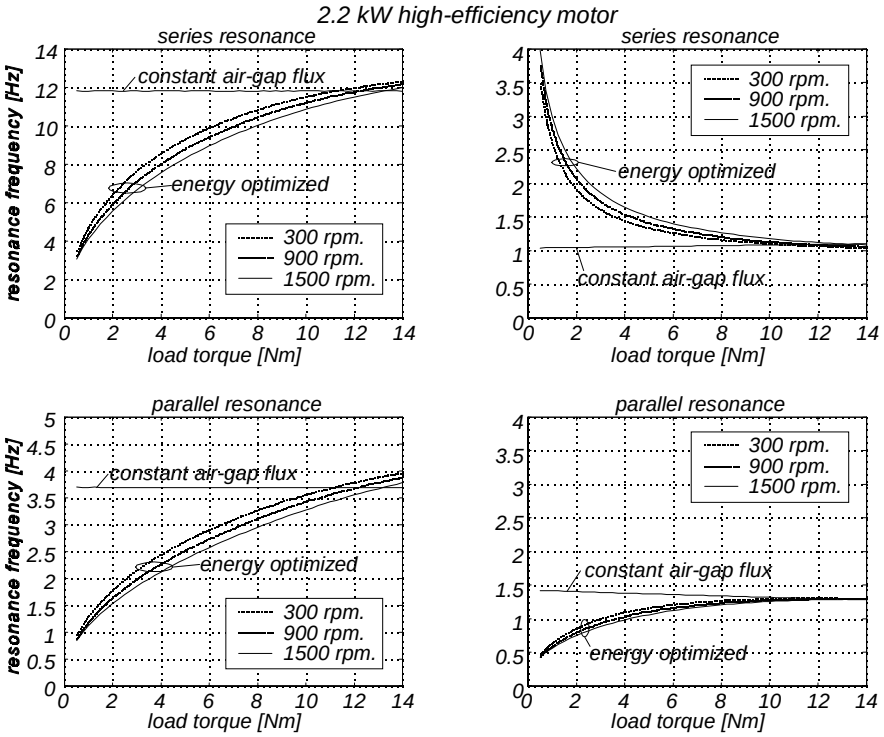

Figure 8.12: *Calculation of resonance stator frequency and damping of the 2.2 kW high-efficiency motor with constant air-gap flux and with optimal efficiency. 300, 900, 1500 rpm.*

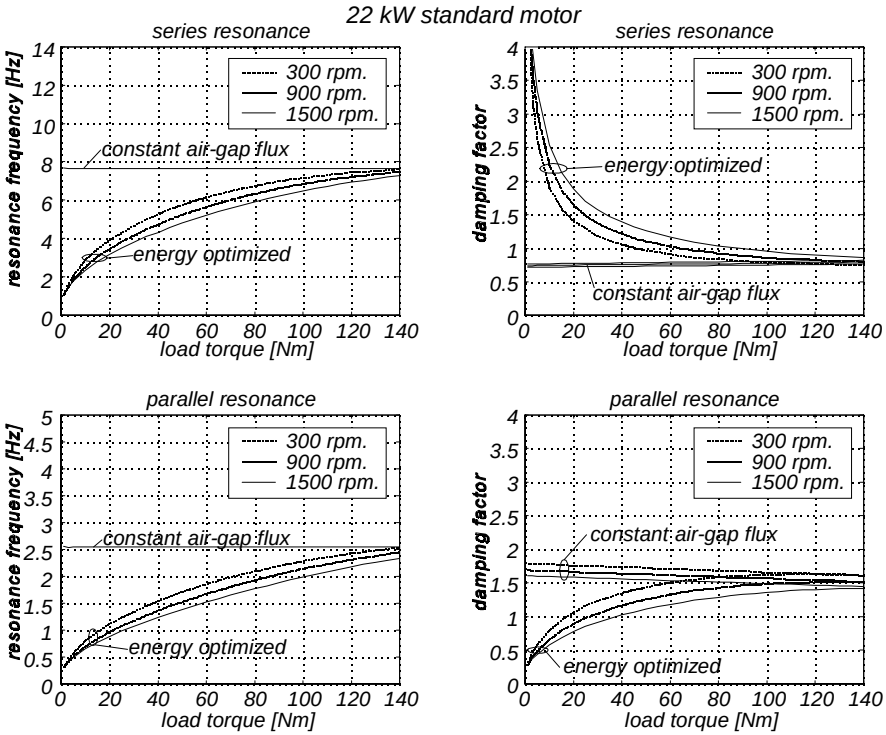

Figure 8.13: *Calculation of resonance stator frequency and damping of the 22 kW standard motor with constant air-gap flux and with optimal efficiency. Speeds: 300, 900, 1500 rpm.*

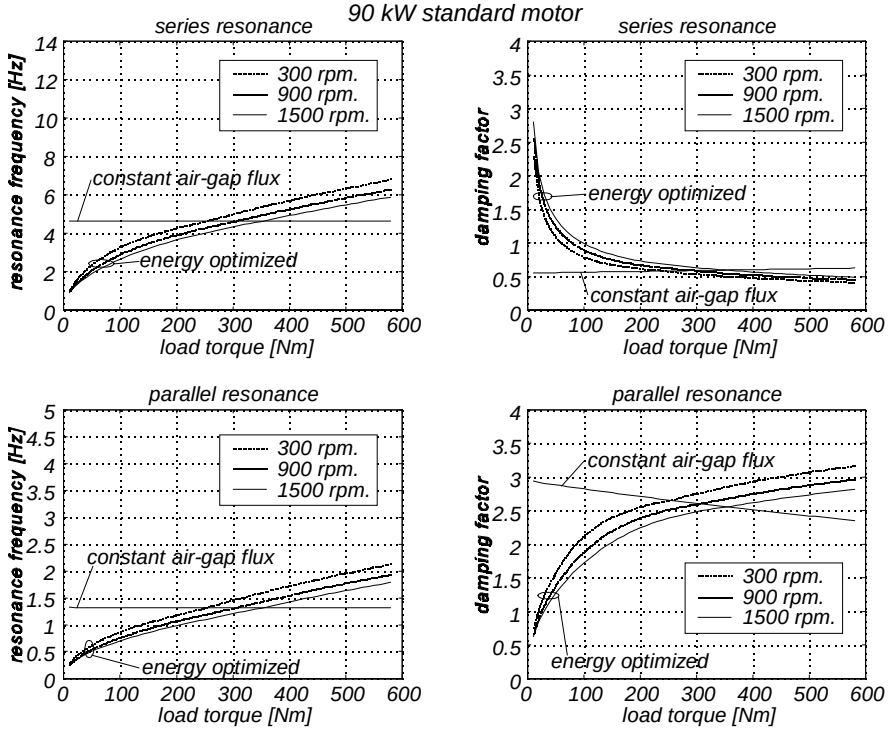

Figure 8.14: *Calculation of resonance stator frequency and damping of the 90 kW standard motor with constant air-gap flux and with optimal efficiency. Speeds: 300, 900, 1500 rpm.*

8.3 Summary.

A systematic analysis of stability is made for open-loop controlled motors, a topic which is not seen before is relation to energy optimal control. Two instability phenomena have been investigated: robustness against load disturbances, and oscillations. The robustness against load disturbances was first analyzed by simulating sudden load steps in cases with nominal magnetization and in cases with flux reduced to the limit of static pull-out. The result was that the limit of pull-out is independent of how the load disturbance is applied. This finding simplifies robustness analysis considerably, because it can then be made from simple steady-state considerations. Comparison of the robustness towards load disturbances for different motors showed that a high-efficiency motor is more robust than a standard motor, and similarly medium-size motors are more robust than small motors. The reason is primarily the relatively higher magnetizing inductance of the high-efficiency and medium-size motors.

The oscillations were analyzed by use of analytical expressions instead of the usual method of linearization and calculation of Eigen-values. The strength of the analytical method, which gives serial and parallel resonance frequencies and damping factors, is that it defines a link from the physical motor parameters to the resonance properties. The finding with respect to energy optimization is that both series and parallel resonance frequencies are reduced by flux reduction. The influence on damping goes either way when the flux is reduced, because the series resonance damping is increased and the parallel resonance damping is decreased. It can not be said beforehand which resonance phenomenon will possibly cause trouble, as this depends on motor size and inertia, so in some cases energy optimization will cause trouble, and in other cases it will reduce the oscillations. But anyway, during start-up where the motor is nominally magnetized, a drive may have to be operated with special control in order to avoid problems with oscillations.

References.

[1] P. C. Krause, O. Wasynczuk, S. D. Sudhoff, “Analysis of electric machinery”, New York, 1995.

[2] B. Peterson, “Oscillations in Inverter Fed Induction Motor Drives”, Tech. Lic. Dissertation, IEA, LTH, Lund, Sweden, 1991.

[3] M. Alaküla, B. Peterson, J. Valis, “Damping of Oscillations in Induction Machines”, Proceed. of PESC’92, Vol. 1, Toledo, Spain, Jul. 1992, pp. 133-138.

Chapter 9

Comparison of Induction Motor Drive and PM Motor Drive Efficiency

Integral horse-power permanent magnet motors have been used for several years as a replacement for dc-motors in applications demanding high dynamics or accurate servo performance. Energy consumption has not been a determining factor here, rather high reliability, high performance and low maintenance. Permanent magnet motors are also used in submersible pumps combining good efficiency with a compact design. An application where the permanent magnet motor has replaced an induction motor for efficiency reasons is refrigerators, but this is only for some hundred watt output power motors. However, as the price of permanent magnets goes down it becomes more and more interesting to use PM motor drives as replacement for induction motor drives. For example, Yaskawa Motors has recently started a production of interior permanent magnet motors in the range 0.4-75 kW as a replacement for variable speed standard induction motor drives, presumably offering a better efficiency. The objective with this chapter is to put the induction motor drive in perspective by evaluating the energy consumption and economical aspects of using a permanent magnet motor drive instead of an induction motor drive in HVAC applications. Focus is put on 2.2 kW and 90 kW drives.

No one is in doubt that PM motors have substantially lower losses than the induction motor at nominal load as there are no rotor core and copper losses, and no magnetizing current to generate stator copper losses. It is, however, interesting to analyze the situation also at light load, where it is possible to reduce the flux in the induction motor, and to see whether the induction motor drive can compete with the permanent magnet motor drive, for which flux-weakening is not feasible.

9.1 Conditions for the Comparison.

Similar comparative studies of this subject have previously been done, of which three are mentioned here. Andersen et al. [1] made a comparison, and constructed an induction motor and several surface mounted PM motors and brush-less dc motors with optimized efficiency

as a key goal. But as the power ratings were very low (100 W), the results can not be extended directly up to the power levels examined here. Slemon [2] compared induction motor and PM motor efficiencies. However, his considerations were purely theoretical and only for nominal load. So he did not consider the most predominant load situation in HVAC, namely light load, and his results are not useable for the cases studied here. A comparison of 0.75 kW permanent magnet and induction motor drives was reported by Hansen [3]. The comparison was done between a PM motor with a nominal efficiency of 0.87, and an induction motor with energy optimal control having a nominal efficiency of 0.78. At quarter load and half speed the efficiencies were 0.82 and 0.63 respectively. It was estimated that for a heat-water pump in house-holds the annual energy consumption can typically be reduced with 14 % by using the PM motor drive instead of the induction motor drive. This gives a good idea of the attainable difference between the two motor types, although a smaller difference can be expected at power levels higher than 0.75 kW.

It is a very difficult task to compare two different motor types in a fair way, and the comparison can be designed in different ways. This comparison is restricted to 4-pole, 50 Hz motors with sinusoidal 400 V supply, although there may be other combinations of these three specifications for which the permanent magnet motor is especially well suited. Then one could set up several different specifications from which the motor drives should be designed, including volume, weight, material cost and manufacturing cost. It should also be specified how the motor drives are tested, for example to know whether the motors should be optimized for low load or high load. Having defined all this, experts should design the two motors, and then an absolute comparison of the two motor drives could be carried out.

This procedure probably formed the basis of the results reported in [3], but it is very time-consuming, and given the limited resources in this project an easier method has been chosen, and the strength of the result is, of course, proportionally weak. It is believed, however, that it is possible to reach some conclusions regarding the performances of the two types of drives.

The methodology used here is to compare the drives in two different pump applications. The induction motor drives are those analyzed in the preceding chapters, the 2.2 kW standard and high-efficiency motor drives, and the 90 kW standard motor drive. The sine-wave permanent magnet synchronous motors (PMSM) are designed with the same stator geometry and core material as their corresponding standard induction motors, and the windings are also the same. The rotors are equipped with surface-mounted radially magnetized sintered NdFeB permanent magnets. Neither brush-less dc-motors nor interior permanent magnet motor are considered. The permanent magnet motors are, of course, not optimized to the same degree as the induction motors, so a comparison of the absolute performances is not possible. But it is possible to answer what the relation is between the performances at high load and at low load, similarly at different speeds, and to get an idea of the converter loss with the different

motors. Finally it will be possible get an idea of the advantage of using permanent magnet motors related to the motor power size, partly with respect to energy consumption and partly with respect to pay-back times.

The pump load and the motors are first described. Then the induction motor losses are calculated with the already established models. For the permanent magnet motors, which are not constructed in practice, the loss calculations are based on experience with the induction motors and on calculations done with a commercial motor designer software. The results are presented both in terms of losses, typical energy consumption and pay-back time. For the rest of the chapter a permanent magnet synchronous motor is referred to as a PMSM.

9.2 Speed and Load Torque Characteristics.

The motors drive water circulating pumps without head, and they are examined in two situations: pressure control and flow control. In both cases the motor speed and load torque are calculated as function of flow. It is first done for the 2.2 kW motor drives. The characteristic curves for a pump equipped with a 2.2 kW mains-connected induction motor are shown on Figure 9.1.

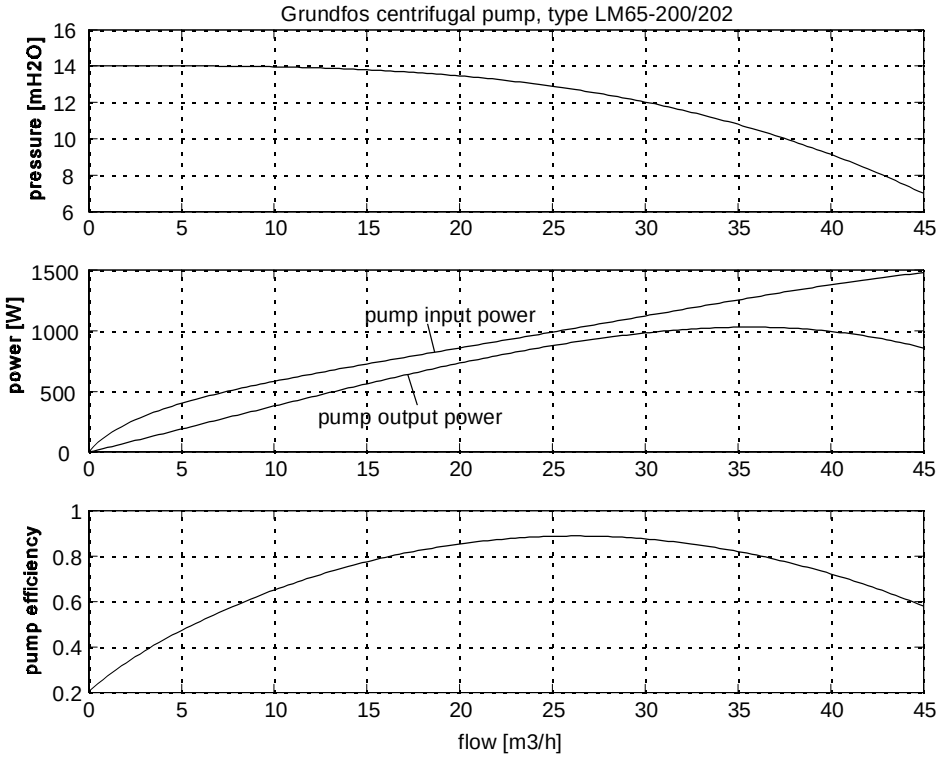

Figure 9.1: *Characteristic curves for a centrifugal pump, Grundfos LM65-200/202, fed by a 2.2 kW induction motor connected directly to the 50 Hz grid.*

9.2.1 Pressure Control.

This control strategy is often used in hot-water distribution installations with variable system characteristic [4]. The pressure is for a given flow controlled according to the linear pressure-flow curve marked with a thick line on Figure 9.2 by varying the speed. If, for example, the system characteristic is equal to the broken line on Figure 9.2, the pump is operating in point A. Increasing the speed to the nominal value would change the operating point to B. The speed in point A is a calculated as

$$n_A = n_B \frac{q_A}{q_B} \qquad (9.1)$$

where n_A, n_B : speed in point A and B.
q_A, q_B : flow in point A and B.

This leads to the speed curve marked with thick line on Figure 9.2. The pump output power is the product of pump pressure and flow, and the pump input power is then calculated by dividing with the pump efficiency. The pump efficiency is approximated by equation (9.2) [5, p. 121], which defines the efficiency in point A from knowledge of the efficiency in point B. Having calculated the pump input power, which is equal to the motor output power, the motor load torque, which is marked with a thick line on Figure 9.2, can easily be calculated.

$$\eta_A = 1 - \left(1 - \eta_{pump,B}\right)\left(\frac{n_B}{n_A}\right)^{0.1} \qquad (9.2)$$

where $\eta_{pump,A}$, $\eta_{pump,B}$: pump efficiency in point A and B.

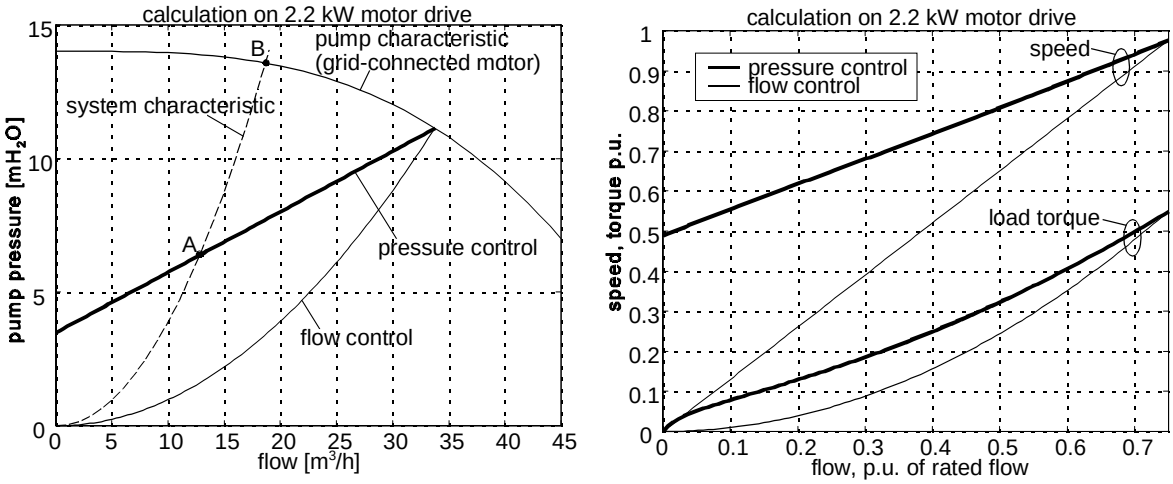

Figure 9.2: *Illustration of the calculated motor load torque and speed with pressure control and flow control for a 2.2 kW motor driving a Grundfos LM65-200/202 pump with variable speed. Left: pressure-flow curves, right: load and speed characteristics.*

9.2.2 Flow control.

In installations where the system characteristic is constant, the flow can be controlled directly with the speed. The pressure-flow curve is marked with a thin line on Figure 9.2. The speed is considered proportional to the flow, and the speed and load torque are calculated by following the same procedure as for the pressure control. The results are shown with thin lines on Figure 9.2 to the right.

9.2.3 Load of 90 kW Drive.

The pump characteristics for the 90 kW drives are obtained by upscaling the curves for the small pump, see Figure 9.3. The p.u. speed and load torque curves are almost equal to those for the 2.2 kW drives.

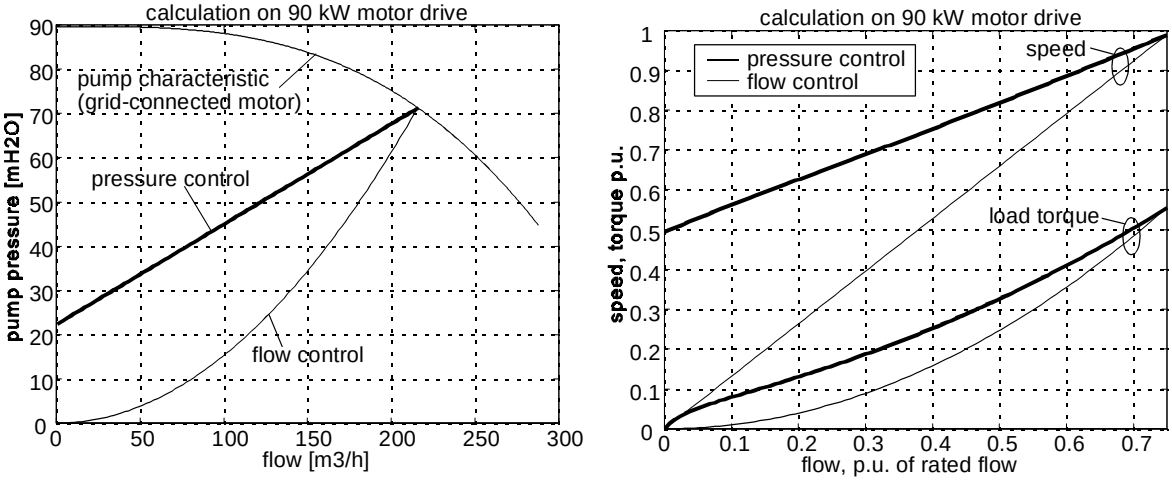

Figure 9.3: *Calculated motor load torque and speed with pressure control and flow control for a 90 kW motor driving a pump with variable speed. Left: pressure-flow curves, right: load and speed characteristics.*

The calculations of the load torque for the 2.2 kW and 90 kW motors show that the motors are never loaded to more than 55 % of rated torque. The situation is not rare in real applications, although is seem obvious to use a smaller motor.

9.3 Description of the Motors.

Cross-sections of the 2.2 kW motors are shown on Figure 9.4, and of the 90 kW motors on Figure 9.5. As may be seen from the figures, the induction motors and the PMSMs use the same stator frame geometries, while the rotors of the PMSMs are equipped with surface mounted permanent magnets. The PMSMs are not constructed physically.

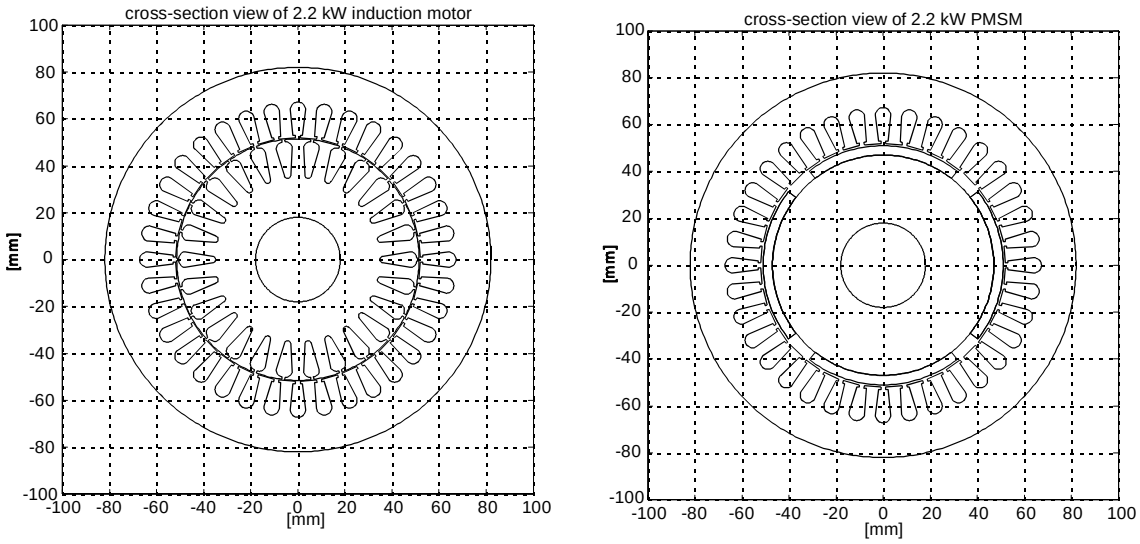

Figure 9.4: *Cross-sections of the investigated 2.2 kW motors. Left: standard and high-efficiency induction motor. Right: sine-wave permanent magnet synchronous motor. Measures are given in [mm].*

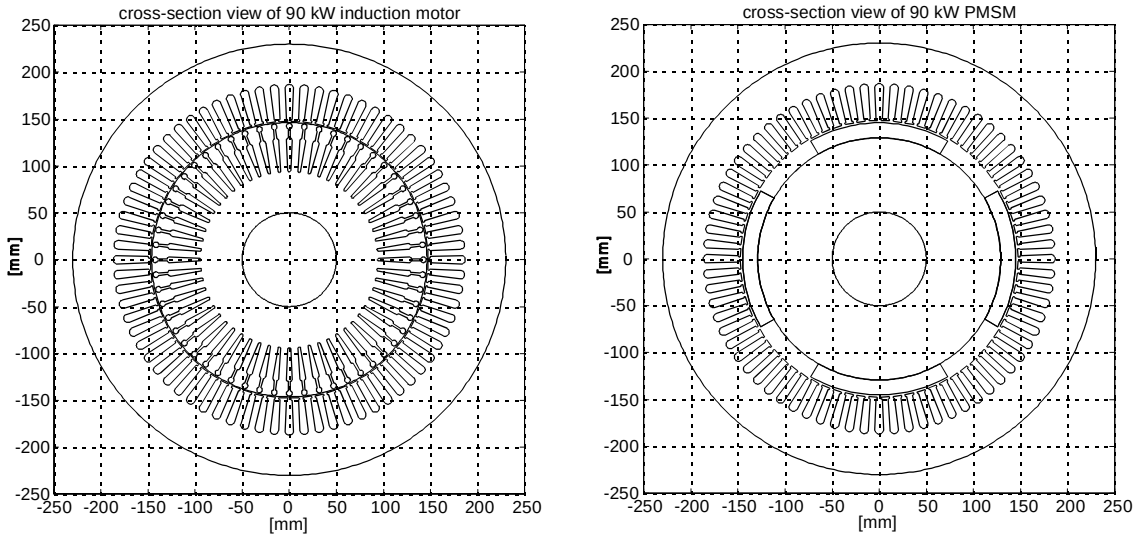

Figure 9.5: *Cross-sections of the investigated 90 kW motors. Left: standard induction motor. Right: sine-wave permanent magnet synchronous motor. Measures are given in [mm].*

9.3.1 Induction Motor Loss Calculation.

The induction motor losses are calculated according to the method in chapter three, and the model constants for the 2.2 kW standard and high-efficiency motors and for the 90 kW standard motor are listed in appendix B. The only difference is that the stator resistances are all calculated with a 80°C winding temperature, and the resistance values are listed in Table 9.1.

9.3.2 PMSM Construction.

The PMSMs which are used for the comparison are not constructed, so the derivation of their efficiencies is based on calculation and on induction motor data. The PMSMs are made with the same stator geometry and core material as their respective standard induction motors, and the rotors are provided with surface mounted permanent magnets of sintered NdFeB. It is assumed that the magnet temperature is 80 °C, so the remnant flux density is 1.07 T and the relative recoil permeability is 1.06, see Figure 9.6.

The PM arc angle of the 2.2 kW PMSM is adjusted to minimize torque ripple. The PM arc angle of the 90 kW PMSM is adjusted to reduce the circulating currents in the delta-connected stator winding to zero. For both motors a skew of one stator slot is applied to reduce torque ripple, and the core stack length is reduced in order to reduce the back-emf, so that the converter can shape a sinusoidal current at full speed. The thickness of the magnets is dimensioned so that they can withstand a fault current which is three times the nominal peak stator current without being demagnetized. Table 9.1 gives a summary of the motor designs.

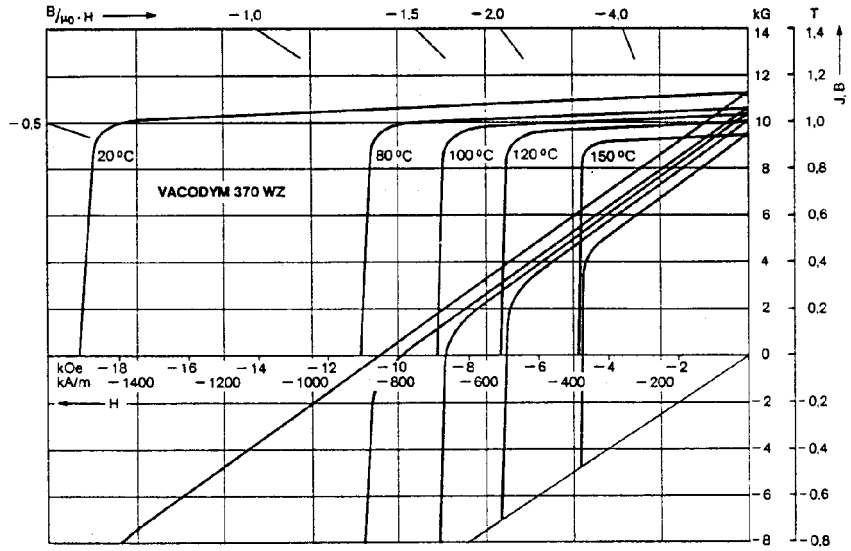

Figure 9.6: *Data sheet for the NdFeB permanent magnet material.*

Table 9.1: Summary of Induction motor and PMSM motor design.

	2.2 kW standard IM	2.2 kW high-eff. IM	2.2 kW PMSM	90 kW standard IM	90 kW PMSM
Stator resistance [Ω]	3.57	2.89	3.38	0.0207	0.0190
Stack length [mm]	90	110	80	250	215
Skew	1 rotor slot	1 rotor slot	1 stator slot	not known	1 stator slot
Magnet arc [elec. °]	-	-	150	-	120
Magnet thickness [mm]	-	-	1.6	-	4
Total PM weight [kg]	-	-	0.62	-	14.8
Air-gap [mm]	0.3	0.3	0.6	1.2	2.4

9.3.3 PMSM Loss Calculation.

All motors are investigated under operating conditions of optimal motor efficiency. For the induction motors this is assured by impressing a set a stator frequency and stator voltage which minimizes motor input power for a given load torque and speed. The permanent magnet in a PMSM with a recoil permeability of 1.06 equal a large equivalent air-gap seen from the stator winding, so the armature reaction from the stator current will not change the air-gap flux level worth mentioning. Hence, the air-gap flux can be regarded as constant and equal to the flux from the permanent magnets with the stator windings open-circuited. The optimal efficiency is therefore defined by maximum torque per ampere stator current, where the copper loss has a minimum. Figure 9.6 shows a vector diagram of the PMSM with maximum torque per ampere. The stator current is in phase with the induced voltage.

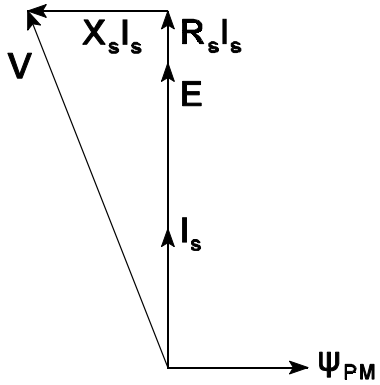

Figure 9.7: *Vector diagram for a PMSM with maximum torque per ampere.*

The produced electromagnetic torque is

$$\tau_{em} = \frac{3z_p E I_s}{\omega_s} \qquad (9.3)$$

where τ_{em} : electromagnetic torque.
z_p : pole-pair number.
E : phase emf.
I_s : stator current.
ω_s : stator angular velocity.

The phase emf is:

$$E = \psi_{PM}\omega_s \qquad (9.4)$$

where ψ_{PM} : permanent magnet flux.

For a given torque, the stator current can be determined by combining (9.3) and (9.4):

$$I_s = \frac{\tau_{em}}{3 z_p \psi_{PM}} \tag{9.5}$$

This enables to calculate the PMSM losses for a given load torque and speed. The stator copper loss and the mechanical losses are calculated as for the induction motors. The core losses are calculated with the same formula as for the induction motor, but as there are no rotor losses, the formula is reduced to (9.6).

$$P_{core} = k_1 |\underline{\psi}_{PM} + L_m \underline{I}_s|^{\nu} f_s + k_2 |\underline{\psi}_{PM} + L_m \underline{I}_s|^2 f_s^2 \approx k_1 \psi_{PM}^{\nu} f_s + k_2 \psi_{PM}^2 f_s^2 \tag{9.6}$$

Equation (9.6) assumes a sinusoidal air-gap flux density waveform. As seen on Figure 9.8 the air-gap flux density is flat on the top, so the factors 0.87 and 0.89 are introduced in equation (9.7) and (9.8) to take that into account. The coefficients of the core loss expressions are determined so that the derived core losses correspond with those calculated with the SPEED motor designer software package. The core loss of the 2.2 kW PMSM is:

$$P_{core} = 2.2 (0.87 \cdot \psi_{PM})^{1.8} f_s + 0.075 (0.87 \cdot \psi_{PM})^2 f_s^2 \tag{9.7}$$

The core loss of the 90 kW PMSM is:

$$P_{core} = 21.2 (0.89 \cdot \psi_{PM})^{1.8} f_s + 0.239 (0.89 \cdot \psi_{PM})^2 f_s^2 \tag{9.8}$$

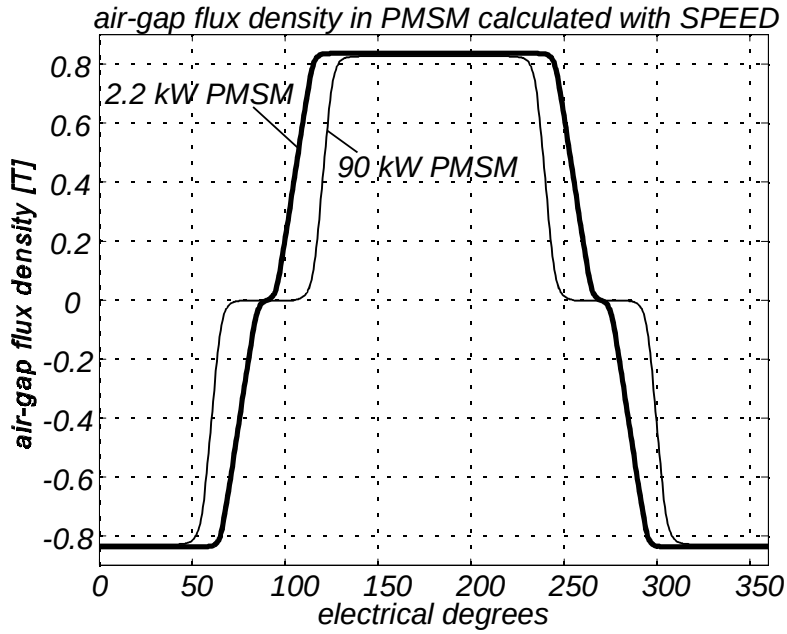

Figure 9.8: *Air-gap flux density from the permanent magnets calculated with the SPEED motor designer software.*

9.4 Result of Calculations for 2.2 kW Motor Drives.

The result of calculations on the 2.2 kW drives are now presented. Two parallel calculations are made for each drive: pressure control and flow control. The speed and torque curves from Figure 9.2 are used.

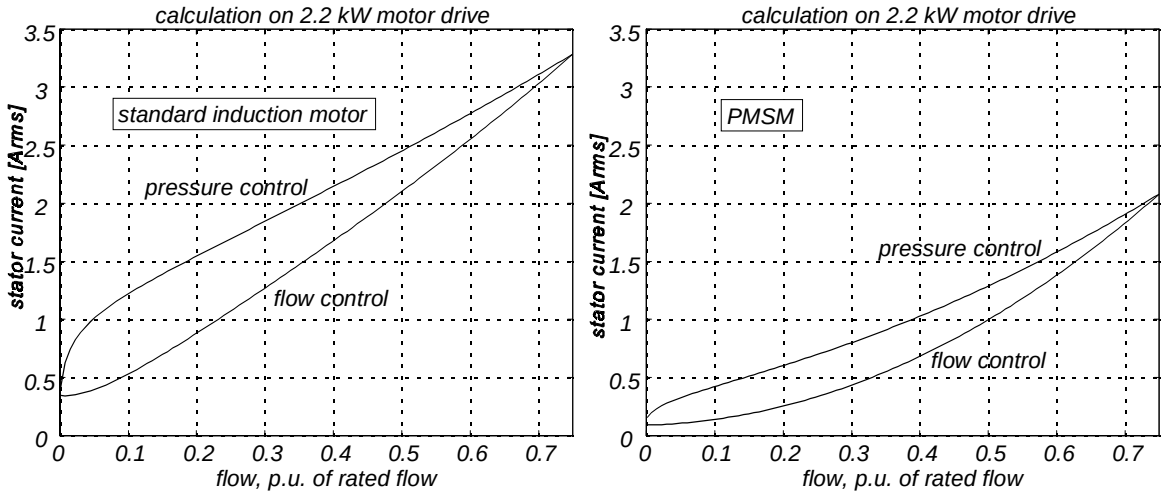

Figure 9.9: *Calculated 2.2 kW motor stator currents.*

Figure 9.9 shows the stator currents for the standard induction motor and the PMSM in the two control cases. The currents for flow control are smallest because the motors in that case are loaded with the lowest torque. The current in the PMSM is lower than in the induction motor because it has no magnetization current and because the NdFeB permanent magnets are quite strong. Figure 9.10 shows the efficiencies.

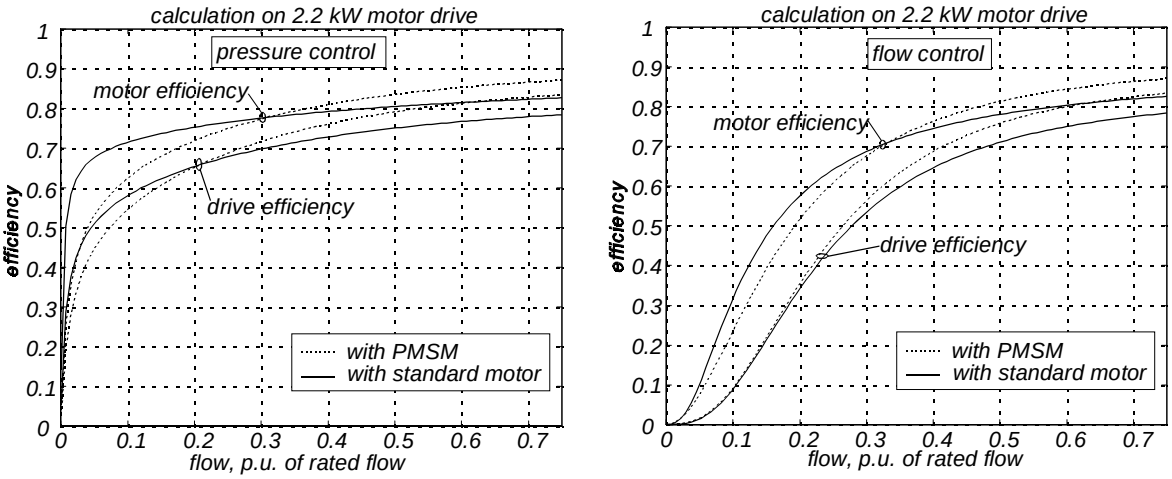

Figure 9.10: *Calculated efficiency for 2.2 kW motor drives with pressure and flow control.*

The calculated drive losses with pressure control are shown on Figure 9.11. At full load the PMSM drive loss is smaller than the induction motor drive loss. The main reason is that the stator copper loss is reduced a lot and the rotor loss is not present. The inverter loss is reduced

a little, while the core loss has increased because of the high permanent magnet flux density. At low flow (low load torque, medium speed) the drive losses are of equal size because the PMSM can not reduce its flux as the induction motor can. Figure 9.11 indicates that the PMSM construction is far from optimal because the core loss is too large compared with the stator copper loss.

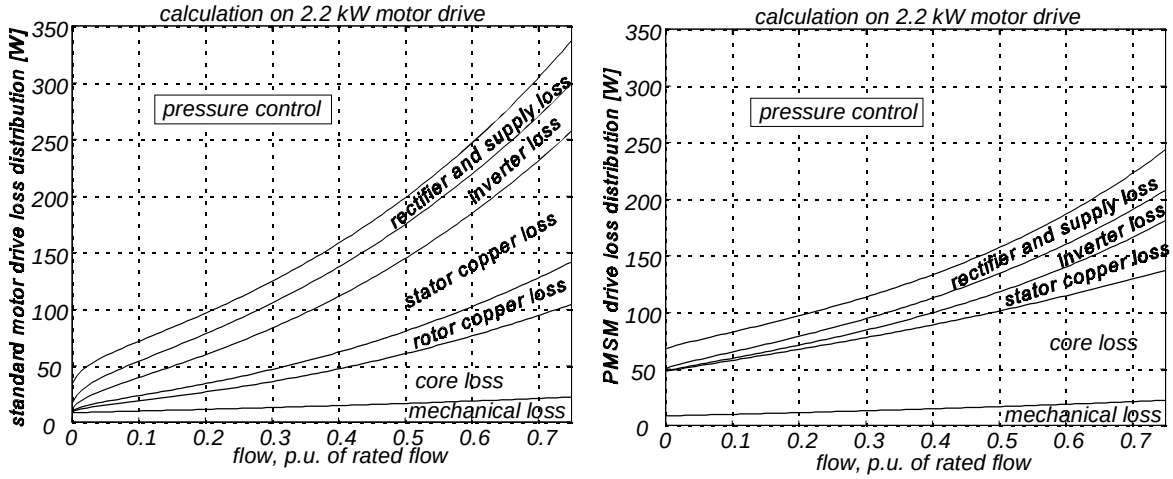

Figure 9.11: *Loss distribution in 2.2 kW motor drives with pressure control. Left: standard induction motor drive, right: PMSM drive.*

Figure 9.12 shows the drive input power. Besides the two drives from Figure 9.10 are also shown the input power for a high-efficiency induction motor drive, for a drive with no losses, and for a mains-connected standard induction motor with throttling valve control.

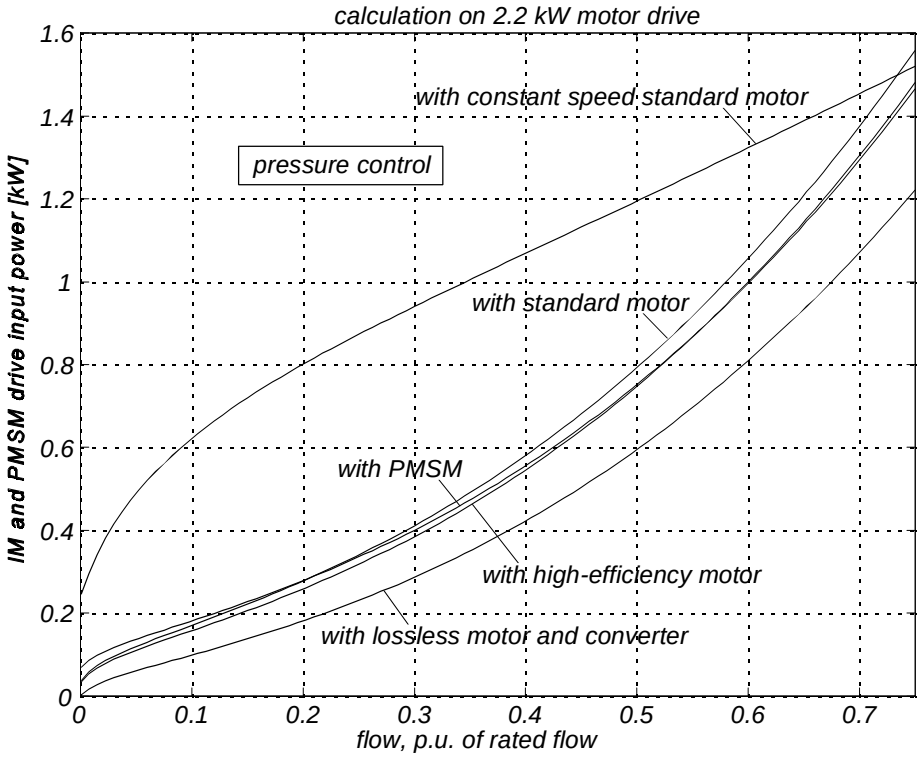

Figure 9.12: *Calculated input power to the 2.2 kW motor drives with pressure control.*

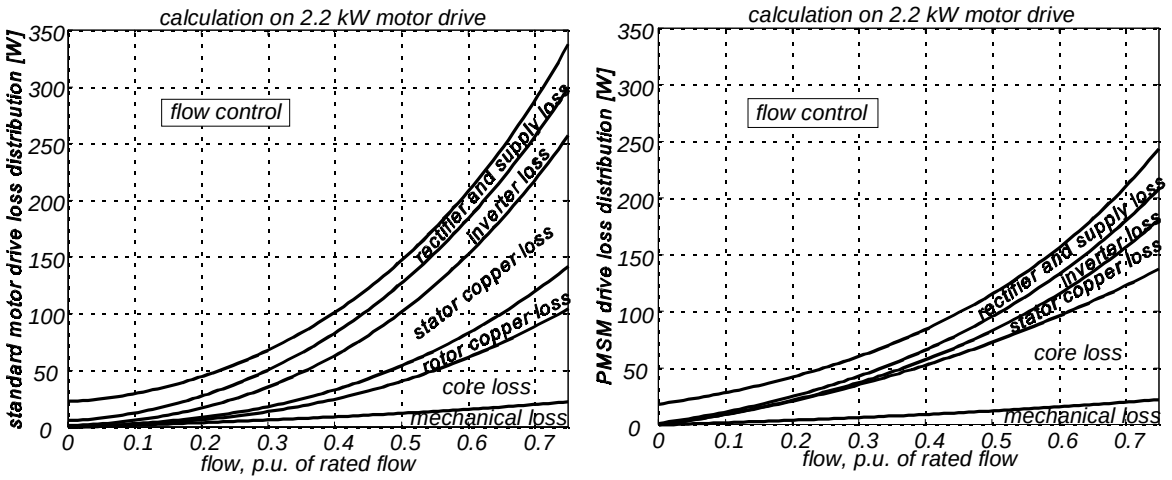

Figure 9.13: *Loss distribution in 2.2 kW motor drives with flow control. Left: standard induction motor drive, right: PMSM drive.*

The difference with a flow controlled drive is, as seen on Figure 9.2, that the speed is low at low flow. This means that the PMSM does not have a large core loss at low flow, and the PMSM has the same low copper losses as with pressure control, see Figure 9.13 and compare with Figure 9.11. The PMSM therefore performs better with flow control than with pressure control compared with the induction motor, which is also seen by comparison of the drive efficiency curves on Figure 9.10. The drive input power with flow control is shown on Figure 9.14.

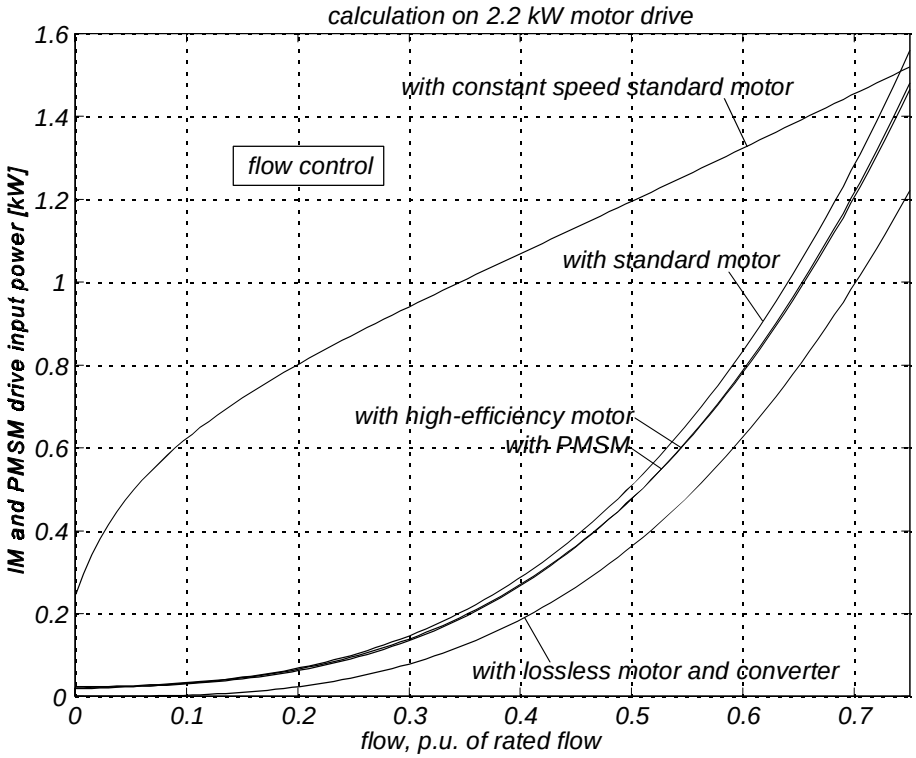

Figure 9.14: *Calculated input power to the 2.2 kW motor drives with flow control.*

9.5 Result of Calculations for 90 kW Motor Drives.

The next three pages present the same calculations as before, but made on the 90 kW drives. The calculations are done using the speed and load torque curves on Figure 9.3. The stator currents are shown on Figure 9.15, and they are similar in shape to the currents for the small drives.

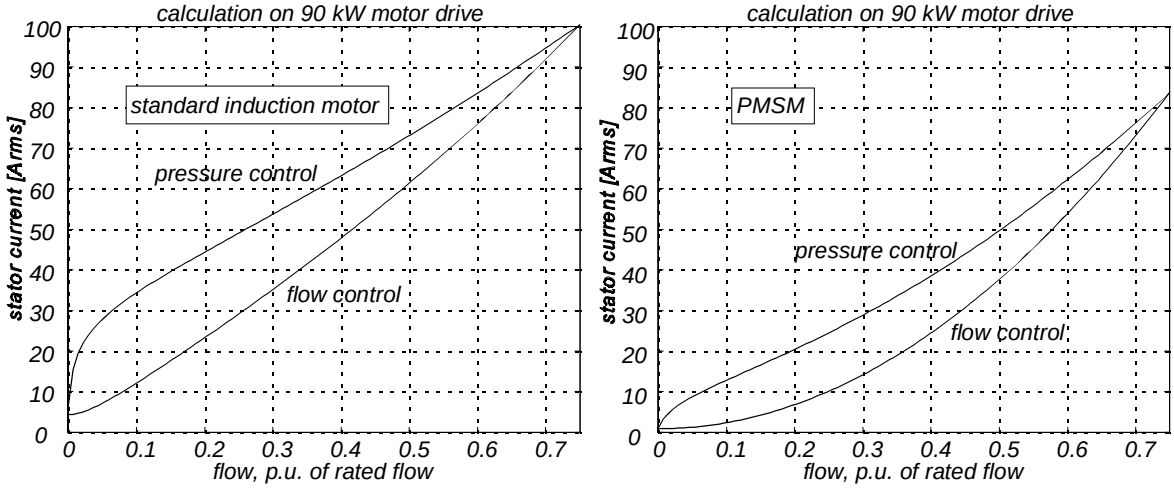

Figure 9.15: *Calculated 90 kW motor stator currents.*

From Figure 9.16 it is seen, as for the small drives, that as the drive efficiency curves cross each other at low flow with pressure control. The PMSM has the highest efficiency at all flows with flow control.

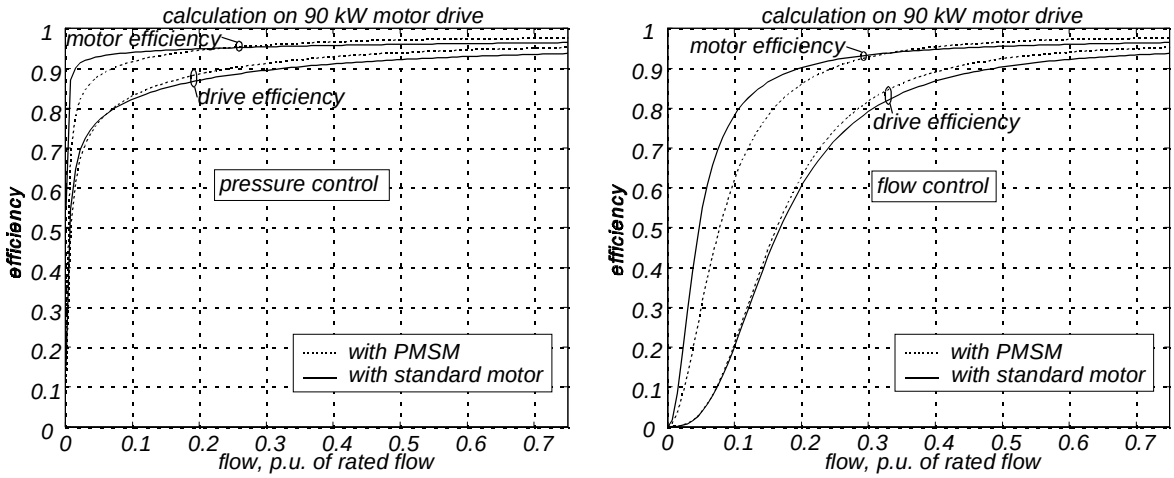

Figure 9.16: *Calculated efficiency of 90 kW motor drives with pressure control and flow control.*

The difference with the loss distribution for the medium-size drive is that while the main loss reduction for the small PMSM compared with the induction motor was reduced copper losses, then the 90 kW PMSM benefits mainly from both reduced copper losses and reduced inverter loss, see Figure 9.17 and Figure 9.19.

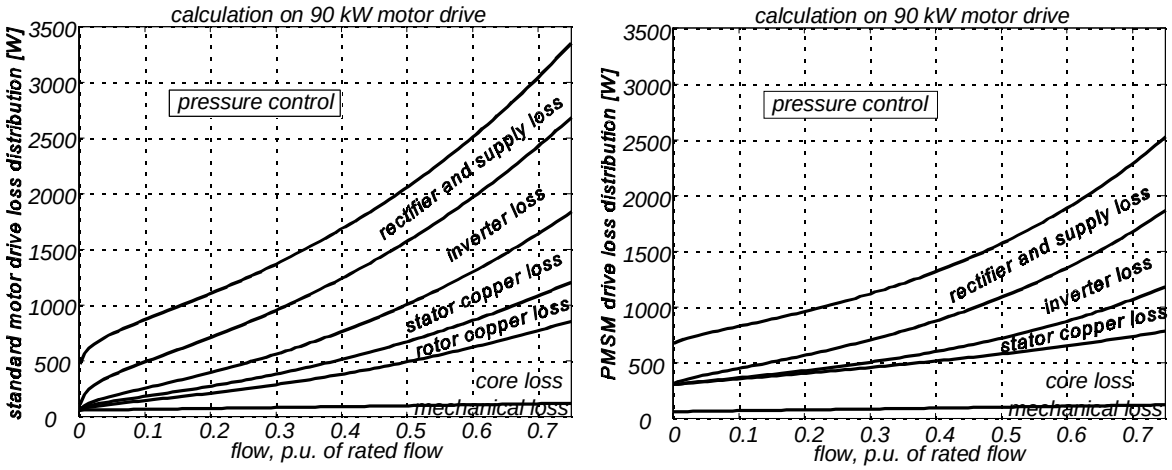

Figure 9.17: *Loss distribution in 2.2 kW motor drives with pressure control. Left: standard induction motor drive, right: PMSM drive.*

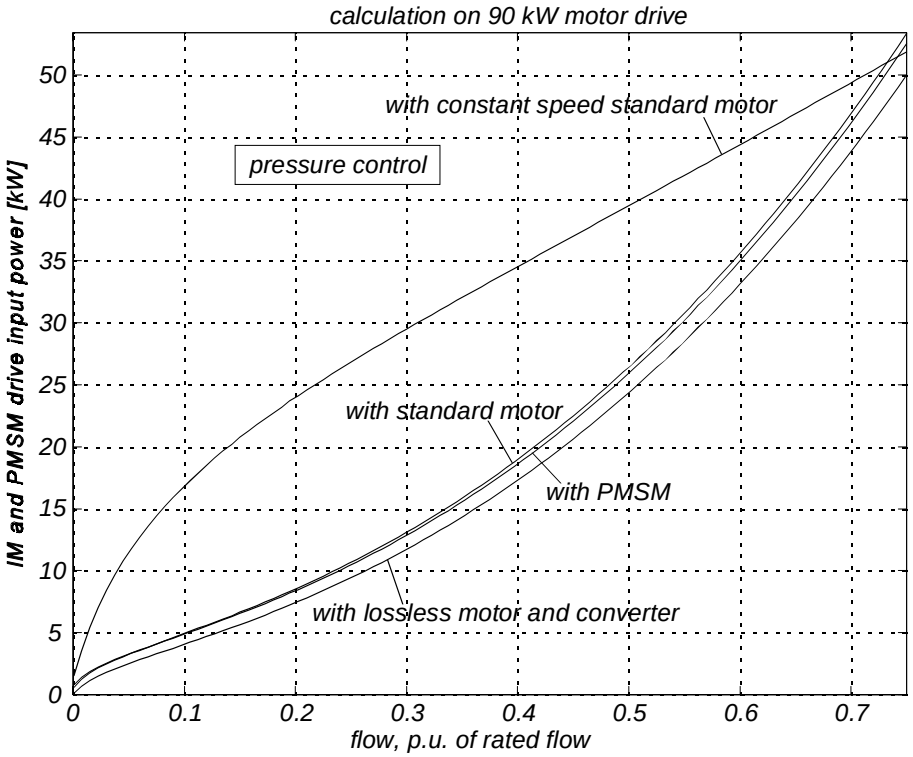

Figure 9.18: *Calculated input power to the 90 kW motor drives with pressure control.*

As the relative loss in the 90 kW drives are smaller than in the 2.2 kW drives, the differences in input power between the two investigated drives becomes even more marginal than it was the case for the small drives, see Figure 9.18 and Figure 9.20.

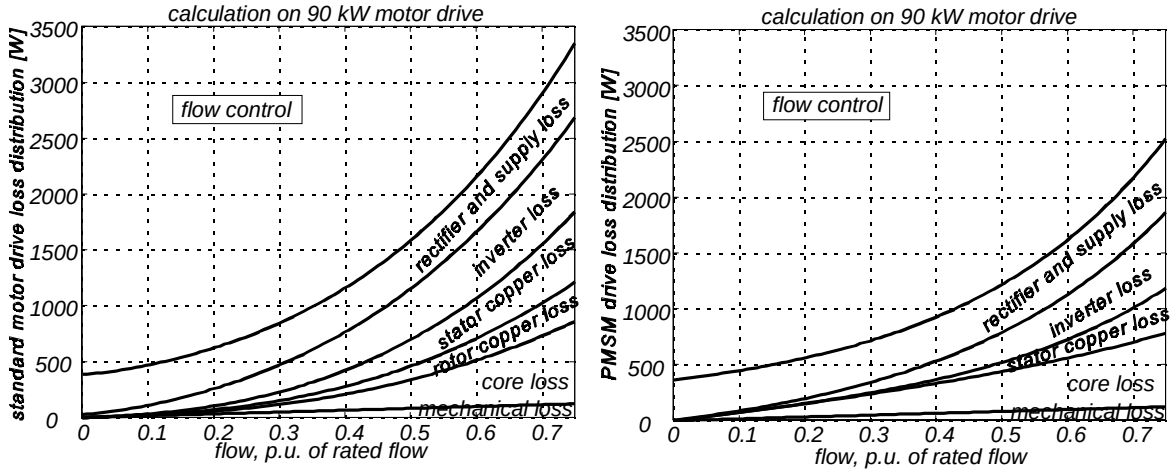

Figure 9.19: *Loss distribution in 2.2 kW motor drives with flow control. Left: standard induction motor drive, right: PMSM drive.*

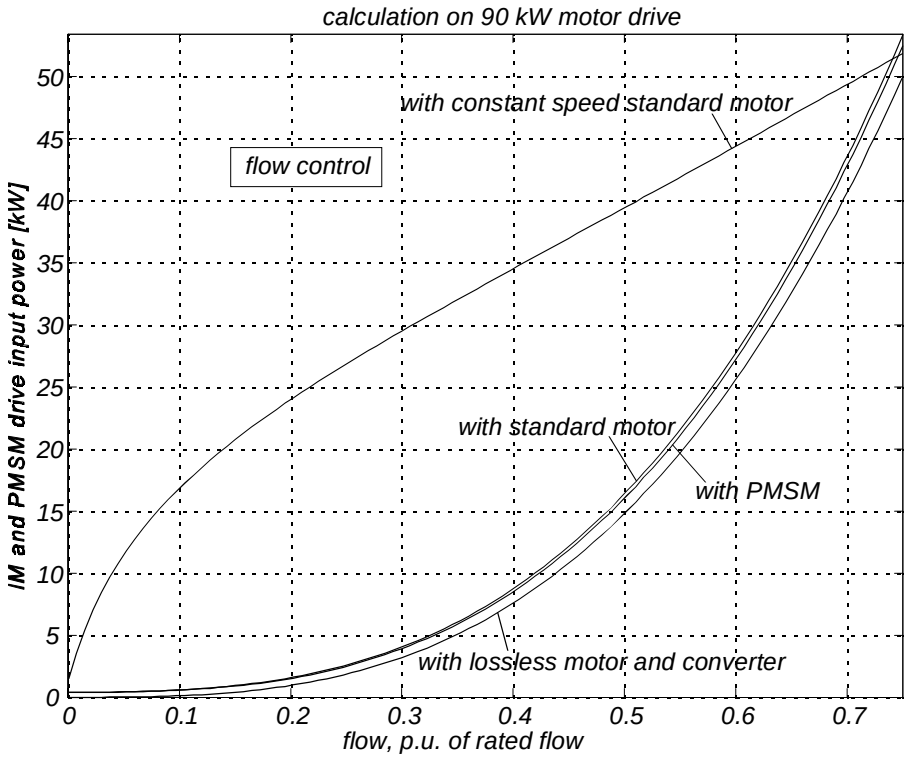

Figure 9.20: *Calculated input power to the 90 kW motor drives with flow control.*

9.6 Profitability.

Given the input power curves as function of flow on Figure 9.12, Figure 9.14, Figure 9.18 and Figure 9.20, the energy consumption and energy cost can be calculated. This is used to calculate typical annual energy cost and to estimate the pay-back times for the drives.

9.6.1 Annual Energy Cost.

The drive input power curves from the preceding sections are now used to calculate the annual energy cost in three load cases which are considered typical. The load profiles are shown on Figure 9.21, and it is seen that the average motor output for pressure control varies between 21-43 % of the rated motor output power, and for flow control between 14-41 % of rated output power.

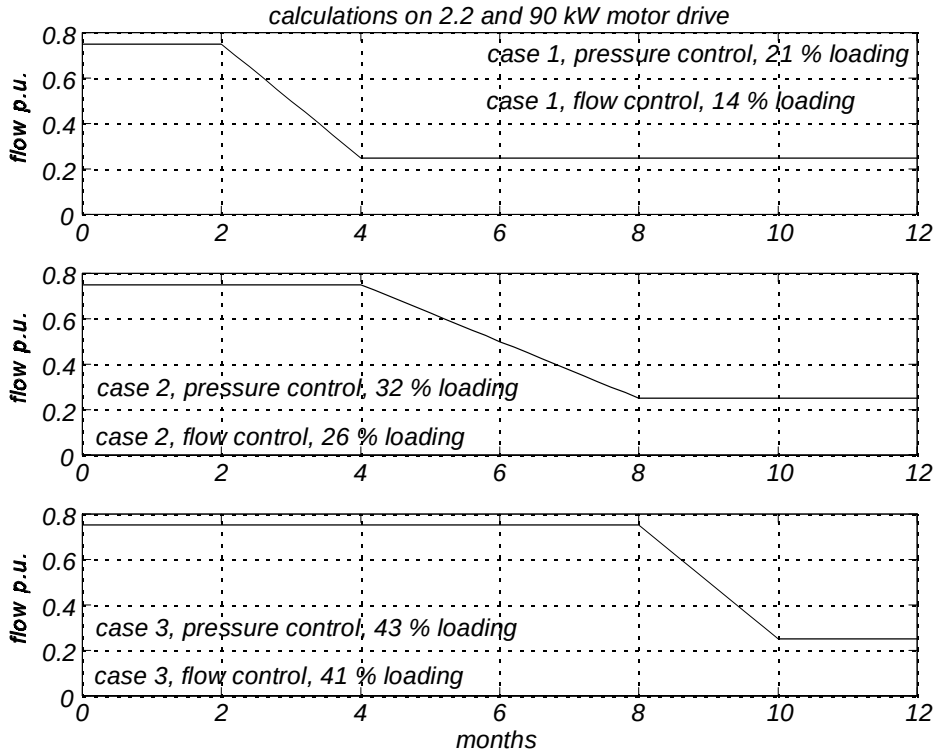

Figure 9.21: *Three load profiles used to calculated annual energy consumption. The average motor output power loadings are indicated in each case.*

The calculated annual energy cost is shown on Figure 9.22 for the 2.2 kW drive and on Figure 9.23 for the 90 kW drive. The electricity price is 0.0705 €/kWh, which is the average industry electricity price in Europe.

The figures show that the lower the load is (case 1), the large is the difference between the constant speed drive and the variable speed drives. Comparing the variable speed drives, the PMSM is in all cases better than the standard induction motor drive, and the difference is

largest for the small drives. At low load the high-efficiency induction motor drive is better than the PMSM drive, but this is because the PMSM construction is not optimized.

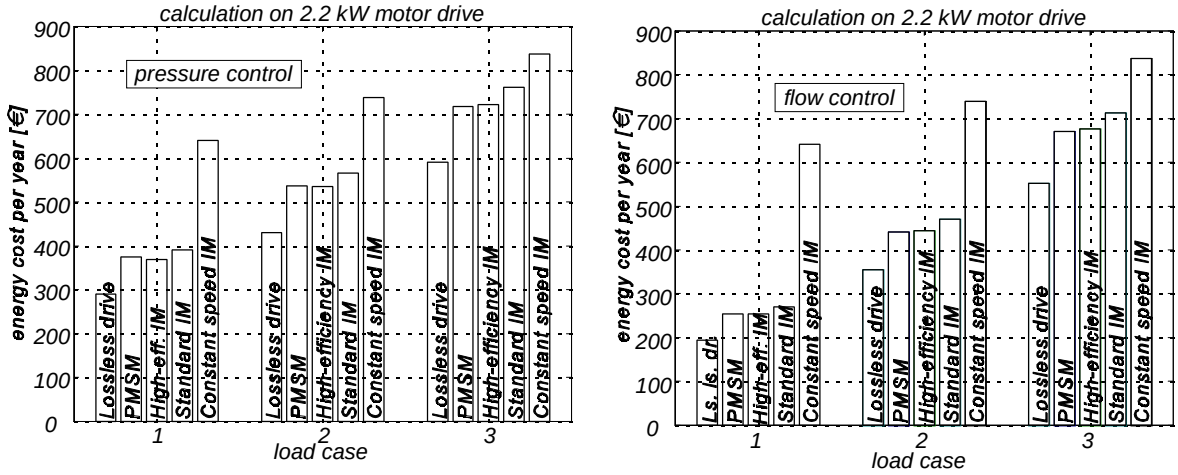

Figure 9.22: *Annual energy cost for the 2.2 kW drives is three cases of load profiles.*

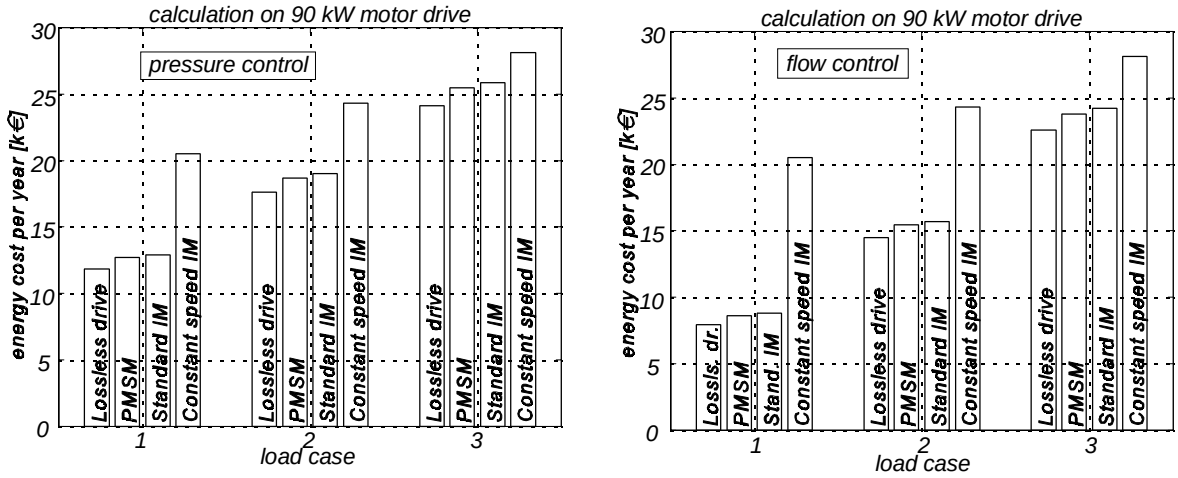

Figure 9.23: *Annual energy cost for the 90 kW drives is three cases of load profiles.*

9.6.2 Pay-Back Time.

The pay-back times are calculated from load case 2 on Figure 9.22 and Figure 9.23, which is the medium load case. Table 9.2 lists the precise annual costs. Listed are also the prices for motors and converters. The induction motor and converter prices are without any reduction. The prices of the converters for the PMSMs are cheaper than the converters for induction motors because they can use smaller converters. The prices of the PMSMs are calculated from the standard induction motor price and adding the price of the permanent magnets. The price for NdFeB magnets is 104 Euro/kg, and it is multiplied with a factor 3.5 to take into account the increased value of the magnets in the final product.

Table 9.2: Prices (in €) used to calculate pay-back times.

	2.2 kW cst. speed	2.2 kW standard	2.2 kW high-eff.	2.2 kW PMSM	90 kW cst. speed	90 kW standard	90 kW PMSM
motor price	350	350	428	576	7903	7903	13290
converter price	0	937	937	831	0	12773	10754
annual energy cost, pressure	739	565	534	535	24320	19013	18699
annual energy cost, flow	739	468	443	441	24320	15708	15437

The pay-back times are calculated for two cases. The first case is a new installation where both a constant speed drive and a variable speed drive can be used. The pay-back times for the variable speed drives are calculated as:

$$pay\text{-}back\ time = \frac{(motor + converter - motor_{stan})}{energy\ cost_{cst} - energy\ cost} \qquad (9.9)$$

where motor : price of induction motor or PMSM.
converter : price of converter for an induction motor or for a PMSM.
$motor_{stan}$: price of standard induction motor.
energy cost : annual energy cost with variable speed drive.
$energy\ cost_{stan}$: annual energy cost with constant speed drive.

The results are listed in Table 9.3. They show that the motor type has only little influence on the pay-back time of a variable speed drive. It is slightly better to use a high-efficiency motor than a standard motor. The PMSM drive benefits from the fact that it can use a smaller converter than the induction motors. But the pay-back times are generally determined by the difference between the energy constant speed drive and the variable speed drives, and how the plant is loaded and controlled. A medium-size drive is in general paid back faster than a small drive.

Table 9.3: Pay-back time in years for a variable speed drive.

drive size	control type	Standard motor drive	High-eff. motor drive	PMSM drive
2.2 kW	pressure / flow	5.4 / 3.5	5.0 / 3.4	5.2 / 3.5
90 kW	pressure / flow	2.4 / 1.5	- / -	2.9 / 1.8

The second case is a new installation where only variable speed drives can be used, and where the pay-back times for buying a high-efficiency motor or a PMSM drive instead of a standard motor drive are calculated. The pay-back times are calculated as:

$$pay\text{-}back\ time = \frac{(motor + converter) - (motor_{stan} + converter_{stan})}{energy\ cost_{stan} - energy\ cost} \qquad (9.10)$$

where
- motor : price of the high-efficiency motor or the PMSM.
- converter : price of converter for the high-efficiency motor or the PMSM.
- $motor_{stan}$: price of standard induction motor.
- $converter_{stan}$: price of converter for the standard induction motor.
- energy cost : annual energy cost for high-efficiency motor or PMSM.
- $energy\ cost_{stan}$: annual energy cost for variable speed standard induction motor.

The results are shown in Table 9.4. They show that the best investment is a small high-efficiency motor, and that a small PMSM is almost just as good. Again, the expensive PMSM benefits from a smaller converter. But the PMSM is too expensive at the 90 kW level. It is not so important whether the plant is pressure controlled or flow controlled.

Table 9.4: Pay-back time in years for using a better motor in a variable speed drive.

motor drive size	control type	High-efficiency motor	PMSM
2.2 kW	pressure/flow	2.5 / 3.1	4.0 / 4.4
90 kW	pressure/flow	- / -	10.7 / 12.4

9.7 Summary.

The aim with this chapter is to set the induction motor drive in perspective by comparing its energy efficiency with that of a PMSM drive in HVAC applications. The chosen method is to compare an induction motor with a PMSM made from an induction motor but with permanent magnets on the rotor surface. This simple method was chosen because of the limited resources, but it is realized that the analysis does not provide results for the two drives which are directly comparable. So it is not possible to fulfil the main purpose of the comparison. The reason for this is that constructing a PMSM from an induction motor results in a PMSM which is far from optimal with respect to efficiency. An absolute comparison requires much more work, for example, the research project which [3] referred to represents 14 years of manpower. When it is chosen to include this comparative analysis in the thesis anyway it is from the point of view that it is better to say something, although formulated in vague terms, than to say nothing.

From the calculation of loss distribution in the drives it is possible to conclude that the PMSM loss is reduced because of reduced copper losses, and especially in the 90 kW drive

at low load also because of lower inverter loss. The induction motor can benefit from flux reduction at low load, but it is only an advantage compared with the PMSM if the speed at the same time is relatively high, because at low speed the core loss is small anyway. In what here is referred to as flow control (speed changes linearly with speed) the induction motor has no advantage of flux reduction compared with the PMSM.

A graphic presentation of the drive input power illustrates that the difference between the investigated variable speed drives is small compared with the constant speed drive, especially for the 90 kW drive.

Calculation of pay-back times indicated that when a variable speed drive is installed instead of a main connected induction motor, the motor type has only a minor influence on the pay-back time of the drive.

When only a variable speed drive can be used, and it is considered to choose a high-efficiency motor or a PMSM instead of a standard motor, it is in a small drive a good idea to change to a high-efficiency motor and possibly also to a PMSM. But a 90 kW PMSM is too expensive.

References.

[1] H. R. Andersen, C. B. Rasmussen, E. Richie, J. K. Pedersen, “Efficiency Comparison of Electrical Motors for Energy Optimized Variable Speed Low Power and Low Cost Household Equipment”, Proceed. of EPE’95, Sevilla, 1995, pp. 3.423 - 3.429.

[2] G. R. Slemon, “High-Efficiency Drives using Permanent-Magnet Motors”, Proceed. of IECON’93, Hawaii, 1993, pp. 725-730.

[3] H.-H. Hansen, DEFU technical report no. 386. DEFU, Postboks 259, DK-2800 Lyngby. (Danish)

[4] T. Heilmann, “Pumper og regulering”, Heilmanns forlag, Højbjerggårdsvej 38, DK-2840 Holte. 1. udg., 1. oplag 1990. ISBN 87-983513-0-3. (Danish)

[5] Pumpeståbi, 2. udgave, 1991, Teknisk Forlag, ISBN 87-571-1327-0. (Danish)

Chapter 10

Conclusion

A large part of the electrical energy consumption goes to Heating, Ventilation and Air-Condition (HVAC) applications and it is well known that in some of these cases the energy consumption can be drastically reduced by using variable speed drives instead of constant speed drives controlled by, for example, throttling valves. A smaller, but still important, improvement in the induction motor drive efficiency can be obtained by adapting the magnetizing level in the motor to the load condition. The basic purpose with this thesis is to demonstrate how energy optimal control can be made for small and medium-size low-cost PWM-VSI drives for HVAC application, without bringing the robustness of the drive below an acceptable level. The low-cost criterion implies a minimum of sensors and relatively simple control algorithms. A number of more specific purposes with the thesis were mentioned in the definition of the problem in Chapter 1, and a summary of the results is presented here.

Measurement of Drive Efficiency and Harmonic Losses.

In order to gain a good comprehension of the losses in electrical drives, extensive efficiency measurements were made on 2.2 kW standard and high-efficiency motor drives, with and without filtered converter output voltages. Similar measurements without filtered converter output voltages were made on 22 kW and 90 kW standard motor drives. The measurements were made within the whole specified operating area (0-1 p.u. load torque and 0.2-1 p.u. speed) in order to discover all possible phenomena.

The experiments on small drives with optimized efficiency and with constant air-gap flux showed that at 0.25 p.u. load torque the drive losses were reduced with 26-36 % for the standard motor drive and with 23-31 % for the high-efficiency motor drive. This indicates that the better the motor construction is, the smaller is the relative improvement by energy optimal control. In both drives the drive efficiency was improved in the operating area below approximately 70 % of rated load torque.

It was found that in small drives the improvement appears mainly due to reduced motor losses, so in that drive size the energy optimal control algorithms do not have to include converter losses. Neither is it necessary to consider harmonic motor losses in the energy optimal control. Experiments with variable switching frequency on a 2.2 kW drive showed a minimum in drive loss around 3-4 kHz.

Analysis of Optimized Drive Efficiency.

Motor and converter models were established with special attention to precise representation of losses and verified against the measurements. The experience was that the motor losses can be modeled satisfactorily with a traditional single phase model with losses represented by stator, rotor and core resistances. The copper resistances take into account the temperature changes in the motor. No attempt has been made to quantify stray load losses, but they are represented inherently through the stator resistance. The inverter losses were modeled by help of off-line measurements of transistor and diode switching energies and of on-state conduction voltages. The losses in the chokes were calculated from their dc-resistances, while the loss in the dc-link capacitor was ignored. The rectifier loss was calculated assuming a constant diode on-state voltage.

The established drive models were used to analyze the drives when operating with and near optimized efficiency. It was demonstrated that around the point of optimal efficiency there is a wide region of air-gap flux, inside which the efficiency is almost constant, so with respect to efficiency it is not important to hit exactly the optimal point. Rather is it a good idea to select an air-gap flux slightly higher than the optimal value in order to ensure a more stable motor. On the other hand, it was shown that the motor will not pull out with optimized efficiency as long as there are no large load disturbances.

Evaluation of Energy Optimal Control Methods.

A review of energy optimal control strategies was presented, and five strategies were selected for further analysis. Based on calculations and tests, the following conclusions can be made concerning the strategies for small drives:

- The displacement power factor control is simple and gives good results, which makes it a good choice for HVAC applications. It was chosen to use a constant reference value for the displacement power factor, and the investigations have not revealed any reason to make the reference variable.
- It appeared that the reference for the constant slip frequency controller has to vary with both speed and load, and as the method furthermore requires a speed sensor, it was disregarded.
- A direct air-gap flux control was tested. The reference was made a function of estimated load and speed, but it could also be made a function of stator frequency and stator current. The result was very good, but the method requires good knowledge of the motor.
- It was demonstrated that the analytical solutions to model-based control proposed in literature do not give satisfactory results as they ignore magnetic saturation. In the tests the problem was solved in a simple and acceptable, but not satisfactory, way.
- The stator current and input power minimizing search controllers, although providing good steady state performance, appeared to have problems in a realistic pump system test with slowly varying load. In the choice between the two strategies, the experience is that it is best to use minimized stator current.

Test of Energy Control Strategies.

In general it is found that the search control is slow, while the other control algorithms converge faster. Comparison with tests of the dynamic properties in a vector controlled drive for CT applications showed that the convergence times could generally be reduced with 50 % in vector controlled drive. It is clear, however, that the dynamics greatly depend on how the drive control is designed.

There is a general need for methods to design the PI-controllers in the cos(φ) control, the direct air-gap flux control and the model-based control. It was in this project done from simple consideration and further fine-tuning with gain-scheduling by trial and error. The search control has the disadvantage that every new application demands a time consuming job of trimming a number of constants in the algorithm.

Tests with a 2.2 kW standard induction motor drive on a pump system demonstrated a 12.6 % reduction in energy consumption by energy optimal control compared with constant air-gap flux control. The average load of the motor during the test was approximately 20 % of rated power. This test revealed that the search control had difficulties to follow the minimum loss operating point in case of slowly varying load and speed.

Energy Optimal Control of Medium-size Drive.

Reliable motor and converter loss models for a 90 kW drive were established on the basis of extensive measurements. An analysis with these models showed that it has virtually no influence on the drive efficiency whether it is the drive efficiency or only the motor efficiency that is optimized. The only reason to include the converter loss in the energy optimal control algorithm should be that it makes the drive more robust against load disturbances because it dictates a higher flux level than if only the motor efficiency is optimized. This phenomenon is more distinct the higher the switching frequency is.

It was found that it is even more troublesome to use the search control in medium-size drives than in small drives because of the relatively smaller losses. But the other energy optimal control strategies which were tested on the 2.2 kW drive can be used on the medium-size drive without problems.

Calculations with constant displacement power factor control and with model-based control showed good results in terms of efficiency. The model-based control was tested on a 22 kW drive with good results.

Instead of seeking an analytical solution to the model-based control it is proposed to solve the optimization numerically off-line, and turn the real-time drive control into a simple principle of controlling, for example, the air-gap flux as function or stator frequency and stator current. With this new method the loss model can include converter losses and a complex motor model with little demand for real-time computational power.

From the experiments with the standard induction motor drives at 2.2 kW, 22 kW and 90 kW graphical relations were formed, which for any motor within that power range show how much the drive efficiency can be improved with energy optimal control, compared with constant air-gap flux control. It should just be kept in mind that the improvement may vary, depending on how well the motor construction is optimized itself. The general tendency is that the improvement gets smaller, the larger the drive is.

If a mains-connected induction motor is over-sized, it results in a degraded efficiency. A small study showed, on the contrary, that in variable speed drives with energy optimal control it is not a disadvantage to use over-sized induction motors, because with flux reduction the core losses are of equal size, but the copper losses are smaller in the over-sized motor. The result may differ if there is large difference between the shaft height of the motors.

Stability.

It is shown that robustness against sudden load disturbances for an open loop controlled motor can be studied from simple steady-state considerations. A comparison of the investigated motors shows that a high-efficiency motor is more robust than a standard motor, and a medium-size motor is more robust than a small motor. If the drive should be able at any time to withstand a sudden increase to nominal load torque it is necessary continuously to monitor the load torque and to increase the motor flux rapidly when a large load disturbance is detected. Experiments showed that this can easily be realized, for example by forcing the flux to its nominal value when a large difference between the flux reference and the calculated flux is detected.

Motor oscillations were studied with respect to flux reduction. There are two resonance phenomena in a motor, and when the flux is reduced, the damping of the first is increased while the damping of the second is decreased. It can not be said beforehand which one will possibly cause trouble, as it depends on the motor and on the load, so flux reduction can both degrade and improve a resonance problem.

Comparison of Induction Motor and PMSM Drives.

Comparisons of energy efficiency were made between induction motor drives, and drives of permanent magnet synchronous motor (PMSM) made from induction motor frames. The conditions of the comparison appeared to be too simplified to make an absolute comparison between the different drives. It was demonstrated, however, that the advantage of flux reduction for the induction motor compared with the PMSM only appears in applications where the speed is relatively high at low load torque, such as the pressure-controlled pump. But in any case, the PMSM benefits from reduced copper and inverter losses. So the induction motor can not compete with the PMSM with regard to energy efficiency.

Economical considerations indicate that when a variable speed drive is installed instead of a constant speed drive, the pay-back time is almost independent of the motor type. When only a variable speed drive can be used, and it is considered to choose a high-efficiency motor or a PMSM instead of a standard motor, it is in a small drive a good idea to change to a high-efficiency motor and possibly also to a PMSM. But a 90 kW PMSM is too expensive.

Unique Contributions in the Thesis.

The unique contributions in this thesis to the field of energy optimal control of induction motors are believed to include a demonstration of the importance of including magnetic saturation and converter loss in the control algorithms, a general comparison of different control strategies with respect to stationary and dynamic performances, analysis of energy optimal control in medium-size drives, proposal of a new implementation of model-based control, a means to determine the expected efficiency improvement with energy optimal control for any drive between 2.2 kW and 90 kW, and a general analysis of stability with respect to flux reduction.

Future Work.

Concerning the future work in the field of energy optimal control, this project revealed that there is a need for methods to design the energy optimizing controllers in a systematic way so that the convergence time for varying load can be minimized. In some applications it might even be relevant to minimize energy consumption during transitions. An automatic routine for determining the many parameters in the search control algorithms is also needed. Furthermore, it might, at least from an academic point of view, be interesting to get an analytical solution to model-based efficiency optimization with inclusion of magnetic saturation and possibly converter losses.

Appendix A

Description of Laboratory Motor Drives

This chapter describes the physical 2.2 kW, 22 kW and 90 kW motor drive systems which are used for experiments in this project. It includes induction motor, mechanical load, converter, digital control system and acquired signals, see Figure A.1.

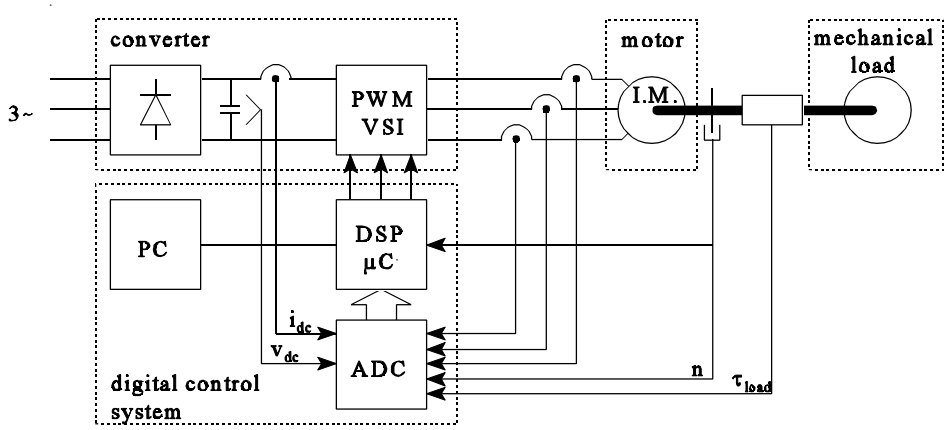

Figure A.1: *Overview of laboratory motor drive system.*

A.1 Mechanical Load.

The 2.2 kW and 22 kW induction motors are loaded with separately excited dc-generators, see Figure A.2. The load torque at a given speed is adjusted by varying the field current and the resistance connected to the armature. It is possible to make a sudden load step by closing or opening the armature circuit with the switch.

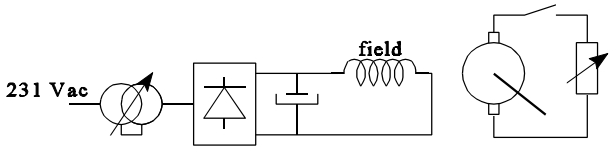

Figure A.2: *Connection of the dc-generator load machine for 2.2 kW and 22 kW drives.*

The 90 kW drive is loaded with a torque controlled permanent magnet synchronous generator drive.

A.2 Motors and Converters.

A diagram of the power electronic converters is shown on Figure A.3. The basic converter is similar for both the 2.2 kW, 22 kW and 90 kW drives. The 2.2 kW drive is additionally equipped with a brake module, and an output filter which can be applied when desired. The 2.2 kW drive converter is connected to the grid through a vario-transformer so that the input voltage to the diode bridge can be varied between 0 and 450 V. This enables to adjust the dc-link voltage from 0 V to 640 V. The 22 kW and 90 kW drive converters are connected directly to the grid.

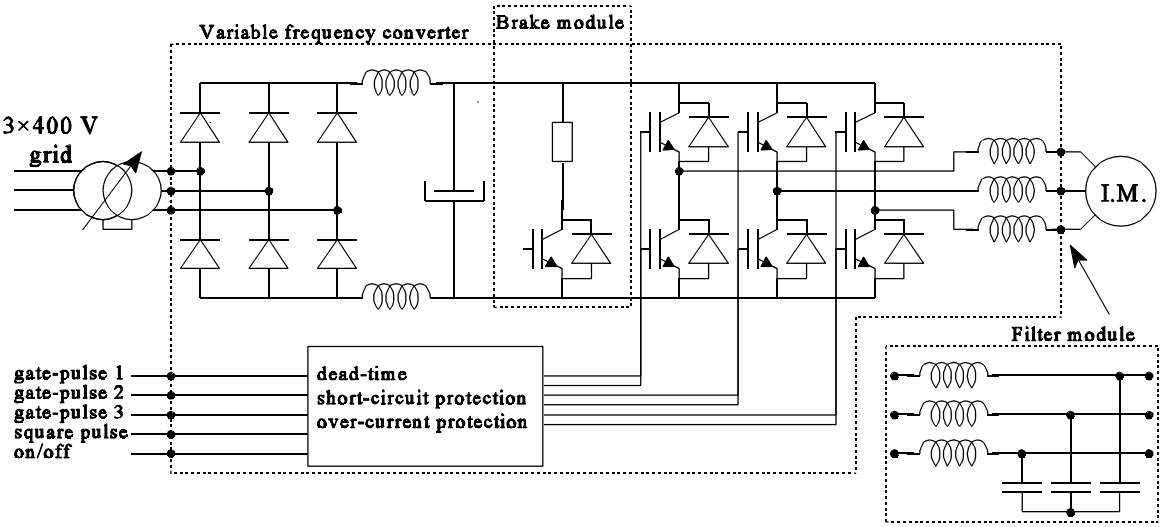

Figure A.3: *Diagram with main components of the power electronic converters. Control electronics, and high frequency components, such as snubbers and RFI-filters, are not shown. Vario-transformer, brake-module and output filter are only used with the 2.2 kW drive.*

The control circuit is taken out of the converter, so the control input to the converter consists of three gate signals, one for each branch, a square-wave signal for a watch-dog timer and an on/off-signal. As shown on Figure A.3, the converter contains a dead-time circuit, as well as short-circuit and over-current protection.

The induction motors used in this project (2.2 kW, 22 kW and 90 kW standard motors, and 2.2 kW high-efficiency motor) are all squirrel-cage norm motors. The motor and converter type specifications are listed in Table A.1, and the model parameters are shown in Appendix B.

Table A.1: Motor and converter type specifications.

Drive	Motor Type	Converter Type	
2.2 kW	*Standard motor* ABB Motor 3~ CI.F IP55 IEC34 MTM100LA28-4 MK110022-S *High-efficiency motor* ABB Motor 3~ CI.F IP55 IEC34 MTM100LB28-4 V290-50A	Danfoss VLT 3004 175H7246 380-415 V 160013G026	Danfoss Brake Module 175H6199 380/500 V, 12.5 A 807302G197 Danfoss RFI/LC filter 175U0253 3×380/500 V, 7.3 A 592902G515
22 kW	ABB Motor 3~ CI.F IP55 IEC34 ABB 400/50Hz, Motor MBT 180L	Danfoss VLT 3032 175H1671 380-415 V 030609G344	
90 kW	ASEA Motor 3~ CI.F IP55 IEC34 400/50Hz, Type 280SMB	Danfoss VLT 3132 380-415 V	

A.3 Digital Control System.

A diagram of the digital control system is shown on Figure A.4. It consists of an analog-to-digital converter, a digital signal processor, a PC, a dual-port-ram, a micro-controller and an interface with galvanic isolation to the converter. Circuit diagrams are shown in [1].

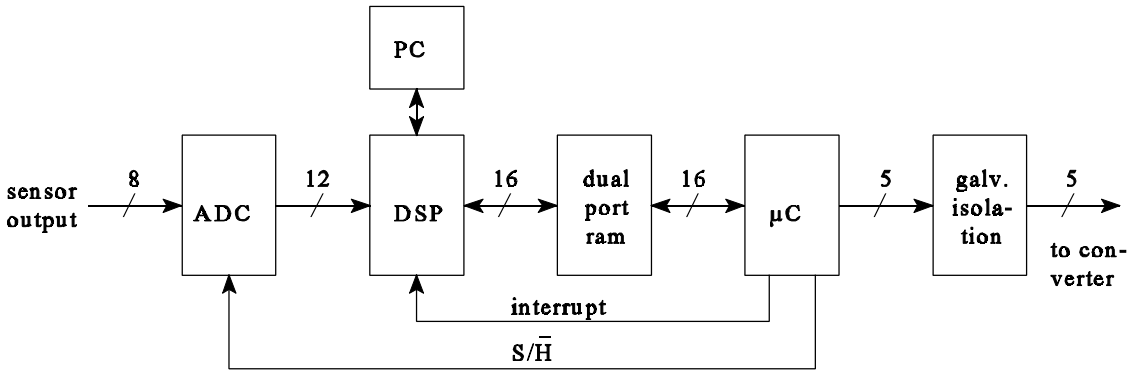

Figure A.4: *Diagram of digital motor drive control system.*

A/D-converter.

The eight input channels are sampled simultaneously by two sample-hold circuits (AD684 from Analog Devices) when a signal is given from the micro-controller. The input voltages are converted with 12-bit resolution by the AD7891 chip from Analog Devices. The conversion time for each channel is 2.3 µs and the conversion is controlled by the DSP. The total conversion time of eight channels is 27 µs, including transmission of results to the DSP.

Digital Signal Processor (DSP).

Most calculations are made the in floating point DSP from Analog Devices: SHARC ADSP-21062, 33.3 MHZ clock frequency. It performs floating point calculation with 32 or 40 bit resolution. The DSP is mounted on the EZ-lab development system (hardware ver. 3) by BittWare Research Systems. The board is placed physically in the PC, which enables exchange of data between the DSP, and the screen and hard-disc. The DSP is programmed in ANSI-C.

The interrupt procedure in the DSP is executed at the beginning of each sampling period when a signal from the micro-controller is given. The output of the DSP are three duty-cycles, one for each inverter-branch. The duty-cycles are written in 16-bit format to the dual-port ram.

Dual-Port Ram.

The dual-port ram consists of two parallelled 8-bit memory-circuits. This gives a total of 128 16-bit memory addresses, accessible from two sides.

Micro-Controller.

The micro-controller is from Siemens, SAB80C167, with 20 MHz clock frequency. It performs calculations in 16-bit fixed point format. The input to the micro-controller are the three duty-cycles which are read from the dual-port ram, and the output are three PWM gate signals, a square-wave and an on/off signal. The PWM signals are generated with a resolution of 50 ns. The micro-controller also generates an interrupt signal for the DSP and a hold-signal of the A/D-converter in the beginning of each sampling period.

Galvanic Isolation.

The galvanic isolation circuit simply passes the PWM, square-wave and on/off signals on to the inverter. The galvanic isolation is provided by fibre-optic cables. The circuit also contains a switch by which it is possible to block the gate-signals manually.

Timing of Communication.

The timing between the individual part of the digital control system is illustrated with two sampling periods on Figure A.5. The figure only shows the actions that are related to the sampling at time t_0.

At time t_0 the micro-controller gives a hold signal to the A/D-converter and an interrupt signal to the DSP. The DSP immediately starts to read to converted values. Thereafter the control algorithms are executed in the DSP. The output of the control part, three duty-cycles, are written into the dual-port ram. At the beginning of the next sampling period, at time t_0+T_s, the duty-cycles are read by the micro-controller, the PWM timer values are calculated and written to the timer buffer registers. These values are automatically loaded into the timer compare registers at time t_0+2T_s. This means that there is a delay of two sampling periods from analog values are sampled, until the output voltage of the converter are applied.

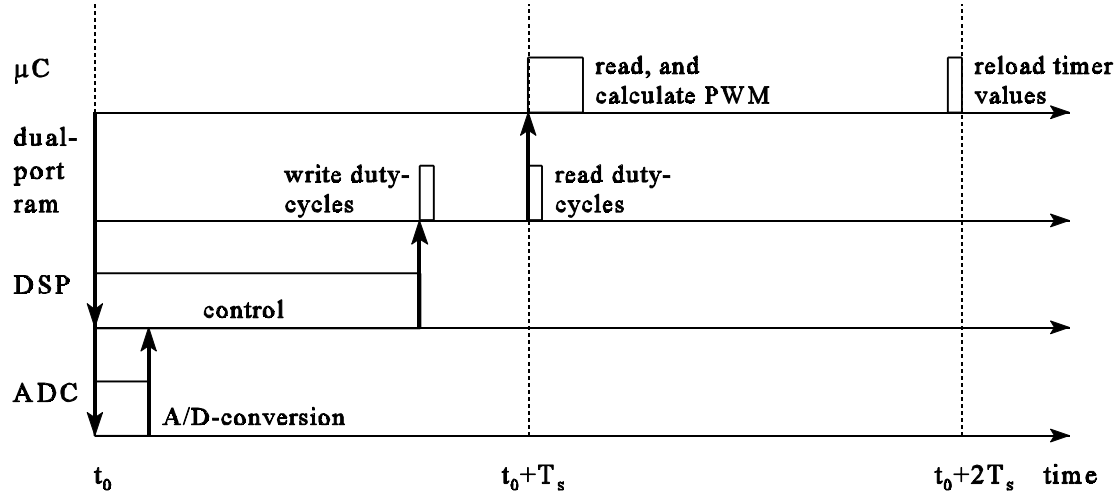

Figure A.5: *Timing of communication between micro-controller, dual-port ram, DSP and A/D-converter.*

A.4 Sensors and Filters.

The currents are measured with Hall-effect sensors, and the dc-link voltage with a voltage divider. The speed is measured with an encoder, and the pulses are both counted in the micro-controller and converted to an analogue voltage. For the 2.2 kW and 22 kW drives the resolution is 2500 pulses/revolution, and for the 90 kW drive the resolution is 1200 pulses/revolution. The bandwidth of the analogue signals are listed in table A.1.

Table A.2: Bandwidth of measured analogue signals.

Measured parameter	Effective bandwidth
Stator currents	10.6 kHz
dc-link current	58 Hz
dc-link voltage	10.6 kHz
speed	723 Hz
load torque	approx. 800 Hz

References.

[1] F. Abrahamsen “Energy Optimal Control Strategies for Electro Motors, low-cost and sensorless PWM-VSI based induction motor control”, Aalborg University, Denmark, ISBN 87-89179-23-4, 1998.

Appendix B

Verification of Motor and Converter Loss Models

The structure of the motor and converter models are described generally in chapter 3. It is the same models that are used for both the 2.2 kW, 22 kW and 90 kW standard induction motors, and the 2.2 kW high-efficiency induction motor. The models are all verified experimentally and the results of the experiments and the determined constants are reported in this appendix.

The models are verified within the specified operating area which is found relevant for HVAC applications, namely 0-1 p.u. load torque and 0.2-1 p.u. speed. The main objective is to model the losses as precisely as possible, using a model which is not unnecessarily complex.

In all cases the losses are determined by the input-output method measuring the input and output powers of the converter with a 12 channel Norma power analyzer and the motor output power from measurement of torque and speed. A scheme of the measuring principle is shown on Figure 4.1.

The general procedure for determination of the model constants is the following, although there are small variations from drive to drive. The motor model constants are initially determined by traditionally tests. The main inductance and possibly the core losses are determined from no-load tests at different stator frequencies. The stray inductance and rotor frequency are determined from a locked-rotor test at 10 Hz stator frequency. The stator resistance is determined by a dc-measurement. No further changes are made to the inductances. Because the resistances depend on temperature, and thereby on the operating point, the rotor resistance is initially adjusted within a reasonable range to make the slip frequency of the loss measurements correspond with the calculated slip frequency. Thereafter the motor losses are adjusted to the measured motor loss by changing primarily the stator resistance keeping in mind its variation with temperature. Concerning the converter loss, small corrections are made to the output filter resistance value, to the dc-filter resistance values and to the diode rectifier conduction voltage.

B.1 2.2 kW Standard Induction Motor Drive.

Loss measurements are made both with and without a converter output filter. The complete data set is provided in [1]. The motor constants are determined from measurements with filtered stator voltages, so the model does no include harmonic losses. These are, however, quite constant, see section 3.2, so this does not influence the development of energy optimal control strategies. The result is shown in Figure B.1 - Figure B.6. The converter losses are verified with the measurements without output filter, see Figure B.7 - Figure B.11.

Table B.1: 2.2 standard motor name-plate.

ABB Motors

Motor 3~ CI.F IP55 IEC34 MTM100LA28-4 MK110022-S					CE
V	Hz	min^{-1}	kW	A	Cosφ
380-420 Y/220-240 D	50	1430	2.2	4.9/8.5	0.81
440-480 Y/250-280 D	60	1720	2.5	4.9/8.5	0.79

Derived nominal data for 2.2 standard motor in star connection.

Number of poles:	4
Output power:	2.2 kW
Stator voltage:	400 V
Stator current:	4.9 A
cos(φ):	0.81
Speed:	1430 rpm
Rated torque at 1430 rpm.:	14.7 Nm
Rated torque at 1500 rpm.:	14.0 Nm
Air-gap flux:	0.66 Wb

The following measurements are made with a LC-filter on the output of the converter. The filter cut-off frequency is 2.5 kHz, and it has the following component values:

$$L_{LC} = 1.35\,mH$$
$$R_{LC} = 1.17\,\Omega$$
$$C_{LC} = 3\,\mu F$$

where L_{LC} : LC-filter inductance.
R_{LC} : equivalent series resistance of LC-filter inductance.
C_{LC} : LC-filter capacitance.

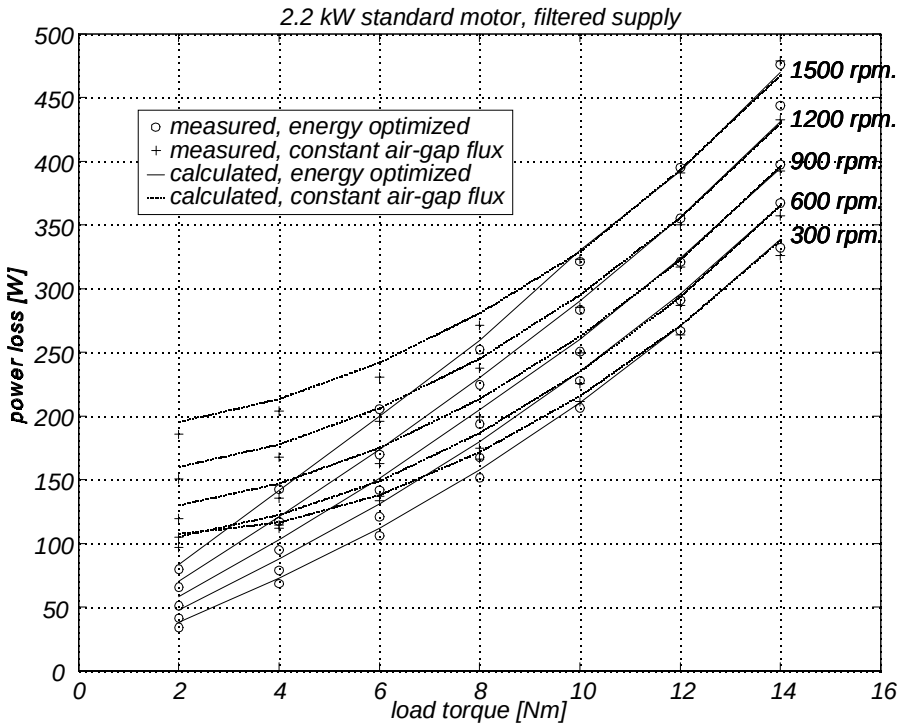

Figure B.1: *Measured and calculated motor power loss for a 2.2 kW standard induction motor fed by an inverter with an output filter.*

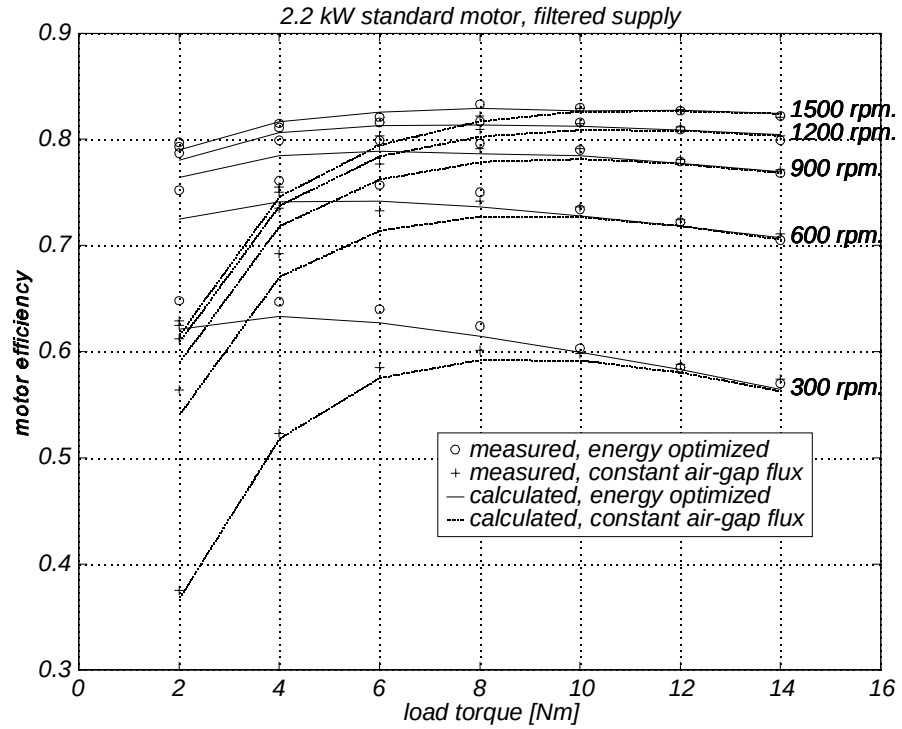

Figure B.2: *Measured and calculated efficiency of a 2.2 kW standard induction motor fed by an inverter with an output filter.*

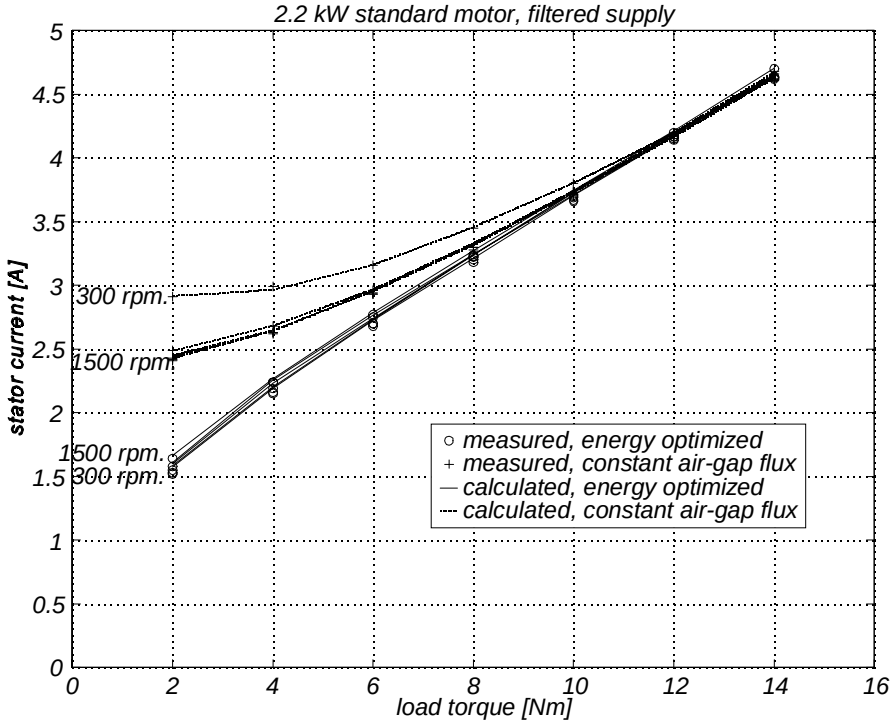

Figure B.3: *Measured and calculated stator current of a 2.2 kW standard induction motor fed by an inverter with an output filter.*

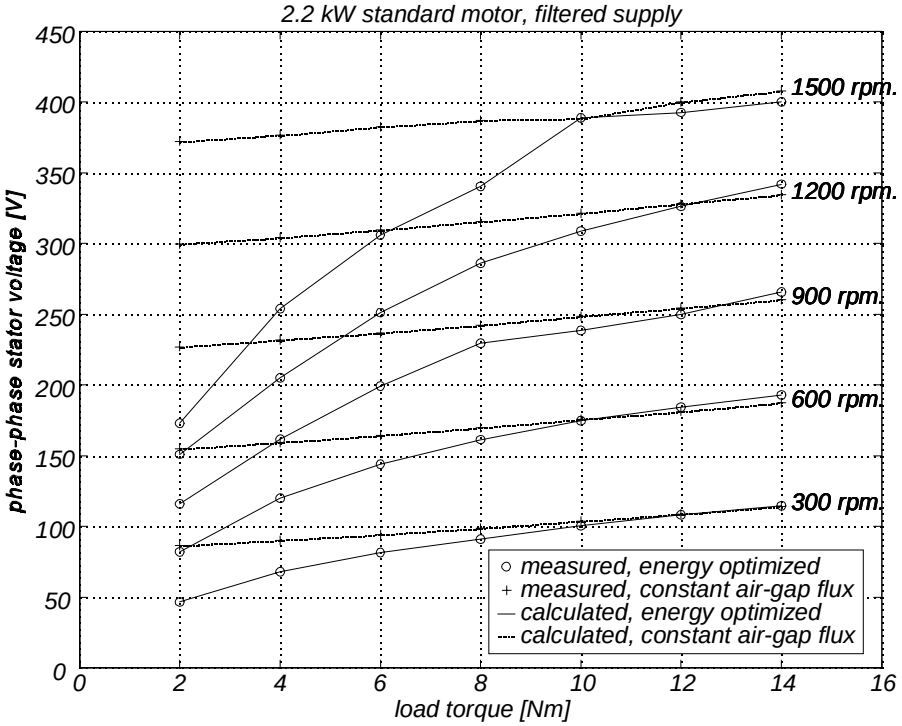

Figure B.4: *Measured and calculated line-to-line voltage for a 2.2 kW standard induction motor fed by an inverter with an output filter.*

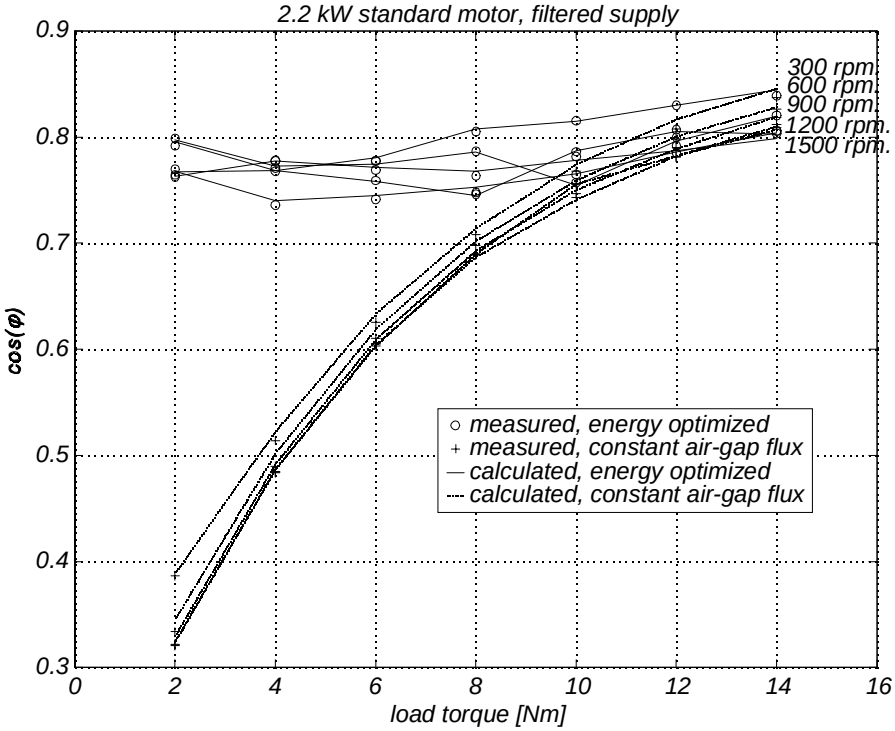

Figure B.5: *Measured and calculated displacement power factor for a 2.2 kW standard induction motor fed by an inverter with an output filter.*

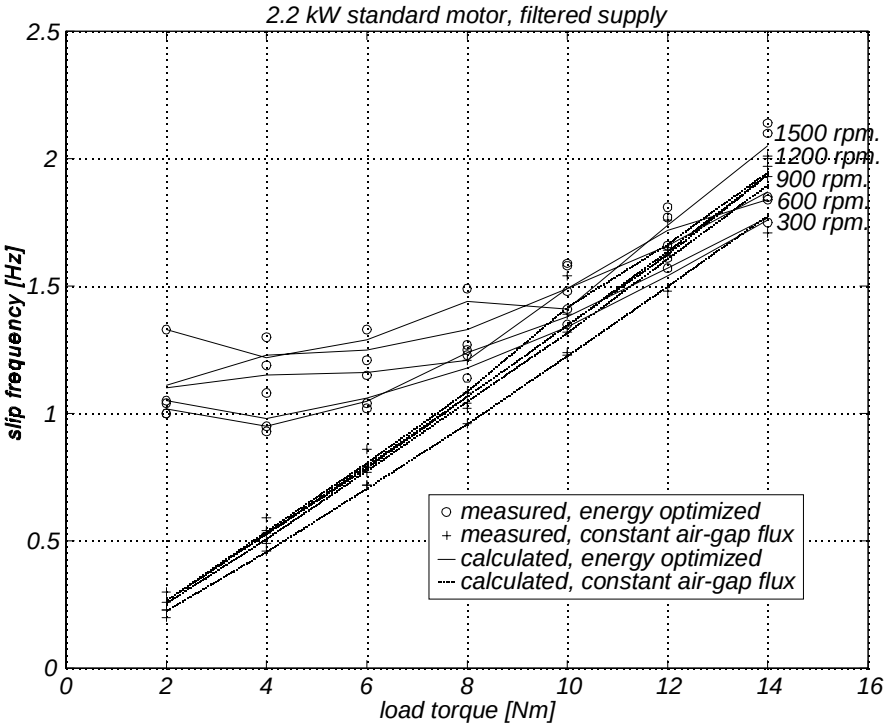

Figure B.6: *Measured and calculated slip frequency for a 2.2 kW standard induction motor fed by an inverter with an output filter.*

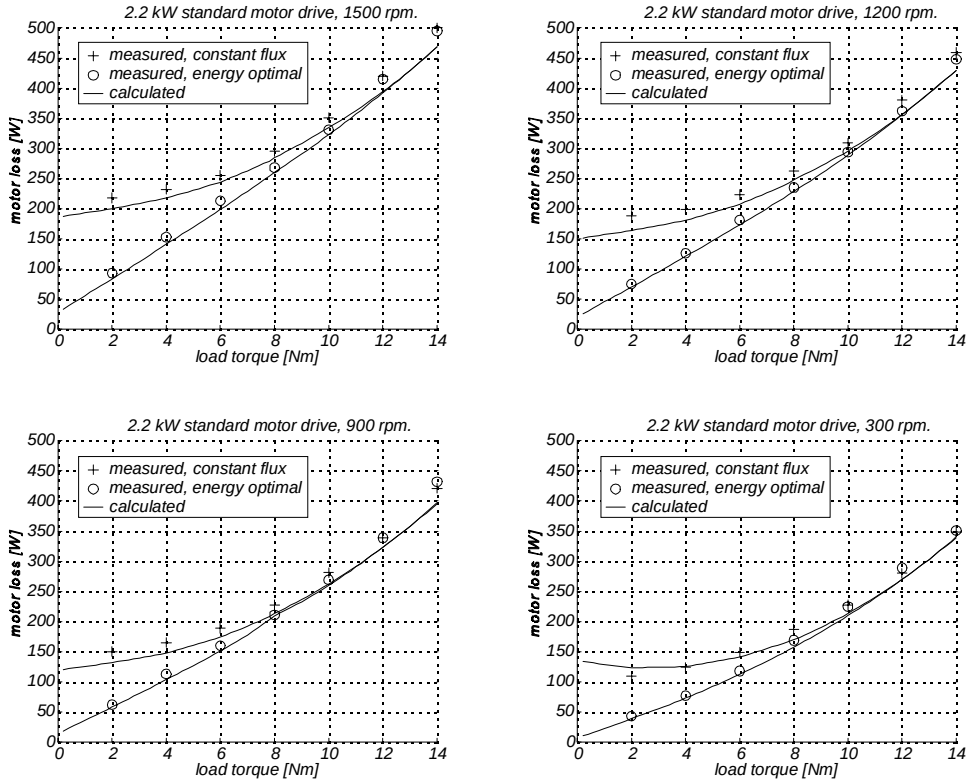

Figure B.7: *Measured and calculated motor loss of a 2.2 kW standard induction motor fed by an inverter.*

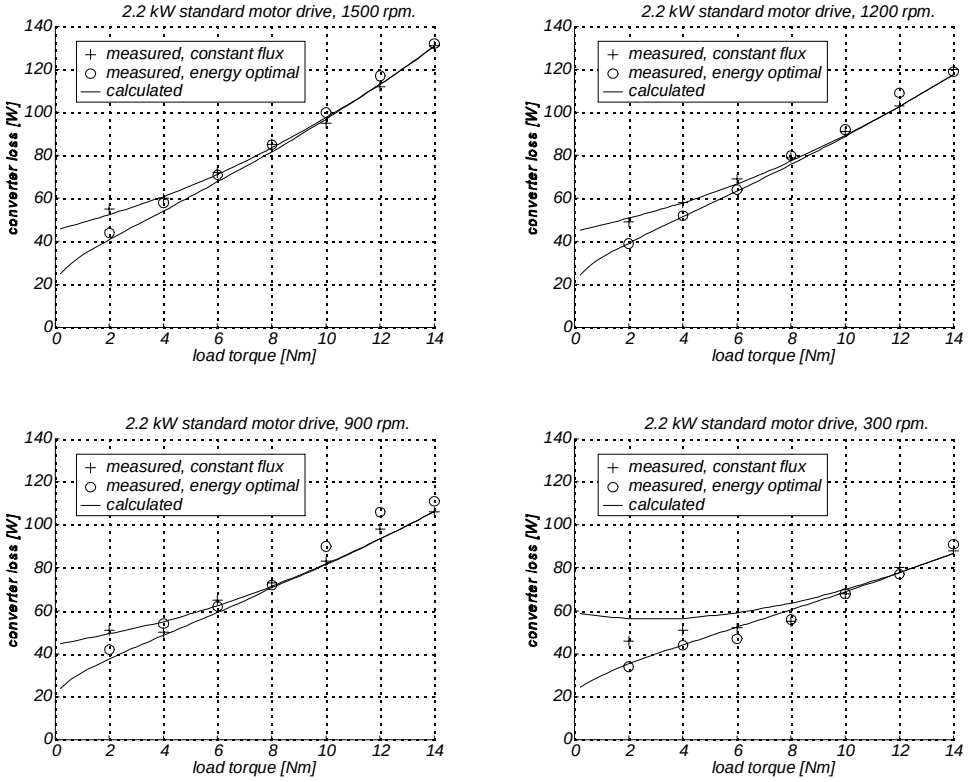

Figure B.8: *Measured and calculated converter loss of a 4 kVA converter feeding a 2.2 kW standard induction motor.*

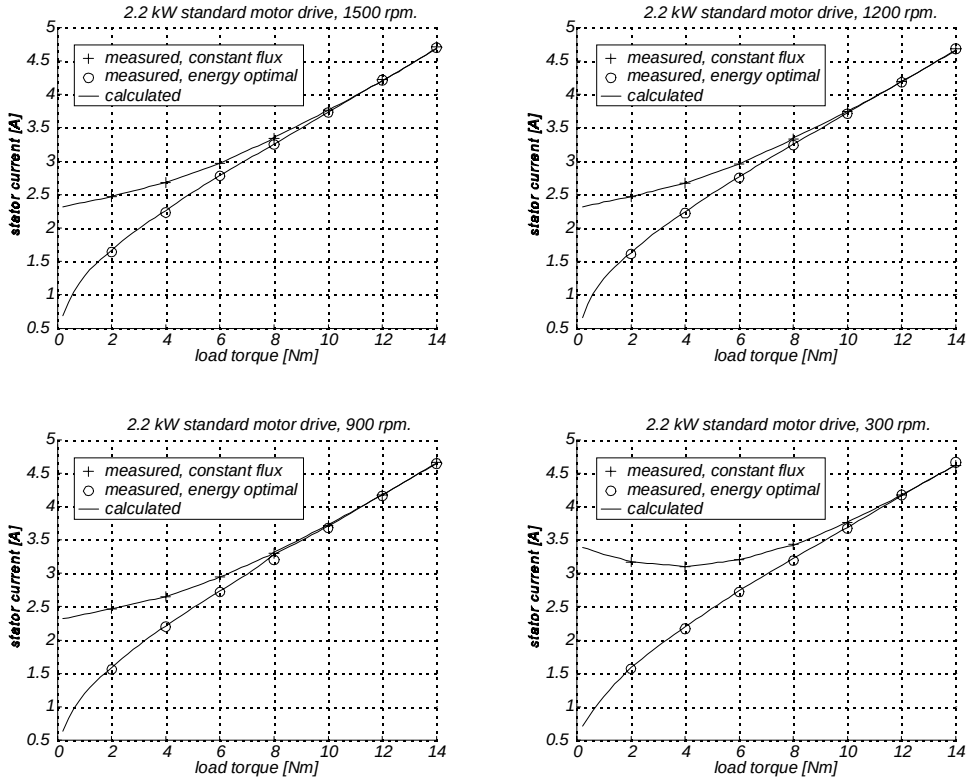

Figure B.9: *Measured and calculated stator current for a 2.2 kW standard induction motor fed by an inverter.*

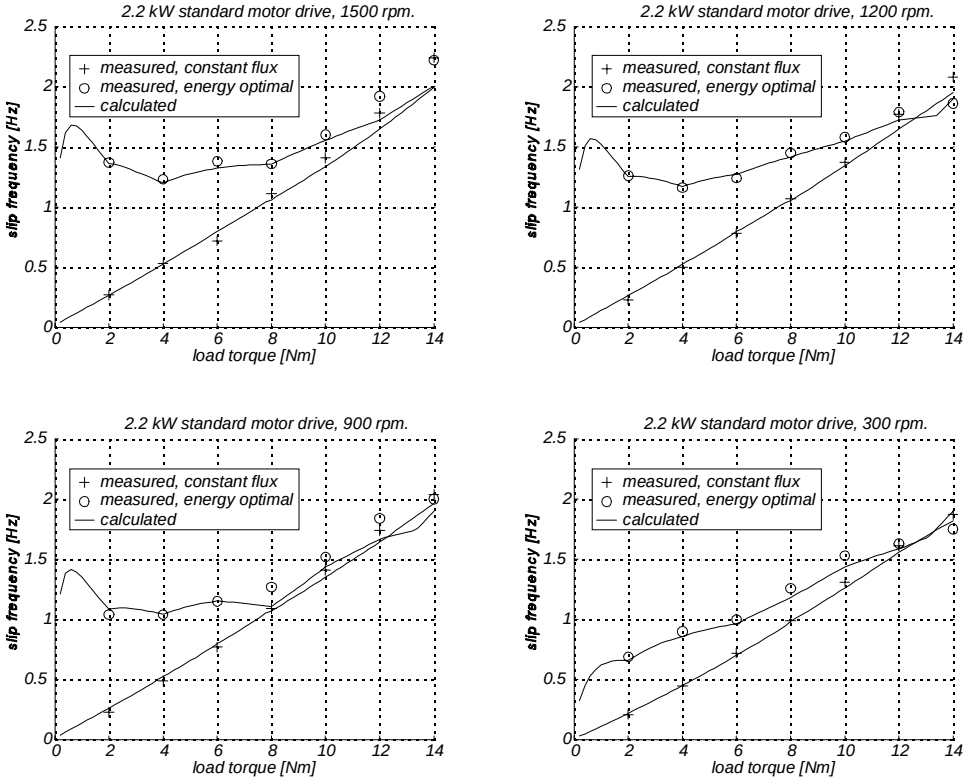

Figure B.10: *Measured and calculated slip frequency of a 2.2 kW standard induction motor fed by an inverter.*

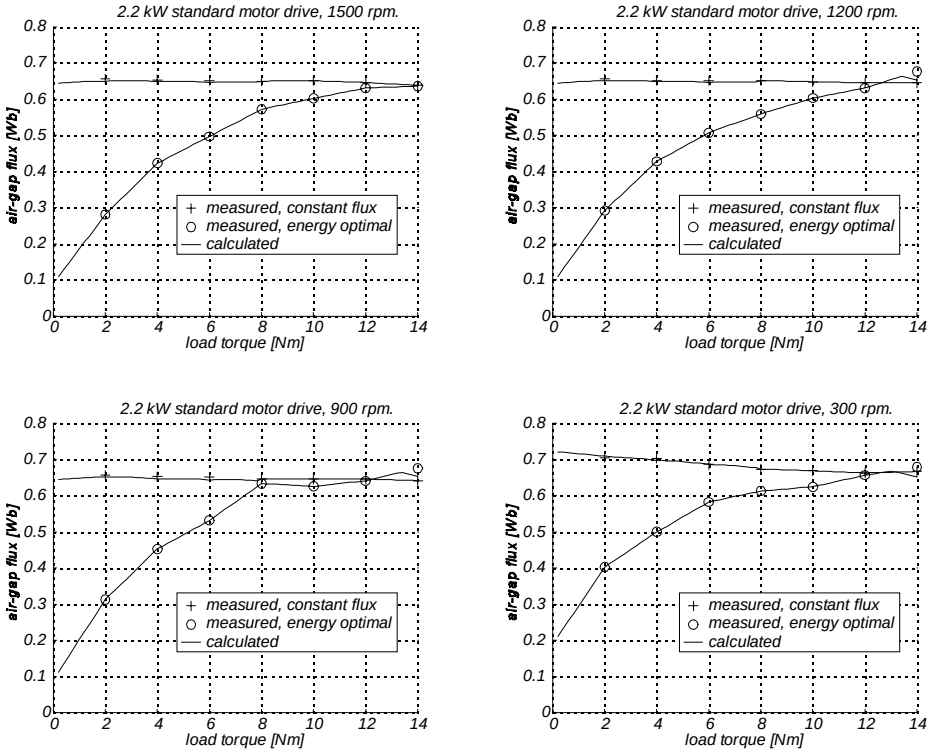

Figure B.11: *Measured and calculated air-gap flux of a 2.2 kW standard induction motor fed by an inverter.*

2.2 kW Standard Motor Model Constants.

All constants are expressed in SI-units.

$$T_{s,over} = 2.8 + 40 \cdot \psi_m + 2.58 \cdot \tau_{load} \quad [°C]$$

$$R_s = 2.89\ (1 + 0.00393\,(T_{amb}[°C] + T_{s,over}[°C] - 20))$$

$$T_{r,over} = 37.5 \cdot \psi_m + 1.67 \cdot \tau_{load} - 14.6 \quad [°C]$$

$$R_r = 1.88\,(1 + 0.0043\,(T_{amb}[°C] + T_{r,over}[°C] - 20))$$

$$L_\sigma = 0.029H$$
$$L_{s\sigma} = 0.013H$$
$$L_{r\sigma} = 0.016H$$

$L_m(i_m)$ $[H]$:

$$i_m < i_{m1}: L_m = L_{m0}$$
$$i_{m1} \le i_m < i_{m2}: L_m = a_1 \cdot i_m^3 + a_2 \cdot i_m^2 + a_3 \cdot i_m + a_4$$
$$i_{m2} \le i_m < i_{m3}: L_m = b_1 \cdot i_m + b_2$$
$$i_{m3} \le i_m: L_m = c_1 + c_2 / i_m$$

$i_{m1} = 0.8$
$i_{m2} = 2$
$i_{m3} = 3$
$L_{m0} = 0.328$
$a_1 = -0.0108796$
$a_2 = -0.0070833$
$a_3 = 0$
$a_4 = 0.328$
$b_1 = -0.064$
$b_2 = 0.427$
$c_1 = 0.043$
$c_2 = 0.576$

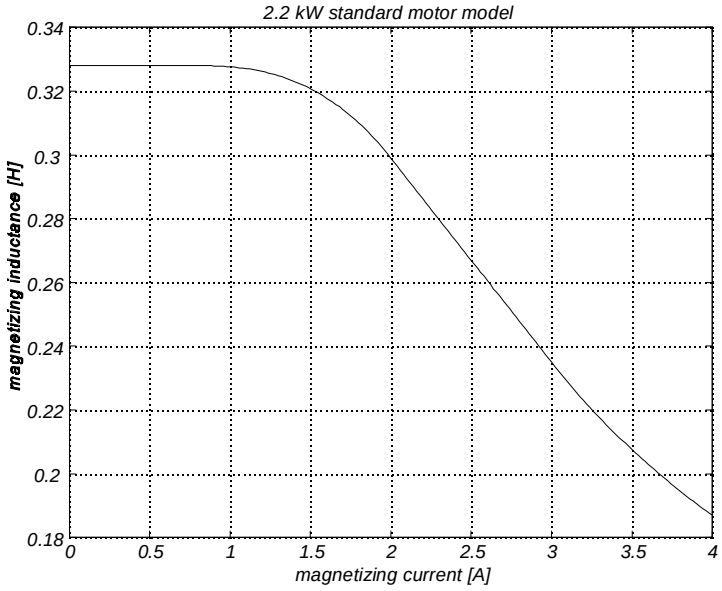

Figure B.12: *2.2 kW standard induction motor magnetizing inductance model.*

$$P_{core} = 3.10\,(1 + 0.69 \cdot s)\,\psi_m^{1.80} \cdot f_s + 0.040\,(1 + 0.69 \cdot s^2)\,\psi_m^2 \cdot f_s^2 \quad [W]$$

$$\tau_{mech} = 0.095 + 1.18 \cdot 10^{-5} \cdot n + 1.6 \cdot 10^{-8} \cdot n^2 \quad [Nm]$$

$$J = 0.007\ kg \cdot m^2$$

4 kVA Converter Model Constants.

$V_{0T} = 1.330$ $A_{swonT} = 0.180 \cdot 10^{-3}$ $V_{0Tlin} = 1.5365$
$R_{0T} = 0.320$ $B_{swonT} = 1$ $R_{0Tlin} = 0.1123$
$B_{conT} = 0.550$ $A_{swoffT} = 0.175 \cdot 10^{-3}$ $V_{0Dlin} = 0.5977$
$V_{0D} = 0.550$ $B_{swoffT} = 1$ $R_{0Dlin} = 0.0492$
$R_{0D} = 0.096$ $A_{swD} = 0.260 \cdot 10^{-3}$ $\alpha = 5.0835 \cdot 10^{-4}$
$B_{conD} = 0.700$ $B_{swD} = 0.670$

$R_{dc1} = 0.014\ \Omega,\ at\ 20°C$ $R_{ac} = 0.075\ \Omega,\ at\ 20°C$ $P_{supply} = 17\ W$
$R_{dc2} = 0.074{+}1.9\ \Omega,\ at\ 20°C$ $V_D = 0.8\,V$

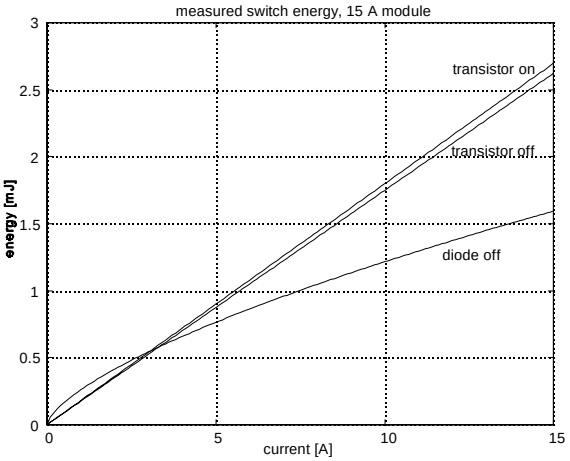

Figure B.14: *Switch energies for 4 kVA inverter.*

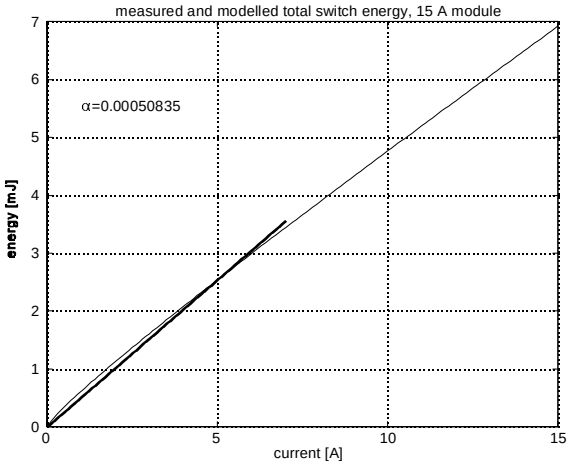

Figure B.13: *Total inverter switch energy.*

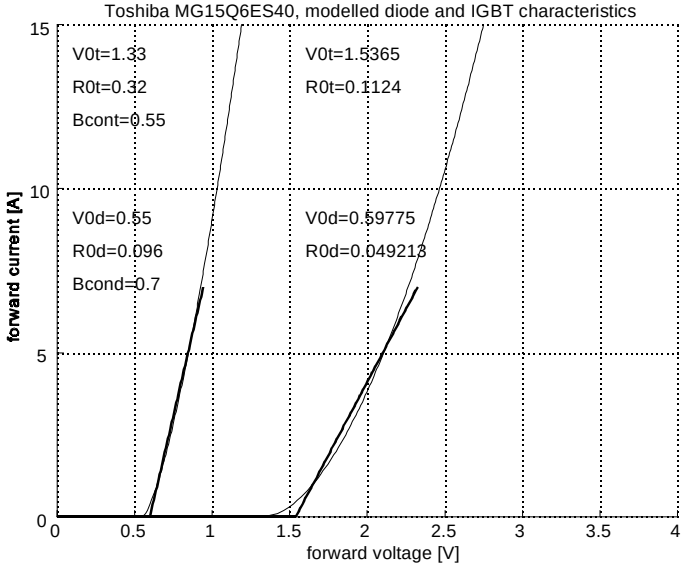

Figure B.15: *Transistor and diode conduction voltages for a 15 A module.*

B.2 2.2 kW High-Efficiency Motor.

The constants for the 2.2 kW high-efficiency motor model are determined in the same way as for the 2.2 kW standard motor. The comparison of measurements and calculations is shown on Figure B.12 - Figure B.17.

Table B.2: 2.2 kW high-efficiency motor name-plate.

ABB Motors

Motor 3~ CI.F IP55 IEC34 MTM100LB28-4 V290-50A					CE
V	Hz	min^{-1}	kW	A	Cosφ
400 Y/230 D	50	1450	2.2	4.7/8.1	0.8

Derived nominal data for 2.2 kW high-efficiency motor in star connection.

Number of poles:	4
Output power:	2.2 kW
Stator voltage:	400 V
Stator current:	4.7 A
cos(φ):	0.80
Speed:	1450 rpm
Rated torque at 1430 rpm.:	14.5 Nm
Rated torque at 1500 rpm.:	14.0 Nm
Air-gap flux	0.67 Wb

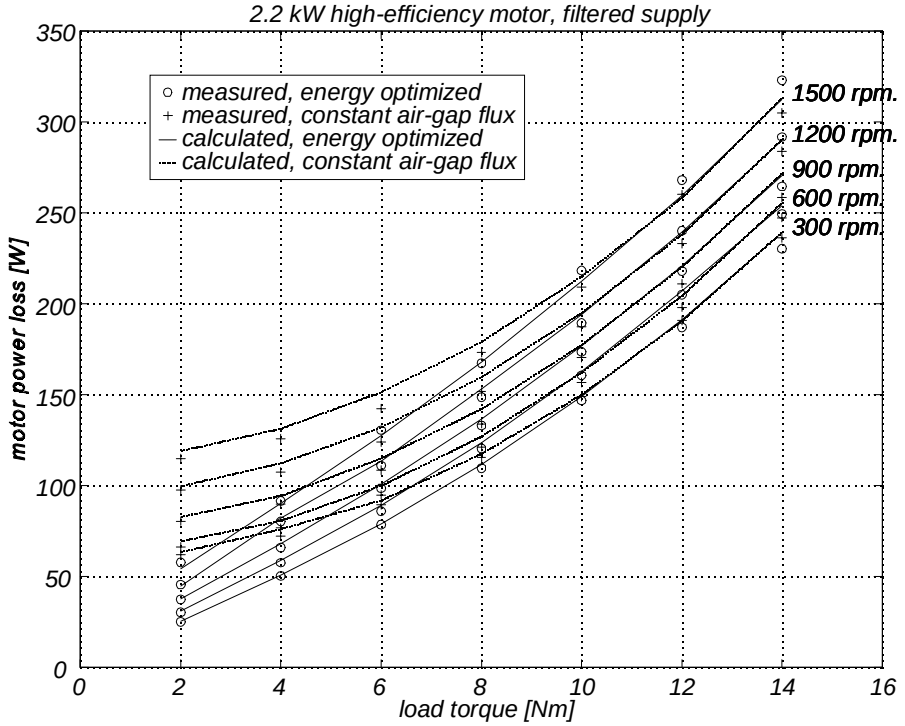

Figure B.16: *Measured and calculated power loss for a 2.2 kW high-efficiency induction motor fed by an inverter with an output filter.*

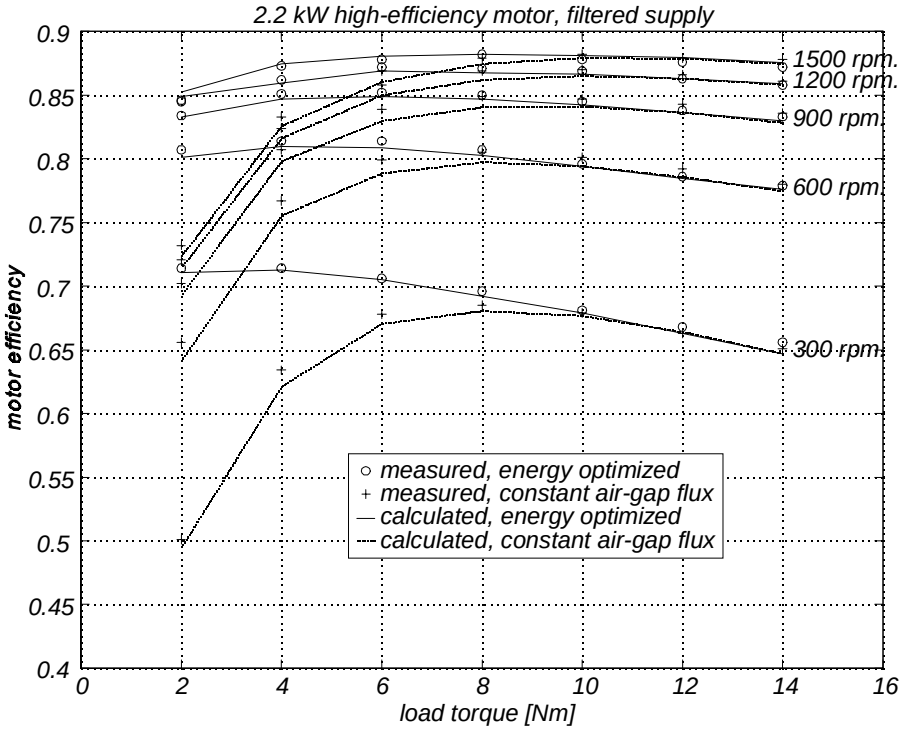

Figure B.17: *Measured and calculated efficiency of a 2.2 kW high-efficiency induction motor fed by an inverter with an output filter.*

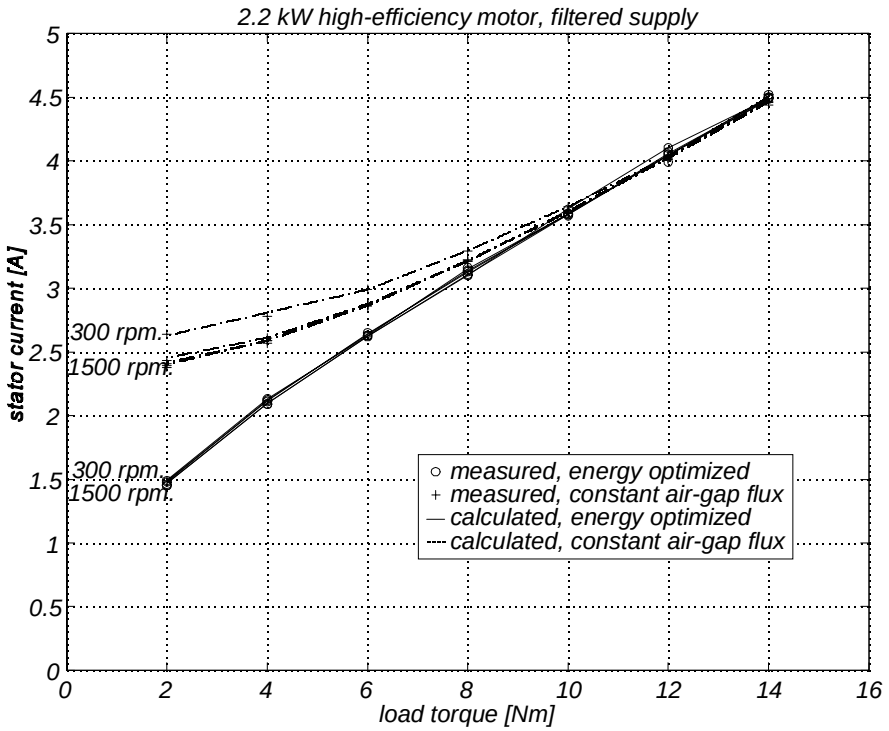

Figure B.18: *Measured and calculated stator current of a 2.2 kW high-efficiency induction motor fed by an inverter with an output filter.*

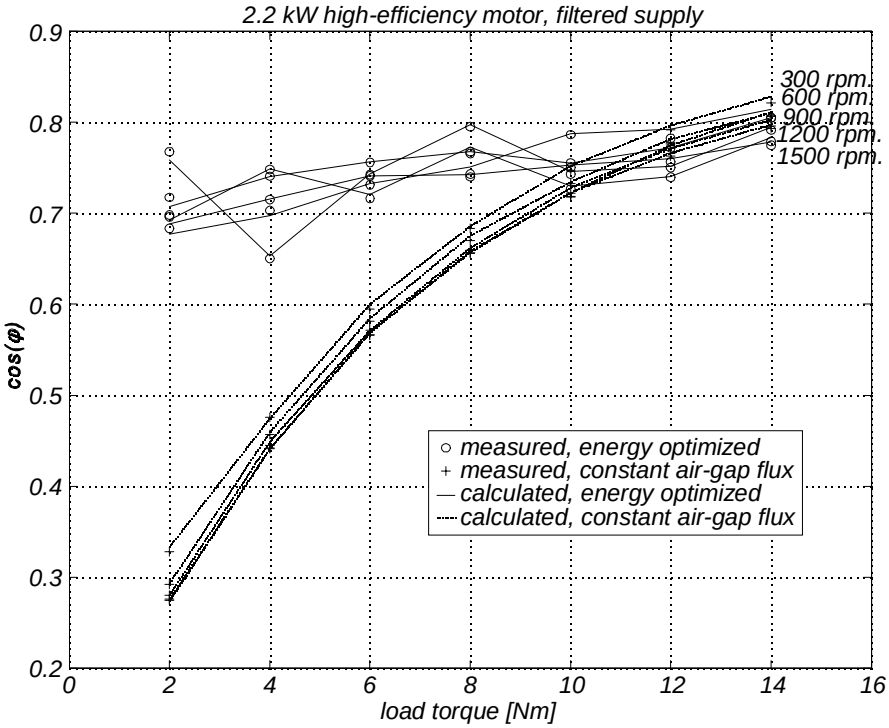

Figure B.19: *Measured and calculated displacement power factor for a 2.2 kW high-efficiency induction motor fed by an inverter with an output filter.*

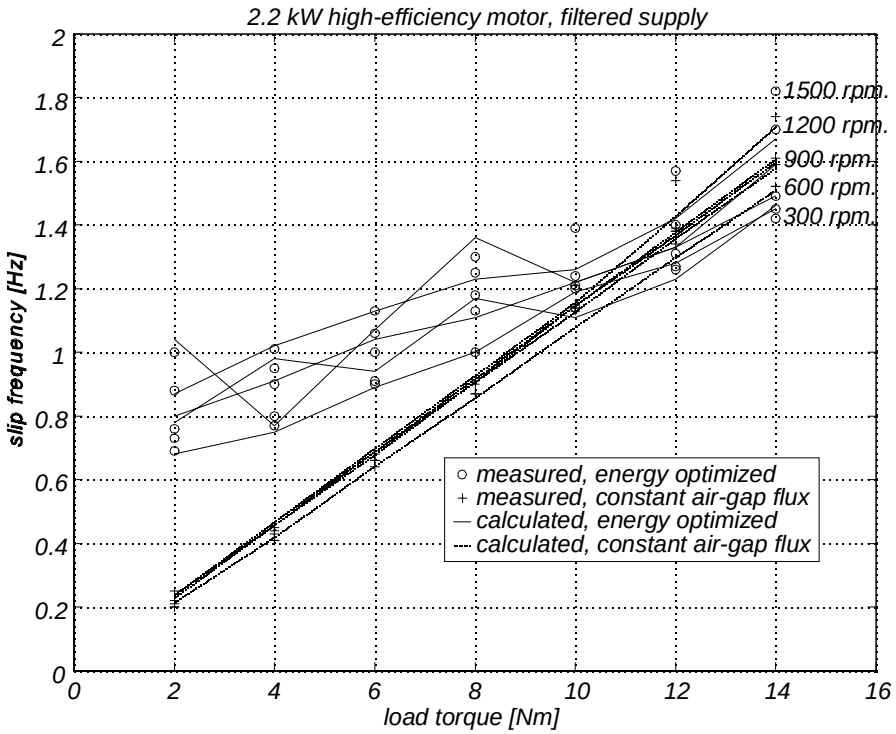

Figure B.20: *Measured and calculated slip frequency for a 2.2 kW high-efficiency induction motor fed by an inverter with an output filter.*

2.2 kW High-Efficiency Motor Model Constants.

All constants are expressed in SI-units.

$T_{s,over} = 12.50 \cdot \psi_m + 2.083 \cdot \tau_{load} - 2.9 \quad [°C]$

$R_s = 2.34 \ (1 + 0.00393 (T_{amb}[°C] + T_{s,over}[°C] - 20.0)) \quad [\Omega]$

$T_{r,over} = 10\,°C \quad R_r = 1.8 (1 + 0.0043 (T_{amb}[°C] + T_{r,over}[°C] - 20)) \quad [\Omega]$

$L_\sigma = 0.027\,H$
$L_{s\sigma} = 0.012\,H$
$L_{r\sigma} = 0.015\,H$

$L_m(i_m)$ $[H]$:

$i_m < i_{m1}$: $L_m = L_{m0}$
$i_{m1} \le i_m < i_{m2}$: $L_m = a_1 \cdot i_m^3 + a_2 \cdot i_m^2 + a_3 \cdot i_m + a_4$
$i_{m2} \le i_m < i_{m3}$: $L_m = b_1 \cdot i_m + b_2$
$i_{m3} \le i_m$: $L_m = c_1 + c_2 / i_m$

$i_{m1} = 0.5$
$i_{m2} = 1.7$
$i_{m3} = 3$
$L_{m0} = 0.365$
$a_1 = 0.0069444$
$a_2 = -0.037500$
$a_3 = 0$
$a_4 = 0.3650$
$b_1 = -0.0600$
$b_2 = 0.4250$
$c_1 = 0.0650$
$c_2 = 0.5400$

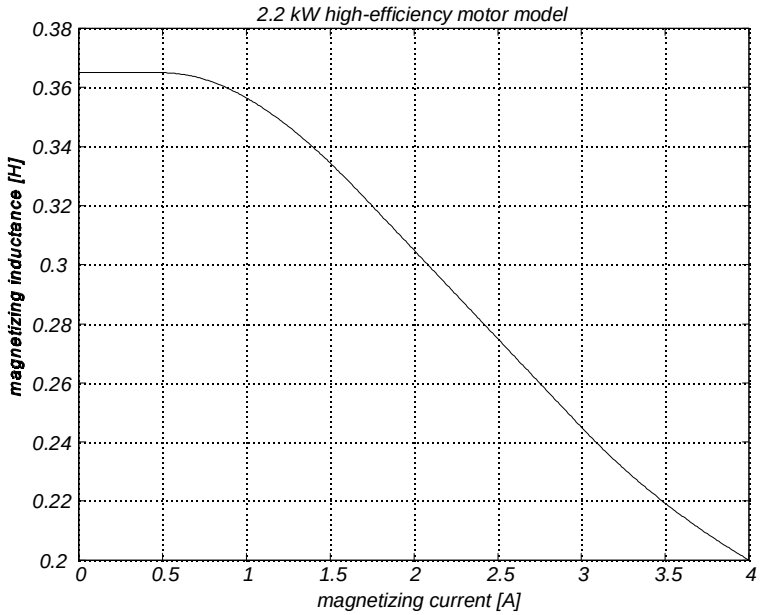

Figure B.21: *2.2 kW high-efficiency motor magnetizing inductance model.*

$P_{core} = (1 + 0.69 \cdot s) \cdot 1.83 \cdot \psi_m^{2.05} \cdot f_s + (1 + 0.69 \cdot s^2) \cdot 0.018 \cdot \psi_m^2 \cdot f_s^2 \quad [W]$

$\tau_{mech} = 0.065 + 1.013 \cdot 10^{-5} \cdot n + 1.1 \cdot 10^{-8} \cdot n^2 \quad [Nm]$

$J = 0.0086 \ kg \cdot m^2$

B.1 22 kW Standard Induction Motor Drive.

Table B.3: 22 kW standard motor name-plate.

ASEA Made in Sweden			
Motor MBT 180L			
3~	50 Hz	No.	
22 kW		1470 o/min.	
		Cl. F	cosφ = 0.84
prim.	381 V	prim.	220 V
Y	43.5 A	Δ	75 A
Sec.	V A		
Cat. no. MK 171 007-AA		IP 54	145 kg.
SEN.	2601	IEC 34-1	

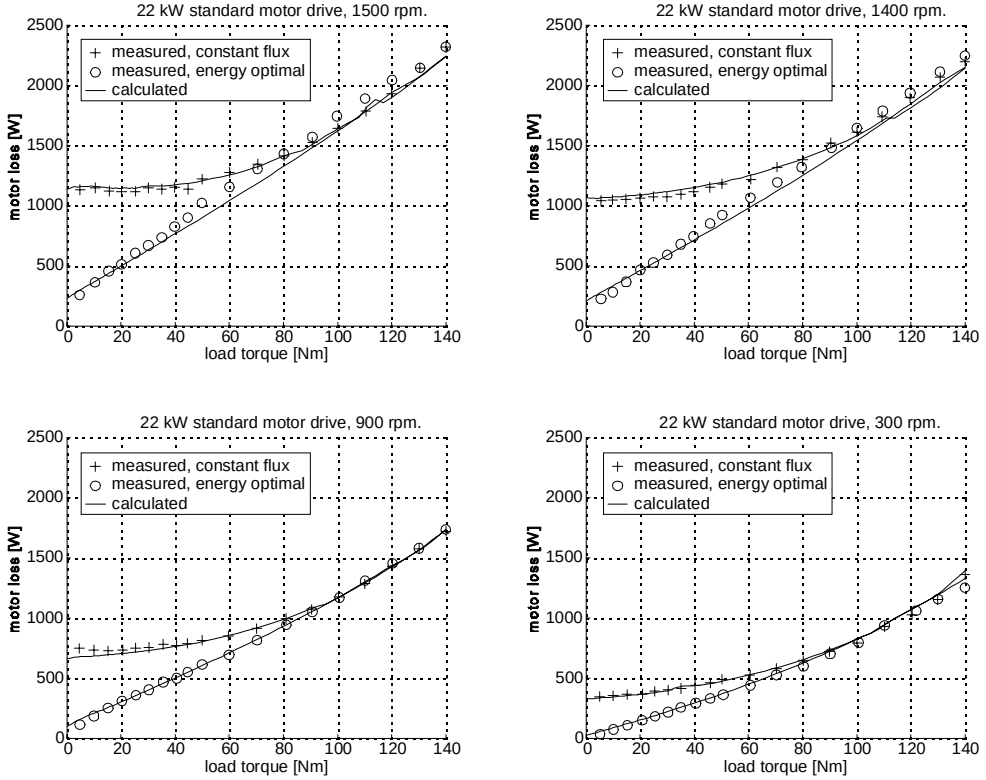

Figure B.22: *Measured and calc. loss of a 22 kW standard induction motor fed by an inverter.*

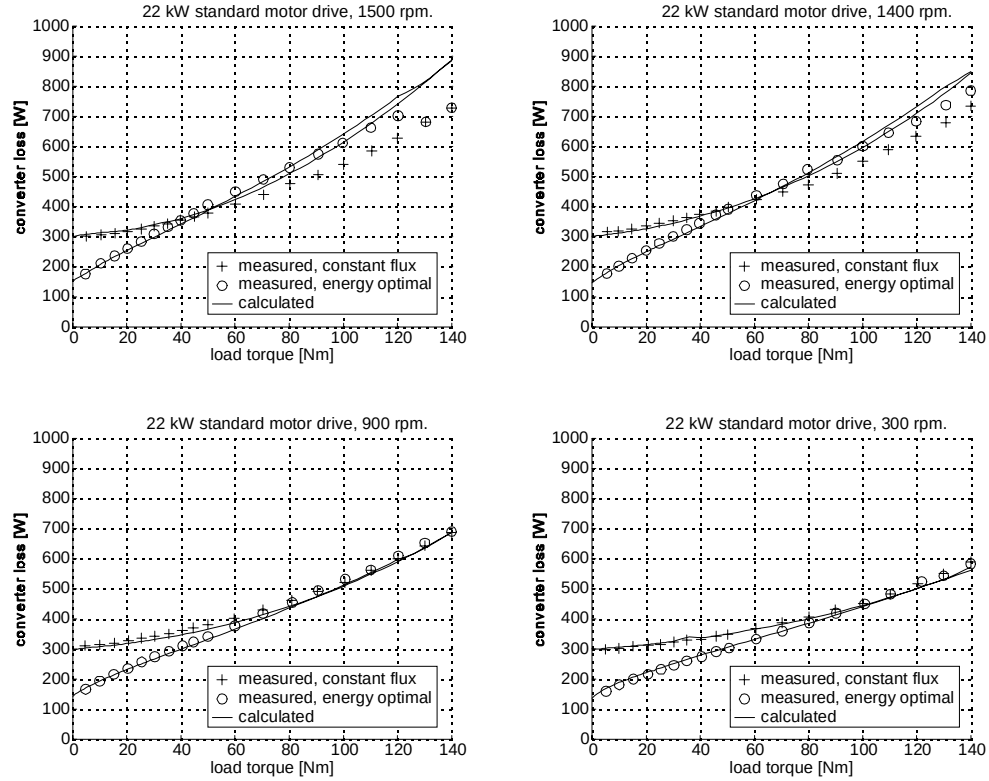

Figure B.23: *Measured and calculated loss of a 32 kVA converter when feeding a 22 kW standard induction motor.*

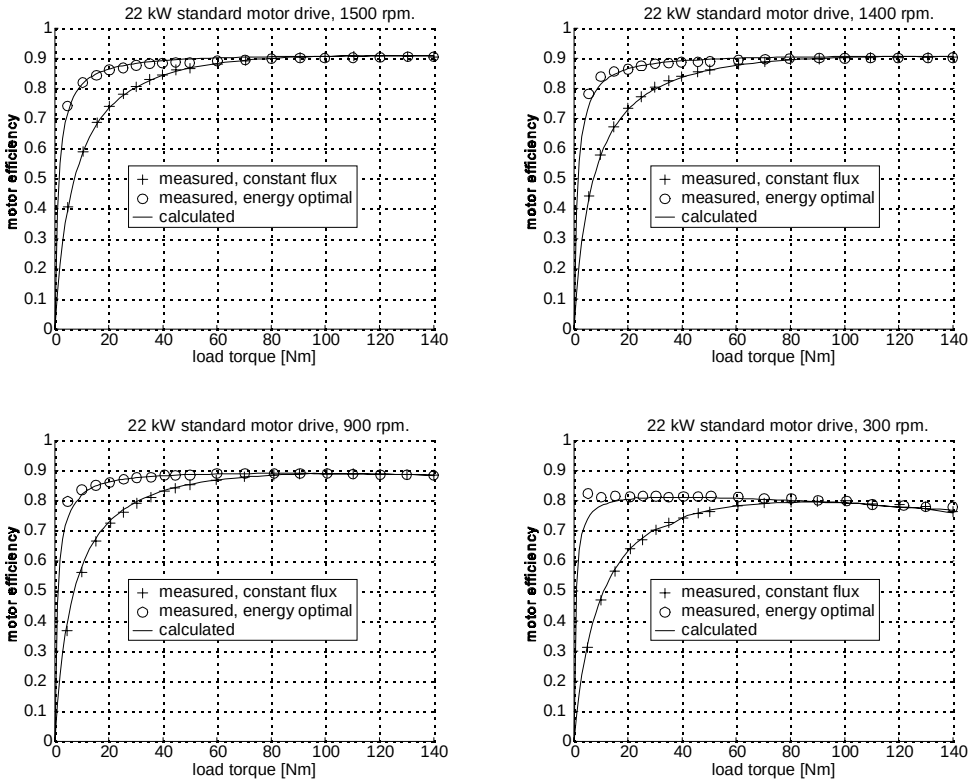

Figure B.24: *Measured and calc. eff. of a 22 kW standard induction motor fed by an inverter.*

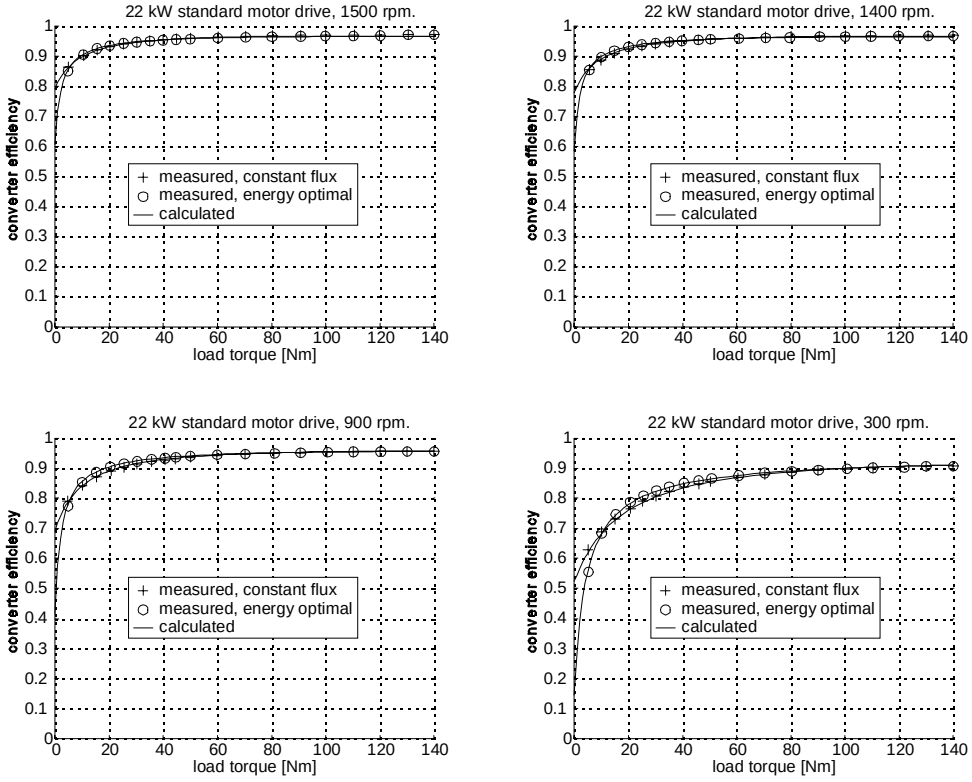

Figure B.25: *Measured and calculated efficiency of a 32 kVA converter feeding a 22 kW standard induction motor.*

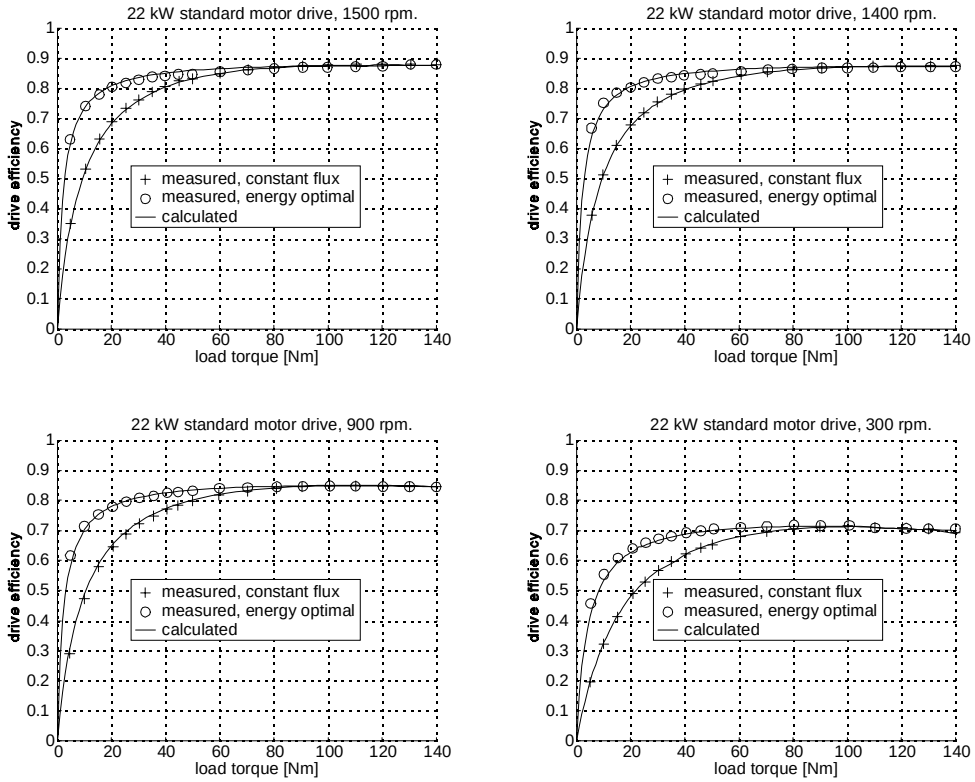

Figure B.26: *Measured and calculated efficiency (motor and converter) of a 22 kW standard induction motor fed by a converter.*

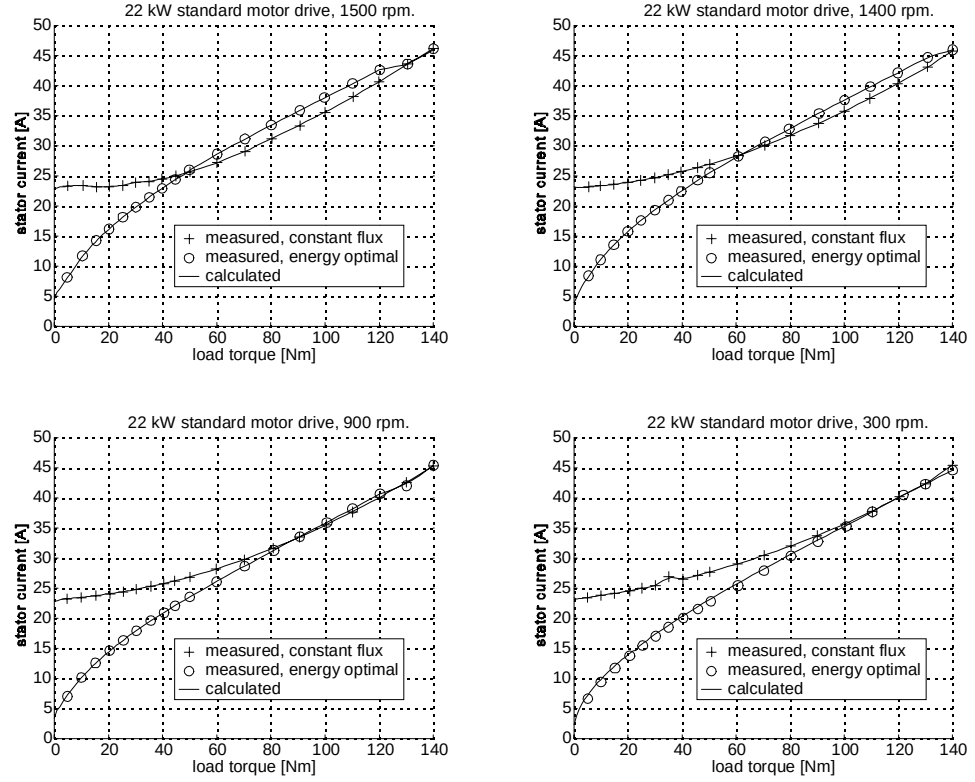

Figure B.27: *Meas. and calc. stator current for a 22 kW standard ind. motor fed by a conv.*

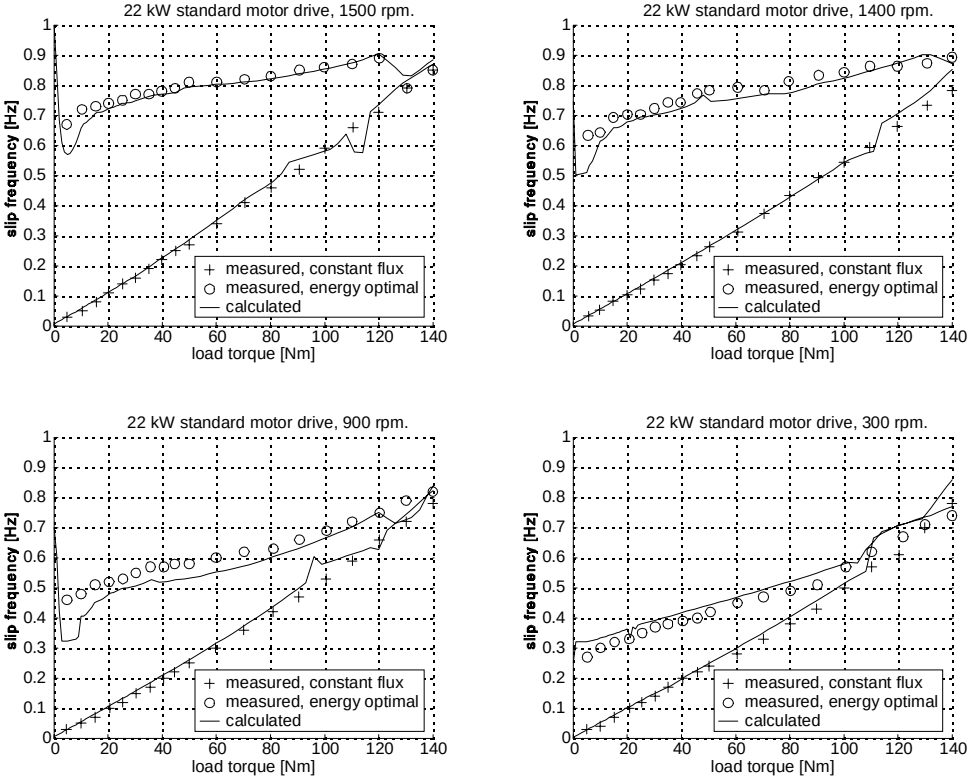

Figure B.28: *Meas. and calc. slip freq. for a 22 kW standard ind. motor fed by an inverter.*

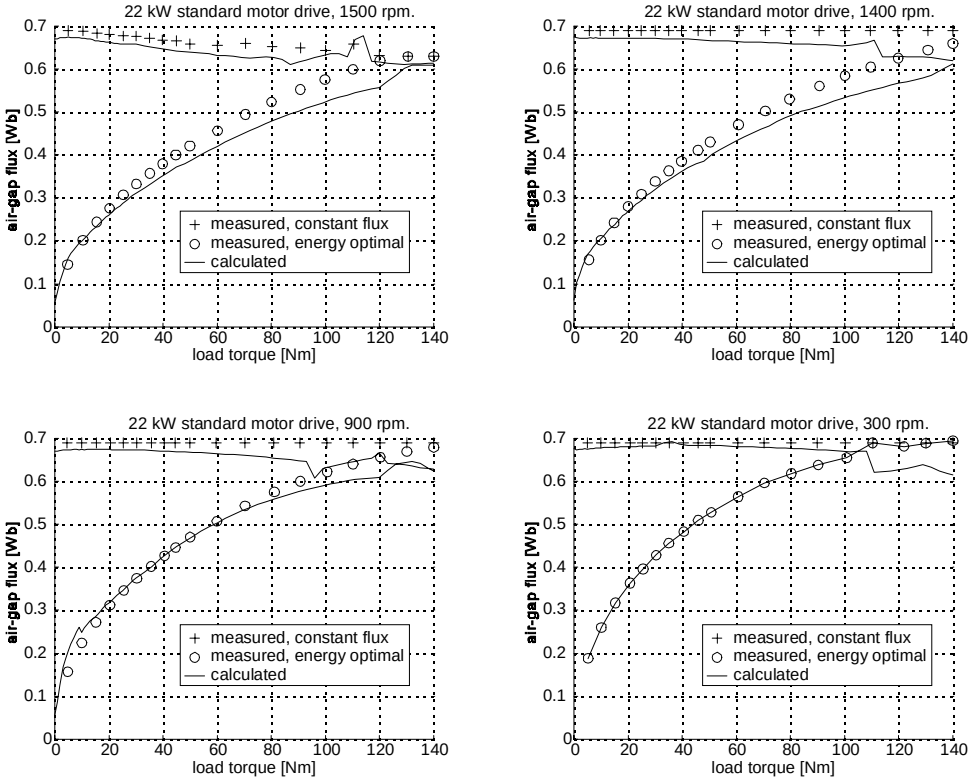

Figure B.29: *Air-gap flux ref. and calc. air-gap flux for a 22 kW standard induction motor.*

22 kW Standard Motor Model Constants.

$R_s = (0.13+0.0145/140\,\tau)(1+(n-300)/10000)\ \Omega$
$R_r = 0.086\ \Omega$
$L_{s\sigma} = 1.21\cdot 10^{-3}\ H$
$L_{r\sigma} = 1.82\cdot 10^{-3}\ H$

$L_m(i_m)\ [H]$:
$i_m < i_{m1}$: $L_m = L_{m0}$
$i_{m1} \le i_m < i_{m2}$: $L_m = a_1(i_m-i_{m1})i_m^3 + a_2(i_m-i_{m1})i_m^2 + a_3(i_m-i_{m1})i_m + a_4$
$i_{m2} \le i_m < i_{m3}$: $L_m = b_1\cdot i_m + b_2$
$i_{m3} \le i_m$: $L_m = c_1 + c_2/i_m$

$i_{m1} = 5$
$i_{m2} = 10$
$i_{m3} = 28$
$L_{m0} = 0.0405$
$a_1 = 3.333333\cdot 10^{-6}$
$a_2 = -9.666666\cdot 10^{-5}$
$a_3 = 0$
$a_4 = 0.0405$
$b_1 = -7.1666666\cdot 10^{-4}$
$b_2 = 0.04566666$
$c_1 = 0.00553333$
$c_2 = 0.56186666$
$\psi_1 = 0.2025$
$\psi_2 = 0.3850$
$\psi_3 = 0.7168$

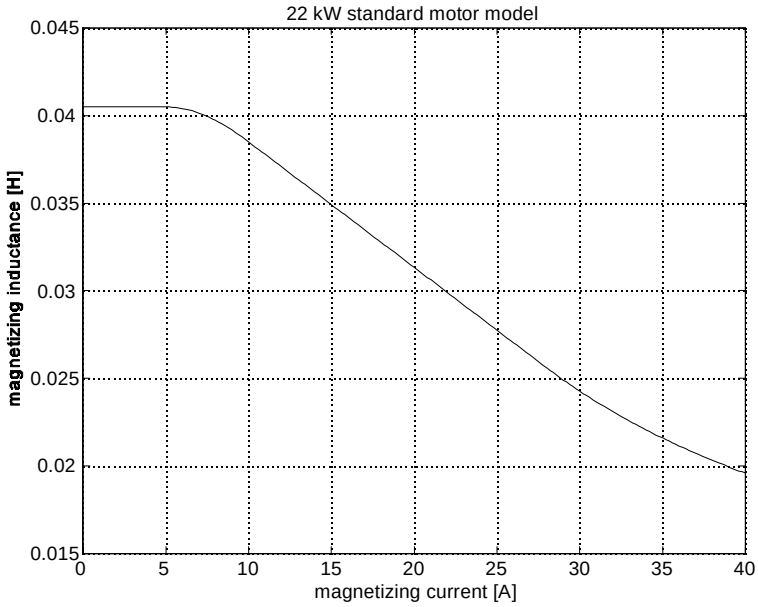

Figure B.30: *22 kW standard induction motor magnetizing inductance model.*

$P_{core} = 18.02(1+0.69\cdot s)\psi_m^{1.80}\cdot f_s + 0.234(1+0.69\cdot s^2)\psi_m^2\cdot f_s^2 \quad [W]$

$\tau_{mech} = 0.4+625\cdot 10^{-6}\cdot n \quad [Nm]$

$J = 0.19\ kg\cdot m^2$

32 kVA Converter Model Constants.

$V_{0T} = 0.6000$ $A_{swonT} = 7.5588 \cdot 10^{-5}$ $V_{0Tlin} = 0.9707$
$R_{0T} = 0.1636$ $B_{swonT} = 1.2209$ $R_{0Tlin} = 0.0228$
$B_{conT} = 0.5711$ $A_{swoffT} = 2.5786 \cdot 10^{-4}$ $V_{0Dlin} = 0.7114$
$V_{0T} = 0.4500$ $B_{swoffT} = 0.8381$ $R_{0Dlin} = 0.0125$
$R_{0T} = 0.1237$ $A_{swD} = 2.2193 \cdot 10^{-4}$ $\alpha = 3.5883 \cdot 10^{-4}$
$B_{conD} = 0.5066$ $B_{swD} = 0.5711$

$R_{dc1} = 0.040\ \Omega,\ at\ 20°C$ $R_{ac} = 0.003\ \Omega,\ at\ 20°C$ $P_{supply} = 120\ W$
$R_{dc2} = 0\ \Omega,\ at\ 20°C$ $V_D = 0.7\,V$

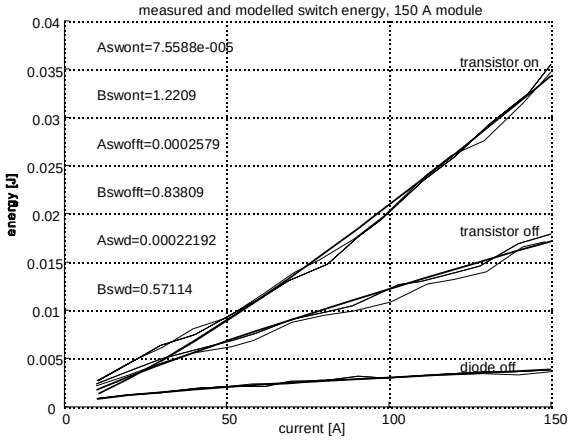

Figure B.31: *Measured and modeled inverter switch energies.*

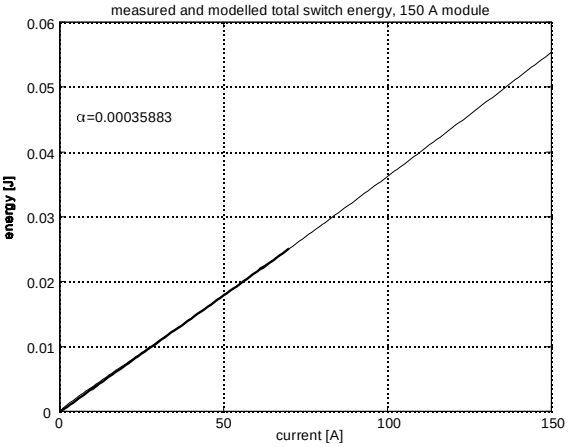

Figure B.32: *Total inverter switch energy.*

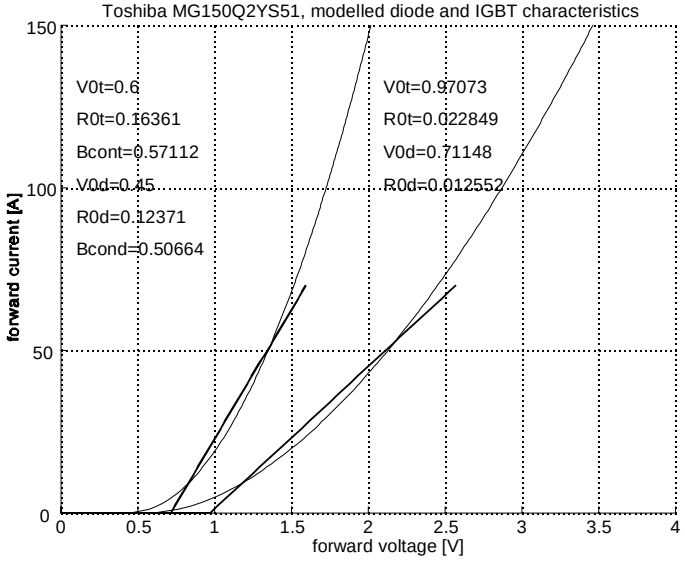

Figure B.33: *Measured inverter transistor and diode conduction voltages.*

B.3 90 kW Standard Induction Motor Drive.

Table B.4: 90 kW standard motor name-plate.

ABB Motors

Motor 3~ CI.F IP55 IEC34 ABB 400/50Hz, Type 280SMB					CE
V	Hz	min^{-1}	kW	A	Cosφ
380-420 D	50	1483	90	158	0.86

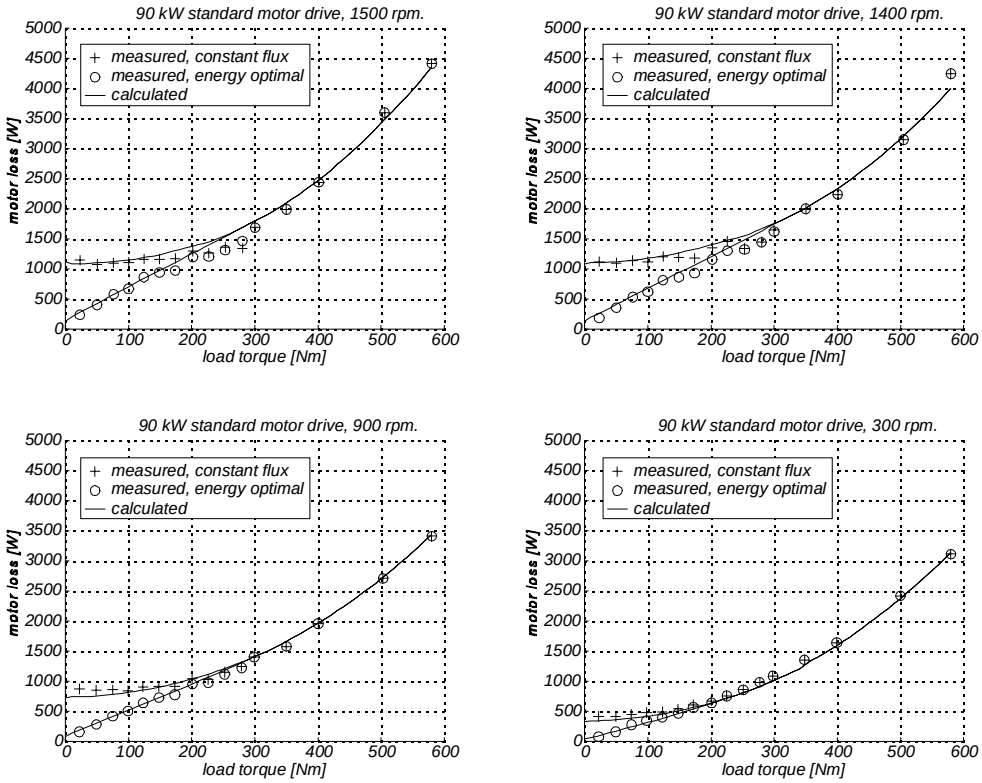

Figure B.34: *Meas. and calc. loss of a 90 kW standard induction motor fed by an inverter.*

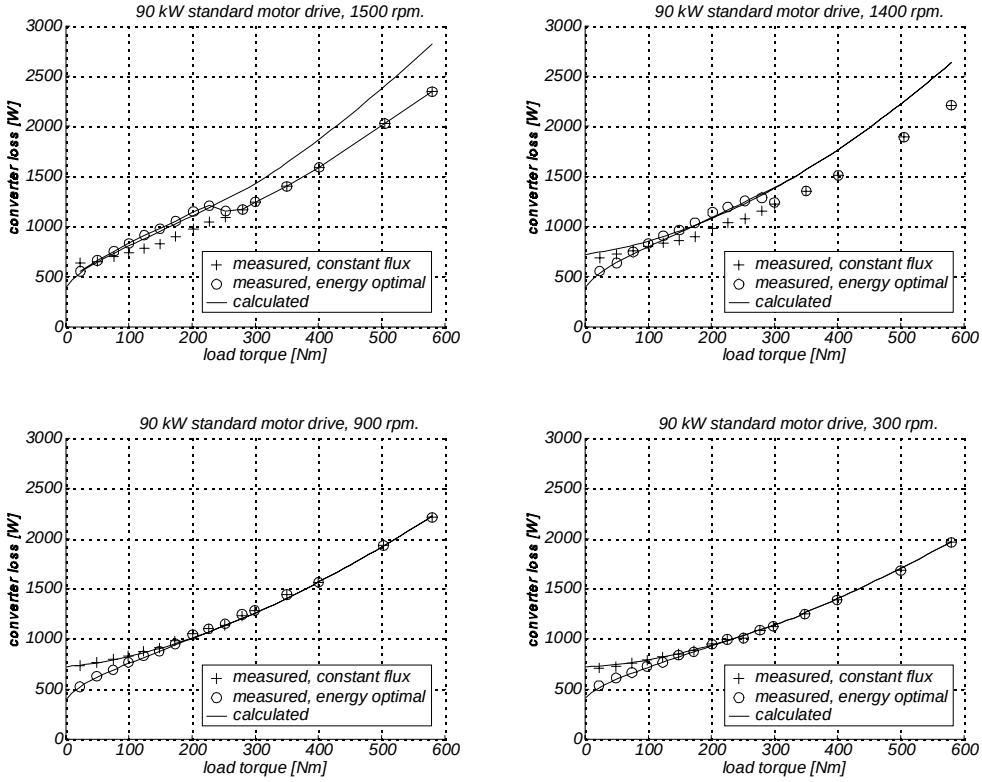

Figure B.35: *Meas. and calc. loss of a converter feeding a 90 kW standard induction motor.*

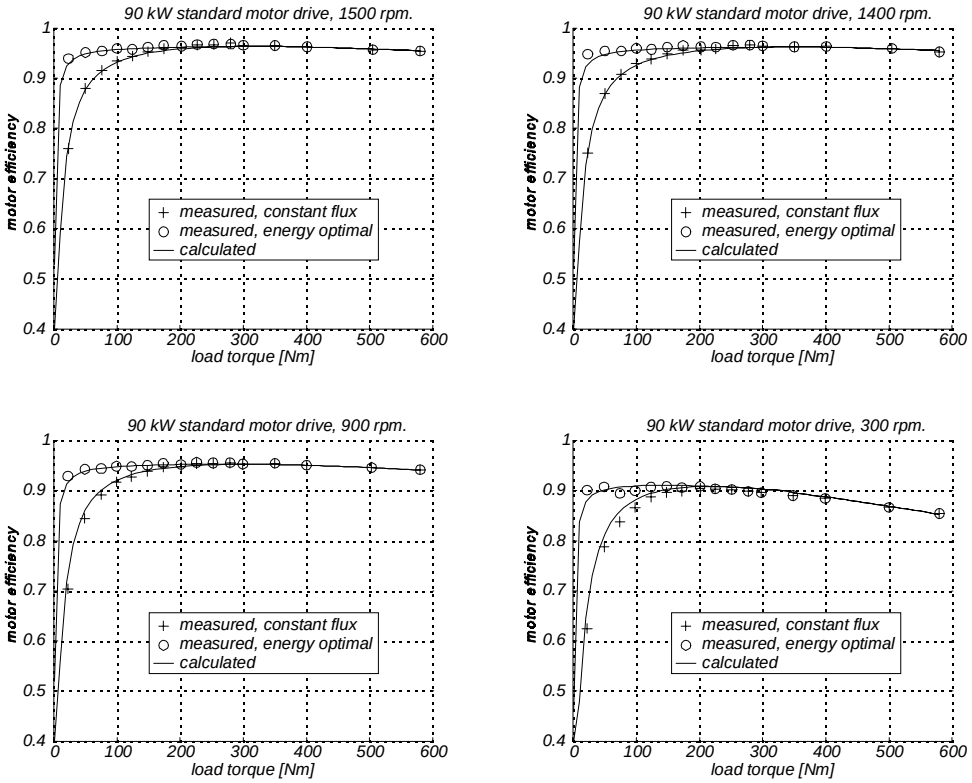

Figure B.36: *Meas. and calc. efficiency of a 90 kW standard ind. motor fed by an inverter.*

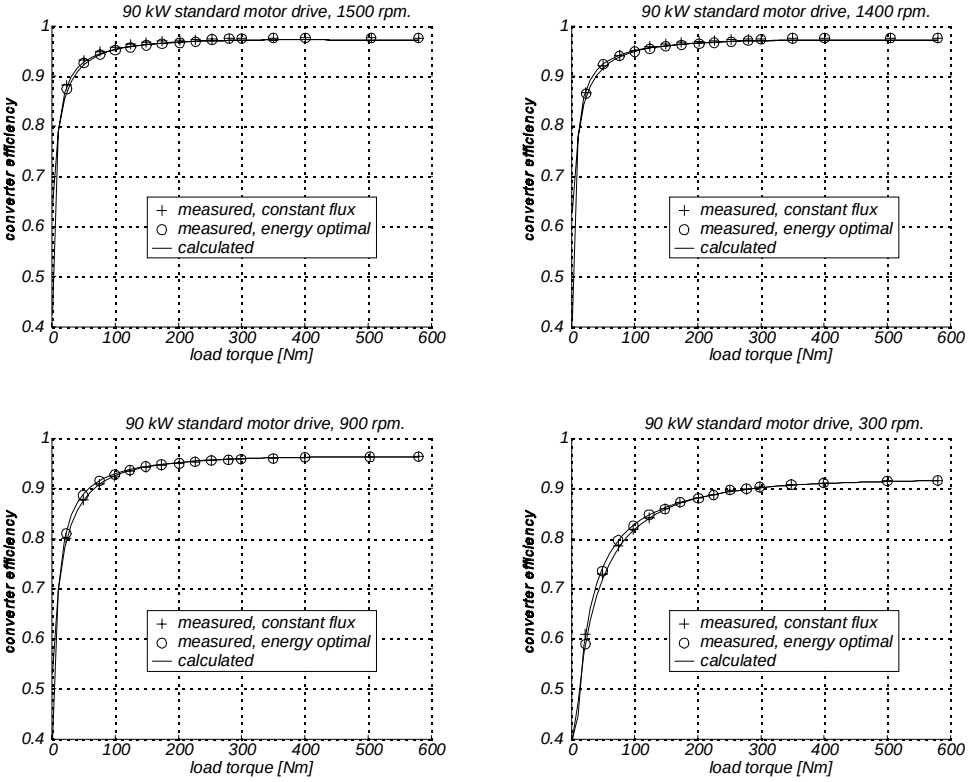

Figure B.37: *Measured and calculated efficiency of a converter feeding a 90 kW standard induction motor.*

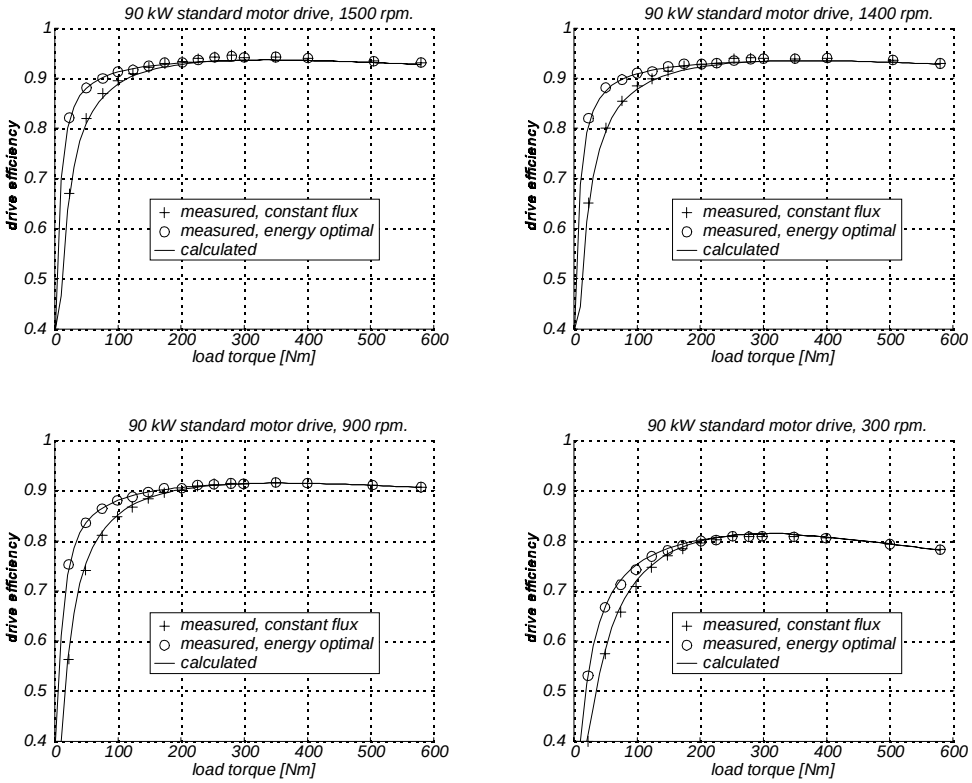

Figure B.38: *Meas. and calc. drive eff. of a 90 kW standard ind. motor fed by a converter.*

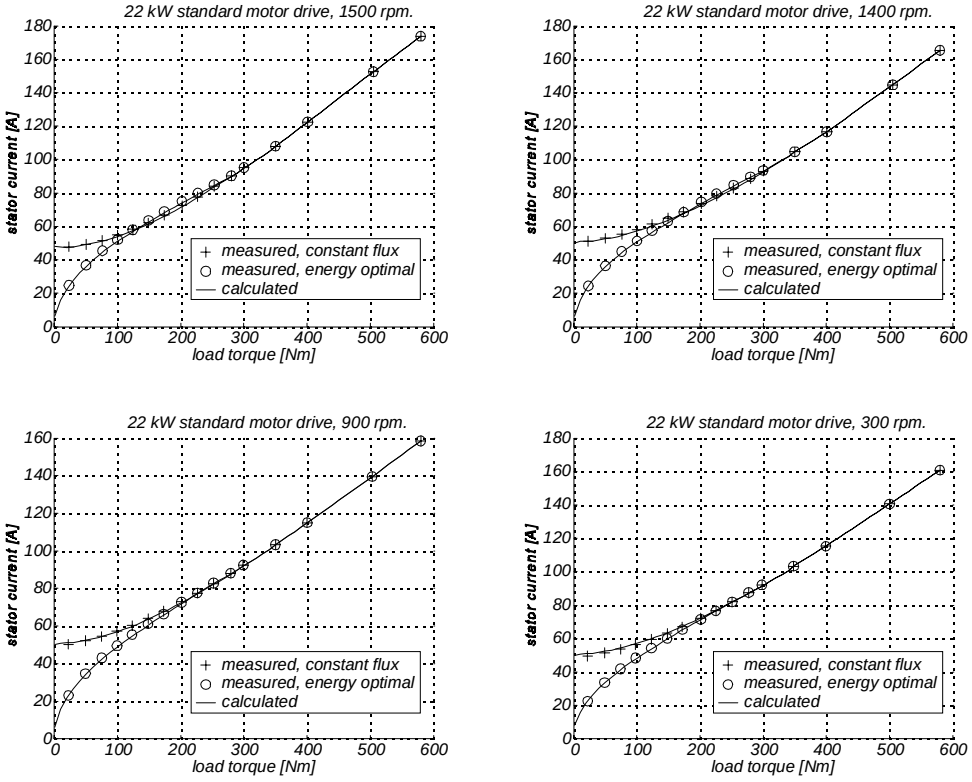

Figure B.39: *Measured and calculated stator current for a 90 kW standard induction motor fed by a converter.*

90 kW Standard Motor Model Constants.

All constants are expressed in SI-units.

$R_s = 0.020 + (0.025-0.020)\tau/580\ \Omega$

$R_r = 0.016\ \Omega$

$L_{s\sigma} = 0.36\ mH$

$L_{r\sigma} = 0.74\ mH$

$L_m(i_m)\ [H]$:

$i_m < i_{m1}: L_m = L_{m0}$

$i_{m1} \le i_m < i_{m2}: L_m = a_1(i_m - i_{m1})i_m^3 + a_2(i_m - i_{m1})i_m^2 + a_3(i_m - i_{m1})i_m + a_4$

$i_{m2} \le i_m < i_{m3}: L_m = b_1 \cdot i_m + b_2$

$i_{m3} \le i_m: L_m = c_1 + c_2/i_m$

$i_{m1} = 20$

$i_{m2} = 40$

$i_{m3} = 50$

$L_{m0} = 0.016$

$a_1 = -2.50 \cdot 10^{-8}$

$a_2 = -2.00 \cdot 10^{-6}$

$a_3 = 0$

$a_4 = 0.016$

$b_1 = -1.10 \cdot 10^{-4}$

$b_2 = 0.0194$

$c_1 = 0.0084$

$c_2 = 0.2750$

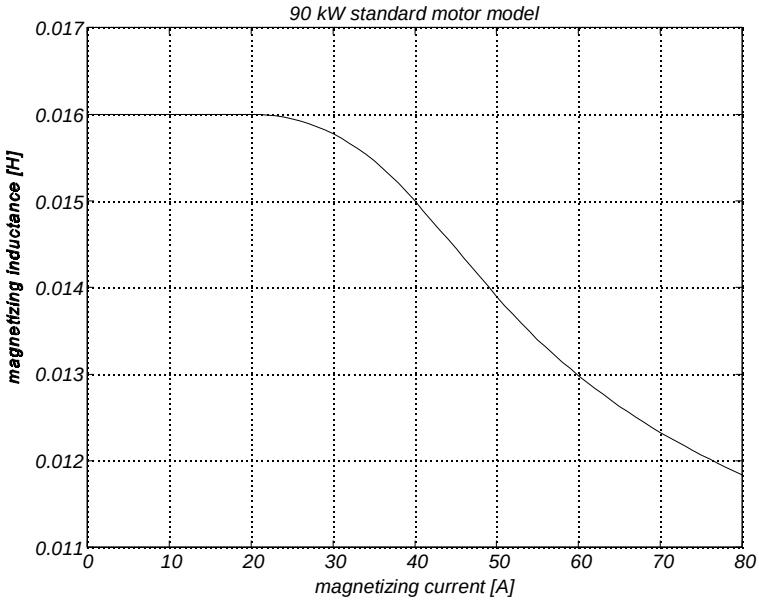

Figure B.40: *90 kW standard induction motor magnetizing inductance model.*

$P_{core} = 29.2 \cdot (1+0.63 \cdot s) \cdot \psi_m^{1.80} \cdot f_s + 0.10 \cdot (1+0.63 \cdot s^2) \cdot \psi_m^2 \cdot f_s^2 \quad [W]$

$\tau_{mech} = 0.8\ Nm$

$J = 1.50\ kg \cdot m^2$

Converter Model Constants.

R_{ac} = 0.0013 Ω, *at converter operating temperature*

V_{0T}	= 0.6000	V_{0Tlin}	= 1.0684
R_{0T}	= 0.1278	R_{0Tlin}	= 0.0058
B_{conT}	= 0.4733	V_{0Dlin}	= 0.8280
V_{0T}	= 0.5000	R_{0Dlin}	= 0.0044
R_{0T}	= 0.0844	α	= $3.3 \cdot 10^{-4}$
B_{conD}	= 0.4975		

R_{dc1} = 0 Ω, *at* 20°C P_{supply} = 360 *W*

R_{dc2} = 0.0076 Ω, *at* 20°C V_D = 1.0 *V*

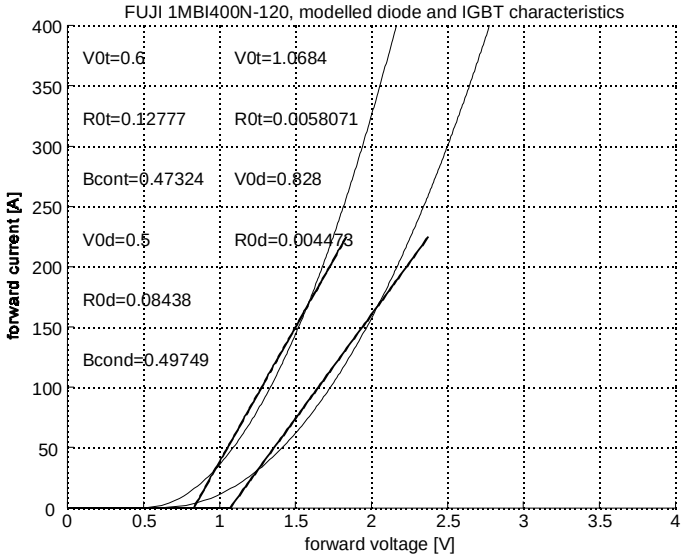

Figure B.41: *Measured inverter transistor and diode conduction voltages.*

B.5 3 kW Standard Induction Motor.

A 3 kW standard induction motor is used in chapter 7 in an analysis of oversized motors. The model of the motor is developed from the 2.2 kW standard induction motor model, as the only difference between the two motors is that the 3 kW motor has a longer stack, fewer windings and a thicker stator copper wire. It is shown here how the model is developed.

Stator Resistance.

It is assumed that the length of the end-winding is equal in the two motors. The length of the stator copper wire is then only increased by the increased stack length:

$$l_{wire,3} = l_{wire,stk,2.2}\frac{l_{stk,3}}{l_{stk,2.2}} + l_{endwind}$$

where $l_{wire,2.2}$, $l_{wire,3}$: length of stator copper wire per phase in 2.2 kW and 3 kW motors
$l_{stk,2.2}$, $l_{stk,3}$: stack length of 2.2 kW and 3 kW motors
$l_{endwind}$: length of end windings

The stator resistance per phase is:

$$R_s = \rho_{cu}\frac{l_{wire,3}}{A_{wire,3}} = 1.79\Omega\ ,\quad 20°C$$

where R_s : stator resistance per phase.
ρ_{cu} : copper resistivity.
$A_{wire,3}$: stator copper wire cross-section area in 3 kW motor

Rotor Resistance.

The rotor resistance is scaled for the increased stack length and for the changed stator winding number as:

$$R_{r,3} = R_{r,2.2}\frac{l_{stk,3}}{l_{stk,2.2}}\left(\frac{N_3}{N_{2.2}}\right)^2$$

where $R_{r,2.2}$, $R_{r,3}$: rotor resistance in 2.2 kW and 3 kW motors, referred to stator.

The stator and rotor resistances are corrected for temperature increase in the same way as for the 2.2 kW motor.

Core Loss.

The core loss is calculated by using the formula for the core loss in the 2.2 kW motor, and by scaling the air-gap flux and the calculated core loss in the following way:

$$P_{core,3} = \frac{l_{stk,3}}{l_{stk,2.2}} P_{core,2.2}\left(\psi_{2.2}, f_s, s\right), \quad \psi_{2.2} = \psi_3 \frac{l_{stk,2.2}}{l_{stk,3}} \frac{N_{2.2}}{N_3}$$

where $P_{core,2.2}$, $P_{core,3}$: core loss in 2.2 kW and 3 kW motors
$\psi_{2.2}$, ψ_3 : air-gap flux linkage in 2.2 kW and 3 kW motors
$N_{2.2}$, N_3 : number of windings in 2.2 kW and 3 kW motors

Magnetizing Inductance.

The magnetizing inductance is calculated by using the formula for the magnetizing inductance in the 2.2 kW motor, and by scaling the magnetizing current and the calculated inductance in the following way:

$$L_{m,3} = \frac{l_{stk,3}}{l_{stk,2.2}} \left(\frac{N_3}{N_{2.2}} \right)^2 L_{m,2.2}\left(i_{m,2.2}\right), \quad i_{2.2} = i_3 \left(\frac{N_3}{N_{2.2}} \right)$$

where $L_{m,2.2}$, $L_{m,3}$: magnetizing inductance in 2.2 kW and 3 kW motors
$i_{2.2}$, i_3 : magnetizing current in 2.2 kW and 3 kW motors

Stray Inductance.

The stray inductances are scaled as:

$$L_{s\sigma,3} = L_{s\sigma,2.2} \left(\frac{N_3}{N_{2.2}} \right)^2, \quad L_{r\sigma,3} = L_{r\sigma,2.2} \left(\frac{N_3}{N_{2.2}} \right)^2$$

where $L_{s\sigma,2.2}$, $L_{r\sigma,3}$: stator stray inductance in 2.2 kW and 3 kW motors
$L_{r\sigma,2.2}$, $L_{r\sigma,3}$: rotor stray inductance in 2.2 kW and 3 kW motors

References.

[1] F. Abrahamsen “Energy Optimal Control Strategies for Electro Motors, low-cost and sensorless PWM-VSI based induction motor control”, Aalborg University, Denmark, ISBN 87-89179-23-4, 1998.

Appendix C

List of Publications

F. Abrahamsen, J. K. Pedersen, F. Blåbjerg, “State-of-the-Art of Optimal Efficiency Control of Low-cost Induction Motor Drives”, Proceed. of PEMC'96, Budapest, Sep. 1996, Vol. 2, pp. 163-170.

F. Abrahamsen, F. Blåbjerg, J. K. Pedersen, “Hvordan får en standard asynkronmotor en højere virkningsgrad?”, Elteknik 09/96.

F. Abrahamsen, F. Blåbjerg, J. K. Pedersen, “Energirigtig drift af asynkronmotorer - uanset last”, Teknisk Nyt Special 07/96.

F. Abrahamsen, F. Blåbjerg, J. K. Pedersen, “Energibesparende drift af elektromotorer”, Installationsnyt Special, No. 11, nov. 1996.

F. Abrahamsen, J. K. Pedersen, F. Blåbjerg, “Analysis of Stability in Low-Cost Energy Optimal Controlled PWM-VSI Fed Induction Motor Drive”, Proceed. of EPE'97, Trondheim, Sep. 1997, pp. 3.717-3.723.

F. Abrahamsen, F. Blåbjerg, J. K. Pedersen, P. Grabowski, P. Thøgersen, E. J. Petersen, “On the Energy Optimized Control of Standard and High-Efficiency Induction Motor in CT and HVAC Applications”, IAS Annual Record, New Orleans, Oct. 1997, pp. 621-628.

F. Abrahamsen, F. Blåbjerg, J. K. Pedersen, “Energibesparende styringer for asynkronmotorer i både CT og HVAC anvendelser”, Teknisk Nyt Special 13/98.

F. Abrahamsen, F. Blåbjerg, J. K. Pedersen, P. Grabowski, P. Thøgersen, “On the Energy Optimized Control of Standard and High-Efficiency Induction Motor in CT and HVAC Applications”, IEEE Trans. on Ind. Appl., Vol. 34, No. 4, Jul/Aug 1998, pp. 822-831.

F. Abrahamsen, “Energy Optimal Control Strategies for Electro Motors, low-cost and sensorless PWM-VSI based induction motor control”, technical report (268 pages) and related publications, ISBN 87-89179-23-4, Feb. 1998.

P. Thøgersen, P. Nielsen, F. Abrahamsen, “Impacts on Energy Savings by Variable Speed Drives from Motor and Converter Technology”, PCIM'99, Nurnberg.

F. Abrahamsen, Jens Birk, F. Blåbjerg, J. K. Pedersen, “Comparison of Induction and PM Motor Efficiency in HVAC Applications”, Proceed. of EPE'99, Lausanne, Sep. 7-9, 1999.

F. Abrahamsen, F. Blåbjerg, J. K. Pedersen, “Evaluation of Variable Speed Electrical Drives for HVAC Applications, Proceed. of EEMODS'99, London, Sep. 20-22, 1999".

F. Abrahamsen, F. Blåbjerg, J. K. Pedersen, P. Thøgersen, “Efficiency Optimized Control of Medium-Size Induction Motor Drives”, IAS Annual Record, Rome, Oct. 2000, (in press).